Potential Energy Surfaces for Quantum Dynamics Simulations: From ab initio Computations to Vibrational State Determinations

by

Ekadashi Pradhan

A thesis submitted in partial fulfillment of the requirements for the degree of

Doctor of Philosophy

Department of Chemistry

University of Alberta

Abstract

Full dimensional potential energy surfaces (PESs) have been constructed using the neural network exponential fitting approach (NN-expnn). High level ab initio energies have been fit to a sum-of-products form (SOP) and the quality of the PESs have been verified by computing vibrational frequencies using the Multi-Configuration Time Dependent Hartree (MCTDH) method. Ground and excited states of CS_2, HFCO and HONO have been explored using this NN-expnn technique.

The ground state PES and dipole moment surfaces (DMS) for CS_2 have been determined at the CASPT2/C:cc-pVTZ, S:aug-cc-pV(T+d)Z level of theory and fit to a SOP form using the NN-expnn method. A generic interface between the NN-expnn PES fitting and the Heidelberg MCTDH software package is demonstrated. The PES has also been fit using the *potfit* procedure in MCTDH. For fits to the low-energy regions of the potential, the neural network method requires fewer parameters than *potfit* to achieve high accuracy - global fits are comparable between the two methods. Using these PESs, the vibrational energies have been computed for the four most abundant CS_2 isotopomers, compared to previous experimental and theoretical data, and shown to accurately reproduce the low-lying vibrational energies within a few wavenumbers.

A local 6D PES for the HFCO molecule was fit in a SOP form using neural network exponential fitting function and validated in MCTDH calculation. The ab initio data were computed at the CCSD(T)-F12/cc-pVTZ-F12 level of theory. The

fit PES has a RMSE of 10 cm^{-1} as compared to the ab initio data up to 10000 cm^{-1} above the zero point energy. The computed vibrational modes, which cover most of the experimentally measured infrared data, are more accurate that those from the previous MP2-based PES. With this PES, intermolecular vibrational redistribution (IVR) in HFCO and DFCO, the effect of IVR on unimolecular dissociation, and control of IVR using optimal control theory can be studied.

A CCSD(T)-F12/cc-pVTZ-F12 computed 6D PES for HONO in the cis-trans region has been fit with the neural network exponential fitting function. The final PES is in SOP form and can directly be used in MCTDH to study spectroscopy and dynamics. The PES is compared with alternate PESs based on CCSD(T)/cc-pVTZ, cc-pVQZ, cc-pV5Z and complete basis set (CBS) extrapolated ab initio data. The vibrational states determined up to 4000 cm^{-1} for cis- and trans-HONO exhibit very good accuracy when compared to experiment (RMSE of 7.5 cm^{-1} for cis-HONO and 8.5 cm^{-1} for trans-HONO). The general NN-expnn fitting method can be applied to other similar 6D molecular systems and has great potential for application to larger systems (9D, etc.) in the future.

A global 6D PES was constructed for HFCO using CCSD(T)-F12/cc-pVTZ-F12 ab initio energies. The SOP form of the final analytical surface was used to compute vibrational frequencies using MCTDH. The equilibrium to HF + CO dissociation part of the potential was very accurate, about 10 cm^{-1} RMSE, compared to recent experiment and theory. The cis-trans-HOCF and HFCO to trans-HOCF regions were also accurate with RMSE of 20 cm^{-1} compared to the ab initio data.

A 6D PES for the HFCO S_1 electronic state was determined based on EOM-CCSD/aug-cc-pVTZ energies. The fundamental vibrational frequencies as computed using MCTDH were in very good agreement with the experimental results. RMSE of 45 cm^{-1} of the fundamental modes was obtained. The vertical excitation energies were also computed at CASSCF, CASPT2, CASPT2-F12, MRCI and MRCI-F12 levels of theory with different active space, (CAS(8,7), CAS(12,9), and full CAS(18,13)). With this newly constructed PES along with the previous S_0 surface (both in SOP form), it is possible to study theoretically stimulated emission pumping (SEP) spectra for the HFCO molecule using MCTDH.

Overall, a MATLAB interface (for constructing PESs by directly fitting of ab initio data into SOP form) to the MCTDH software package has been successfully implemented and tested on a diversity of problems. In the future, the present PES fitting method may serve as an alternative to the conventional *potfit* approach for adopting PESs for use in MCTDH.

Preface

Chapter 2 of this thesis has been published as E. Pradhan; J. L. Carreón-Macedo; J. E. Cuervo; M. Schröder and A. Brown, "Ab Initio Potential Energy and Dipole Moment Surfaces for CS_2: Determination of Molecular Vibrational Energies," *J. Phys. Chem. A*, **2013**, *117*, 6925. Initial MATLAB code for the PES fitting was developed by J. E. Cuervo and M. Schröder. Ab initio computations to obtain energies were carried out by J. L. Carreón-Macedo. I completed the main important work on this chapter, from MATLAB code development, python interface to MCTDH, PES fitting, MCTDH vibrational state computation, dipole surface fitting and was involved in the paper writing. All research reported in the other chapters is executed solely by myself with the help of my supervisor Professor Alex Brown.

Acknowledgements

I want to thank Dr. Alex Brown who supervised me throughout my research work and thesis writing. This thesis would not have been completed without his constant guidance. I am thankful to my co-workers. I want to thank my friends and family members for their support during my Ph.D.

Table of Contents

List of Tables

List of Figures

List of Abbreviations and Acronyms

1D	*One dimensional*
2D	*Two dimensional*
3D	*Three dimensional*
ANN	*Artificial neural network*
aug-cc-pV5Z	*Dunning's augmented, correlation-consistent valence quintuple-ζ basis set*
aug-cc-pVDZ	*Dunning's augmented, correlation-consistent valence double-ζ basis set*
aug-cc-pVQZ	*Dunning's augmented, correlation-consistent valence quadruple-ζ basis set*
aug-cc-pVTZ	*Dunning's augmented, correlation-consistent valence triple-ζ basis set*
CA	*Complementary auxiliary*
CARS	*Coherent anti-stokes Raman scattering*
CASPT2	*Complete active space second order perturbation theory*
CASPT2-F12	*Explicitly correlated, complete active space second order perturbation theory*
CASSCF	*Complete active space self-consistent field*
CBS	*Complete basis set extrapolation*
CC	*Coupled cluster method*

CCSD(T)	*Coupled cluster singles doubles and perturbative triples*
CCSD(T)-F12	*Explicitly correlated, coupled cluster singles doubles and perturbative triples*
CCSD	*Coupled cluster singles doubles*
CMF	*Constant mean field*
CSF	*Configuration state functions*
CVDR	*Correlation discrete variable representation*
DFT	*Density functional theory*
DMS	*Dipole moment surface*
DVR	*Discrete variable representation*
EOM-CCSD	*Equation of motion coupled cluster singles and doubles*
F12	*Explicitly correlated energy*
HF	*Hartree Fock*
HF-SCF	*Hartree Fock self consistent field*
HO	*Harmonic oscillator*
IMLS	*Interpolating moving least squares*
IVR	*Intramolecular vibrational energy redistribution*
KEO	*Kinetic energy operator*
LMA	*Levenberg-Marquardt algorithm*
MCSCF	*Multiconfiguration self-consistent field*
MCTDH	*Multiconfigurational time-dependent Hartree method*
MO	*Molecular orbital*
MP2	*Møller-Plesset second order perturbation theory*
MP3	*Møller-Plesset third order perturbation theory*
MP4	*Møller-Plesset* 4^{th} *order perturbation theory*

MRCI	*Multireference configuration interaction*
MRCI-F12	*Explicitly correlated, multireference configuration interaction*
MSE	*Mean-squared error*
MSI	*Modified Sheppard interpolation*
NMR	*Nuclear magnetic resonance spectroscopy*
NN	*Neural network*
NN-expnn	*Neural network exponential fitting techniques*
OCT	*Optimal control theory*
OCT-MCTDH	*Optimal control theory implemented in MCTDH*
PES	*Potential energy surface*
PIP	*Permutation invariant polynomial*
PIP-NN	*Permutation invariant polynomial Neural Network*
QSAR	*Quantitative structure-activity relationship*
RHF	*Restricted Hartree Fock self consistent field*
RMSD	*Root-mean squared deviation*
RMSE	*Root-mean squared error*
SEP	*Stimulated emission pumping*
SOP	*Sum-of-products*
SPF	*Single particle function*
VPT2	*Vibrational second-order perturbation theory*
ZPE	*Zero-point energy*

List of Symbols

Å	*angstrom*
θ	*bond angle*
r	*electron coordinate or bond length*
R	*nuclear coordinate*
M_A	*nuclear mass*
Z_A	*nuclear charge*
$\hat{H}$	*Hamiltonian operator*
ψ	*wavefunction*
$\Phi_i(q_i)$	*spin orbital*
α	*up spin*
β	*down spin*
$\hat{T}$	*cluster operator*
$\hat{T}_1$	*cluster of all single excitations*
$\hat{T}_2$	*cluster of all double excitations*
$\hat{Q}_{12}$	*projector*
V_{CBS}	*CBS extrapolated energy*
L_{max}	*highest angular momentum*
a_{ij}^{kl}	*weight parameter connecting* k^{th} *node in the* i^{th} *layer to* l^{th} *node of the* j^{th} *layer*
x_m^l	*sum of all the weighted value*

G_i	*input node*
b_m^l	*bias*
w_{qp}	*weight parameter*
b_q	*bias parameter*
f_i	*random number*
X_{scaled}	*scaled data*
x_{max}	*maximum of unscaled data*
x_{min}	*minimum of unscaled data*
f	*number of degrees of freedom*
χ	*time-dependent primitive basis functions*
$\Phi^{(k)}$	*single particle function*
$\hat{h}_r^{(k)}$	*potfit Hamiltonian operator operates on the k^{th} particle only*
ϕ	*dihedral angle*
D_0	*dissociation energy*
μ	*dipole moment operator*
ν	*frequency*

Chapter 1

Introduction

1.1 Motivation

The goals of this thesis are to generate and test high quality, multidimensional potential energy surfaces (PESs) that will be computationally effective for spectroscopic and quantum dynamics applications for moderate to large sized molecules (i.e., containing from 3 to, perhaps, 10 atoms). Among many other competitive mathematical PES fitting approaches [e.g., permutation invariant polynomial neural network (PIP-NN), PIP interpolated moving least squares (PIP-IMLS)], the neural network exponential fitting (NN-expnn) method, developed by Carrington and Manzhos[1,2] is selected. In the NN-expnn approach, the PES is fit to a sum-of-products (SOP) form which can be directly utilized in the multiconfigurational time-dependent Hartree (MCTDH) method[3] to study spectroscopy and dynamics. None of the other above mentioned methods generate a SOP form for the final PES. Thus, refitting to the SOP form before use in MCTDH is required for computational efficiency.

MCTDH has been shown[3–7] to be an efficient and accurate method to study spectroscopy and full dimensional quantum dynamics in a diversity of molecular systems. However, in MCTDH, the sum-of-products form of the wave function and the Hamiltonian operator are required to obtain computational efficiency. In general, the kinetic energy operator (KEO) is always or can be, written in the SOP form. Therefore, the challenge becomes expressing the potential in the requisite SOP form.

The motivation behind using the NN-expnn fitting method comes from the fact that the traditional *potfit* method in MCTDH for fitting a PES is impossible to implement beyond a six-dimensional (6D) PES, i.e., beyond four atoms. The limitation arises because the *potfit* algorithm requires, and must store, the energy data on a grid. As an example, for a nine-dimensional (9D) system, i.e., 5 atoms, if 10 grid points are taken along each dimension, the total number of data points required is 10^9. Computing a large number of data points, especially using any sort of high-level ab initio approach, is not tractable. Even if one could compute the data, its storage would be prohibitive. The computational cost of the underlying ab initio points is why many (most) MCTDH computations for isolated molecules are based on PESs refit using the *potfit* algorithm from a previous analytical surface. On the other hand, the NN-expnn fitting procedure is general and does not require data on a grid but rather randomly selected data can produce a high quality PES.[1,2,8] Therefore, one of the motivations of this thesis work is to implement the NN-expnn method as a general replacement for *potfit* in MCTDH such that full dimensional quantum dynamics of 6D, and larger, systems can be studied. At the same time, this thesis aims to present the most accurate PES of a system available from the underlying ab initio electronic structure. The accuracy of a PES is reflected in the quality of computational results for spectroscopy (e.g., vibrational state energies) and quantum dynamics (e.g., reaction rates). For ground electronic states, the ab initio electronic structure computations are carried out primarily with the explicitly correlated coupled cluster singles, doubles, and perturbative triples excitation (CCSD(T)-F12) method. For one system, the multireference complete active space second order perturbation theory (CASPT2) was utilized. The equation of motion coupled cluster singles and doubles (EOM-CCSD) method was used as a basis for the excited electronic state PES.

In this thesis, the overall computational approach is termed as NN-expnn-MCTDH, where (i) ab initio electronic structure computations are carried out to determine electronic energies for a variety of molecular geometries, (ii) the energy data is fit directly using the NN-expnn approach and the fitting parameters converted into an MCTDH operator file, and (iii) vibrational states are computed using block improved relaxation[9] in MCTDH to validate the PES quality. The utility of this specific potential energy surface fitting approach is exemplified through applications to several specific molecules: CS_2, HFCO and HONO. The motivation for examining these specific systems is touched upon in the Thesis Overview (Section 1.5) and expanded upon in the corresponding research chapters.

In the following sections, a brief overview of the three computational components that form the basis of the present work are provided: (i) the ab initio computational methods used for determining ground and excited electronic states, (ii) the potential energy surface fitting procedures, and (iii) the approaches used for the determination of the vibrational frequencies. While a basic general introduction is given to most of the topics in each of the above components, one major topic will be the primary focus in each of these sections; further theoretical, mathematical and computational details are available from the primary references and are not presented here. In the ab initio methods section, the theoretical details of the explicitly correlated coupled cluster with singles doubles and perturbative triples, CCSD(T)-F12, method will be emphasised (see Section 1.2.1.4). In the PES fitting procedures, neural network fitting, including that with exponential neurons to obtain a sum-of-products form suitable for use in MCTDH, will be discussed (see Section 1.3.2.1). Finally, for determining vibrational states, the approaches available in the Heidelberg MCTDH software package are discussed.

1.2 Electronic Structure Computations

The Schrödinger equation is the basic building block of quantum chemistry:

$$\hat{H}(\hat{r}, \hat{R})\Psi(\hat{r}, \hat{R}) = E\Psi(\hat{r}, \hat{R}) \tag{1.1}$$

where the Hamiltonian operator $\hat{H}(\hat{r}, \hat{R})$ and wavefunction $\Psi(\hat{r}, \hat{R})$ depend explicitly on the coordinates of all the electrons ($\hat{r}$) and nuclei ($\hat{R}$) in the system (molecule).

The (non-relativistic) Hamiltonian operator in atomic units is given by

$$
\begin{aligned}
\hat{H}(\hat{r},\hat{R}) = &-\frac{1}{2}\sum_{A}\frac{1}{M_A}\nabla_A^2 - \frac{1}{2}\sum_{i}\nabla_i^2 - \sum_{i,A}\frac{Z_A}{|r_i - R_A|} \\
&+ \sum_{i<j}\frac{1}{|r_j - r_i|} + \sum_{A<B}\frac{Z_A Z_B}{|R_B - R_A|}
\end{aligned}
\tag{1.2}
$$

where the terms represent the kinetic energy of the nuclei (of mass M_A/m_e), kinetic energy of the electrons, electron-nuclei attractions, electron-electron repulsion, and nuclear-nuclear repulsion. While, in principle, any property can be determined from the wavefunction Ψ, Eq. (1.1) is rarely solved directly for molecular applications but rather the Born-Oppenheimer approximation is invoked. Within the Born-Oppenheimer approximation, the electronic and the nuclear motion of a molecule are treated as separable. One utilizes the fact that electrons are much less massive compared to the nuclei, and hence move much faster. Therefore, the nuclear motion is negligible with respect to the electronic motion, and one can solve the electronic Schrödinger equation for fixed positions of the nuclei. From this, one obtains the electronic energy for a given set of nuclear coordinates. Mapping out this energy as a function of nuclear coordinates, $V(\overrightarrow{R})$, leads to the concept of the potential energy surface (PES). The PES can then be used to construct the nuclear Schrödinger equation, where the Hamiltonian operator is

$$\hat{H} = -\frac{1}{2}\sum_{A}\frac{\nabla_A^2}{M_A} + V(\overrightarrow{R}). \tag{1.3}$$

The solution of this equation is discussed further in Sec. 1.4. Thus, the wave function of a molecule can be presented as a product of an electronic and nuclear part, i.e.,

$$\Psi_{molecule}(\vec{r}_i, \vec{R}_j) = \Psi_{electronic}(\vec{r}; \vec{R})\Psi_{nuclear}(\vec{R}). \tag{1.4}$$

Several methods for computing the electronic energies are presented below.

1.2.1 Ground Electronic State

1.2.1.1 Hartree-Fock Self-Consistent Field (HF-SCF)

The most basic electronic structure computation is a HF-SCF[10,11] determination of the electronic wave function. Restricted HF (RHF) computations are based on a single determinant. where the (N-electron) electronic wavefunction is written as,

$$\Psi(q_1, q_2, ...q_N) = \frac{1}{\sqrt{N!}} \begin{vmatrix} \Phi_1(q_1) & \Phi_2(q_1) & \cdots & \Phi_N(q_1) \\ \Phi_1(q_2) & \Phi_2(q_2) & \cdots & \Phi_N(q_2) \\ \vdots & \vdots & \vdots & \vdots \\ \Phi_1(q_N) & \Phi_2(q_N) & \cdots & \Phi_N(q_N) \end{vmatrix}. \quad (1.5)$$

In Eq. (1.5), each $\Phi_i(q_i)$ is a spin orbital that depends on both the spatial (r_i) and spin (α or β) coordinates. If one assume that each orbital can be written as a linear combination of one electron atomic basis functions, the standard Hartree-Fock-Roothan equations can be derived. In general, the HF-SCF procedure neglects electron correlation (save for that accounted for through the proper anti-symmetrization of the wavefunction). To deal with the accurate description of the correlation energy, a variety of post-HF methods have been developed; however HF-SCF is required for the initial guess wave function.

1.2.1.2 Møller-Plesset perturbation theory (MP2)

Møller-Plesset (MP) perturbation[12] theory utilizes Rayleigh-Schrödinger perturbation theory to incorporate effects of electron correlation and, hence, can lead to expansion to different orders, i.e., MPn. The zeroth-order wavefunction is that from a HF-SCF computation and the perturbation is the correlation potential. However, the MP method is not variational, and, therefore, the calculated energy may be lower than the true ground state energy. Although various orders of MP perturbation theory are available, e.g. second order (MP2), third order (MP3), fourth order (MP4), MP2 is widely used for computational efficiency since higher order MPn methods may be divergent. The MP2 method is useful due to the availability of analytic energy gradients and Hessians, which allow for efficient geometry optimizations and computation of harmonic vibrational frequencies. In this thesis, the MP2 method[13,14] was used to optimize geometries prior to the use of much more computationally expensive coupled cluster theory methods (including explicitly correlated versions).

1.2.1.3 CCSD, CCSD(T)

CCSD(T)[14] is considered as the "gold standard method of quantum chemistry." The coupled cluster wave function is expressed using an exponential ansatz,

$$|\Psi\rangle = e^{\hat{T}} |\Phi_0\rangle \tag{1.6}$$

where Φ_0 is the initial Slater determinant constructed from (usually) HF molecular orbitals and $\hat{T}$ is the cluster operator. The cluster operator, is written as

$$\hat{T} = \hat{T}_1 + \hat{T}_2 + \hat{T}_3 + ... \tag{1.7}$$

where $\hat{T}_1$ is the cluster of all single excitations, $\hat{T}_2$ is the cluster of all double excitations, etc. The exponential operator $e^{\hat{T}}$ can be expressed, by a Taylor series expression, as

$$\begin{aligned} e^{\hat{T}} &= 1 + \hat{T} + \frac{\hat{T}^2}{2!} + ... \\ &= 1 + \hat{T}_1 + \hat{T}_2 + \frac{\hat{T}_1^2}{2} + \hat{T}_1\hat{T}_2 + \frac{\hat{T}_2^2}{2} + ... \end{aligned} \tag{1.8}$$

The CCSD(T) method includes all single and double excitations (i.e., $\hat{T} = \hat{T}_1 + \hat{T}_2$) and the triple excitations are included perturbatively. The CC methods provide some of the most accurate results for ground state properties using ab initio electronic structure theory. However, their high computational cost usually limits applications to small molecules, such as those considered in this thesis. A modification of the CC methods, using explicitly correlated techniques (designated by F12),[15,16] came with improved treatment of electronic correlation and faster convergence to the complete basis set limit. In the following section, the CCSD(T)-F12 method will be described briefly.

1.2.1.4 Explicitly Correlated Methods

For closed shell CCSD-F12, the wave function ansatz is

$$\Psi_{CCSD} = e^{\hat{T}_1 + \hat{T}_2} \Psi_{HF}, \tag{1.9}$$

where the $\hat{T}_1$ and $\hat{T}_2$ are the cluster operators:

$$\hat{T}_1 = t_a^i \hat{E}_{ai}, \tag{1.10}$$

and

$$\hat{T}_2 = \hat{T}_{ab}^{ij} \hat{E}_{bj} + \tau_{\alpha\beta}^{ij} \hat{E}_{\alpha i} \hat{E}_{\beta j}. \tag{1.11}$$

Here i and j ... refer to the occupied orbitals, a and b to the external (virtual) orbitals and α and β to a complete orbital basis set. t_a^i and T_{ab}^{ij} are the conventional single and double amplitudes from coupled cluster theory. In the F12 variant, $\tau_{\alpha\beta}^{ij}$ is an additional term which is approximated as

$$\tau_{\alpha\beta}^{ij} = \left\langle \alpha\beta \left| \hat{Q}_{12} \hat{F}_{12} \right| kl \right\rangle T_{kl}^{ij}, \tag{1.12}$$

where the projector,

$$\hat{Q}_{12} = 1 - |rs\rangle \langle rs| - |mx\rangle \langle mx| - |xm\rangle \langle xm| \,. \tag{1.13}$$

The r and s denote the full molecular orbital (MO) basis and x the complementary auxiliary (CA) orbital basis. When α and β belong to the orbital basis, or if at least one of them corresponds to an occupied orbital, $\tau_{\alpha,\beta}^{ij} = 0$. The correlation factor $\hat{F}_{12}$ is a simple Slater function, i.e.,

$$F(r_{12}) = e^{-\beta r_{12}}. \tag{1.14}$$

In the present CCSD-F12 implementation, a simple product of Gaussian functions is used to replace the Slater function. The triples correction to CCSD-F12 can be obtained perturbatively; there is no F12 triples corrections. By default two different energies are computed, CCSD(T)-F12A and CCSD(T)-F12B; the interested reader is referred to the original papers[15,16] for the difference. Practically speaking, the F12A (F12B) approach slightly overestimates (underestimates) the correlation energy and there is strong basis set dependence to the energies. The recommendations are that the F12A method be used for cc-pVDZ-F12 and cc-pVTZ-F12 basis sets and F12B should be utilized for cc-pVQZ-F12 and cc-pV5Z-F12 basis sets.

1.2.2 Excited Electronic State Computations

The excited electronic states geometries, vibrational energies and vertical excitation energies were computed using several different ab initio electronic structure methods. EOM-CCSD, complete active space self-consistent field (CASSCF), internally-contracted multi-reference configuration interaction, (MRCI), CASPT2, MRCI-F12 and CASPT2-F12 methods were used to compute vertical excitation energies. Geometry optimizations and harmonic vibrational frequency computations were carried out for those methods where analytic gradients (Hessians) were available, i.e., CASSCF and CASPT2, or where numerical approaches were computationally tractable, i.e., EOM-CCSD and MRCI. In this section, an extremely brief introduction to these methods is provided along with references to the original papers where further theoretical and computational details can be found.

1.2.2.1 EOM-CCSD

The EOM-CCSD method[17] is used to compute the excitation energies using the equation-of-motion (EOM) procedure; in Molpro,[18,19] EOM-CCSD is limited to computing energies for singlet excited states. The accuracy of EOM-CCSD depends on the relative contribution of the single excitations to the singlet excited state. The more single excitations dominate, the better is the expected accuracy in the EOM-CCSD excitation energy. In this thesis, I have utilized the EOM-CCSD method to generate ab initio data to fit an S_1 PES for the HFCO molecule.

1.2.2.2 CASSCF

In the (CASSCF) method,[20–24] the occupied orbital space is split into inactive core and active valence orbitals. Within the active valence space, electrons are allowed to distribute in all possible ways, i.e., full configuration interaction within a subset of all orbitals. The inactive core orbitals are doubly occupied in all configurations. The accuracy of a CASSCF calculation compared with an observed value depends on the choice of the active space. CASSCF results can also be significantly improved by using them as a basis for methods including dynamical electron correlation, i.e., MRCI and CASPT2 approaches.

1.2.2.3 MRCI

In the multi reference configuration interaction (MRCI) method (implemented in Molpro[25–29] and numerous prior/competing implementations[30–35]), a configuration interaction computation is performed from the configuration state functions (CSFs) generated from a CASSCF computations. Although very accurate, the MRCI approach is very computationally costly, and thus generally restricted to very small molecular systems.

1.2.2.4 CASPT2

In CASPT2 method,[36–40] the orbital space is split into closed, active and external shells based on their occupancies in the reference wavefunction. The closed-shell orbitals are doubly occupied inactive orbitals in all reference configurations. The active orbital space is allowed to perform all kinds of excitations within it. The external or secondary orbital space contains unoccupied virtual orbitals. In the CASPT2 method, second order perturbation theory is used to incorporate dynamical correlation, thus describing excited states more accurately than CASSCF. It requires large computational resources.

1.2.2.5 CASPT2-F12 and MRCI-F12

Second order multireference perturbation theory with explicit correlation, CASPT2-F12[41] and explicitly correlated multireference configuration interaction, MRCI-F12[42–44] are used to improve the convergence in the correlation energies with the basis set size.

1.2.3 Dunning-style Basis Sets and Complete Basis Set Extrapolation

In this thesis work, I have used only correlation consistent basis sets derived by Dunning and co-workers.[45] They found that Hartree-Fock optimized basis sets are not ideal for use in computations incorporating electron correlation computations.

Thus, the correlation consistent basis sets were optimized using correlated (CISD) wave functions. The basis sets are designated as cc-pVXZ, where X=D, T, Q, 5, 6, 7. The prefix "aug" is added to those basis sets that have diffuse functions added for every angular momentum present in the basis, e.g., aug-cc-pVDZ[45,46] has diffuse s, p, and d for the C atom. The cc-pVTZ-F12[47–49] basis set was used for the explicitly correlated computations in this thesis work. The Dunning basis sets are designed such that they converge smoothly to the complete basis set (CBS) limit. The Dunning-style basis sets have been adapted for use with explicitly correlated computations; that is, with an increasing number of basis functions, the electronic energy decreases, and (eventually, for an "infinite" number of basis functions) reaches the CBS limit. The convergence of ab initio energies to the CBS limit is very slow when post-HF computations are performed. Therefore, instead of using a infinite number of basis functions, the CBS limit can be determined by extrapolating the correlation energy from a few carefully selected basis sets. In this thesis, the CBS extrapolation[50–52] is done using the CCSD(T)/aug-cc-pVTZ, aug-cc-pVQZ and aug-cc-pV5Z computed energies. The total CBS extrapolated energy is

$$E_{CBS}^{tot} = E_{CBS}^{SCF} + E_{CBS}^{corr}, \tag{1.15}$$

where the SCF correlation energy, E_{CBS}^{SCF}, is assumed same as the CCSD(T)/aug-cc-pV5Z SCF energy, E_{AV5Z}^{SCF}. From the aug-cc-pVTZ to aug-cc-pV5Z basis sets, the SCF energy change is insignificant compared to the correlation energy change for CCSD(T) computations. The correlation energy is

$$E^{corr} = E^{tot} - E^{SCF}, \tag{1.16}$$

where E^{corr} is the correlation energy, E^{tot} is the total energy, and E^{SCF} is the SCF energy. There are two types of extrapolation methods used to reach the CBS limit: two and three point extrapolation:

$$V(x) = V_{CBS} + Ae^{-Bx} \tag{1.17}$$

and

$$V(x) = V_{CBS} + Ax^{-3} \tag{1.18}$$

Equation (1.17) is for three point extrapolation where V_{CBS}, A and B are the unknown parameters to be solved. The x is the same as L_{max} (or l_{max}), the highest orbital angular momentum in the basis. Therefore, the value of x equals 2 for aug-cc-pVDZ, 3 for aug-cc-pVTZ, 4 for aug-cc-pVQZ, and 5 for aug-cc-pV5Z. Not surprisingly, a minimum of three different basis sets are required to use the three point extrapolation method. Equation (1.18) is a two point extrapolation method where x is the same as defined for equation (1.17). However, the two point extrapolation requires only two different basis sets to solve the CBS energy, V_{CBS} and A, but to get consistent results, at least one extra basis set is generally required.

1.3 Potential Energy Surface Fitting

In chemical physics, the potential energy surface (PES) is one of the most basic features to represent a quantum chemical system. Almost all the properties of a quantum chemical system directly or indirectly depend upon the PES. From a known PES, one can extract various properties of a system using available computer simulation methods. The PES is defined as the functional form (analytical form) of the potential energy of a system constructed upon the atomic positions (geometry/internal coordinate) as the parameters. As an example, the Morse oscillator[53] has the form

$$V(r) = D_0[1 - e^{-\alpha(r-r_0)}]^2, \tag{1.19}$$

where D_0 is the dissociation energy, α is the pre-exponential factor, r_0 is the equilibrium distance and the r is the distance coordinate. The independent variables or the coordinates should represent all the degrees of freedom present in a system. As the number of degrees of freedom depends on the molecular size (atom number), the PES of a system could range from very simple (in the case of small molecules) to very complex (systems that contain large numbers of atoms). Ideally, any suitable coordinates, e.g., internal, polyspherical, cartesian or polar, should be able to be used to represent the PES. The PES is necessary to solve the nuclear Schrödinger equation, see Eq. (1.3). It is not mandatory to have a PES, e.g., the potential energy can be known at discrete points (DVR approach[54,55]), but a PES makes it possible to use a variety of dynamics methods. One of the disadvantages of the DVR method is that the PES information is stored for a particular set of points. Thus, if the representation is changed in any way, the electronic Schrödinger equation must be solved again. Alternatively, within the ab initio MD method,[56] the potential energy is computed "on the fly" at required geometries. However, this method is computationally costly. Thus computationally efficient methods, and hence less accurate than high level wave-function based methods, must be employed, e.g., DFT. If the potential energies computed during the electronic structure calculations are represented in the form of an analytical function, the computational cost of potential evaluations in the dynamics simulation can be overcome. A PES is constructed through fitting or interpolating potential energies at many different nuclear configurations. The potential energy of a given nuclear configuration is obtained by solving the electronic Schrödinger equation. Constructing a PES is challenging for high dimensional systems. With increasing dimensionality, the number of energy computations required to generate a suitable data set for fitting is very high and fitting an analytical form to the high dimensional data is even harder. When considering PES fitting methods, almost all can be categorized into two different types: physically intuitive and generalized mathematical. The physically intuitive approaches are based on utilizing predefined physically motivated fitting functions[57–60] for the interatomic distances and angles. If the functional form is chosen appropriately, the PES representation is compact with few fitting parameters and generally can be very accurate. The main drawbacks are that physically motivated PES are usually local (i.e., represent specific regions of the PES which may then be connected with switching functions), restricted to the specific system of interest (although there can be similar PES representations for analogous systems), and cannot be transferred or utilized for general problems.

The generalized mathematical methods, on the other hand, are not predefined but entirely depend on the efficiency and the flexibility of the functional form. Examples are spline methods,,[61,62] interpolating moving least squares (IMLS),[63,64] modified Sheppard interpolation (MSI) using Taylor expansion,[65,66] genetic algorithms,[67] and Gaussian approximation methods.[68] If fit carefully, the final PES can be highly accurate and computationally efficient. On the other hand, special care must be taken for fits to non-physically motivated functional form. The permutationally invariant polynomial method (PIP) by Bowman and co-workers[69–72] works well for small to moderate sized molecules, especially those with a large numbers of symmetry equivalent nuclei. To enforce permutation invariance, one must use interatomic redundant coordinates. One advantage of the PIP-approach is that it can be transferred directly between different problems without changing the general form of the PES, i.e., in principle these are "black box" methods. Guo and co-workers developed a neural network (NN) based method which exhibits permutational invariance[73] symmetry (PIP-NN).[74–76] This recently developed method takes advantage of the black box efficiency of neural networks for the PES fitting.

NN based methods are an example of a mathematical PES fitting method. It is a black box method; once the network is constructed, it can automatically be optimized to give the desired output. The neural network exponential fitting method (NN-expnn) is one of the very recently developed PES fitting methods in the generalized mathematical category.[1] In the following section, the NN based methods with an emphasis on NN-expnn, will be discussed. Being a black box method, a NN does not require any predefined form. It is a general method and portable to other science areas. NN based methods can be used to fit input with target into a multivariable functional form. In general NN based methods are highly accurate in the high input density region and very weak in extrapolation; beyond the boundary of the data incorporated into the fit, it could give less accurate, or even entirely erroneous, results. NN based PES fitting methods[2,77–84] are equally accurate for small as well as moderate sized molecules. If the exponential transfer function is used in the NN method, the PES would be a sum-of-products form (SOP). The SOP is one of the special focus in this thesis, as SOP accelerates quantum dynamics simulation[4,85,86] in MCTDH. This thesis will demonstrate how selective numbers of points could give a highly accurate PES using the NN-expnn method. As the thesis is aimed primarily at constructing efficient PESs for quantum dynamics simulations, it is very important to describe what an effective PES should be.

The ideal PES has several important characteristics:

(1)*Accuracy.* The PES must be sufficiently accurate to determine the desired properties, i.e., of sufficient accuracy to compare with or interpret, experimental measurements, or to make predictions for new experiments that can be subsequently validated. The accuracy of the PES is impacted by the choice of method utilized to obtain the energies for fitting. The accuracy is also reflected in the fitting error, which is usually measured by the root mean square error (RMSE); the larger the RMSE, the less accurate the PES.

(2) *Scope of systematic improvement.* It should be possible to improve the accuracy of the PES, or make it more general, systematically when required. This improvement could be obtained by adding additional ab initio data or by incorporating additional functional parameters.

(3) *General applicability.* A PES should be very general and applicable equally to all different types of interaction present in a system.

(5) *Sufficiently High Dimensionality.* The PES must describe all the degrees of freedom in a system.

(6) *Self sustainability.* In this context, self sustainability refers to the lack of a need for manual control when performing the fitting, e.g., NN-based PES fitting is an automatic "black box" method requiring little (to no) human choice in the fitting process.

(7) *Easily transferable.* The potential should be general and easily transferable to other similar systems.

(8) *Easy and quick evaluation.* One should be able to compute the potential energy easily and quickly. A simple functional form and a small number of fitting parameters make this possible.

(9) *Easy and quick construction.* Constructing the PES should be easy and fast. Some high dimensional PES are impossible to construct because they need grid like data, e.g., one cannot go beyond 6D fitting with *potfit.*[87,88]

(10) *Ready computation of gradients and Hessians.* The gradient and the Hessian should be easily accessed. These are required, for example, in many classical dynamics

integration schemes.

(11) *Experimental data refinable.* It is nice to have a PES that one can refine to experimental data, e.g. to provide accurate comparison to experimentally measured vibrational frequencies.

Now, in the following sections, the general features of NN, feed forward NN, fitting functions, training algorithm (mainly Levenberg Marquardt algorithm, LM), and post processing will be discussed.

1.3.1 Artificial Neural Network

An artificial neural network (ANN) is an information processing prototype which is inspired by the function of neurons in biological nervous systems. Its most close relevance will be with the way brain processes information. Like a nervous system, the ANN is constructed by a significant number of interconnected fitting functions (neurons) with the goal of solving targeted problems. The ANN learns something like people learn, i.e., by encountering real world (training data) and storing information. An ANN could be designed for specific problem solving, like pattern recognition (in our case, finding the shape of the PES), through a learning process. While the biological NN learns the environment through adjustment in the synaptic connections between two neurons, the ANN does so by connecting one layer after another by weight and bias parameters. Kohonen[89] stated "Artificial neural networks are massively parallel interconnected networks of simple (usually adaptive) elements and their hierarchical organizations, which are intended to interact with the objects of the real world in the same way as biological nervous systems do." A NN is highly capable of deriving meaning (recognize) from complicated (very complex) data. A NN can extract patterns (detect trends) that are too complex to be noticed by humans or by other computer techniques. Once trained properly with a given set of input data, a NN becomes an information expert within the data set boundary and sometimes extended outside the boundary (extrapolation sometime becomes accurate with the selection of transfer functions). Adaptive learning, self-organization, real-time operation, etc., are other advantages one can get using Neural Networks. Presently, NNs are widely used in chemistry and physics in forms such as data analysis tools.[90–92] NN techniques are used in NMR and mass spectrometry,[93,94] kinetics studies, protein structure predictions,[95,96] quantitative structure and reactivity (QSAR) models,[97–99] clinical chemistry,[100] polymer science,[101] nuclear spin prediction,[102] atomic energy levels detection,[103,104] nucleic acid sequence analysis,[105] Schrödinger equation solving,[54,106–109] enzyme kinetics, and constructing potential energy surfaces[110] and many more. Specific examples of NNs application in fitting PESs include, correlated energy of diatomic molecules and heavy atoms,[111] CBS converged energies, bond energy, enthalpy and heat of formation estimation.[112] These again demonstrate the ability of NNs to tackle complex data analysis.

1.3.1.1 Feed-forward neural network

A feed forward neural network is named after the fact that it only allows information to flow in one direction; the forward direction, from the input to the output. Only feed-forward NNs have been successfully applied to construct PESs so far. In this thesis, I used feed-forward NNs. In a feed forward neural network, a number of nodes (or neurons) are organized in a desired number of layers. Three main layers in a NN include: the input layer which consists of the input matrix elements or the coordinates; the hidden layers where input signals are transformed into functional forms using transfer functions; and the output layer where the output is processed. Overall, the NN results in an analytical functional form of the input coordinates $G = \{G_i\}$. The hidden layers serve the key purpose of fitting, i.e., provide the functional form of the input coordinates using transfer functions. There may be one or more hidden layers depending on the type of NN. Nodes or the neurons are connected to the adjacent layers (either to the input coordinates or to the next layer's neurons) by "weight" parameters. These weight parameters are the fitting parameters when training is performed. Each neuron is also provided with a "bias" parameter to give more flexibility to the fitted surface. A typical single layer feed forward neural network is presented in Figure 1.1. The input layer is connected to the first hidden layer's neurons by weights. It can be seen that throughout the network, weights and biases are connected in the forward direction; from input to the hidden layer to the output layer. The weight parameters are presented by the symbol a_{ij}^{kl} which connects the i^{th} node in the k^{th} layer to the j^{th} node of the l^{th} layer. In the feed forward neural network, only connections between two adjacent layers are possible, so, $l = k + 1$. Usually the input layer is designated as the 0^{th} layer. A bias parameter b_i^k is added to each node. Weights and biases are real valued parameters.

The scheme of computation is as follows: First, the input coordinates are supplied in the first layer. Nodes in the input layer represent each degree of freedom. Next, the hidden layers sum up all the weighted value (x_m^l) of the input nodes ($\{G_i\}$) along with the bias (b_m^l),

$$x_m^l = b_m^l + \sum_{i=1}^{N_i} G_i a_{im}^{l-1,l} \tag{1.20}$$

This is nothing but the linear combination of degrees of freedom considering weights as coefficients. Here m is the number of nodes in l^{th} hidden layer and N_i is the number of nodes in $(l-1)^{th}$ node. In the following step, a non-linear transformation of the output x_m^l is performed in the first hidden layer. This procedure is how the functional form of the analytical PES arises which provides the numerical output value of the node. The transfer function is called an activation function or neuron.

$$y_m^l = f_m^l(x_m^l) \tag{1.21}$$

A general expression of any specific node in the l^{th} hidden layer is given as,

$$y_m^l = f_m^l(x_m^l) = f_m^l(b_m^l + \sum_{i=1}^{N_{l-1}} y_i^{l-1} a_{im}^{l-1,l}). \tag{1.22}$$

Here, N_l is the number of nodes in the l^{th} layer. In this way, all the nodal outputs are collected and passed out to the next layer until the final output is reached. The final output has the functional form,

$$\begin{aligned} E &= f_1^l(x_1^l) \\ &= f_1^l\{b_1^l + \sum_{k=1}^{N_k} a_{k1}^{(l-1),l}.f_k^{(l-1)}(...f_k^2[b_k^2 + \sum_{j=1}^{N_2} a_{jk}^{12}.f_j^1(b_j^1 + \sum_{i=1}^{N_1} a_{ij}^{01}.G_i)])\}. \end{aligned} \tag{1.23}$$

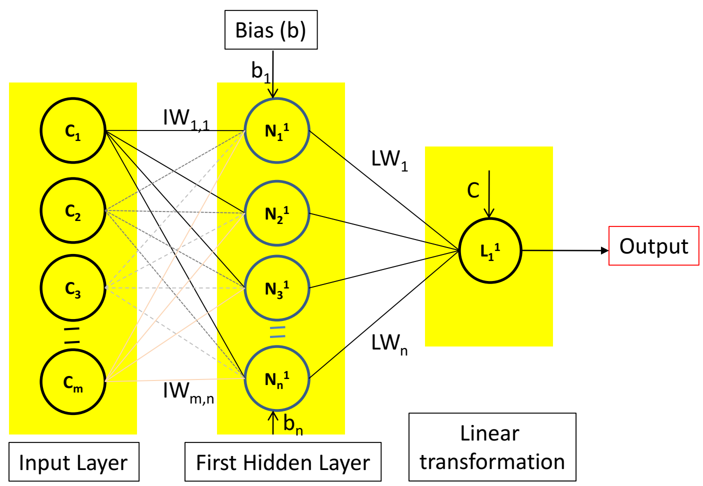

Figure 1.1: *Neural Network Architecture: A 'm' dimensional single layer feed-forward neural network connecting the energy and 'n' coordinates C_1 to C_m by transfer functions through their weights and biases*

So, the final PES is the sum of the activation functions or neurons. The feed forward NN used in this thesis work (see Figure 1.1) is a single hidden layer consisting of exponential transfer functions. The output layer is a single node with a purelinear transfer function. Here the input weights are termed as "IW". The weights of the hidden layer nodes towards the linear transformation are termed as "LW".

1.3.2 Transfer Functions and Exponential Neurons

Nodes are the basic building blocks of a NN. Inside each node exists the fitting functions called neurons, as they build the connection between coordinates and the functional value. The default activation function in a MATLAB Neural network is the sigmoidal function which has the form,

$$\sigma(x) = \frac{1}{1+e^{-x}} \tag{1.24}$$

The sigmoidal neuron is often used and it has very general scientific application. The sigmoidal neuron output ranges between 0 to 1 and exhibits asymptotic behaviour beyond -4 to +4 of the input range. So, sigmoidal functions are localized functions which is good for parameterizing the initial weight matrix. Hyperbolic tangent and error functions are also used as transfer function in PES fitting. The latter two functions have very similar shape like sigmoidal function (see Figure 1.2).

$$\sigma(x) = \tanh(x) = \frac{\sinh(x)}{\cosh(x)} = \frac{(e^{2x}-1)}{(e^{2x}+1)} \tag{1.25}$$

$$\sigma(x) = erf(x) = \frac{2}{\sqrt{\pi}} \int_0^x e^{-t^2} dt \tag{1.26}$$

The activation function could be in many different forms, such as linear,

$$\sigma(x) = x \tag{1.27}$$

or as a Gaussian activation function,

$$\sigma(x) = e^{-\alpha x^2}. \tag{1.28}$$

The linear transfer function is used in almost every network, during transferring output data from the last hidden layer. The pure linear neuron uplifts (or downgrades)

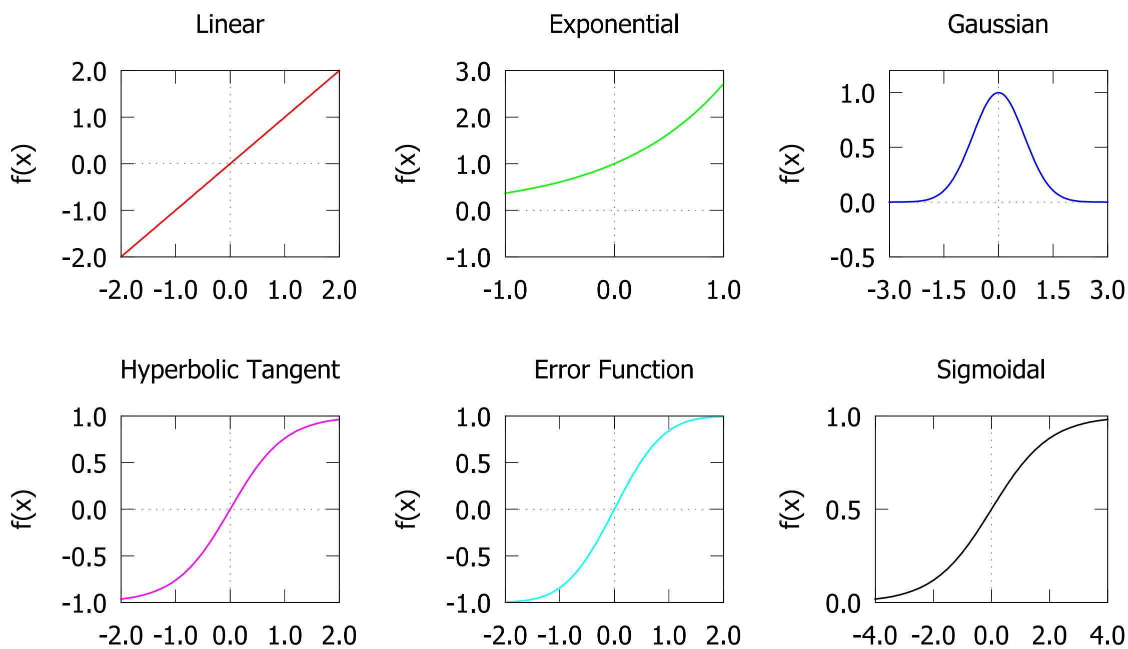

Figure 1.2: *Different types of transfer functions (neurons); linear (red), exponential (green), gaussian (blue), hyperbolic tangent (purple), error function (cyan) and sigmoidal (black); range and functional values.*

the entire data set to the real target by adjusting any constant bias. There are other activation functions, like cosine function,[113] etc., but none of these neurons give the final form as sum-of-products function. The sum-of-products form is my goal in this project because the analytical PES will be used in MCTDH which needs SOP form of the PES for faster computation of nuclear dynamics. Carrington and Manzhos found that an exponential neuron[1] can generate sum-of-products form of the final PES. They build the exponential fitting function,

$$\sigma(x) = e^x. \tag{1.29}$$

This exponential function is nonlinear, monotonic, smooth and most importantly, the PES is a sum-of-products form of coordinates x_i. Flexibility in the exponential neuron is shown in Figure 1.3. The final PES is a large number of terms summed over the total number of neurons in the form,

$$h(x) = c_1 f(c_2 x + c_3) + c_4 \tag{1.30}$$

where c_1 and c_2 are the weights and c_3 and c_4 are the bias parameter. By adjusting these parameters, the transfer function can be shifted up and down or left and right, slopes are changed and they are rescaled. All these are shown in Figure 1.3 with the exponential transfer function. Very recently, Zhang and co-workers[114] generated sum-of-products form using an error function as the activation function. This form was based on a different types of NN fitting, where a product neuron is used instead of the traditional sum; the product approach is less efficient and more restrictive.

1.3.2.1 Sum-of-products form using Neural Network

The sum-of-products form is the main focus of my research. Thus here I discus how SOP is obtained using exponential neurons. The functional form of a typical single layer Neural Network is,

$$\begin{aligned} V(x) &= c + \sum_{i=1}^{N} LW_i \ F(\sigma) \\ &= c + \sum_{i=1}^{N} LW_i \ F\Big(\sum_{j=1}^{D} (IW_{ij} x_j + b_i)\Big) \end{aligned} \tag{1.31}$$

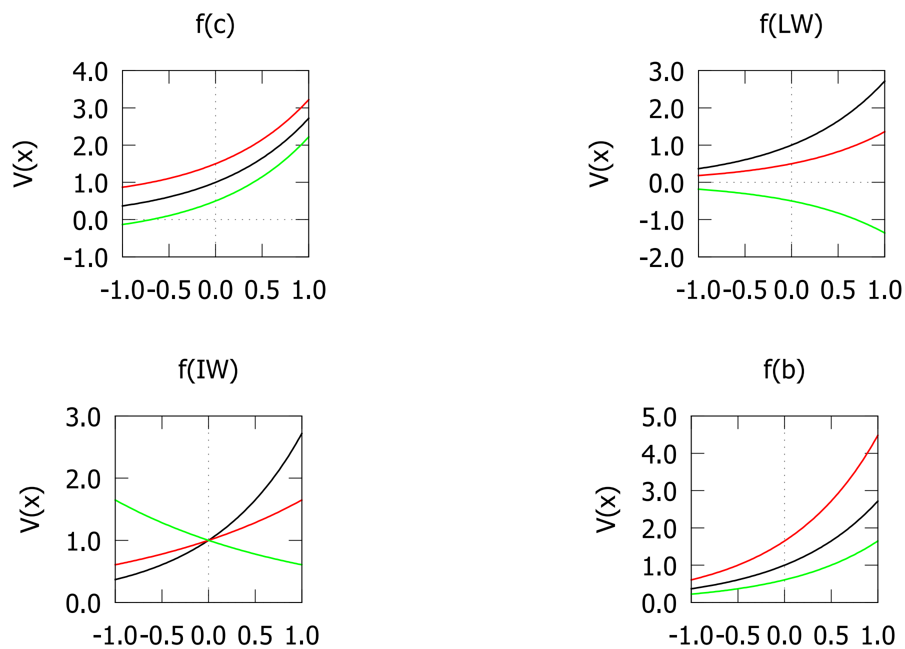

Figure 1.3: *Role of different parameters in a single exponential neuron;* $V(x) = c + LW.f(IW.x + b)$, $f(IW.x + b) = e^b.e^{IW.x}$. *Each plot contains exp(x) (black), +0.5 (red) and -0.5 (green) of the parameter (c, LW, IW and b).*

where IW_{ij} is the weight of input coordinate x_j to the i^{th} node of the hidden layer. b_i is the bias of the node. LW_i is the weight of i^{th} neuron to the linear transformation node or the output layer with the final bias of c. Now, replacing $F(\sigma)$ with exp(x), we obtain

$$
\begin{aligned}
V(x) &= c + \sum_{i=1}^{N} LW_i e^{(\sum_{j=1}^{D}(IW_{ij}x_j + b_i))} \\
&= c + \sum_{i=1}^{N} LW_i \ e^{b_i} \prod_{j=1}^{D} e^{IW_{ij} \ x_j} \\
&= \sum_{i=1}^{N} \tilde{c}_i \prod_{j=1}^{D} e^{IW_{ij} \ x_j}
\end{aligned}
\tag{1.32}
$$

Equation (1.32) is a sum over all the neurons and product over all the coordinates.

1.3.2.2 Training Neural Network

Once the neural network architecture is established with suitable transfer functions, the optimization of parameters is done to get the best fitted PES. The fitting is named as training in NN. Depending on the size of the NN, the fitting parameters vary and so does the training effort. A typical feed forward NN used in this thesis has a total number of parameters,

$$
N_p = \sum_{k=1}^{M_h+1} (N_{k-1}N_k + N_k) \tag{1.33}
$$

where N_p is the total number parameters (weights and biases) in a M_h hidden layer neural network. N_k is the number of nodes in k^{th} layer. For the input layer, the number of nodes (N_0) is same as the number of input coordinates. The output layer ($M_h + 1$) is just a single node. As an example, a single layered 30 neurons fit PES of the CS_2 molecules has 151 fitting parameters. In constructing the input for MCTDH, it further reduced to 121 for the fact that LW and b are collapsed to a single parameter ($LW.e^b$). In the training process, the weight and bias parameters are first randomly (some other initialization methods are also used) initialized. An efficient optimization algorithm is then used to minimize the error between the fitted output to the target. Among many available optimization methods, the back propagation algorithm, the Kalman filter[115] and the Levenberg Marquardt (LM)[116,117] algorithm are mostly used. It has been reported[77] that LM is the most efficient algorithm to minimize large number of weight parameters. Throughout this thesis, the LM algorithm is used.

1.3.2.3 Scaling of Data Sets

The scaling of data is done before the fitting is initiated. All the data sets, i.e., coordinates and energies, are scaled between -1 to 1 such that the lowest value is set to -1 and highest possible value to +1. All the remaining data are arranged accordingly in the space. Before fitting, all data (coordinates and energies) were scaled to lie between [-1, 1] by

$$X_{scaled} = \frac{X - x_{min}}{x_{max} - x_{min}} \tag{1.34}$$

where the maximum and minimum of a particular coordinate are x_{max} and x_{min}. X is the data before scaling which after scaling appears as X_{scaled}. The scaled data gives smooth convergence and a gradually decreasing RMSE for the fit. After the fitting is done, rescaling back to the original scale is particularly important. The rescaling procedure is as following,

$$X_{rescale} = \frac{X + 1}{2} \tag{1.35}$$

here, x_{min} is -1 and x_{max} is +1.

1.3.2.4 Input Coordinates and Symmetry Functions

The symmetry is important for those systems with permutational invariant symmetry (one that gives the energy same with the exchange of two identical atoms). In constructing PESs, one could tackle the symmetry by two different ways: (i) by including in the training set symmetric coordinates and the corresponding equal energies (symmetric copies of points) and (ii) by using some PIP symmetry operation to the input layer. Even though we used the first method for the CS_2 molecule, the final PES is not entirely symmetric as during the training, two symmetric coordinates were connected to the hidden layer by two different random weights, and those weights were optimized using random steps in the LM algorithm. Although the PIP-NN method by Guo and co-workers gives a symmetric potential, the final PES is not in the particular SOP required for MCTDH. The symmetry might not be an issue for the vibrational states and nuclear dynamics study but in some other areas, it may be an issue if the exact symmetry plays key role.

1.3.2.5 Quality Control of a Fit: RMSE and MSD

Direction of the fitting process is monitored by calculating several quantities. The root mean squared error (RMSE) is the most important quantity to monitor, where

$$RMSE = \sqrt{\frac{1}{N}\sum_{i=1}^{N}(E_{i,ref} - E_{i,NN})^2}. \tag{1.36}$$

Sometimes, the mean absolute error (MAE) or mean absolute deviation (MAD) is used to analyse error,

$$MAE = \frac{1}{N}\sum_{i=1}^{N}\left|E_{i,ref} - E_{i,NN}\right|. \tag{1.37}$$

Numerically, the RMSE is larger than the MAE because of the squared term present in the equation. During the fitting process, the RMSEs of the training and the validation sets are calculated. The training set is the data used to determine the parameters of the fit (train the network). The validation set consists of independent data against which the network is tested during the course of the training. If the RMSE increases beyond a specific threshold, the fitting is terminated and restarted. Hence the validation set ensures there is not overfitting of the data. If the error for the training set is lower than a desired value, the fitting process completes and stop. The fit is then checked by determining the RMSE for a test set of data. For further analysis, we post process the data set by computing the RMSEs in different energy ranges. As expected, the RMSE in the lower energy region would be lower than in the higher energy region.

1.4 Vibrational State Computations

1.4.1 VPT2

The vibrational second-order perturbation theory (VPT2) approach[118–120] is useful for computing anharmonic vibrational frequencies of fundamental modes along with overtones and combination bands. VPT2 has been implemented in several ab initio software packages (e.g. Gaussian09,[121] GAMESS-US,[122,123] Molpro[18,19] and CFOUR;[124] the implementation in CFOUR is used throughout this thesis). In a VPT2 computation, the zeroth order vibrational wave functions are obtained via the harmonic approximation, i.e., the zeroth order Hamiltonian is that for the harmonic oscillator (normal mode), $\hat{H}_{HO}$. The anharmonicity is included as a perturbation, i.e., the total Hamiltonian is

$$\hat{H}_{VPT2} = \hat{H}_{HO} + \hat{H}_{anharm}. \tag{1.38}$$

The anharmonic perturbation includes both cubic and quartic force constants and corresponding normal mode displacements (q_i). The anharmonic vibrational wavefunctions and energies are obtained by second order perturbation theory using all non-resonant harmonic energy terms followed by a variational treatment of the relevant resonant interactions. The second order perturbation theory is applied to the PES approximated by a Taylor expansion in the normal coordinates, q_i, that includes the quartic, and all cubic, and semidiagonal quartic force constants.

$$V(q_1, q_2, ..., q_N) \cong \frac{1}{2}\sum_{i} w_i q_i^2 + \frac{1}{6}\sum_{ijk} f_{ijk} q_i q_j q_k + \frac{1}{24}\sum_{ijk} f_{ijkk} q_i q_j q_k q_k \tag{1.39}$$

In Eq. (1.39), f_{ijk} and f_{lmno} are obtained by numerical differentiation of the (usually) analytic Hessian at geometries slightly displaced from the equilibrium.

In addition to providing data for overtones and combination bands, VPT2 provides improved vibrational energies relative to the experimental measurements compare to the harmonic results. As it is a perturbative approach, it can not (in general) compute vibrational frequencies for highly excited states.

1.4.2 MCTDH Theory

The Multiconfiguration Time-Dependent Hartree method (MCTDH)[3–7] is a very efficient algorithm to solve the time-dependent Schrödinger equation for distinguishable particles. The efficiency of the MCTDH method arises from writing functions of large numbers of degrees of freedom as the sum-of-products of low degrees of freedom. The multidimensional wavefunction is written as sum-of-products form of low dimensional functions, often called single particle functions (SPFs):

$$\begin{aligned}\Psi(q_1,...,q_f,t) &= \Psi(\{q\}_1,...,\{q\}_p,t) \\ &= \sum_{j_1}^{n_1}...\sum_{j_p}^{n_p} A_{j_1,...,j_p}(t)\prod_{k=1}^{p}\Phi_{j_k}^{(k)}(\{q\}_k,t) \\ &= \sum_J A_J\Phi_J,.\end{aligned} \tag{1.40}$$

The number of degrees of freedom is denoted by *f*. The p denotes the number of MCTDH particles, sometimes called a combined mode. As an example, there will be n$_k$ combined modes for the k^{th} particles. In this equation, the SPFs, $\phi(\{q\},t)$, could be one or multiple dimensional functions. The coordinate {q} is collective one,$\{q\} = \{q_k,...,q_l\}$. The expansion coefficients are designated as $A_J = A_{j_1,...,j_f}$. Φ_J are Hartree products of SPFs. These SPFs are represented as a linear combination of time-dependent primitive basis functions χ:

$$\Phi_{j_k}^{(k)}(\{q\}_k,t) = \sum_{i_k=1}^{N_k} c_{i_kj_k}^{(k)}(t)\chi_{i_k}^{(k)}(\{q\}_k). \tag{1.41}$$

For the SPFs, the discrete variable representation (DVR) is commonly used. The MCTDH equations of motion are derived by applying the Dirac-Frenkel variation principle to the wavefunction *ansatz*:

$$i\dot{A} = \sum_L \langle\Phi_J\,|H|\,\Phi_L\rangle \tag{1.42}$$

$$i\Phi^{(k)} = (1-P^{(k)})(\rho^{(k)})^{-1}\,\langle\mathbf{H}\rangle^{(k)}\,\Phi^{(k)} \tag{1.43}$$

where a vector notation, $\Phi^{(k)} = (\Phi_1^{(k)}, ..., \Phi_{n_k}^{(k)})^T$, is used. The MCTDH equations conserve the norm and, for time independent Hamiltonians, the total energy. MCTDH contains time dependent Hartree (TDH) and the standard method (i.e., propagating the wave packet on the primitive basis) as limiting cases. One can simplify MCTDH to TDH when all $n_k = 1$. Increasing the n_k recovers the number of primitive basis functions until the standard method is used. For fast convergence, MCTDH uses variationally optimized SPFs. As the mean field calculation at every time step is required to solve the MCTDH equations of motion, a fast algorithm must be used. A quick solution to this is to build high dimensional objects as sum-of-products of low dimensional objects. Thus the Hamiltonian is built in product form as

$$\hat{H} = \sum_{r=1}^{s} C_r \sum_{k=1}^{p} \hat{h}_r^{(k)}, \tag{1.44}$$

where the operator $\hat{h}_r^{(k)}$ operates on the kth particle only and where the C_r are numbers. Within this approach, the matrix elements of the Hamiltonian can be expressed by a sum-of-products of monomode integrals,

$$\left\langle \Phi_J \left| \hat{H} \right| \Phi_L \right\rangle = \sum_{r=1}^{s} c_r \prod_{k=1}^{p} \left\langle \phi_{j_k} \left| \hat{h}_r^{(k)} \right| \phi_{l_k} \right\rangle \tag{1.45}$$

The mean fields, $\langle \mathbf{H} \rangle^{(k)}$, are evaluated in the similar way.

1.4.3 Eigenstates by Relaxation and Improved Relaxation

The ground and all other vibrational states are obtained by improved relaxation[7,125] as well as block improved relaxation. In MCTDH, the ground state wavefunction is obtained by propagating an initial wavefunction in negative imaginary time followed by normalization.

$$\Psi(t) = e^{-Ht}\Psi(0) \left\| e^{-Ht}\Psi(0) \right\|^{-1} \tag{1.46}$$

The initial wavefunction is expanded with the eigenfunctions of the Hamiltonian $\hat{H}$. As time approaches infinity, the $\Psi(t)$ converges to the ground state, $\Psi(0)$. This ground state can serve later as an initial state for subsequent propagation with a different Hamiltonian.

While relaxation is a useful approach for obtaining a few eigenstates (one state at a time), it fails when the density of states is high. A better method for computing an eigenstate uses improved relaxation.[7,125] Improved relaxation is a combination of diagonalization of the Hamiltonian and the principle of relaxation. Improved relaxation is carried out through the following steps: (i) Define the initial state which should have reasonable overlap with the desired eigenstate. (ii) Diagonalization of the Hamiltonian in the initial basis is performed next. (iii) The mean fields $\mathcal{H}^{(\kappa)}$ are built and the SPFs are relaxed over a suitable time interval. (iv) The Hamiltonian matrix κ is then rebuilt in the new configurations (Hartree products) and diagonalized. (v) The entire process is repeated iteratively until the convergence is reached. For computing the ground state, the lowest energy is taken where as for any excited state, the eigenvector of the Hamiltonian is taken which has greatest overlap with the initial state. Block improved relaxation is very efficient for computing eigenstates in a small energy window.[9] Energy energy states in the high energy region of the PES are often computed using the block improved relaxation method.

1.4.4 Potential Representation (*potfit*)

1.4.4.1 The *potfit* algorithm

The *potfit* algorithm[87,88] is a default procedure in MCTDH to build a multidimensional potential energy surface into a sum-of-products form. The *potfit* algorithm only operates on a product grid. In the fitting procedure, no polynomial or spline functions are used. The *potfit* algorithm assumes that the values of a PES are given in product grid, i.e.,

$$V[q_{i_1}^{(1)}, ..., q_{i_p}^{(p)}] \equiv V_{i_1 \ldots i_p}, \tag{1.47}$$

where $q_{i_k}^{(\kappa)}$ denotes grid points of the κth 1D grid with $1 \leqslant i_\kappa \leqslant N_\kappa$. The N_κ is the number of grid points for the κth particle and p denotes the number of particles or the number of degrees of freedom. The variable {q} may be one or a multidimensional coordinate. Now, the potential density matrix $\rho^{(\kappa)}$ is defined as,

$$\rho^{(\kappa)}_{nm} \equiv \sum_{i_1=1}^{N_1} \cdots \sum_{i_{\kappa-1}=1}^{N_{\kappa-1}} \sum_{i_{\kappa+1}=1}^{N_{\kappa+1}} \cdots \sum_{i_p=1}^{N_p} V_{i_1 \ldots t_{\kappa-1} n i_{\kappa+1} \ldots i_p} V_{i_1 \ldots t_{\kappa-1} m i_{\kappa+1} \ldots i_p}. \tag{1.48}$$

The orthonormal eigenvectors of $\rho^{(\kappa)}_{nm}$ are called natural potentials $(\nu^{(\kappa)}_{ij})$. The natural potentials are 1D functions defined on the set of grid points $\{q^{(\kappa)}_i\}$ such that $\nu^{(\kappa)}_j(\{q\}^{(\kappa)}_i)=\nu^{(\kappa)}_{ij}$. Corresponding eigenvalues of these natural potentials are termed as natural weights $(\lambda^{(\kappa)}_j)$. Natural weights are considered to be in decreasing order, $\lambda^{(\kappa)}_j > \Lambda^{(\kappa)}_{j+1}$. With selected set of expansion orders $\{m_k\}$, the *potfit* potential is approximated as,

$$\begin{aligned} V(\{q\}^{(l)}_{i_1}, ..., \{q\}^{(p)}_{i_p}) & \\ &\approx V^{app}(\{q\}^{(1)}_{i_1}, ..., \{q\}^{(p)}_{i_p}) \\ &= \sum_{j_1=1}^{m_1} \cdots \sum_{j_p=1}^{m_p} C_{j_1 \ldots j_p} \nu^{(1)}_{j_1}(\{q\}^{(1)}_{i_1}) \ldots \nu^{(p)}_{j_p}(\{q\}^{(p)}_{i_p}), \end{aligned} \tag{1.49}$$

where the expansion coefficients $C_{j_1, \ldots j_p}$ are the overlap between the potential and the natural potentials.

1.4.5 The Kinetic Energy Operator

The kinetic energy operator (KEO) plays an important role in MCTDH efficiency. In general (i) a sum-of-products form and (ii) a compact KEO leads to faster convergence in MCTDH.

1.4.5.1 Coordinate Systems

A suitable coordinate system for the molecule of interest is crucial as the choice must minimize the correlation between degrees of freedom. Inappropriate coordinate system selection leads to complex and artificial correlation which slows down convergence. The polyspherical coordinate system has been used successfully in

MCTDH computations for many small molecular systems including HFCO[126–128] and HONO[129–131] considered in this thesis. In the polyspherical coordinate system, the KEO is represented in terms of spherical coordinates (r, θ and ϕ). It is an exact representation of the KEO of an N-atom system. It has the following characteristic: (i) Gives compact and exact expression of the KEO. (ii) If desired, includes rotational and Coriolis coupling. (iii) Spectral basis sets are easily achieved. (iv) General expression of the KEO is available in two different forms. (v) Flexible to use different underlying vectors such as, Jacobi, Radau, valence, satellite or combinations of these. (vi) It is always separable, i.e., it can be written as a sum-of-products form of monomodal operators. In this thesis, for the HFCO and the HONO molecule, the polyspherical coordinate system was used.

1.5 Thesis Overview

The thesis presents critical tests of the neural network with exponential neurons approach to fitting PESs to the sum-of-products form. Importantly, the research develops and utilizes an interface to generate the prerequisite[8] MCTDH operator files needed for further quantum dynamics studies. The PESs developed are based on high-level ab initio data; hence, prior to developing the full dimentional PESs, the important stationary points (minima and TSs) are located and characterized. The thesis demonstrates the versatility of the NN-expnn approach and applies it to a number of molecules.

In Chapter 2, the 3D potential energy and dipole moment surfaces of the CS_2 molecule have been fit to sum-of-products form using the NN-expnn approach; to test the accuracy of the fit, vibrational energies for various isotopomers have been computed using the Lanczos algorithm as implemented in MCTDH and compared to experiment. The CS_2 PES represent the first direct fit of ab initio data using the NN-expnn approach. Importantly the study utilized a newly developed interface to generate requisite MCTDH operator files. In future, the PES can be used to study coherent anti-stokes Raman scattering (CARS) using OCT-MCTDH, and, hence develop understanding of the corresponding experiments. While a variety of fitting algorithms can be applied for 3D PESs, the initial study reported in Chapter 2 set the stage for studying larger systems with more complicated PESs.

In Chapter 3, a 6D PES for HFCO encompassing the equilibrium and transition state (to HF + CO) geometries is fit to CCSD(T)-F12/cc-pVTZ-F12 ab initio data using the NN-expnn approach and interfaced to MCTDH. The high quality (near spectroscopic accuracy) of the PES is determined through computation of vibrational energy levels and their comparisons to experimental data. The development of a new HFCO PES was motivated by recent computational work by Gatti and co-workers investigating IVR in HFCO (DFCO) both with and without driving by an external field.[126–128] Optimal control of these processes was not pursued as the underlying PES was not sufficiently accurate. The new accurate PES of HFCO can be used as a basis for examining the optimal control of dynamics.

In Chapter 4, the NN-expnn method for PES fitting is applied to HONO, a molecule of great experimental and theoretical interest due to the low energy cis-trans isomerization barrier (4000 cm^{-1}) and the asymmetric double well PES (for trans and cis isomers). The PES fitting, and subsequent quantum dynamics, are challenging. Previous work on the cis-trans isomerization by the Gatti group[129–131] was based on a PES fit to CCSD(T)/cc-pVQZ(-g functions) ab initio data. In Chapter 4, new PESs for HONO are developed using the NN-expnn approach based on two different sets of ab initio data: (i) CCSD(T)-F12/cc-pVTZ-F12 and (ii) CCSD(T) with complete basis set (CBS) extrapolation. The PESs are tested by determining vibrational state energies and comparing with experimental measurements and previous computational results.

A global S_0 PES of HFCO (encompassing the equilibrium, cis-HOCF, trans-HOCF, and transition states between them) had yet to be developed. The previous PES[132] was restricted to the equilibrium and unimolecular dissociation regions by a cut-off energy of 24000 cm^{-1}. Due to lack of a global HFCO surface, the intriguing competition between unimolecular dissociation and conversion to trans-HOCF could not be explored.[126] In Chapter 5, the local HFCO PES developed and tested in Chapter 3 is extended to a global PES.

In their work examining control of IVR in HFCO,[128] Gatti and co-workers suggested using excitation/de-excitation via the electronic excited S_1 PES. The excited state has been explored experimentally using Stimulated Emission pumping (SEP).[133] In Chapter 6, vertical excitation energies to the low-lying S_1 and T_1 states are determined using a variety of electronic structure theory methods, i.e., EOM-CCSD, CASSCF, CASPT2 and MRCI. The stationary points, and corresponding harmonic frequencies, are computed using the same methods. By comparing with available experimental data, a cost effective and sufficiently accurate method (EOM-CCSD) is identified and then used to generate ab initio data for fitting an S_1 PES. The excited state PES is fit using the NN-expnn method and vibrational frequencies are computed using block improved relaxation in MCTDH.

The final chapter (Chapter 7) summarizes the most important conclusions that can be drawn from the research presented in the Thesis. In addition, the more general conclusions that can be made from the specific research projects are discussed. Potential future directions are provided.

Chapter 2

Ab Initio Potential Energy and Dipole Moment Surfaces for CS_2: Determination of Molecular Vibrational Energies

*

2.1 Introduction

The use of femtosecond pulse shaping in a non-resonant coherent anti-Stokes Raman scattering (CARS) process to selectively excite or suppress molecular vibrational modes of CS_2 in the gas and liquid phases was recently reported by Scaria and coworkers.[134] The Stokes pulse was optimized using phase-only shaping and a learning algorithm in a feedback controlled closed loop approach. As they point out, this approach has several open questions: the mechanism for the mode control, the effects of the changes in the phase and amplitude of the spectral components of the excitation pulses, and the role of the intermolecular processes in the control of the molecular modes. In order to understand these experiments, one requires (i) accurate potential energy and dipole moment surfaces and (ii) a method for simulating the CARS process and its control. Here the ab initio determination of the ground state potential energy surface (PES) and the corresponding dipole moment surface for CS_2 are reported.

*A version of this chapter was published in the *J. Phys. Chem. A*, **2013**, *117*, 6925.

Importantly, how these surfaces can be fit to a sum-of-products form to facilitate their future use in optimal control theory multiconfiguration time-dependent Hartree (OCT-MCTDH) simulations[6,135,136] of the control of CARS processes, are discussed.

The ground state structure and corresponding vibrational spectrum of CS_2 has been the subject of much experimental[137–145] and theoretical[138,146–154] scrutiny. Empirical PESs have been determined by fitting to accurately reproduce the measured vibrational spectra.[138,146–149] The most recent of these fitted PESs[146,147] has been used to determine highly excited vibrational states up to 20000 cm^{-1}. A global PES has also been determined using the many-body single value surfaces of Murrell and Guo[149] refined by non-linear least squares fitting to the observed vibrational frequencies up to 10000 cm^{-1}.[148] A PES valid for vibrational energies up to 5000 cm^{-1} has also been derived by fitting to experimental rotation-vibration data.[138] The molecular constants of CS_2 have been determined by a general rovibrational analysis including all data known up to 1985.[141] Our main future goal is the study of coherent control processes and to do so, a global dipole moment surface is also required in addition to the global PES. Therefore, new ab initio electronic structure calculations at the complete active space with second order perturbation theory (CASPT2) level have been carried out to determine the global potential energy and dipole moment surfaces. Once the ab initio data has been determined, the surfaces must be fit to an analytical form to ease their use in dynamics calculations. Since the PES will eventually be used for the study of the control of quantum dynamics with the optimal control theory multi- configuration time-dependent Hartree (OCT-MCTDH) approach,[6,135,136] the PES will be fit to a sum-of-products form as required for the efficient use of the MCTDH ansatz.[3–5] In the present work, the fitting will be accomplished using artificial neural networks (NNs) with exponential neurons[1,2] and these results will be compared to those from *pot-fit*,[87,88] as implemented in the MCTDH software package.[3] Further details regarding the use of NNs for fitting PESs are provided in recent reviews.[83,84,155]

The chapter is organized in the following manner. First, the computational methods used for determining the ab initio potential energy and dipole moment surfaces for CS_2, the fitting of the surfaces, and the calculation of the vibrational eigenenergies

Table 2.1: *Comparison of Equilibrium Bond Lengths (Å) for CS_2*

Method	Reference	r_{CS}
CASPT2/C:cc-pVTZ, S:aug-cc-pV(T+d)Z	This work	1.563
Full CCSD/6-311++G(d,p)	Ref.[152]	1.557
Full CCSD(T)/aug-cc-pv(T+d)Z	Ref.[156]	1.5557
Full CCSD(T)/cc-pCVQZ	Ref.[150]	1.5533
Full MP2/6-31+G(d)	Ref.[151]	1.561
Full MP2/aug-cc-pVTZ	Ref.[151]	1.557
B3LYP/6-31+G(d)	Ref.[151]	1.563
B3LYP/aug-cc-pVTZ	Ref.[151]	1.557
BLYP/aug-cc-pVTZ	Ref.[151]	1.571
Experiment	Ref.[138]	1.5549 ± 0.004
Experiment[a]	Ref.[137]	1.55448 ± 0.00020

[a]Value represents the best combined experiment/theory estimate.

are discussed. In the Results and Discussion section, the fits to the PES and dipole moment surfaces are analyzed. The vibrational energies obtained for four isotopomers of CS_2 are presented and compared to previous theoretical and experimental results. I then present final remarks on the NN fitting of PESs to sum-of-products forms for use in MCTDH and discuss briefly the future application of the CS_2 surfaces in the optimal control of CARS processes.

2.2 Computational Methods

2.2.1 Ab Initio Methods

To determine the potential energy and dipole moment surfaces, complete-active-space self-consistent-field (CASSCF)[23,24] computations were first performed. For the CASSCF calculations, a (12,10) active space, i.e., twelve electrons in ten orbitals, was utilized. The active space consisted of 6 doubly occupied orbitals [two A' (σ), two A'' (π) and two non-bonding] and 4 unoccupied orbitals [two A' (σ^*) and two A'' (π^*)]. Tests showed that this active space is a good compromise between accuracy and the cost of the calculation when compared with an active space that considers all the valence electrons, i.e., sixteen electrons in twelve orbitals. To improve the convergence

Table 2.2: *Comparison of Theoretically Determined Harmonic Frequencies (cm^{-1}) for CS_2 at the Equilibrium Geometry with Experimental Fundamental Frequencies.*

Method	Reference	ν_1	ν_2	ν_3
CASPT2/C:cc-pVTZ, S:aug-cc-pV(T+d)Z	This work	659	393	1549
Full CCSD(T)/aug-cc-pv(T+d)Z	Ref.[156]	674	400	1560
MCSCF/6-31G(d)	Ref.[153]	727	429	1572
CIS-MP2/6-311+G(d)	Ref.[154]	684	371	1637
Full MP2/6-31+G(d)	Ref.[151]	685	390	1635
B3LYP/6-31+G(d)	Ref.[151]	673	404	1551
B3LYP/aug-cc-pVTZ	Ref.[151]	674	403	1551
BLYP/aug-cc-pVTZ	Ref.[151]	645	384	1501
Experiment[a]	Ref.[157]	672.848	398.099	1558.787

[a] These values represent the harmonic parameters determined from a fit to the experimental data.

of the wavefunction (especially at geometries far from equilibrium), state-averaged CASSCF was used and included the first two states for each of the two symmetries of the C_s point group. While other numbers of states for state-averaging could be utilized, the choice of four states provided a reasonable description for the ground state in both the Franck-Condon region and asymptotically. The CASSCF orbitals and wavefunction were used as reference for CASPT2[38] computations - computations that were well-behaved based upon the aforementioned four-state state-averaged CASSCF results. The basis sets for the carbon atom and for the sulphur atoms were cc-pVTZ[45,46] and aug-cc-pV(T+d)Z,[158] respectively. The basis set for sulphur allows for a better description of the electronic density in this polarizable atom. All electronic structure computations were carried out with the Molpro software package.[18] The ground state equilibrium geometry was determined using the CASPT2 analytic gradients available in Molpro.[159] For the linear equilibrium structure, the CASPT2 optimized geometry gave an r_{CS} bond length of 1.563 Å (2.954 au), which is within 0.01 Å of the best theoretical and experimental determinations,[137,150,156] see Table 2.1. The (numerical) harmonic frequencies determined at the CASPT2 level are also in good agreement with previous calculations on CS_2, see Table 2.2. The modes labeled ν_1, ν_2, and ν_3 correspond to the symmetric stretch, *cis*-bend, and asymmetric stretch, respectively.

To build the ab initio potential energy and dipole moment surfaces for CS_2, we have used valence coordinates: the two C-S bond lengths (r_1 and r_2) and the S-C-S bond angle (θ). The bond lengths were varied from 1.263 to 2.463 Å in steps of 0.100 Å. The bond angle spanned a range from 110° to 180° in 5° steps. This choice results in a three-dimensional ($r_1 \times r_2 \times \theta$) grid of $13 \times 13 \times 15 = 2535$ points of which 1365 are symmetry unique. Note that the current PES does not include the high-energy cyclic-CS_2 isomer.[151,160,161] In terms of the Cartesian components of the dipole moment vector, the molecule is chosen to lie in the yz-plane, where the y-axis is chosen to bisect the bond angle θ and the linear molecule is chosen to lie along to the z-axis.

2.2.2 Fitting the Potential Energy and Dipole Surfaces

To use the PES efficiently in the MCTDH software package, it needs to be fit to a product form. In the present work, two options are considered: (i) using *potfit*[87,88] as implemented in the MCTDH software package[3] and (ii) using a NN fit with a sum-of-products form using exponential neurons.[1] Since the vibrational eigenergies are determined exactly, i.e., without invoking the MCTDH ansatz, fitting to product form is not strictly required. However, doing so allows easy integration with MCTDH and a test of the NN sum-of-products PES fitting to MCTDH operator file interface we have developed. Also, for future work using the OCT-MCTDH approach,[6,135,136] the MCTDH ansatz will have to be invoked as the current implementation does not allow the use of exact wavefunctions.

When using *potfit*, the error at the 2535 grid points was essentially zero (as expected when including the complete expansion). It is important to emphasize that *potfit* is not a fit per se, as it operates on the grid points only and does not fit the potential to continuous functions. As discussed by Manzhos and Carrington,[1] the error is then only reflected in the points included in generating the natural potentials and not the root mean-square error (RMSE) at random test points on the potential. In order to use *potfit* with the DVR used for determining the vibrational energies, see the following section, we must spline fit the natural potentials which can result in errors in the potential. However, as shown in the results, the *potfit* potential leads to accurate vibrational eigenvalues and, hence, must be an accurate reflection of the true potential.

A NN consists of a set of non-linear functions (neurons) organized into layers. Often the neurons used are sigmoid functions. However, we choose to use a single layer with exponential neurons so that the potential is written as a sum of N products,[1] i.e.,

$$V^{NN}(x_1, x_2, ...x_D) = \sum_{q=1}^{N} \tilde{c}_q \prod_{p=1}^{D} e^{w_{qp} x_p}. \tag{2.1}$$

The parameters $\tilde{c}_q$ (coefficients) and w_{qp} (weights) are optimized using the Levenberg-Marquardt (LM) algorithm to obtain a good fit.[81] Manzhos et al. tested a number of methods for determining the parameters[77] and concluded that LM "converged most quickly and produced the best fit." With a single-layer NN fit, the important parameter is the number of neurons (N) used. For the NN fits, which do not require data on a uniform grid, we choose an energy cut-off (E_{cut}) for the data points to include in the fit. The data set is also reduced to include only the symmetry unique points. From this set of symmetry- and energy-selected data, 80% of the points were selected at random (the training set) and used to fit the parameters of the NN, 10% of the points were used for ensuring that the training data was not overfit (the validation set), and 10% were used to test the quality of the fit at grid points not used for training (test set). For each symmetry-unique data point in the initial training set, an additional point involving the exchange of the two sulfur atoms was added to create the final training set. Usually we iterated several times (10-50) with different random training, validation, and test sets in order to minimize the RMSE on the test set. Further details regarding the use of NNs for fitting PESs are provided in recent reviews.[83,84,155] In addition to fitting the PES using NNs, the y- and z-components of the dipole moment (μ_y and μ_z, respectively) are also fit to sum-of-products form using NNs. The selection of the points for training, validation, and testing followed a similar procedure as for the PES regarding the inclusion of symmetry-related points; no energy cut-off was utilized and the training, validation, and test sets came from the entire 1365 symmetry unique points.

2.2.3 Determining Eigenenergies

To determine the vibrational eigenenergies, a kinetic energy operator is needed. In valence coordinates, the kinetic energy operator is given by[162]

$$\begin{aligned}\hat{T} &= \frac{p_1^2}{2\mu_{CS_1}} + \frac{p_2^2}{2\mu_{CS_2}} + \frac{j^2}{2\mu_{CS_1} r_1^2} + \frac{j^2}{2\mu_{CS_2} r_2^2} + \frac{p_1 p_2 \cos\theta}{m_C} \\ &\quad - \frac{p_1 p_\theta}{m_C r_2} - \frac{p_2 p_\theta}{m_C r_1} - \frac{\cos\theta j^2 + j^2 \cos\theta}{2 m_C r_1 r_2}\end{aligned} \tag{2.2}$$

where

$$p_k = -i\frac{\partial}{\partial r_k}, \quad k = 1, 2, \tag{2.3}$$

$$p_\theta = -i\frac{\partial}{\partial \theta}\sin\theta, \tag{2.4}$$

and

$$j^2 = -\frac{1}{\sin\theta}\frac{\partial}{\partial\theta}\sin\theta\frac{\partial}{\partial\theta}. \tag{2.5}$$

The reduced mass is $\frac{1}{\mu_{CS_i}} = \frac{1}{m_C} + \frac{1}{m_{S_i}}$ where m_C and m_{S_i} represent the masses of carbon (^{12}C = 12.0 amu or ^{13}C = 13.003354 amu) and sulfur isotope i (^{32}S = 31.97207070 amu, ^{33}S = 32.97145843 amu, or ^{34}S = 33.96786665 amu), respectively. The kinetic energy operator can be readily implemented in the Heidelberg MCTDH software package[3] using the built-in operators. For each degree of freedom (r_1, r_2 and θ) we have used 100 primitive basis functions; sine DVR for the bond lengths and (restricted) Legendre DVR for the bond angle. A restricted Legendre DVR (Leg/R), restricts the angular motion to a smaller interval than 0 to π. Using Leg/R, one may speed-up the wave-packet propagation as relatively smaller number of grid points (compare to the FBR/DVR) are used. The grids used were $2.4 \leq r_i \leq 4.05$ a.u. and $110° \leq \theta \leq 180°$. In the present work, the vibrational eigenstates have been calculated exactly using the Lanczos algorithm[163–165] available in the MCTDH software[3,166] with 11000 Lanczos iterations. For the relatively small problem under consideration, there was no need to optimize carefully the number of basis functions or number of Lanczos iterations - the present choices were sufficient to converge the reported eigenvalues to $\ll 0.01$ cm^{-1}.

Table 2.3: *Root Mean Square Errors (RMSEs) Over the Training and Test Sets for PESs with Different Energy Cut-offs (E_{cut}) that are Fit to Product Form Using NNs.*

E_{cut}/cm^{-1}	# Neurons	N_{train}	RMSE$_{train}$/cm^{-1}	N_{test}	RMSE$_{test}$/cm^{-1}
20,000	30	303	1.0	38	1.6
30,000	30	624	3.0	76	7.5
50,000	30	1516	40.3	190	53.9

2.3 Results and Discussion

2.3.1 Neural Network Fits of the Potential Energy and Dipole Surfaces

To fit the potential energy surface using NN, three different values of E_{cut} were considered: 20000 cm^{-1}, 30000 cm^{-1}, and 50000 cm^{-1}. The RMSE at the training and test points for CS_2 PES fits with an exponential NN as a function of the number of nodes is illustrated in Figure 2.1. As can be clearly seen, the test point RMSE for the fits up to 20000 and 30000 cm^{-1} reaches $\leq$ 10 cm^{-1} for greater than 15 neurons. The RMSE for the fit to 50,000 cm^{-1} is significantly larger and a larger number of neurons is required. It should be noted that a *potfit* with $\approx$ 200 terms, i.e., approximately the number of parameters in a NN fit with 50 neurons, exhibits a RMSE for the fit of of only 45 cm^{-1} - a value comparable to the NN fit up to 50,000 cm^{-1}. For determining the vibrational eigenenergies, the PES fits with 30 neurons were utilized for all energy cut-offs. The RMSEs for these fits and the total number of ab initio data points included in the training and test sets are given in Table 2.3. For the fit up to 50000 cm^{-1} with 30 neurons, the overall RMSE for the training set is 40.3 cm^{-1} while the RMSE of training (test) points with energies between 0 and 10000 cm^{-1} is 16.1 (17.0) cm^{-1} and for 10000 to 20000 cm^{-1} it is 11.9 (11.3) cm^{-1}. Thus, the fit is significantly better at low energies. Plots of the NN fit PES (E_{cut} = 50000 cm^{-1} and $N = 30$) for the linear configuration with r_1 and r_2 varied are given in Figure 2.2 and Figure 2.3 for different contour spacings, i.e., 0.1 eV and 0.01 eV, respectively. The corresponding plot for $r_2 = r_{eq} = 1.563$ Å with r_1 and θ varied is given in Figure 2.4, respectively. From these plots, it is clear that the fitted PES is smooth and contains no “holes,” i.e., regions with large (artificially) low energies.

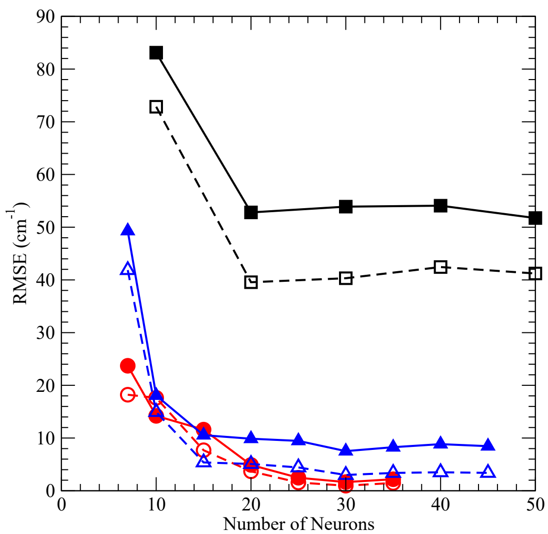

Figure 2.1: *The RMSE at the training (dashed lines, open symbols) and test (solid lines, filled symbols) points for CS_2 PES fits with an exponential NN as a function of the number of neurons for different value of E_{cut}: 20000 cm^{-1} (red, circles), 30000 cm^{-1} (blue, triangles), and 50000 cm^{-1} (black,squares).*

Both components of the dipole moment, i.e., μ_y and μ_z, have been fit using NN in sum-of-products form with 50 neurons using all of the 1365 symmetry unique data points (where 80% are used for fitting, 10% for validation, and 10% for testing). The RMSE over the training (test) set for the μ_y- and μ_z-components are 0.00886 a.u. (0.00916 a.u.) and 0.03126 a.u. (0.03151 a.u), respectively. Increasing the number of neurons in the NN does not significantly improve the fitting, e.g., for 75 neurons, the RMSEs for the training (test) sets are 0.00696 a.u. (0.00954 a.u.) and 0.03076 a.u. (0.03350 a.u.) for the μ_y- and μ_z-components, respectively. Figure 2.5 and Figure 2.6 present plots of the μ_y and μ_z dipole moments for $r_2 = r_{eq} = 1.563$ Å and r_1 and θ varied. As can be seen, the NN fit leads to a smooth dipole moment surface in both cases.

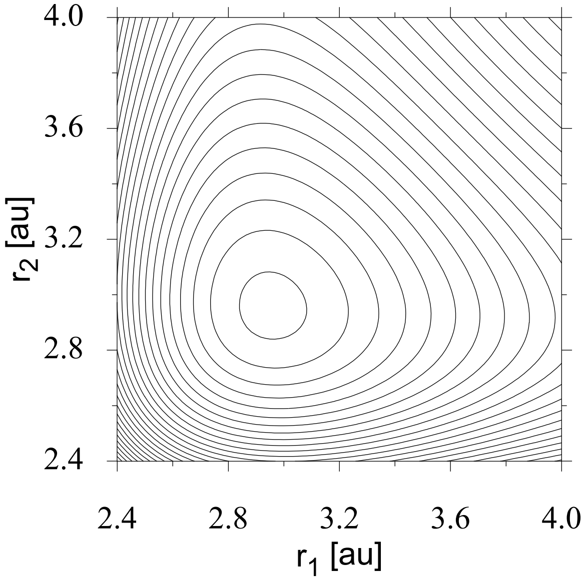

Figure 2.2: *2D PES as a function of r_1 and r_2 with fixed $\theta = 180°$ for CS_2 using the CASPT2/C:cc-pVTZ, S:aug-cc-pV(T+d)Z method and fit with an exponential NN up to 50000 cm^{-1} with 30 neurons. The minimum contour is 0.1 eV (806 cm^{-1}) and each contour represent an increase of 0.3 eV (2417 cm^{-1}).*

2.3.2 The Vibrational Energies

The PESs discussed above have been used to compute the low-lying vibrational states of $^{12}C^{32}S_2$. We were interested to see if, and how, the energy cut-offs used in the NN fitting impacted the determination of the energies of the low-lying vibrational states. Also, we wished to compare the energies using the NN fit to those obtained on the *potfit* PES. While the goal of the present work is not the reproduction of the experimentally measured vibrational transition frequencies (these can be obtained accurately using the empirical PES[146]), the vibrational energies determined in the current work will be compared to experimental measurements.[140–142,157]

The vibrational states determined on the three NN PESs and on the *potfit* PES are given in Table 2.5. As can be seen, there is good agreement between the NN and *potfit* vibrational energies (typically differences of less than 10 cm^{-1}). Importantly, there is also good agreement between our results on the ab initio PES and those of

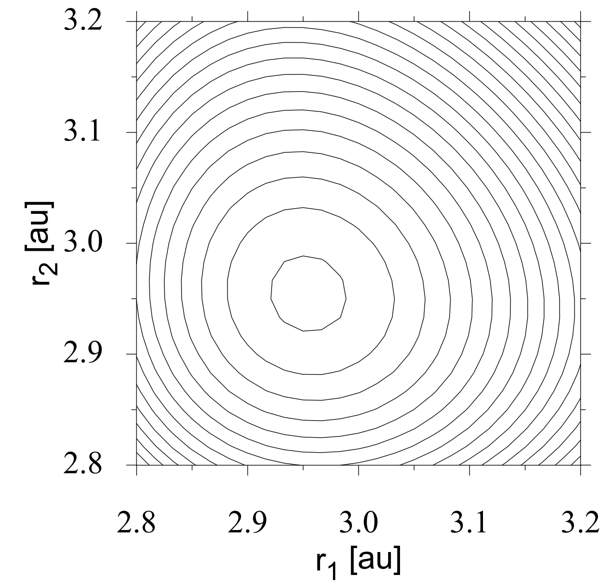

Figure 2.3: *2D PES as a function of r_1 and r_2 with fixed $\theta = 180°$ for CS_2 using the CASPT2/C:cc-pVTZ, S:aug-cc-pV(T+d)Z method and fit with an exponential NN up to 50000 cm^{-1} with 30 neurons. The minimum contour is 0.01 eV (80.6 cm^{-1}) and each contour represent an increase of 0.03 eV (241.7 cm^{-1}).*

Zhou and co-workers,[146] which were based on an empirical PES designed to reproduce the experimentally observed results. The fit by Zhou et al.[146] has an RMSE of 0.20 cm^{-1} for the 86 vibrational levels included in the fitting up to 6000 cm^{-1}. A similar fit to the experimental data of Zuniga et al.[148] has an RMSE of 0.344 cm^{-1} for the 49 levels included in the fit. The purely ab initio results reported here (for $E_{NN_{50}}$) have an RMSE over the 20 levels up to 3100 cm^{-1} of 23.1 cm^{-1} (Mean absolute error = 20.5 cm^{-1}). The agreement is quite good, and the discrepancies with experiment primarily reflect the limitations of the underlying electronic structure theory rather than the PES fitting. For example, if we examine the RMS difference between the ab initio data points and the empirical potential,[146] it is 57.2 cm^{-1} for energies up to 5000 cm^{-1} (42 data points), 125.9 cm^{-1} for energies up to 10000 cm^{-1} (115 data points), and 339.2 cm^{-1} for energies up to 20000 cm^{-1} (379 data points). However, the current potential (with the highest energy cut-off) represents a global fit up to 50,000

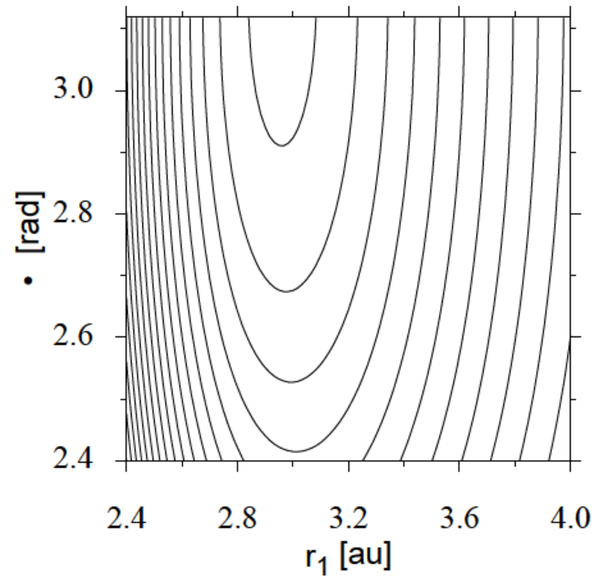

Figure 2.4: *2D PES as a function of r_1 and θ with fixed $r_2 = 2.954$ a.u. (1.563 Å) for CS_2 using the CASPT2/C:cc-pVTZ, S:aug-cc-pV(T+d)Z method and fit with an exponential NN up to 50000 cm^{-1} with 30 neurons. The minimum contour is 0.1 eV (806 cm^{-1}) and each contour represent an increase of 0.3 eV (2417 cm^{-1}).*

cm^{-1} rather than over a limited energy range like the previous empirical potentials.

To further test the PES, vibrational energies were determined for several isotopomers of CS_2 including $^{32}S^{12}C^{34}S$, $^{32}S^{12}C^{33}S$, and $^{13}C^{32}S_2$. The energies for transitions to the lowest-lying ($J = 0$) vibrational states (1,0,0), (0,2,0), and (0,0,1) are given in Table 2.4. Not surprisingly, there is good agreement between the present computations and the previously reported results[143–146] (differences < 11 cm^{-1}, with shifts reproduced to < 1 cm^{-1}).

2.4 Summary

In the present work, new global PES and dipole moments surfaces for CS_2 based upon CASPT2/C:cc-pVTZ,S:aug-cc-pV(T+d)Z ab initio computations are reported. The ab initio data is fit to sum-of-products form using the neural network method with exponential neurons. The quality of the fits depends upon the energy cut-offs and

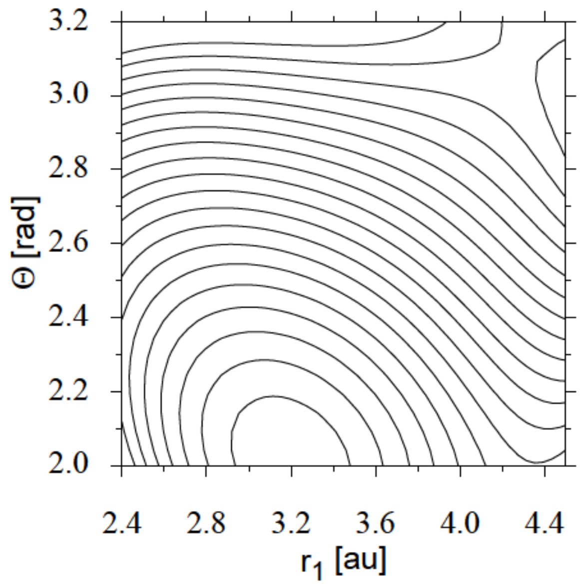

Figure 2.5: *2D μ_y dipole moment surface for CS_2 with $r_2 = 2.954$ a.u. (1.563 Å) using the CASPT2/C:cc-pVTZ, S:aug-cc-pV(T+d)Z method and fit with an exponential NN up to 50000 cm^{-1} with 50 neurons. The minimum contour is 0.0 a.u. and each contour represent an increase of 0.01 a.u.*

the number of neurons, but overall excellent fits to both training (included in the fit) and test (external to the fit) data sets can be achieved with a modest number of neurons (fitting parameters). The sum-of-products form used permits ready use by the MCTDH software package.[3] While other neural network fits to sum-of-products form have been reported,[1,2] the present work presents one of the first, and only, NN fits directly to ab initio data - many NN fits are refits of analytical PESs. Clearly, the NN approach presents an attractive alternative to *potfit* for fitting triatomic PES and dipole moment surfaces. Additional tests on tetra-atomic, and larger, systems where the fits are directly to ab initio data are currently underway. Importantly, we have accurate global potential energy and dipole moment surfaces for CS_2 that should permit future OCT-MCTDH studies.

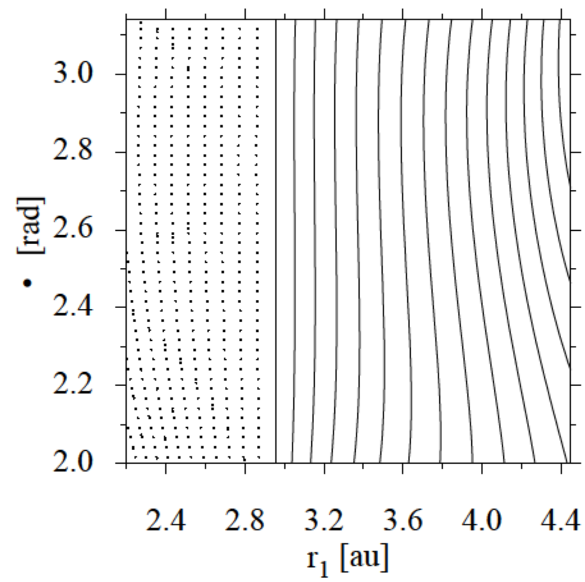

Figure 2.6: *2D μ_z dipole moment surface for CS_2 with r_2 = 2.954 a.u. (1.563 Å) using the CASPT2/C:cc-pVTZ, S:aug-cc-pV(T+d)Z method and fit with an exponential NN up to 50000 cm^{-1} with 50 neurons. The minimum contour is -1.4 a.u. (at $r_1 \approx 4.4$ au) and each contour represents an increase of 0.10 a.u. Negative and positive values are shown as solid and dotted lines respectively. As expected the dipole moment is zero when r_1 = 2.954 a.u. (1.563 Å).*

Table 2.4: *Low-lying Vibrational Eigenvalues for Minor CS_2 Isotopes, and Corresponding Isotopic Shifts (ΔE), as Determined on the NN PES (Fit Up to 50,000 cm^{-1}) as Compared to Previous Theoretical and Experimental Results.*[a]

(v_1,v_2,v_3)	$E_{NN_{50}}$	$\Delta E_{NN_{50}}$	E_{calc}[b]	ΔE_{calc}	E_{obs}
		$^{32}S^{12}C^{34}S$ [8% isotopic abundance]			
(1,0,0)	637.51	-9.30	648.66	-9.39	648.37[c]
(0,2,0)	796.7	-2.16	799.63	-2.27	—
(0,0,1)	1529.43	-3.46	1532.00	-4.75	1531.89[d]
		$^{32}S^{12}C^{33}S$ [1.4% isotopic abundance]			
(1,0,0)	642.04	-4.77	653.24	-4.81	—
(0,2,0)	797.74	-1.12	800.73	-1.17	—
(0,0,1)	1531.10	-1.79	1533.67	-1.78	1533.57[d]
		$^{13}C^{32}S_2$ [1% isotopic abundance]			
(1,0,0)	646.30	-0.51	657.29	-0.76	657.24[e]
(0,2,0)	773.7	-25.16	776.58	-25.32	776.55[e]
(0,0,1)	1482.97	-49.92	1485.44	-50.01	1485.33[e]

[a] Energies in cm^{-1}. v_1: C-S symmetric stretching, v_2: *cis*-bending, v_3: asymmetric stretching; [b]Ref. 146; [c] Ref. 143; [d] Ref. 144; [e] Ref. 145.

Table 2.5: *The Zero-point Energy and Twenty Lowest-lying Vibrational (l = 0) Eigenvalues for $^{12}C^{32}S_2$ (89% Isotopic Abundance) as Determined on the potfit and NN PESs as Compared to Previous Theoretical and Experimental Results.*[a]

(v_1,v_2,v_3)	$E_{NN_{20}}$	$E_{NN_{30}}$	$E_{NN_{50}}$	E_{potfit}	$E_{calc}{}^b$	$E_{obs}{}^c$
(0,0,0)	1499.45	1499.58	1516.07	1511.63	—	—
(1,0,0)	646.69	646.63	646.81	650.11	658.05	658.00
(0,2,0)	792.01	792.74	798.86	790.96	801.90	801.30
(2,0,0)	1291.16	1291.05	1291.45	1296.37	1313.82	1313.70
(1,2,0)	1426.50	1427.14	1432.83	1428.30	1447.21	1447.40
(0,0,1)	1533.74	1533.75	1532.89	1546.33	1535.45	1535.35
(0,4,0)	1598.72	1599.66	1606.61	1596.44	1619.82	1619.78
(3,0,0)	1933.31	1933.17	1933.85	1938.97	1967.22	1966.97
(2,2,0)	2059.07	2059.61	2064.83	2062.41	2090.67	2094.00
(1,0,1)	2172.67	2172.60	2171.85	2178.98	2185.60	2185.47
(1,4,0)	2223.74	2224.56	2230.80	2224.01	2255.45	2254.70
(0,2,1)	2312.98	2313.62	2318.42	2324.68	2324.57	2324.55
(0,6,0)	2416.78	2417.75	2423.68	2414.23	2450.09	2450.05
(4,0,0)	2573.06	2572.90	2573.90	2578.07	2618.11	2616.00
(3,2,0)	2689.74	2690.19	2694.88	2693.53	2732.32	2727.00
(2,0,1)	2809.30	2809.16	2808.59	2809.65	2833.41	2833.19
(2,4,0)	2847.18	2847.89	2853.42	2848.84	2889.62	2889.70
(1,2,1)	2939.59	2940.10	2944.4	2945.68	2961.91	2961.76
(0,0,2)	3033.62	3034.48	3039.63	3032.96	3057.84	3057.63
(1,6,0)	3054.20	3054.18	3052.41	3065.64	3077.42	3077.40
(0,4,1)	3107.12	3107.88	3113.35	3116.34	3129.96	3129.98
RMSE[d]	26.5	26.1	23.1	24.0	1.5	—

[a] Note that all vibrational energies are relative to the ZPE (0,0,0). The NN PESs NN_{20}, NN_{30} and NN_{50} are for fits up to 20000 cm^{-1}, 30000 cm^{-1} and 50000 cm^{-1}, respectively. Energies are given in cm^{-1}. v_1: C-S symmetric stretching, v_2: *cis*-bending, v_3: asymmetric stretching.

[b] Ref. 146. Based on an empirical potential designed to reproduce experimentally observed results.

[c] From Refs. 140–142,157

[d] As compared to the experimental measurements. Note that not all levels presented here were included in the fit of Zhou et al. 146

Chapter 3

Vibrational Energies for HFCO using a Neural Network Sum of Exponentials Potential Energy Surface

3.1 Introduction

Laser control of quantum dynamics for medium to large size molecules, i.e., containing greater than 3 atoms, is an interesting and challenging task. Laser control involves shaping a laser pulse to manipulate chemical processes on the molecular scale.[167–170] For example, laser control can direct a reaction to proceed in a particular direction to give a desired product, product ratio or, in the case of vibrational excitation, to produce a desired quantum (superposition) state. After pioneering research demonstrating control principles for small molecules (2-3 atoms),[171,172] efforts have been made to apply laser control to photochemical processes in much larger molecules ($\geq$4 atoms).[173–176] However, both theory and experiment are difficult for large systems with a significant number of vibrational degrees of freedom. The present work is motivated by simulations using the multi-configuration time dependent Hartree (MCTDH) approach of laser-driven (control of) intramolecular vibrational redistribution (IVR) in the HONO and HFCO molecules;[128,130,177] molecules of moderate but still challenging size for quantum dynamics simulations. In particular, the goal of the present work is to develop and test a new potential energy surface (PES) for HFCO, as the previous simulations were limited by the accuracy of the one available.[132]

The structure, spectroscopy and dynamics of HFCO have undergone extensive experimental[133,178–186] and theoretical[132,187–202] scrutiny. Moore and co-workers[133,178–180] studied the vibrational states of HFCO/DFCO on the ground and first few excited electronic states. Using the stimulated emission pumping technique, they investigated highly excited vibrational states of HFCO and DFCO, near and even above the dissociation limit. These experiments drew the attention of other researchers to investigate the role of particular states on IVR. To understand the findings of Moore and co-worker, Yamamato and Kato (YK) fit a six dimensional ground electronic state potential energy surface (PES) for HFCO based on 4140 MP2/cc-pVTZ level of theory computed energies.[132] The cc-pVTZ basis sets were truncated by removing f-functions from O, C, F and d-functions from H. The analytical surface was fit up to 24500 cm^{-1} above the minimum and the RMSE was 525 cm^{-1}. Even with this (relatively, and by modern standards) poor quality of the PES, they were able to study successfully power spectra, intramolecular dynamics, dissociation products energy distributions, dissociation rates of CH stretching and out-of-plane bending modes.[132,197,198] The YK potential has been used by Viel and co-workers[196] to compute vibrational states of HFCO and DFCO; in the same study, they also utilized the alternate Wei and Wyatt (WW) PES for HFCO.[200] In addition to Viel's work, other groups have used the YK PES to examine the vibrational states of HFCO and DFCO.[199,201,203,204] Using the YK PES, Gatti and co-workers investigated IVR and IVR driven (and, hence, possibly controlled) by an external field in HFCO and DFCO.[126,128] They investigated IVR after excitation above the dissociation limit of C=O or C-F stretching modes. In principle, coupling of these modes with the out-of-plane bending mode, which is close to the dissociation reaction coordinate, could facilitate the dissociation. It was determined that DFCO dissociates but HFCO does not. However, the optimal control of these processes was not pursued as the YK PES underlying the dynamics was not sufficiently accurate.

The present focus is on constructing a new highly accurate PES for the HFCO molecule that can be used for studying quantum dynamics including IVR and optimal control of IVR. Fitting the 6D PES to the sum-of-products form desired for future MCTDH dynamics simulations is challenging. For example, using the conventional *potfit* approach[87,88] requires a large number of data points for the fit as they must be sampled on a uniform grid. As a simple example, if 10 points are sampled per degree of freedom, one million data points are needed for a 6D system; an insurmountable task if using a high-level ab initio determination of the data. The sampling issue could be addressed using the recently developed extension to multi-grid *potfit*.[205] Here we will use the neural network fitting with exponential neurons approach[1,77,78] to develop a PES in sum-of-prdocuts form. In our recent work,[8] see Chapter 2, we developed and tested a direct interface between the PES-fitting and MCTDH. This method gives sum-of-products form which can directly be used in MCTDH to study dynamics. In that work, we demonstrated the utility of the method for CS_2, i.e., only 3D. Here we extend the approach to a 6D PES.

The chapter is organized as follows. First, the computational methods are discussed including the ab initio electronic structure techniques, the Neural Network with exponential neurons PES fitting procedure, and the methods used to determine the vibrational energies in MCTDH. In the Results and Discussion section, the important stationary points on the PES are characterized. The quality of the new PES fit is analyzed in terms of RMSE. The vibrational frequencies of fundamental and combination modes of HFCO and DFCO, as determined on the new PES, are determined and compared ot previous computational and experimental results. The chapter concludes by summarizing the results, discussing the potential use of the new PES in future dynamics studies, and, more generally, the applicability of the fitting method in future for other similar and larger systems.

3.2 Computational Methods

3.2.1 Ab initio Methods/Electronic Structure Computations

The majority of the ab initio electronic structure computations were performed using the explicitly correlated coupled cluster method with single, double and perturbative triple excitations [CCSD(T)-F12].[15,16,206] For the CCSD(T)-F12 computations, the cc-pVTZ-F12 basis set was used for all atoms.[47] The ground state equilibrium geometry of HFCO as well as the geometries of the cis- and trans-isomers (denoted as cis-HOCF and trans-HOCF) were determined at the CCSD(T)-F12/cc-pVTZ-F12 level of theory using numerical gradients. The transition states were also determined at the same level of theory, where the initial Hessian for the search was determined at the MP2/aug-cc-pVTZ level of theory. All stationary points were verified by computing harmonic vibrational frequencies via numerical Hessians. By default, both F12A and F12B energies[15,206] were obtained in a single point calculation; the F12A energies are reported in this work. All CCSD(T)-F12 electronic structure computations were carried out with MOLPRO.[18,19] The default convergence criteria in MOLPRO were used in geometry optimizations and single point energy calculations.

Infrared frequencies and intensities of the fundamental modes were also determined within the harmonic limit and accounting for anharmonicity at the MP2/aug-cc-pVTZ[207–209] and CCSD(T)/aug-cc-pVTZ levels of theory[210–212] using CFOUR.[124] The required geometry optimizations and electronic structure computations used the default convergence criteria in CFOUR. The harmonic frequencies and corresponding intensities were computed using analytic Hessians. The anharmonic vibrational frequencies and the intensities of the fundamental modes were determined at the VPT2 (second-order) level of perturbation theory[118–120] as implemented in CFOUR.[124]

3.2.2 Fitting the Potential Energy Surface

A body fixed polyspherical coordinate system was used for the HFCO molecule, see Figure 3.1. The C-H, C-F and C=O bond distances are designated as $R_{CH} = R_1$, $R_{CF} = R_2$ and $R_{CO} = R_3$ respectively, while θ^{BF}_{HCO}, θ^{BF}_{FCO} and ϕ^{BF} are the H-C-O,

Table 3.1: *Grid lengths and parameters of the primitive basis set employed for each degree of freedom. HO is the harmonic oscillator (Hermite) DVR.*

Mode Combinations	(R_1, cosθ_1)		(R_2, cosθ_2)		(R_3, ϕ)	
Primitive basis	HO-DVR	HO-DVR	HO-DVR	HO-DVR	HO-DVR	HO-DVR
# of basis functions	10	13	14	14	10	40
Grid length (a.u.)	[1.41,3.35]	[-0.99,0.135]	[2.06,3.62]	[-0.91,-0.055]	[1.75,2.93]	[1.48,4.82]
Number of SPFs	10		14		10	

F-C-O bond angles and the dihedral angle between them, respectively. Grids along physical coordinates were carefully chosen to restrict the PES to be confined to the equilibrium HFCO geometry and the transition state to dissociation into HF + CO. The range chosen for each coordinate is given in Table 3.1; the numerical details for the MCTDH computations, discussed later, are also provided.

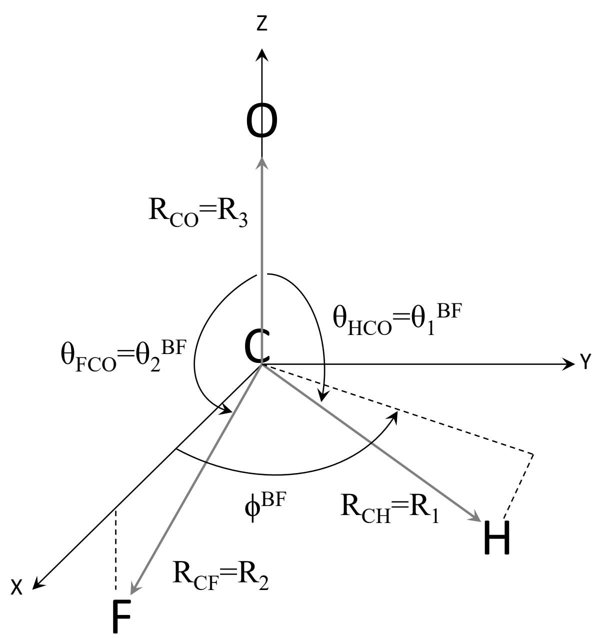

Figure 3.1: *Valence Body-Fixed Polyspherical Coordinate System used for the HFCO Molecule. R_2 lies in the xz Plane*

The neural network (NN) toolbox in MATLAB was used to fit the six-dimensional (6D) PES of the HFCO molecule into a sum-of-products form. The sum-of-products form is required for efficient quantum dynamics simulations using the MCTDH[3–7] approach. In general, neural networks use sigmoidal fitting functions but in the current work, an exponential fitting function is utilized as proposed by Manzhos and Carrington[1] to obtain a sum-of-products form for the final PES, i.e.,

$$V^{NN}(x_1, x_2, ...x_D) = \sum_{q=1}^{N}(e^{b_q}C_q)\prod_{p=1}^{D} e^{w_{qp}x_p} + V_{shift} = \sum_{q=1}^{N}\tilde{c}_q\prod_{p=1}^{D} e^{w_{qp}x_p} + V_{shift}. \quad (3.1)$$

Here V^{NN} is the neural network fitted PES as a function of the number of neurons (N) and the x_1 to x_D degrees of freedom. The fitting parameters consist of weights, w_{qp}, biases, b_q, which are incorporated into the constant $\tilde{c}_q$, and a final constant shift parameter, V_{shift}. The final form is a sum over all the neurons and a product over all the dimensions.

To generate data for PES fitting, one-dimensional (1D) and two-dimensional (2D) grids were generated along the physical coordinates centred at both the equilibrium geometry and the transition state to the dissociation channel HF+CO. In addition to the 1D and 2D grid data, geometries were selected randomly from the 6D grid, where the ranges for the 6 degrees of freedom are defined in Table 3.1. However, the random grid points were restricted using an energy filter,[2,77,81] i.e.,

$$\frac{E_{cut} - V^0_{total}}{E_{cut}} > f_i \quad (3.2)$$

where E_{cut} is a chosen cut-off energy and f_i is a random number between 0 to 1. The total energy, V^0_{total}, that was filtered was determined by summing over all the 1D potentials from the equilibrium geometry. These 1D potentials were fit to Morse (R_1, R_2 and R_3) and polynomial (cosθ_1, cosθ_2 and ϕ) functional forms, see Table B5 and Table B6 in Appendix B and the accompanying discussion. As the energy from the sum over 1D potentials will always be greater than the exact (anharmonic) energy at any geometry, the filter puts more data in the lower energy region of the PES. Therefore, the full data set for the PES-fitting consists of the random energy-filtered data plus 1D and 2D grid data.

The data set was split into training, testing and validation sets. The training set contains 80% of the total data data, including the random energy-filtered geometries plus the 1D and 2D grid data at the equilibrium and transition state to dissociation geometries. The training set was used to fit the PES. A validation set of 10% of the data was used to guide the fit to avoid over-fitting of the training set. A test set of 10% of the data was used to examine the quality of the fit at the end of the fitting procedure.The Levenberg-Marquardt algorithm was used to determine the fitting parameters, see Eq. (3.1). Before fitting, all data (coordinates and energies) were scaled to lie between [-1, 1] by

$$X_{scaled} = \frac{X - x_{min}}{x_{max} - x_{min}} \tag{3.3}$$

where the maximum and minimum of a particular coordinate (or the energy) are x_{max} and x_{min}. X is the data before scaling which after scaling appears as X_{scaled}. The scaled data lead to smooth convergence and a gradually decreasing RMSE for the fit. A one-stage fitting procedure in a loop over 10-20 iterations has been applied in this work to further reduce the RMSE.

3.2.3 Eigenenergy Calculation

Block improved relaxation[9] as implemented in the Heidelberg multiconfiguration time-dependent Hartree (MCTDH) package[3] was used to compute the vibrational state energies. For efficiency in MCTDH, the wavefunction, kinetic energy operator (KEO) and the potential energy operator must all be in sum-of-products form. In the present work, we have employed the KEO used previously in the study of intramolecular vibrational energy redistribution (IVR) of highly excited HFCO.[126–128] Primitive grids for each degree of freedom utilize harmonic oscillator (HO) basis functions. The grid sizes and the number of primitive basis functions are given in Table 4.1. Combination modes have been used in the single particle functions (SPFs). The number of SPFs and the mode combinations are also given in Table 3.1. Improved relaxation[7,125] was used to obtain wavefunctions and assign the vibrational states.

3.3 Results and Discussion

3.3.1 Equilibrium Geometry

3.3.1.1 Stationary points; Structure; Energies

The optimized equilibrium and transition state geometries along with the corresponding relative energies at the CCSD(T)-F12/cc-pVTZ-F12 level of theory are given in Table 3.2. The results for the equilibrium and transition state geometries are in

Table 3.2: *Structural Parameters (bond lengths in Å; angles in degrees) and Relative Energies (in cm^{-1}) of HFCO Isomers and Corresponding Transition States at the CCSD(T)-F12/cc-pVTZ-F12 Level of Theory.*

Structure	$R_1^{(CH)}$	$R_2^{(CF)}$	$R_3^{(CO)}$	θ_1^{HCO}	θ_2^{FCO}	ϕ^a	Energy^b
Equilibrium	1.091	1.341	1.179	127.8	122.7	180	0
Cis-isomer	1.883	1.341	1.295	28.9	106.8	0	15180
Trans-isomer	1.828	1.317	1.308	30.4	104.5	180	14809
$TS_{trans\leftrightarrow cis}$	1.930	1.320	1.332	27.3	106.5	90.3	21013
$TS_{eq\leftrightarrow trans}$	1.246	1.320	1.260	59.2	115.4	180	26416
$T_{dissociation}$	1.136	1.854	1.132	170.6	121.6	0	16993

^{a} Dihedral angle between HCO and FCO planes.
^{b}Relative energy, including harmonic ZPE, with respect to the equilibrium geometry in cm^{-1} unit. The zero point corrected energy (E_0) is the sum of the total energy (E_{tot}) and the zero point energy (E_{ZPE}), i.e., $E_0 = E_{tot} + E_{ZPE}$.

good agreement with previous computations[191,202] and, where available, experimental measurements[185,186,213] (see Table B1 and Table B2, Appendix B). The bond lengths are within 0.01 Å and the bond angles within 0.5 degrees of the previous calculations and within the experimental error bars for the experimental determinations (for equilibrium structure only). The transition state for unimolecular dissociation of HFCO to HF and CO is determined to lie 16993 cm^{-1} (48.55 kcal/mol) above the equilibrium with the zero-point energy correction and this agrees well with the experimental value of 43-49 kcal/mol.[133,183] Trans-HOCF is 14809 cm^{-1} above the equilibrium energy and 371 cm^{-1} (1.06 kcal/mol) more stable than cis-HOCF. The cis- and trans- isomers are separated by a transition state with a relative energy (compared to the trans-isomer) of 6204 cm^{-1}. The barrier height for the equilibrium geometry to trans-HOCF conversion was found to be 26416 cm^{-1}. This relatively high barrier isolates the cis-trans conversion process from unimolecular dissociation. A cut-off energy of 20000 cm^{-1} and a carefully chosen grid (in Table 3.1) restricts the potential to be in the region consisting of only equilibrium HFCO and the transition state to unimolecular dissociation.

3.3.1.2 Harmonic and Anharmonic Frequencies

While the full-dimensional PES is needed for future dynamics studies, it is interesting to compare fundamental vibrational frequencies for HFCO obtained through harmonic and anharmonic computations. Frequencies obtained from MP2/aug-cc-pVTZ, CCSD/aug-cc-pVTZ and CCSD(T)/aug-cc-pVTZ computations were compared with previous experimental measurements[181] along with results from a CCSD(T)-F12/cc-pVTZ-F12 harmonic calculation. The harmonic and anharmonic frequencies for the fundamental modes of HFCO are given in Table 3.3 and Table 3.4, respectively. Previous CCSD(T)/cc-pVTZ results by Vazquez and Stanton[187] are also reported. The root means square errors (RMSE) compared to the experimental data are provided.

The RMSE for the harmonic fundamental modes determined using MP2/aug-cc-pVTZ, CCSD/aug-cc-pVTZ, CCSD(T)/aug-cc-pVTZ and CCSD(T)-F12/cc-pVTZ-F12 were 74 cm^{-1}, 82 cm^{-1}, 60 cm^{-1} and 62 cm^{-1}, respectively. For the anharmonic computations, the RMSEs for the fundamental modes were greatly reduced to 16.5 cm^{-1}, 26 cm^{-1} and 8 cm^{-1} for MP2/aug-cc-pVTZ, CCSD/aug-cc-pVTZ and CCSD(T)/aug-cc-pVTZ, respectively. The ability to determine CCSD(T)-F12 anharmonic frequencies via VPT2 is only accessible numerically, i.e., using finite differences to obtain numerical gradients, Hessians, and higher order derivatives, and, hence, are not computed. Previous theoretically determined frequencies by Stanton and co-workers[187] using the CCSD(T)/cc-pVTZ(Frozen Core) method have a RMSE 66 cm^{-1} for the harmonic frequencies but for anharmonic calculation, the RMSE was 12 cm^{-1}. As expected, improved treatment of electron correlation from MP2 to CCSD(T) to CCSD(T)-F12 improves the harmonic frequencies as does increasing the size of the basis (cc-pVTZ to aug-cc-pVTZ). Interestingly, the CCSD(T)/aug-cc-pVTZ and CCSD(T)-F12/cc-pVTZ-F12 harmonic frequencies are of comparable accuracy. Not surprisingly, similar observations were made for DFCO; the harmonic and anharmonic frequencies for the fundamental modes are given in Appendix B: Tables B3 and B4. While the harmonic and anharmonic modes are useful for spectroscopy, a full-dimensional PES is important for studying high-lying vibrational modes and for quantum dynamics simulations.

3.3.2 NN fit of the PES

The PES fitting was initiated by dividing the total data set, see Section 3.2.2, of ab initio energies as determined at the CCSD(T)-F12/cc-pVTZ-F12 level of theory, into training, testing, and validation sets. PES fits were generated using two different cut-off energies, see Eq. (3.2), of 20000 cm^{-1} and 30000 cm^{-1}. The sum over 1D potentials, V^0_{total}, needed for the energy filtering, was based on 1D potentials fit to CCSD(T)-F12/cc-pVTZ data around the equilibrium geometry. The following forms were utilized: a 9^{th} order polynomial for ϕ, a 5^{th} order polynomial for cosθ_1 and cosθ_2, and Morse potentials for R_1, R_2 and R_3. The fitting parameters are given in Appendix B: Tables B5 and B6. In the training set for the PES with a 30000 cm^{-1} cut-off energy, 8000 random data, 440 1D data, 1500 2D data at equilibrium and 800 2D data at the transition state were used. The test set was 1000 random data and the validation set contained 999 random data. The PES with a 20000 cm^{-1} cut-off energy was fit to a training set of 7000 random, 400 1D and 1300 2D data points at equilibrium and 750 2D data points at the dissociation transition state.

The RMSE versus the number of neurons used in the fit is shown in Figure 3.2. The numerical results associated with this figure are given in Appendix B: Table B7. Not surprisingly, the RMSE decreases as the number of neurons (fitting parameters) increases; however, the RMSE plateaus and does not approach zero due to the use of the validation set. From 55 to 70 neurons, the RMSE decreases very slowly and essentially converges to 20 cm^{-1} after 75 neurons for the 20000 cm^{-1} cut-off potential energy surface and to 35 cm^{-1} for the 30000 cm^{-1} PES. While the training set RMSE

Table 3.3: *Theoretical Harmonic and Experimentally Measured Fundamental Frequencies (in cm^{-1}) of HFCO*

	Present Results				Previous Results	
Mode	MP2^a	CCSD^a	CCSD(T)^a	CCSD(T)-F12^b	CCSD(T)^c	Experiment[181]
ν_5 FCO bend	660.4	680.7	663.9	670.0	673.1	662.5
ν_6 out of plane bend	1035.0	1052.9	1030.2	1026.6	1038.5	1011.0
ν_2 CF stretch	1073.6	1121.3	1086.8	1093.2	1112.9	1064.8
ν_4 HCO bend	1375.3	1394.7	1370.4	1374.8	1388.2	1342.5
ν_3 CO stretch	1846.6	1906.9	1858.5	1870.6	1874.6	1836.9
ν_1 CH stretch	3157.6	3147.2	3120.2	3121.2	3120.9	2981.0
RMSE	74	82	60	62	66	

^{a}aug-cc-pVTZ basis set.
^{b}cc-pVTZ-F12 basis set.
^{c}cc-pVTZ basis set from Ref. 187.

Table 3.4: *Theoretical Anharmonic and Experimental Fundamental Frequencies (in cm^{-1}) of HFCO*

	Present Results			Previous Results		
Mode	MP2[a]	CCSD[a]	CCSD(T)[a]	CCSD(T)[b]	Obs.[c]	Intensity[d]
ν_5 FCO bending	652.3	673.5	656.1	665.5	662.5	17.8
ν_6 out of plane bending	1016.5	1034.4	1012.9	1019.0	1011.0	0.5
ν_3 CF stretching	1046.1	1096.1	1060.7	1088.3	1064.8	132.7
ν_4 HCO bending	1342.8	1362.7	1337.4	1355.0	1342.5	1.1
ν_3 CO stretching	1814.7	1875.3	1825.2	1841.5	1836.9	191.1
ν_1 CH stretching	3006.5	3005.7	2969.8	2973.1	2981.0	17.5
RMSE	16.5	26	8	12	-	-

[a]aug-cc-pVTZ basis set.
[b]cc-pVTZ basis set from Ref. 187.
[c]experimental results from Ref. 181.
[d]Experimental intensities (in km/mol) from Ref. 182.

for the PES with a 20000 cm^{-1} (30000 cm^{-1}) cut-off using 75 neurons was 20 cm^{-1} (35 cm^{-1}), the test set RMSE for energies between 0 to 10000 cm^{-1} was 10 cm^{-1} (12.5 cm^{-1}) and 25 cm^{-1} (26.3 cm^{-1}) for points between 10000-20000 cm^{-1}. This demonstrates the quality of the PES in the lower energy region. A RMSE of 20 cm^{-1} should be sufficient for future quantum dynamics studies of HFCO. The RMSE could be reduced further by removing the validation set but this could lead to over-fitting and subsequent "holes" in the PES. A further minor decrease in the RMSE was found by going to large numbers of neurons (more than 100 NN) but this large number of fitting parameters make dynamics calculation very slow in MCTDH. An optimal number of 75 NN was selected for both the 20000 cm^{-1} and 30000 cm^{-1} cut-off potentials for calculating vibrational states using MCTDH. The MCTDH operator files, i..e, the fitting parameters, for the two PES are provided in Appendix B.

In comparing this current PES with previous fits, the Yamamato and Kato[132] (YK) PES has a RMSE of 1.5 kcal/mol (525 cm^{-1}) which is more than twenty five times larger than that of the present fit (20 cm^{-1}). Another PES by Wei and Wyatt[200] (WW) has a RMSE larger than the YK PES. These two PESs were used previously in both vibrational state computations[196,199,201] and quantum dynamics simulations.[126–128]

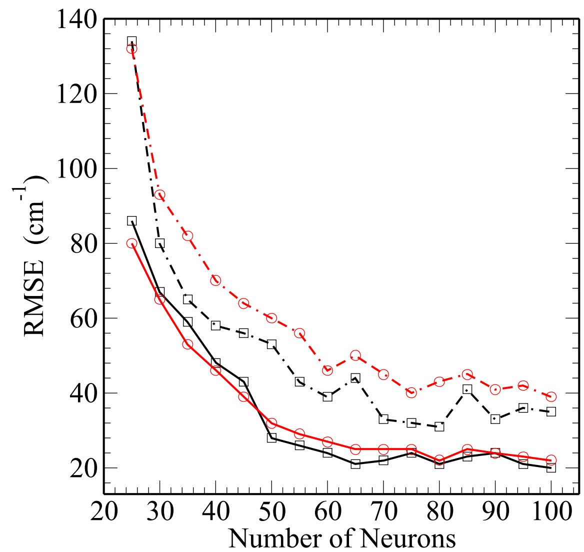

Figure 3.2: *RMSE versus Number of Neurons for the PES with a 20000 cm^{-1} (Solid) and 30000 cm^{-1} (Dashed) cut-off Energies. Training Set (Squares with Black) and TestSet (Circles with Red)*

3.3.3 Vibrational Energies

The quality of the PES is validated by computing and comparing fundamental, overtone and combination band vibrational energy levels with previous computational results[196,199,201] and experimental measurements.[196] The vibrational frequencies were computed using block improved relaxation[9] in the MCTDH software package[3] and the NN fit PES with the 20000 cm^{-1} cut-off energy. The energies were converged to 0.1 cm^{-1} for the first 150 states and were all assigned. The vibrational states were assigned using improved relaxation with initial guess method. State assignments were also verified by plotting the wavefunction probability density followed by counting number of nodes along specified modes. The vibrational energies determined based on this NN fit PES of CCSD(T)-F12/cc-pVTZ-F12 ab initio data are given in Table 3.5. The CCSD(T)-F12/NN results agree much better with experiment[196] than the previously available computations based on the YK or WW PESs. The RMSE of the states below 5000 cm^{-1} was 2.5 cm^{-1} which is much better than previous full dimensional calculation by Viel *et al.*[196] on the YK[132] and WW[200] PESs. Their calculations on the YK and WW PESs gave 28 cm^{-1} and 92 cm^{-1} RMSE, respectively. Most of the states were found to agree with those assigned by Viel *et al.*[196] albeit with energies much closer to the experimental measurements. However, new assignments were made for some states. The experimental peak at 4302.9 cm^{-1} was assigned previously as 002010 but, in the present work, it is assigned as the 100020 state with an energy of 4302.0 cm^{-1}. Interestingly, we found the 002010 state matches with the experimental peak at 4307.5 cm^{-1}; a peak assigned previously as the 100100 state which has an energy of 4291 cm^{-1} according to the present work. Another experimental peak at 4493.9 cm^{-1} was found to be the 001200 state while it was previously assigned as the 010102 state; the current results determine this 010102 state to have an energy of 4415 cm^{-1} which is far from experiment. The assignment of the 001200 state can be seen in Figure 3.3. From this plot, it is clear that there are two nodes along the HCO bending mode and a single node along the C=O stretching mode. An experimental peak at 4705.2 cm^{-1} is assigned by this work as 001031 while the

Table 3.5: *Selected Vibrational Energies (in cm^{-1}) for States up to 5000 cm^{-1} for HFCO from the Present PES Compared with Experimental Measurements and Previous Computations.*

Assignment ($n_1n_2n_3n_4n_5n_6$)	Expt[b]	This work	Ref. 196 WW	Ref. 200 YK	Ref. 201 YK[a]
000010	662.6	664.1	626.4	659.4	658.1
000001	1011.2	1012.8	968.8	1020.5	1019.2
010000	1064.9	1067.8	1017.8	1051.5	1049.5
000020	1324.1	1327.5	1255.1	1317.7	1314.8
000100	1342.3	1338.2	1371.1	1372.2	1370.3
010010	1719.3	1725.1	1639.5	1704.6	1699.0
001000	1836.8	1835.6	1770.5	1827.9	1821.3
020000	2115.6	2114.9	2029.2	2090.8	2085.3
010100	2412.0	2399.0	2376.1	2418.3	2412.9
001010	2494.2	2494.9	2393.4	2484.0	2474.4
001001	2841.0	2841.0	2727.5	2843.5	2833.3
011000	2895.0	2898.4	2787.1	2876.1	2863.9
100000	2981.2	2976.0	2974.4	3039.2	3003.2
001020	3150.6	3153.8	3016.2	3139.4	3126.2
002000	3652.8	3650.9	3526.7	3648.1	3623.7
001002	3838.1	3839.8	3686.9	3855.1	-
100020	4302.9	4301.6	4138.3	4304.3	-
002010	4307.5	4307.1	4335.9	4403.1	-
001200	4493.9	4495.7	4323.5	4458.8	-
002001	4653.1	4649.1	4474.4	4662.6	-
012000	4705.2	4710.9	4546.4	4698.9	-
001031	4817.6	4815.5	4649.9	4865.7	-
002020	4955.0	4959.0	4758.0	4960.4	-
	RMSE	2.5	92	28	12

[a] Vibrational assignments taken from Ref. 201 or present work.
[b] Experimental values from private communication as mentioned in Ref. 196.

previous work assigned it as the 001003 state. The 001003 state has a energy of 4832 cm^{-1} which is far from experiment.

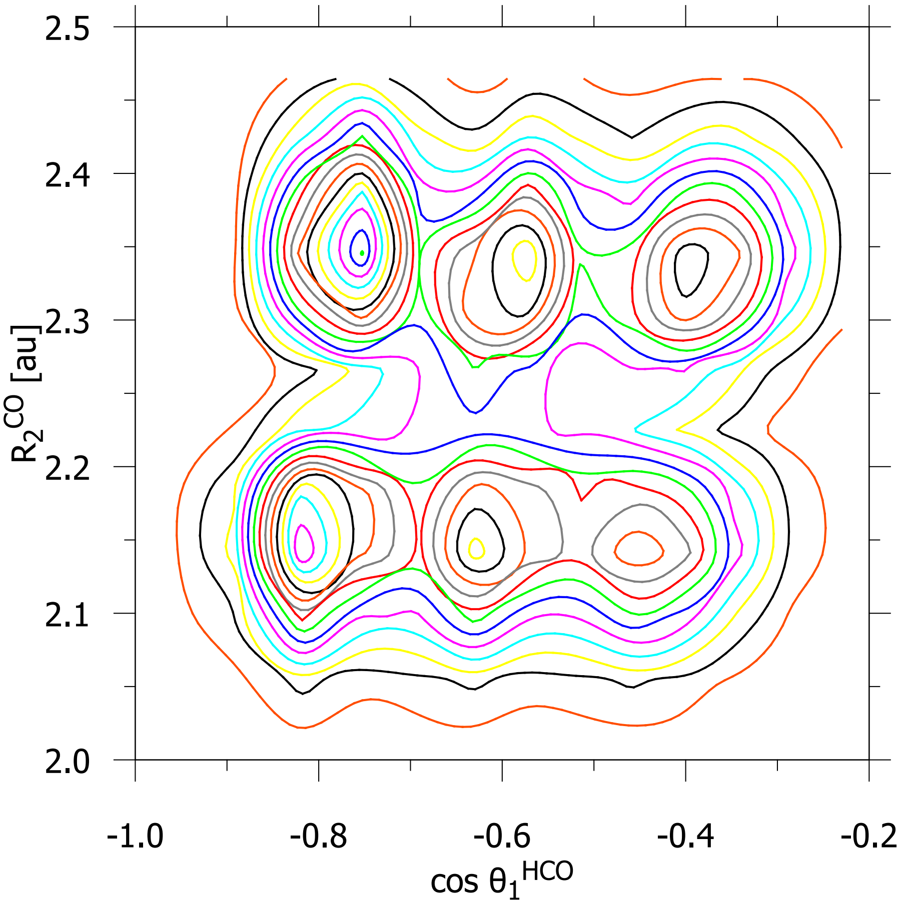

Figure 3.3: *Probability density plot of 001200 state. The state has experimental energy of 4493.9 cm^{-1} energy while caculated value is 4495.7 cm^{-1}. The contour plot was made at equilibrium geometry of other modes.*

During the state assignment, we found some states that were very close in energy with other states. The assignment of these states was made from (approximate) probabilities of the transitions, especially for combination modes. From the measured and calculated values for the intensities of the fundamentals,[128,181,182] see Table 3.4, states containing modes (ν_2 and ν_3) would be higher priority than weak modes in the case of a transition to a combination mode. For example, the experimental peak at 4705.2 cm^{-1} is in-between the computationally determined 4700.4 cm^{-1} and 4711.0

Table 3.6: *Computed Fundamental Vibrational Energies (in cm^{-1}) of DFCO on the Present PES Compared with Experimental Measurements and Previous Computations.*

Fundamental Mode	YK-MCTDH[204]	Expt.[214]	YK-Davidson[203]	This work
ν_1 CD stretch	2276.0	2261.7	2275.4	2258.2
ν_2 CF stretch	1066.0	1073.2	1066.2	1074.3
ν_3 CO stretch	1783.0	1796.8	1783.7	1795.3
ν_4 DCO bend	980.0	967.9	979.8	966.0
ν_5 FCO bend	652.0	657.5	653.0	658.7
ν_6 Out-of-plane bend	863.0	857.4	857.9[a]	859.2
RMSE	10.5	-	9.7	2.0

[a] Based on reported $2\nu_6$ value reported divided by 2.

cm^{-1} energy levels. The state with the energy of 4711.0 cm^{-1} was assigned to be the 012000 state, and the one at 4700.4 cm^{-1} was assigned to be the 110010 state. Here we assigned 012000 to be the experimental state of energy 4705.2 cm^{-1} as 012000 is a two mode combination state but the 110010 state involves three modes. Also, the 012000 state involves one quanta of excitation along the C-F stretching and 2 quanta of excitation along the C=O stretching which is much more probable as can be seen from the experimental intensities that the ν_2 and ν_3 modes are the most intense modes.

Additional tests of the PES in terms of vibrational state energies were carried out for DFCO. The fundamentals and other energy levels match well with experimental results. The fundamental frequencies determined along with previous computations and experimental measurements are provided in Table 3.6; other vibrational levels are given in Appendix B: Table B8. The previous MCTDH results based on a *potfit* of the YK PES have a RMSE 10 cm^{-1} for the fundamental frequencies while the results based on the present PES give a RMSE of only 2.0 cm^{-1}, reflecting the high quality of the NN PES.

3.4 Conclusion

We presented a new full dimensional (6D) potential energy surface for HFCO in a limited region describing the equilibrium geometry up to (and beyond) the transition state to unimolecular dissociation. The present work is the first direct fit of CCSD(T)-F12/cc-pVTZ-F12 ab initio data into a 6D PES using the neural network fitting procedure with exponential neurons. Previous 6D PESs generated using this approach have been re-fits of available analytical PESs. The NN sum-of-products form PES can be, and, in the present work, has been, used in MCTDH. Comparatively few randomly selected data points along with 1D and 2D grid data make this method more efficient that *potfit*. The quality of the fit depends upon the cut-off energy and the number of neurons; due to the presence of the validation set to prevent over-fitting, the RMSE of the fit eventually stops improving with an increased number of neurons. The present PES has a much smaller RMSE relative to the ab initio data (20 cm^{-1}) compared to the previous fit[132] (525 cm^{-1}) and is based on a much higher-level of electronic structure theory (CCSD(T)-F12/cc-pVTZ-F12 vs MP2/pVTZ). The vibrational state energies determined (up to 5000 cm^{-1}) based on the PES have a RMSE of only 2.5 cm^{-1} when compared to the experiment. The method can be applied to fit other 6D systems and, in principle, for large systems (although data sampling may become an issue). Further investigation for other molecules is underway. With the improvement in accuracy and its computational efficiency for use in MCTDH, the NN fit PES may overcome the weaknesses of the previous MP2/*potfit* PES for computations such as the (optimal) control of IVR in HFCO.[128]

Chapter 4

Fitting a 6D Asymmetric Double-Well Potential Energy Surface with Neural Network Exponential Fitting Functions: Application to HONO

4.1 Introduction

Nitrous acid, HONO, plays an important role in atmospheric chemistry, astrochemistry, and geochemistry.[215–222] HONO is formed in the atmosphere from water vapour, NO and NO_2 oxides, and it can be decomposed into OH and NO via photolysis. Hence HONO plays an important role in OH chemistry and that for the nitrogen oxides which are involved as catalysts for tropospheric ozone production.[223,224] While recent research focuses on the atmospheric impact of HONO, e.g., the investigation of the gas phase sources of the HONO in the troposphere,[225] HONO is also of fundamental theoretical and experimental interest, and in particular, its spectroscopy, structure, and dynamics in the electronic ground and first few excited states. Many important photofragmentation reactions and the UV-VIS absorption spectrum involving the first singlet excited state have been studied experimentally[226–230] and theoretically.[231–235] However, in this chapter, we are solely interested in the ground electronic state.

Besides its photophysical and photochemical importance, HONO is one of the smallest molecules to exhibit trans-to-cis isomerization in its ground electronic state. The structures (bond lengths and bond angles) and dipole moments have been measured for both cis- and trans-HONO.[236–240] Vibrational frequencies of fundamental modes as well as overtones and several combination modes for both isomers have been determined experimentally.[237,238,241] The relative stability of the trans- and cis-isomers has been of interest, and it has been determined that trans-HONO is more stable than cis-HONO.[242] The trans$\leftrightarrow$cis barrier height has been examined both theoretically and experimentally and shown to be between 3050 to 4340 cm^{-1}.[242] Many of the experiments exploring the isomerization and spectroscopy have been carried out in cold matrices.[243–254] The cis-trans isomerization process was first observed by monitoring the OH stretching mode[243] in an N_2 matrix. Khriachtchev *et al.*[254] showed that exciting the first overtone of the OH or N=O stretching mode accelerates the trans-cis isomerization process in a Kr matrix. From the matrix assisted experiments, it was concluded that the cis-to-trans conversion is faster than the trans-to-cis process; a conversion that exhibit strong mode specificity. Interestingly, in the gas phase, neither the cis nor trans OH stretching mode can induce the isomerization process.[131] To date, no experimental evidence exists to support the 1,3 H exchange between the two oxygen atoms. On the other hand, for the HNO_2 tautomer experimental fundamental mode frequencies[255] are available but no specific examination of the HONO-HNO_2 rearrangement has been made. The spectroscopy and intramolecular dynamics of HONO can be investigated theoretically to understand these various experimental measurements.

The starting point of many theoretical studies is an evaluation of the underlying PES. The S_0 PES has been examined previously by a variety of different methods with a focus on specific aspects of the spectroscopy or dynamics. A 6D PES based on interpolating DFT energies was constructed to study vibrational spectra by Luckhaus.[256] Anharmonic vibrational frequencies were calculated using the VSCF method based on an MP2/6-311++G(2d,2p) computed PES.[254] A recent analytical PES of HONO was constucted using MP4/6-31++G(d,p) computed ab initio energies and the interpolating moving least-squares (IMLS) approach by Pham and Guo[257] to investigate the reaction rate of cis-trans isomerization. A very recent article studied anharmonic vibrational frequencies of cis-HONO and DONO in a variational calculation based upon ab initio electronic structure at the MP2/aug-cc-pVTZ level of theory.[258]

Most relevant for the present study, a six dimensional PES of HONO encompassing the cis- and trans-isomers was fit to the sum-of-products form based on the 638 CCSD(T)/cc-pVQZ(-g) ab initio points.[131] The analytical surface was used to compute vibrational states up to 3650 cm^{-1} in a full dimensional calculation using MCTDH.[3] In a series of papers, Gatti and co-workers[129,130,177] explored the intramolecular dynamics of HONO with and without an external laser field in the cis-trans region using this PES (and a DFT-based dipole moment surface, when needed). These simulations are targeted to the available experiments[259–261] studying laser control of torsional motion of molecules. However, questions remain as to whether the PES of Richter et al. is sufficiently accurate for quantum control studies. Several aspects could be considered regarding the previous PES: (i) Truncated basis sets were used, (i.e., cc-pVQZ removing the g-functions). As the basis was designed including the g-functions, it is not entirely clear what effect the truncation might have. (ii) The use of diffuse functions in the basis (aug-) could be examined. (iii) The PES obtained is based upon only 638 (judiciously chosen) data points. Therefore, in the present work, we aim to determine, and test, a new PES for HONO.

If the analytical PES is in a sum-of-products form, it greatly reduces the computational cost when using MCTDH to study the quantum dynamics. One possible approach to obtain the sum-of-products form is to use *potfit*.[87,88] However *potfit* requires data on a grid and beyond 6D, is impossible; the limit on dimensionality can be circumvented using multi-grid *potfit*.[262] An alternative method for obtaining sum-of-products form was developed by Manzhos and Carrington using a 1-layer neural network with exponential neurons;[1,2] what is referred to here as NN-expnn. While Manzhos and Carrington focused on refitting existing analytical PESs, we have extended the NN-expnn method to directly fit ab initio data and provide an MCTDH operator file for the PES,[8] see Chapters 2 and 3.

In this chapter, we discuss the construction of a highly accurate NN-expnn fit

PES for the S_0 state of HONO in the restricted region consisting of cis-HONO, trans-HONO and the transition state of cis-trans conversion. Two different ab initio electronic structure approaches are used to determine the data upon which the fit is based: (i) Explicitly correlated coupled cluster single double and perturbative triple excitation, CCSD(T)-F12, with the cc-pVTZ-F12 basis set or (ii) CCSD(T) computations extrapolated to the complete basis set limit. This chapter reveals new aspects of the accurate PES as well as conveys the potential of using NN-expnn for other molecules.

The chapter is organized as follows: Section 4.2 presents the computational methods utilized in this work, including the ab initio electronic structure techniques (Sec. 4.2.1), the Neural Network PES fitting with exponential neurons approach (Sec. 4.2.2), the method implemented in MCTDH for determining the vibrational states (Sec. 4.2.3). In Section 4.3, the results of the ab initio computations (including stationary point geometries and relative energies), the PES fits and the vibrational frequencies including state assignments are discussed. A summary and possible future directions are presented briefly in Section 4.4.

4.2 Computational Methods

4.2.1 Ab initio Electronic Structure Techniques

The explicitly correlated coupled cluster method with single, double and perturbative triple excitations,[15,16] CCSD(T)-F12, was used with the cc-pVTZ-F12 basis set[47] in the majority of the ab initio electronic structure computations. The lowest energy equilibrium geometry for the S_0 state of HONO (the trans-isomer) was determined at the CCSD(T)-F12/cc-pVTZ-F12 level of theory using numerical gradients. All other stationary points, i.e., intermediates and transition states, on the S_0 surface were determined at the same level of theory. For geometry optimization of the transition states, the initial Hessian was determined at the MP2[13,14]/aug-cc-pVTZ[45,46] level of theory. The harmonic vibrational frequencies were computed using numerical Hessians to verify the nature of the stationary points (minima or transition states).

The CCSD(T)-F12 method provides two energies, F12A and F12B (see Ref. [16 and 15] for details); the F12A energy is utilized for the PES fitting, see Section 4.2.2, and all relative energies refer to F12A values. The CCSD(T)-F12 computations were carried out using the Molpro electronic structure package.[18] Geometry optimizations and single point energy calculations were performed using the default convergence criteria.

As an alternative to and as a point of comparison for the CCSD(T)-F12/cc-pVTZ-F12 PES, ab initio data were also determined through extrapolation to the complete basis set (CBS) limit. The basis set extrapolation[50–52] was performed using the CCSD(T)/aug-cc-pVTZ, aug-cc-pVQZ and aug-cc-pV5Z computed energies. These basis sets will sometimes be abbreviated as AVTZ, AVQZ, and AV5Z, respectively. The correlation energy, E^{corr}, is

$$E^{corr} = E^{tot} - E^{SCF}, \tag{4.1}$$

where E^{tot} is the total energy and E^{SCF} is the SCF energy. The total energy at the complete basis set limit is then

$$E^{tot}_{CBS} = E^{SCF}_{CBS} + E^{corr}_{CBS}, \tag{4.2}$$

where E^{corr}_{CBS} is the extrapolated correlation energy and the complete basis set SCF energy, E^{SCF}_{CBS}, is taken to be the CCSD(T)/aug-cc-pV5Z SCF energy, E^{SCF}_{AV5Z}. From aug-cc-pVQZ to aug-cc-pV5Z, the SCF energy change is not significant compared to the correlation energy change, e.g., at the trans-isomer equilibrium geometry E^{SCF}_{AV5Z} - E^{SCF}_{AVQZ} = 0.0031 au, while the total energy change, E^{tot}_{AV5Z} - E^{tot}_{AVQZ} = 0.01692 au. Three-point and two-point extrapolation to the complete basis set limit were performed using the following equations:

$$E(x) = E_{CBS} + A\ e^{-Bx} \tag{4.3}$$

and

$$E(x) = E_{CBS} + A\ x^{-3}. \tag{4.4}$$

Equation (4.3) is for three-point extrapolation where E_{CBS} is the complete basis set limit energy while A and B are the (other) unknown parameters to be determined.

The value of x is equal to L_{max} (or l_{max}), i.e., the highest orbital angular momentum in the basis. The value of x equals 3, 4, and 5 for the aug-cc-pVTZ, aug-cc-pVQZ and aug-cc-pV5Z basis sets, respectively. A minimum of three different basis sets are required to use the three point extrapolation method as in Eq.(4.3); the use of the aug-cc-pVDZ basis set in the extrapolation is discouraged and, hence, we do not use it here. Equation (4.4) is used for two point extrapolation where x is same as in Equation (4.3). The Molpro software package[18,19] was used for the CCSD(T)/aug-cc-pVXZ (X=T, Q, Z) ab initio electronic structure computations described above.

To compare with the CCSD(T)-F12/cc-pVTZ-F12 harmonic frequencies as well as those computed using MCTDH with the full-dimensional PES, the anharmonic (and, hence, corresponding harmonic) fundamental infrared frequencies as well as intensities for the cis-HONO and the trans-HONO isomers were computed at the MP2/aug-cc-pVTZ and CCSD(T)[14]/aug-cc-pVTZ levels of theory using the CFOUR software package.[124] The harmonic frequencies were computed using analytical gradients and the anharmonic frequencies were determined using second-order perturbation theory (VPT2)[118–120] in CFOUR.

4.2.2 Neural Network Fitting of the Potential Energy Surface

For fitting the PES, the HONO molecule is represented in a valence (or internal) polyspherical coordinate system as shown in Fig. 4.1. The N=O, O-N and O-H bond distances are assigned as R_1, R_2, and R_3, respectively. The O=N-O, H-O-N and dihedral angles are designated as θ_1, θ_2 and ϕ . The PES was restricted to the region of the S_0 surface which contains the cis-HONO and trans HONO isomers as well as the corresponding transition state. The restriction was accomplished using an energy cut-off (7500 cm^{-1}) and suitably chosen grid lengths along the six physical coordinates. The coordinate ranges are given in Table 4.1; the table also contains information related to the MCTDH computations, see Sec.4.2.3. The PES fitting utilized the Neural Network toolbox (nftool) implemented in MATLAB. Rather than using the default sigmoidal functions available in MATLAB, an exponential fitting

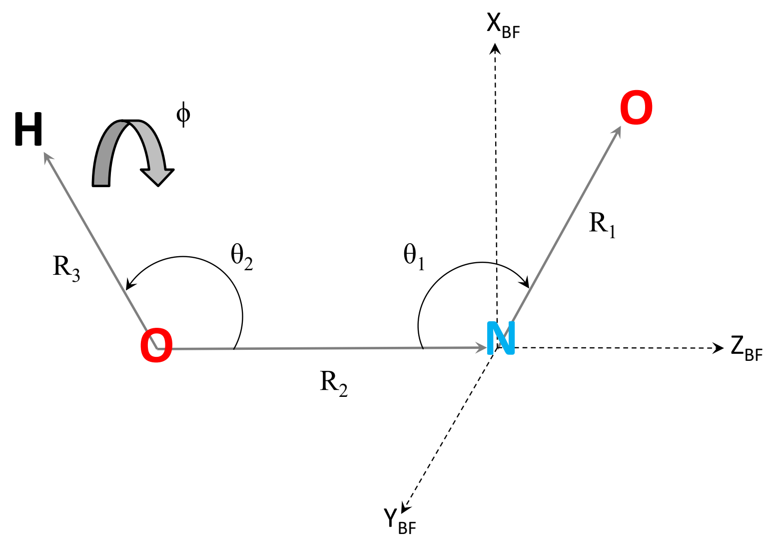

Figure 4.1: *The HONO molecule in the valence polyspherical coordinate system.*

Table 4.1: *Grid lengths used for the physical coordinates for the HONO PES. Also provided are the type and number of primitive basis functions and single particle functions (SPFs) used in the MCTDH computations (see Sec.4.2.3).*

Coordinates	$R_1^{N=O}$	$\cos\theta_2^{HON}$	$\cos\theta_1^{ONO}$	R_2^{ON}	R_3^{OH}	ϕ
Grid Length [min , max]	[1.9,2.6]	[-0.65,0.25]	[-0.65,-0.1]	[2.1,3.25]	1,3,2.45]	[0,3.14]
Primitive Basis	13	18	16	16	18	32
Basis Function Types	HO	HO	HO	HO	HO	sin/cos[a]
SPF	16^b		16^c		5	11

[a] sin DVR for A' and cos DVR for A'' state computations.
[b] For the ($R_1^{N=O}$, $\cos\theta_2^{HON}$) combined mode.
[c] For the (R_2^{ON}, $\cos\theta_1^{ONO}$) combined mode.

function (referred to as an exponential neuron)[1,263] was utilized to generate a sum-of-products form for the analytical potential energy surface. The sum-of-products form is particularly important for computational efficiency in studying quantum dynamics using the MCTDH approach.[3–7] The sum-of-products form is

$$V^{NN}(x_1, x_2, ...x_D) = \sum_{q=1}^{N}(e^{b_q}C_q)\prod_{p=1}^{D} e^{w_{qp}x_p} + V_{shift} = \sum_{q=1}^{N}\tilde{c}_q\prod_{p=1}^{D} e^{w_{qp}x_p} + V_{shift}. \quad (4.5)$$

Here V^{NN} is the neural network fitted PES as a function of the number of neurons (N) and the x_1 to x_D degrees of freedom; we will refer to potentials fit to this form as NN-expnn PESs. The fitting parameters consist of a constant shift (V_{shift}), weights (w_{qp}) and biases (b_q); the biases are incorporated into the constant $\tilde{c}_q$. The final form is a sum over all the neurons and a product over all dimensions.

To generate data for the PES fitting, one-dimensional (1D) and two-dimensional (2D) grids were utilized along the physical coordinates from both the equilibrium geometries (cis- and trans-) and from the transition state for cis-trans isomerization. In addition to the 1D and 2D grid data, geometries were selected randomly from the 6D grid. However, they were restricted using an energy filter,[2,77,81] i.e.,

$$\frac{E_{cut} - V^0_{tot}(x_i)}{E_{cut}} > f_i \quad (4.6)$$

where E_{cut} is a chosen cut-off energy and f_i is a random number between 0 to 1. The total (approximate) energy $V^0_{tot}(x_i)$, that was filtered was determined by summing over the 1D potentials from the trans-HONO equilibrium geometry. Note that if the final ab initio energy exceeded the cut-off energy, it was discarded from the data set used for fitting.

To obtain the sum over 1D energies, $V^0_{tot}(x_i)$, the potentials for the bond distances (R_1, R_2, and R_3) were fit to Morse functional form:

$$V(r_i) = A_0[1 - e^{-A_1(r_i - A_2)}]^2. \quad (4.7)$$

The bond angles (in their cosine form) were fit to a 4th order polynomial, i.e.,

$$V(\cos\theta_i) = A_0 + A_1\cos(\theta_i) + A_2(\cos\theta_i)^2 + A_3(\cos\theta_i)^3 + A_4(\cos\theta_i)^4. \quad (4.8)$$

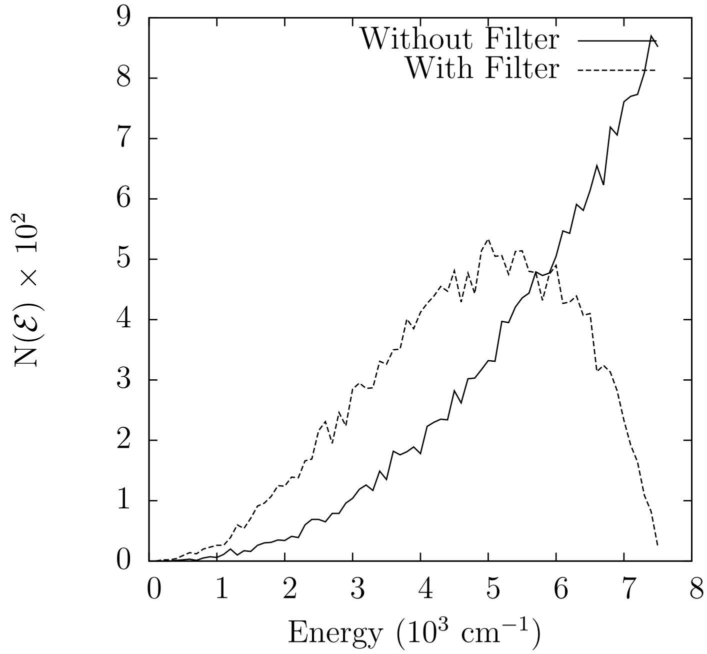

Figure 4.2: *Distribution of energy points with and without the energy filter, see Eq.(4.6). The distribution is taken over 20000 points generated from the sum over 1D analytical surface, $V^0_{tot}(x_i)$, for energies up to 7500 cm^{-1}, where N(ϵ) gives the number of points found within a 250 cm^{-1} energy window.*

The dihedral angle was fit to cos(nx) form:

$$V(\phi) = A_0 + A_1\cos(\phi) + A_2\cos(2\phi) + A_3\cos(3\phi) + A_4\cos(4\phi). \qquad (4.9)$$

The fitting parameters are presented in Tables C4 and C5 in Appendix C. As the energy from the sum-over 1D cut potential will always be greater than the anharmonic energy at any geometry, the filter puts more data in the lower energy region of the PES. Using the energy filter, the selected random data are distributed more strongly/densely around the lower energy region, see Fig.4.2. Therefore, the total data set for the PES fitting consists of random energy-filtered data plus 1D and 2D grid data.

The random data set was split into training, testing and validation sets. The training set contains 80% of the random data plus the 1D and 2D grid data at the equilibrium (cis- and trans-) and the cis $\leftrightarrow$ trans transition state geometries. The training set was used to fit the PES. A test set of 10% of the random data was used to test the quality of the fit at the end of the fitting procedure. A validation set of 10% of the random data was used to guide the fit to avoid over-fitting of the training set. The Levenberg-Marquardt algorithm was used to determine the fitting parameters, see Eq.(4.5). Before the fitting is initiated, all data (coordinates and energies) were scaled to lie between [-1, 1] by

$$X_{scaled} = \frac{X - x_{min}}{x_{max} - x_{min}} \tag{4.10}$$

where the maximum and minimum of a particular coordinate (or energy) are x_{max} and x_{min}. X is the data before scaling which after scaling appears as X_{scaled}. The scaled data leads to smooth convergence and a gradually decreasing RMSE for the fit as the number of neurons is increased. A one-stage fitting procedure in a loop over 10-25 iterations has been applied in this work to further reduce the RMSE.

4.2.3 Eigenenergy Determination

Block improved relaxation[9] as implemented in the Heidelberg Multiconfiguration time-dependent Hartree (MCTDH) package[264] was used to compute the vibrational state energies. Block improved relaxation enables accurate computation of the vibrational states in a designated energy window. For efficiency in MCTDH, the wavefunction, kinetic energy operator (KEO), and the potential energy operator must all be in sum-of-products form. The NN-expnn fitted PES for HONO is designed to be in a sum-of-products form. In the present work, we have used the KEO from previous theoretical studies of HONO by Gatti and co-workers.[129,130,177] As the molecule is represented in a polyspherical coordinate system, the final form of the KEO is a sum-of-products for single mode operators. Primitive grids for the bond angles and bond distances use harmonic oscillator (HO) basis functions. The out-of-plane bending mode was presented as sin or cos DVR. The cos DVR is for computing A'' states and the sin DVR is for computing A' states. The grid sizes and the number of primitive basis functions are given in Table 4.1. Combination modes have been used for the single particle functions (SPFs) grid. As ONO bending and ON stretching modes are strongly coupled to each other, these two modes were used as two mode combination in the SPF basis. Also, HON bending and N=O stretching modes were used as combination modes in the SPF. The number of SPFs and the mode combinations are also provided in Table 4.1. Improved relaxation[7,125,265,266] was used to obtain wave functions and assign the vibrational states.

4.3 Results and Discussion

4.3.1 Stationary Points, Structure and Relative Energies

The CCSD(T)-F12/cc-pVTZ-F12 optimized geometries (for minima and transition states) and the corresponding relative energies (as compared to the energy of the trans-HONO global minimum) are given in Table 4.2 and 4.3, respectively. The structures include cis-HONO, trans-HONO, and the cis↔trans transition state. The geometries of the HNO_2 tautomer as well as the transition states for 1,3 and 1,2 H-atom migration are given in Table C1 in Appendix C. The harmonic frequencies used to determine the ZPE corrections for each species are given in Table 4.4. Anharmonic fundamental frequencies can also be used to determine the ZPE (see Table C2) of a stationary point, but the ZPE of the transition states are harder to determine, thus anharmonic ZPE corrections to the transition states are rarely performed. The results for the geometries are in excellent agreement (bond lengths within 0.01 $\mathring{A}$ and bond angles within 0.1°) with the experimental[241,267] and the previous theoretical calculations,[131,256,268] including for the transition state. The ground state minimum energy structure of the HONO molecule is the trans-HONO conformer. The relative energies and structures of all the intermediates and transition states on the S_0 surface are shown schematically in Figure 4.3. The cis-/trans-HONO energy difference has been considered in several previous studies (experiment[239,242,243,252] and theory[256,269–273]). At the CCSD(T)-F12/cc-pVTZ-F12 level of theory (including ZPE), the cis-HONO minimum is just 122 cm^{-1} above the trans-HONO minimum. The cis-trans energy difference using different computational methods is plotted in Figure 4.4; the corresponding numerical data is given in Table 4.5. The ZPE corrected cis-trans energy

Table 4.2: *CCSD(T)-F12/cc-pVTZ-F12 (F12) and CCSD(T)/aug-cc-pVXZ (X=Q, 5) optimized geometries including bond distances (Å) and angles (degrees), of trans-HONO, cis-HONO and the transition state ($TS^{\#}_{cis\leftrightarrow trans}$). Also provided are experimental and previous theoretical results.*

Isomers	Methods	$R_1^{N=O}$	R_2^{ON}	R_3^{OH}	θ_1^{ONO}	θ_2^{HON}	ϕ
	Expt.[267]	1.169	1.428	0.957	110.70	102.10	180.00
trans-HONO	F12	1.170	1.419	0.966	110.69	102.27	180.00
	AVQZ	1.171	1.423	0.966	110.68	102.22	180.00
	AV5Z	1.171	1.420	0.966	110.69	102.27	180.00
	Ref [131][a]	1.170	1.426	0.964	110.70	101.90	180.00
	Ref [256][b]	1.166	1.433	0.969	111.20	102.90	180.00
	Ref [268][c]	1.173	1.453	0.966	110.50	101.40	180.00
	Expt.[241]	1.185	1.390	0.978	113.60	104.00	0.00
cis-HONO	F12	1.183	1.385	0.976	113.24	104.83	0.00
	AVQZ	1.184	1.387	0.976	113.26	104.80	0.00
	AV5Z	1.183	1.385	0.975	113.24	104.83	0.00
	Ref [131][a]	1.183	1.390	0.974	113.20	104.40	0.00
	Ref [268][c]	1.187	1.414	0.974	113.00	104.30	0.00
$TS^{\#}_{cis\leftrightarrow trans}$	F12	1.161	1.492	0.967	111.19	103.44	86.90
	AVTZ	1.165	1.507	0.970	111.11	103.08	86.71
	AVQZ	1.162	1.496	0.967	111.20	103.39	86.85
	Ref [131][a]	1.164	1.506	0.962	110.50	100.70	86.40

[a] CCSD(T)/cc-pVQZ; [b] CCSD(T)/TZP; [c] CCSD(T)/TZ2P; [a] B3LYP/6-311++G**

Table 4.3: *Relative energies (in cm^{-1}) without (ΔE) and with (ΔE_{ZPE}) zero-point energy corrections of HONO isomers on the S_0 PES at the CCSD(T)-F12/cc-pVTZ-F12 level of theory compared with previous calculations. Energies reported relative to the lowest energy trans-HONO isomer.*

Intermediates	ΔE (cm^{-1})	Δ_{ZPE}	ΔE_{ZPE}	Previous
trans-HONO	0	0	0	0
cis-HONO	124.0	-2.0	122.0	130.0[a]
H-NO_2	2769.3	379.8	3149.1	2783.2[b]
$TS^{\#}_{cis\leftrightarrow trans}$	4070.4	-455.8	3614.6	4105.0[c]
$TS^{\#}_{trans\leftrightarrow H-NO_2}$	20656.5	-1174.9	19481.6	19290.3[b]
$TS^{\#}_{1,3-Hshift}$	10778.3	-919.4	9859.9	9896.5[b]
OH+NO[e]	18211.6	-1611.2	16600.2	16772.0[d]

[a] Experimental results from Ref. 242; [b] B3LYP/6-311G(3df, 3pd) results from Ref. 272; [c] CCSD(T)/aug-cc-pVQZ (-g functions) results from Ref. 131; [d] DROPS measured results from Ref. 274; [e] Open shell optimized RCCSD(T)-F12[206]/cc-pVTZ-F12

difference using the CCSD(T)-F12/cc-pVTZ-F12 level of theory is near the complete basis set (CBS) limit as one can observe from the the CCSD(T)/aug-cc-pVXZ (X=T, Q, and 5) energy differences; the CBS limit (including ZPE) has not been determined since the geometries are subtly different for different basis sets.

Table 4.4: *Harmonic vibrational frequencies and zero point energies (ZPE) (both in cm^{-1}) for the trans-HONO, cis-HONO, HNO_2, TS_ct (transition state of cis-trans isomerization), TS_12(transition state of trans-HONO tautomerization to H-NO2) and TS_13 (transition state of 1,3-H migration of Hydrogen). All results determined at the CCSD(T)-F12/cc-pVTZ-F12 level of theory.*

Frequencies	trans	cis	HNO_2	TS_ct	TS_12	TS_13	OH+NO
	577.0	649.0	788.0	593.0(i)	2125.5(i)	1962.3(i)	
	636.0	679.0	1040.3	555.7	465.2	1019.3	
	836.0	899.0	1385.5	788.4	692.0	1238.4	
	1320.0	1350.0	1511.5	1121.2	1293.4	1283.2	
	1732.0	1677.0	1649.4	1730.7	1584.2	1366.2	1916.7
	3780.0	3623.0	3265.8	3773.3	2496.3	2135.2	3741.9
ZPE	4440.5	4438.5	4820.3	3984.7	3265.6	3521.1	2829.3

The global PES is complicated with several closely spaced (in terms of relative energies) intermediates. The cis and trans isomers are separated by a transition state

Table 4.5: *The energy difference (in cm^{-1}) between trans-HONO and cis-HONO without ZPE correction (ΔE) and with ZPE correction (ΔE_{ZPE}) as determined using various levels of theory.*

Method	ΔE(cm^{-1})	ΔE_{ZPE}(cm^{-1})
MP2 /aug-cc-pVTZ	179.5	198.9
CCSD(T)/aug-cc-pVTZ	167.9	171.4
CCSD(T)/aug-cc-pVQZ	136.0	137.7
CCSD(T)/aug-cc-pV5Z	122.4	127.7
CCSD(T)-F12A/cc-pVTZ-F12	122.0	120.0
CCSD(T)-F12B/cc-pVTZ-F12	124.0	122.0

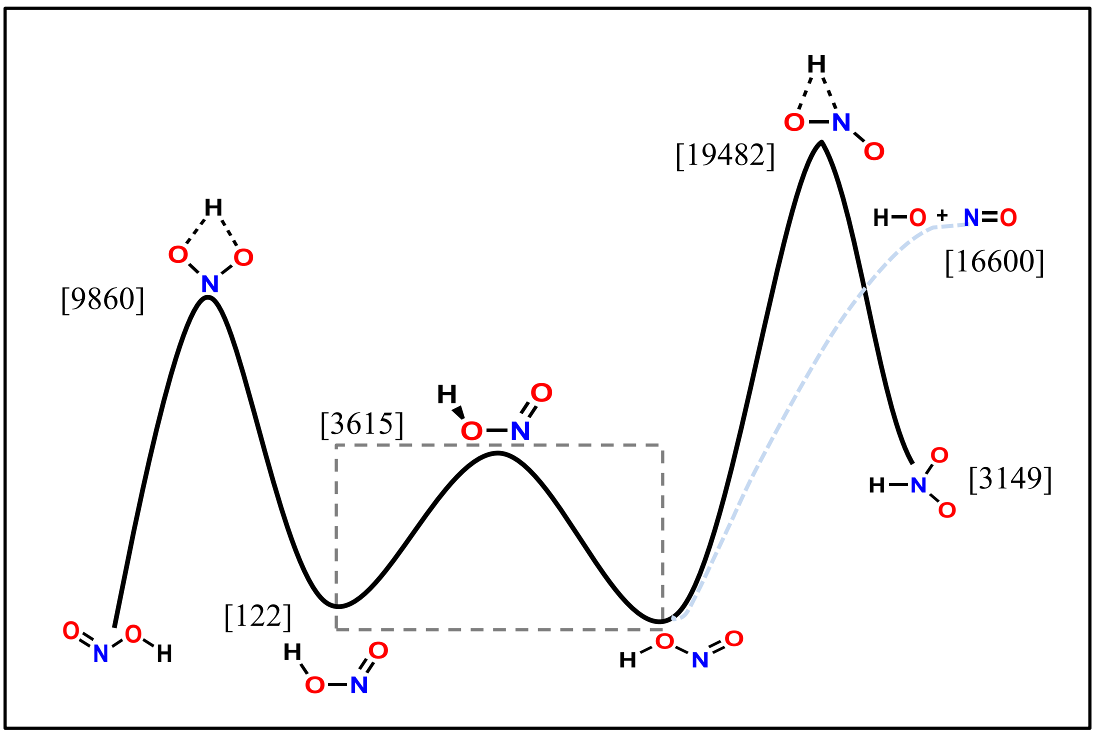

Figure 4.3: *Schematic of the stationary points on the S_0 PES of HONO. Relative energies including ZPE (as compared to trans-HONO) computed at the CCSD(T)-F12/cc-pVTZ-F12 level of theory are also provided.*

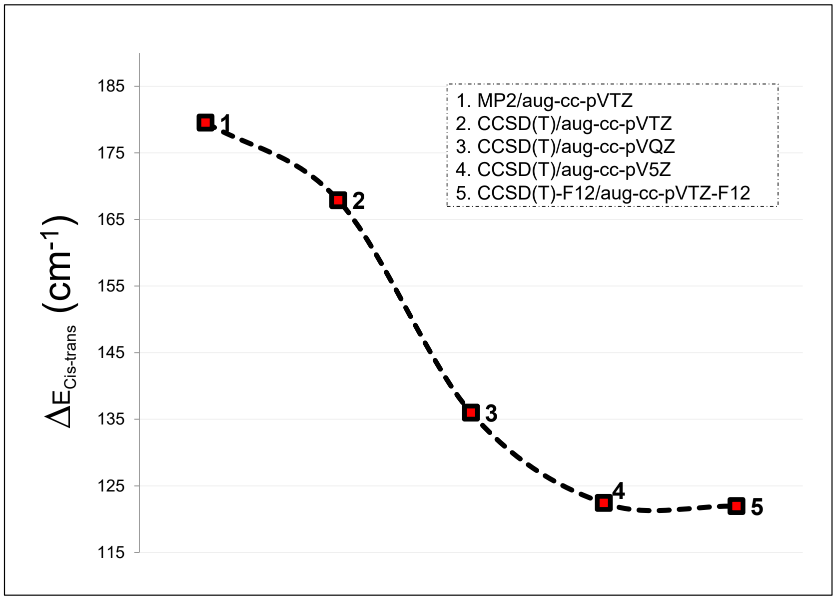

Figure 4.4: *Cis-trans energy difference including ZPE ($\Delta E_{cis \leftrightarrow trans}$) using different computational methods.*

with an energy of 3615 cm^{-1} (relative to the trans- minimum). The CCSD(T)-F12/cc-pVTZ-F12 value is comparable to the previous theoretical[256,269–273] and experimental[239,242,243,253] estimation of the barrier, i.e., values between 3050 - 4100 cm^{-1}. The transition state for 1,3 H-atom migration which also connects the cis- and trans- isomers, has a relative energy (including ZPE) of 9860 cm^{-1}, which is high relative to the cis-trans region, including the transition state, of the PES. The HNO_2 tautomer has an energy (including ZPE) of 3149 cm^{-1} above the minimum energy trans isomer. However, accessing the HNO_2 tautomer is energetically unfavourable as the energy barrier is the highest on the PES (19482 cm^{-1}). The experimental dissociation barrier was reported to be 16772 cm^{-1}, as determined in a double-resonance overtone photofragmentation spectroscopy (DROPS) experiment by Rizzo and co-workers.[274] In this chapter, the dissociation barrier is calculated to be 16660 cm^{-1} above the trans- minimum. Based on the relative energetics and geometries of the stationary points on the global PES, the cis-trans isomerization process can be captured in a more localized PES by restricting the cut-off energy to 7500 cm^{-1} and the bond lengths and bond angles to the grids discussed (see Table 4.1) such that it avoids the 1,3 H-atom migration transition state and the equilibrium HNO_2 tautomer.

4.3.2 Harmonic and Anharmonic Frequencies

To provide comparisons for the MCTDH determined vibrational frequencies, see Section 4.2.3, the harmonic frequencies have been determined using several methods/basis set combinations: MP2/aug-cc-pVTZ, CCSD(T)/aug-cc-pVXZ (X=T, Q, 5), and CCSD(T)-F12/cc-pVTZ-F12. The fundamental frequencies of trans-HONO are given in Table 4.6 and for cis-HONO in Table 4.7; the experimental measurements are provided for comparison. For the trans-HONO isomer, the RMSD with respect to the experiment is 72 cm^{-1} using MP2 whereas it is 73.0, 85.0 and 86.6 cm^{-1} for CCSD(T) with the aug-cc-pVTZ, aug-cc-pVQZ and aug-cc-pV5Z basis sets, respectively. Perhaps, surprisingly, the agreement between the fundamental harmonic frequencies and experiment gets worse when increasing the size of the basis. The RMSE for the CCSD(T)-F12/cc-pVTZ-F12 computed harmonic frequencies of trans-HONO was 86.6 cm^{-1}. Similar trends were found for the cis-HONO isomer. The RMSEs were 74.0, 78.0, 88.0, 91.0 and 89.0 cm^{-1} for the MP2, CCSD(T)/aug-cc-pVXZ (X=T, Q, 5) and CCSD(T)-F12/cc-pVTZ-F12 methods, respectively.

The anharmonic fundamental frequencies at the MP2/aug-cc-pVTZ and CCSD(T)/aug-cc-pVTZ levels of theory are presented in Table 4.8 (for trans-HONO) and in Table 4.9 (for cis-HONO). As expected the anharmonic frequencies exhibit significantly better agreement with the experiment than the harmonic results. For the CCSD(T)/aug-cc-pVTZ computed anharmonic frequencies, the RMSE of trans-HONO is 8.6 cm^{-1} and for the cis-HONO isomer, the RMSE is 9.0 cm^{-1}.

4.3.3 Neural Network PES Fitting

The PES fitting has employed two different approaches for generating the energy data: (i) energy from the previous[131] analytical potential energy surface and (ii) high level ab initio data. The use of the analytical PES permitted the exploration of the parameters defining the data sampling that could impact the quality of the

Table 4.6: *Harmonic frequencies (in cm^{-1}) of the fundamental modes for trans-HONO. The intensities (in km/mol) are provided when determined.*

Mode	MP2/AVTZ[a]	CCSD(T)			F12[b]	Expt.[c]
		AVTZ[a]	AVQZ	AV5Z 5		
OH	3754.8 (90.4)	3760.0 (72.9)	3779.3	3782	3780.0	3590.7
N=O	1659.9 (108.6)	1715.4 (133.2)	1728.3	1729.6	1732.0	1699.8
HON	1283.4 (174.5)	1306.1 (170.1)	1315.7	1317.0	1320.0	1263.1
O-N	805.3 (159.4)	815.9 (145.6)	830.0	833.7	836.0	790.1
ONO	602.5 (196.0)	617.4 (121.8)	630.4	634.0	636.0	595.6
Torsion	586.5 (99.3)	565.1 (97.2)	575.7	576.0	577.0	543.8
RMSE	71.9	72.6	84.6	86.4	86.5	-

[a] Harmonic frequencies and intensities from CFOUR software[124]
[b] CCSD(T)-F12/cc-pVTZ-F12 level of theory
[c](Torsion, ONO bend) from Ref. 275; (ON streching, HON bend) from Ref. 276; N=O stretching from Ref. 237; and OH stretching from Ref. 277

Table 4.7: *Harmonic vibrational frequencies (in cm^{-1}) of the fundamental modes of cis-HONO. The intensities (in km/mol) are provided when determined.*

Mode	MP2/AVTZ[a]	CCSD(T)			F12[b]	Expt.[c]
		AVTZ[a]	AVQZ	AV5Z		
OH	3591.2 (37.6)	3608.4 (29.3)	3622.7	3625.6	3623.0	3426.2
N=O	1610.7 (141.7)	1658.3 (166.5)	1670.4	1674.0	1677.0	1640.5
HON	1320.2 (7.0)	1337.4 (9.6)	1348.0	1351.2	1350.0	1302.0
O-N	884.2 (359.4)	876.4 (298.5)	895.0	898.3	899.0	851.0
ONO	634.0 (36.3)	631.9 (26.2)	645.4	648.7	649.0	609.0
Torsion	693.7 (97.7)	667.5 (97.3)	681.4	685.0	679.0	638.5
RMSE	74.0	78.1	88.3	90.6	89.4	-

[a] Harmonic frequencies and intensities from CFOUR software;[124] [b] CCSD(T)-F12/cc-pVTZ-F12 level of theory; [c] From Ref. 241

Table 4.8: *Anharmonic frequencies (in cm^{-1}) and in parenthesis corresponding intensities (in km/mol) of trans-HONO.*

Mode	MP2/AVTZ	CCSD(T)/AVTZ	Experiment[e]
OH	3575.0 (76.7)	3576.0 (59.2)	3590.7
N=O	1633.1 (109.8)	1690.0 (141.8)	1699.8
HON	1233.4 (163.4)	1259.0 (159.5)	1263.1
O-N	756.2 (121.3)	785.8 (127.9)	790.1
ONO	565.7 (231.2)	596.0 (131.4)	595.6
Torsion	551.2 (96.5)	534.0 (94.3)	543.8
RMSE	35.8	8.6	-

[e](Torsion, ONO bend) from Ref. 275; (ON streching, HON bend) from Ref. 276; N=O stretching from Ref. 237; and OH stretching from Ref. 277

Table 4.9: *Anharmonic frequencies (in cm^{-1}) and in parenthesis corresponding intensities (in km/mol) of cis-HONO.*

Mode	MP2[a]	MP2/AVTZ	CCSD(T)/AVTZ	Experiment[c]
OH	3422.3(64)	3408.5(30.2)	3421.4 (21.9)	3426.2
N=O	1599.1(197)	1587.5(136.9)	1629.2 (158.9)	1640.5
HON	1336.3(12)	1249.5(1.4)	1288.7 (0[b])	(1302)[d]1315.2
O-N	881.6(347)	840.8(336.4)	844.5 (280.2)	851.0
ONO	622.9(27)	598.5(60.3)	604.8 (35.9)	609.0
Torsion	836.5(121)	651.7(95.2)	628.2 (94.3)	638.5
RMSE	84.9	32.2	9.0	-

[a]Variational computations based on MP2/aug-cc-pVTZ ab initio data from Ref. 258
[b] Very low intensity.
[c](Torsion, ONO bend) from Ref. 275; (OH stretching, N=O stretching) from Ref. 238; HON bending in a Kr matrix from Ref. 254; and ON stretching from Ref. 276
[d]Extremely low intensity; represents a best estimate for the gas phase result based on the measured value of 1315.2 cm^{-1} in a Kr matrix experiment from Ref. 254

fit. In refitting the available analytical PES,[131] several different cut-off energies were considered, i.e., 5000, 6000, 7500 and 10000 cm^{-1}, as well as different data training set combinations (including the 1D, 2D, and 3D grids as well as the selection of random data with, e.g., different numbers of data points from the cis, trans and TS regions). The details and the corresponding RMSEs (selected samples of) of these fits are given in Appendix C in Tables C11 and C12. Typically, the best RMSE that can be obtained is 15 cm^{-1}. However, if the validation set is removed (possibly leading to overfitting), the RMSE can be reduced to 2 cm^{-1}. From the tests refitting the analytical PES, it is clear that the NN-expnn method is capable of accurate fitting of an asymmetric double well PES with a low energy barrier. We can also adopt the data sampling guidelines developed for use when computing high level ab initio data for fitting a new HONO PES.

For the direct fitting of the ab initio data, a cut-off energy of 7500 cm^{-1} was selected based on the information learned from refitting the analytical PES, the analysis of the stationary points on the ab initio PES, and with the aim to restrict the PES to the cis-trans region consisting of only cis-HONO, trans-HONO and the transition state of the cis-trans isomerization process, $TS_{cis \leftrightarrow trans}$. In the NN fitting process, the training, test and validation sets were built by dividing the entire data set. Among the random data (of 10000 points), 8000 were chosen in the training set. The test and validation sets were 1000 random data each. In addition to the random data, in the training set, selected grids of 1D and 2D data at the cis, trans and the transition state geometries were included. A total of 1591 1D and 2D cuts were included in the training set. The information about the 1D and 2D grids is provided in Appendix C: Tables C6 to C8. As discussed in Section 4.2.2, the use of scaled data leads to a smooth decrease in the RMSE as the numbers of neurons increases. Without scaling, the quality of the fit does not systematically improve beyond 50 NN. The effect of scaling the data on the RMSE of the fit as the number of neurons is increased is plotted in Figure C1. The RMSE with increasing the number of neurons (fitting parameters) is shown in Figure C2 and the corresponding numerical data is provided in Table C9. As expected, the RMSE decreases as the number of neurons is increased;

however beyond 70 neurons, the RMSE does not change significantly. The lack of improvement for an increased number of neurons is due to the presence of the validation set to prevent overfitting. We choose the PES fit with 80 neurons for use in the MCTDH calculations of the vibrational state frequencies. The RMSE is 15.0 cm^{-1} for the PES with 80 NN. Although the overall RMSE is 15 cm^{-1}, examining the lower energy region of the PES reveals that up to 3000 cm^{-1}, the RMSE is 4.5 cm^{-1}, while up to 6000 cm^{-1} (as in the Table C10), the RMSE is 6.5 cm^{-1}. The MCTDH operator files for the 80 NN single stage fit PES with a 7500 cm^{-1} cut-off energy (based upon CCSD(T)-F12/cc-pVTZ-F12 or CBS extrapolated ab initio data) are provided in Appendix C. The quality of the NN-expnn fitted PES can also be verified by analyzing 1D or 2D cuts of the PES. As an example, the 2D cut for the HON and out-plane-bending modes (with all other parameters set at their equilibrium values) is illustrated in Figure 4.5.

4.3.4 Vibrational States from MCTDH

Once a PES has been obtained in sum-of-products form, it can be utilized for subsequent computations of vibrational state energies, and, if desired, wavefunctions using MCTDH. The resulting vibrational energies, as determined using different PESs, are discussed in the following sections.

4.3.4.1 Refit of the analytical PES

As a first test, the low-lying vibrational states have been determined using the NN-expnn refits of the previous analytical PES,[131] with different cut-off energies. The computed energies for the fundamental modes, along with the previous computations of Richter et al.[131] are shown in Tables C11 and C12 for trans- and cis-HONO, respectively. For the trans-HONO isomer, the computed energies are within 1 cm^{-1} of those determined on the Richter et al. PES (an exception is the N=O stretch mode with a deviation of 8.0 cm^{-1}). For the cis-HONO isomer, the agreement is better as most are within 1 cm^{-1} of those determined on the Richter et al. PES (the N=O stretch mode deviates by 4.5 cm^{-1}).

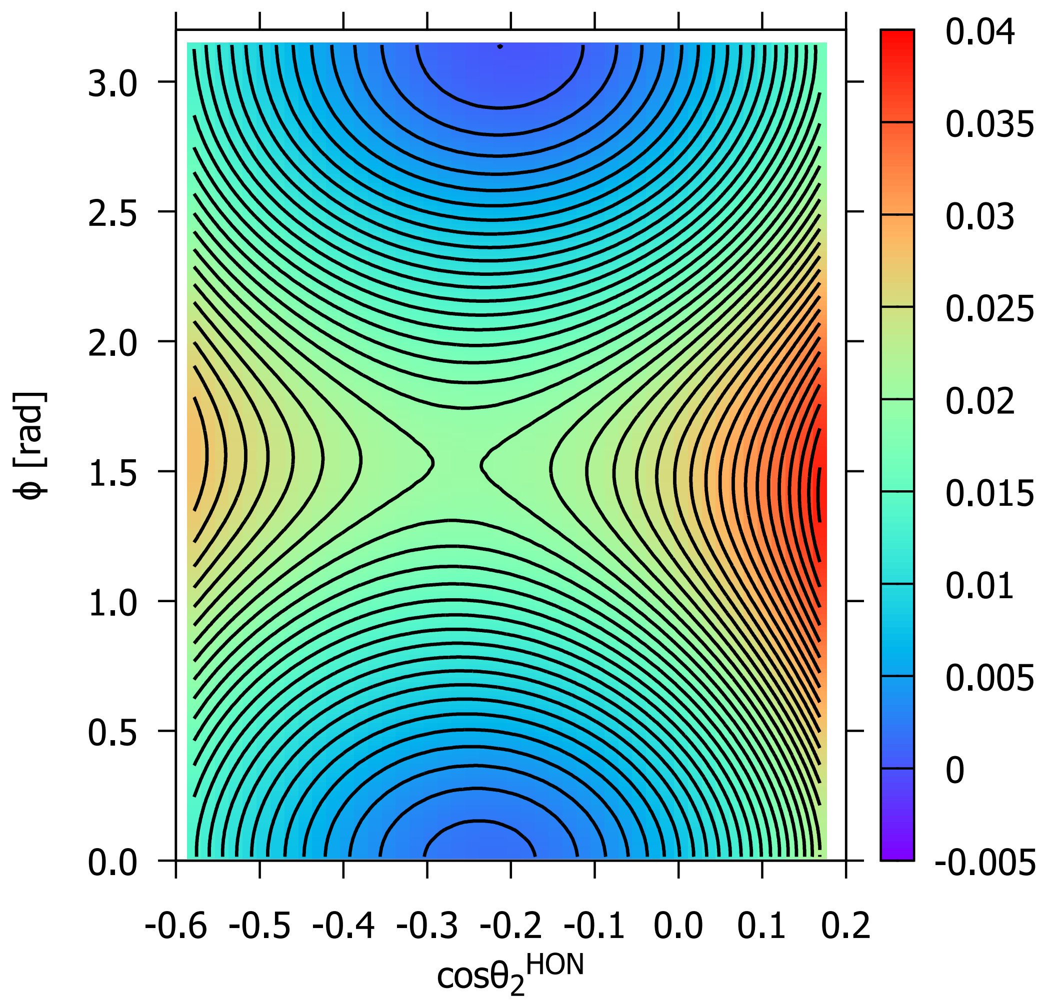

Figure 4.5: *HONO S_0 surface 2D contour plot of ϕ vs $cos\theta_2^{HON}$ with all other geometrical parameters fixed at the trans-HONO equilibrium geometry. Contours represent 0.001 au or 220 cm^{-1} intervals.*

The refitting of the previous analytical PES and the good agreement with the corresponding vibrational energies provides confidence that the NN-expnn-MCTDH procedure is efficient for fitting the asymmetric double-well HONO PES and for determining accurate vibrational energies. Hence, the decision to determine new accurate HONO PESs based upon high level CCSD(T)-F12/cc-pVTZ-F12 and CCSD(T)/CBS ab initio data.

4.3.4.2 New HONO PESs

In this section, we focus on the fundamental vibrational modes for the trans- and cis-HONO isomers determined based on the NN-expnn fits (with 80 neurons) to the CCSD(T)-F12/cc-pVTZ-F12 and CCSD(T)/CBS ab initio data. The vibrational states determined based upon the CCSD(T)-F12/cc-pVTZ-F12 and the CBS extrapolated NN-expnn fit PESs are compared with the experimental results[237,238,254,275–277] and previous theoretical results,[131] see Tables 4.10 and 4.11. The absolute differences as compared to the experiment range from 0.3-17.4 on the CCSD(T)-F12 PES (0.3-12.9 on the CCSD(T)/CBS PES) and the RMSE is 9.7 cm^{-1} (7.0 for CBS PES) for the trans-HONO isomer. Interestingly, despite improvement in the underlying ab initio electronic structure (from CCSD(T)/cc-pVQZ (-g functions)) the RMSE of 9.7 cm^{-1} is comparable to the previous results of Gatti and co-workers[131] (RMSE of 8 cm^{-1}). More precisely, in this work, the out-of-plane bending mode is more accurate (off by 0.3 cm^{-1} and 1.1 cm^{-1} for the CCSD(T)-F12/cc-pVTZ-F12 and the CBS extrapolated NN-expnn fit PESs, respectively) than the theoretical result by Gatti and co-workers[131] (off by 6.0 cm^{-1} from the experiment). The OH stretching, N=O stretching and HON bending modes are also accurately computed (differences less than 5 cm^{-1}) and comparable to those determined in the previous theoretical work. The ONO bending and O-N stretching modes are the two modes which differ from experiment by more than 15 cm^{-1} (more than 10 cm^{-1} for the CBS PES). These two modes are highly coupled, and even in the previous work,[131] these modes deviated most significantly from the experiment. Overall, the CBS extrapolated results for trans-HONO are more accurate than those from CCSD(T)-F12 for the N=O and ON stretching plus HON and ONO bending modes.

For cis-HONO, the CCSD(T)-F12/cc-pVTZ-F12-MCTDH results are quite accurate when compared to the experimental measurements (RMSE of 2.9 cm^{-1}). The CBS extrapolated results are also very accurate with a RMSE of 3.9 cm^{-1}. The maximum deviation is found for the HON bending mode; 19 cm^{-1} for the CCSD(T)-F12 PES and 16 cm^{-1} for the CBS PES as compared to the experimental measurement[241] of of 1302.0 cm^{-1}. However, it should be emphasized that this value was an estimate[278] as the experimentally measured gas phase spectral peak was too low in intensity to assign. This large difference for the HON bending mode is also reflected in the work by Gatti and co-workers[131] (10 cm^{-1} difference). A more recent experiment in a Kr matrix[254] reports the HON bending frequency to be 1315.2 cm^{-1} which we include in the comparison. Except for the HON bending mode, the agreement with the other five modes is excellent. The OH stretch, N=O stretch and ONO bending modes are almost exact (differences less than 1 cm^{-1}) when compared with the experiment. The out of plane bending mode and O-N stretching mode have differences below 3 cm^{-1}. Overall, the current results show better agreement with the experiment than the previous MCTDH results.[131] The largest deviation for the CBS result is for the ONO bending mode, differing 8.6 cm^{-1} from the experiment. Overall the accuracy of the cis-HONO frequencies is better than for trans-HONO.

Additional data for selected overtones and combination modes, including their assignment and frequencies (based on the CCSD(T)/CBS 80 NN PES fit) are provided in Appendix C: Tables C15 and C16 for the trans-HONO and cis-HONO isomers, respectively. These computed values are compared with the previously observed values.[237,238,275,279–281] Gatti and co-workers[131] also computed overtones and combination modes frequencies of cis- and trans-HONO isomers up to 3650.0 cm^{-1}. Our (and their) assigned first overtones of N=O stretching mode ($2\nu_2$) are in good agreement with the observed values:[237,238] for trans-HONO, a computed value of 3374.5 cm^{-1} (3367.4 cm^{-1}) as compared to the observation at 3372.1 cm^{-1}, and for cis-HONO 3264.7 cm^{-1} (3253.6 cm^{-1}) for the computation relative to the measurement of 3257.9 cm^{-1}. Overtones of N=O and OH modes are important to consider because these are the modes

Table 4.10: *The fundamental vibrational energies for trans-HONO as determined on potential energy surfaces based on different levels of ab initio theory. (See main text for discussion of PESs). Differences from the experimental measurements, see Table 4.8, are provided in bold.*

Mode	CCSD(T)			CCSD(T)-F12	CBS	Previous[131]
	AVTZ	AVQZ	AV5Z	VTZ-F12		MCTDH
OH stretch	3577.4	3592.9	3595.1	3593.5	3586.4	3590.2
	-13.3	**2.2**	**4.4**	**2.8**	**-4.3**	**-0.5**
N=O stretch	1688.0	1701.6	1704.9	1705.7	1700.1	1698.3
	-11.8	**1.8**	**5.1**	**5.9**	**0.3**	**-1.5**
H-O-N bend	1258.7	1267.4	1268.8	1269.3	1266.6	1267.4
	-4.6	**4.3**	**5.7**	**5.5**	**2.8**	**3.6**
O-N stretch	788.3	799.8	802.8	804.1	800.1	796.5
	-1.8	**9.7**	**10.7**	**14.0**	**10.0**	**6.4**
O-N-O bend	596.8	608.6	612.3	613.0	608.5	600.9
	1.2	**13**	**16.7**	**17.4**	**12.9**	**5.3**
Torsion	530.7	539.4	543.9	543.5	542.7	537.8
	-13.1	**-4.4**	**0.1**	**-0.3**	**-1.1**	**-6.0**

Table 4.11: *The fundamental vibrational energies for cis-HONO as determined on potential energy surfaces based on different levels of ab initio theory. (See main text for discussion of PESs). Differences from the experimental measurements, see Table 4.9, are given in bold.*

Mode	CCSD(T)			F12	CBS	Previous[131]
	AVTZ	AVQZ	AV5Z	VTZ-F12		MCTDH
OH stretch	3417.6	3428.8	3431.0	3426.1	3426.0	3435.8
	-8.6	**2.6**	**4.8**	**-0.1**	**-0.2**	**9.6**
N=O stretch	1628.9	1643.0	1645.8	1639.8	1640.7	1636.8
	-11.6	**2.5**	**5.3**	**-0.7**	**0.2**	**-3.7**
H-O-N bend	1306.6	1322.2	1321.9	1321.1	1318.4	1312.0
O-N stretch	847.6	865.0	865.6	854.2	861.2	850.1
	-3.4	**14.0**	**14.6**	**3.2**	**10.2**	**-0.9**
O-N-O bend	605.2	616.9	620.3	609.8	617.6	617.0
	-3.8	**7.9**	**11.3**	**0.8**	**8.6**	**8.0**
Torsion	627.4	633.9	637.5	636.0	636.5	631.8
	-11.3	**-4.6**	**-1.0**	**-2.5**	**-2.0**	**-6.7**

involves in the isomerization. For the combination of N=O and N-O stretching modes, ($1\nu_2$,$1\nu_3$), the computed frequency 2515.9 cm^{-1} (2476.7 cm^{-1}) can be compared to the experimentally observed value of 2492.9 cm^{-1}. The computed frequencies and state assignments obtained in this work of the overtones and combination modes are in excellent agreement with the previously determined results.

4.4 Conclusions

In this chapter, the stationary points (minima and transition states) on the global HONO PES have been located and characterized based on CCSD(T)-F12/cc-pVTZ-F12 computations. We have demonstrated the capability of the NN-expnn method to fit a potential energy surface localized around the cis- and trans-isomers for the HONO molecule. The CCSD(T)-F12/cc-pVTZ-F12 and CCSD(T)/CBS levels of theory have been used to generate the ab initio data for the energies. Vibrational states up to 4000 cm^{-1} have been determined for both the cis- and trans-HONO isomers; the RMSE with respect to the experiment is less than 10 cm^{-1}. Based on the vibrational energies, the PES appears to be only (perhaps, surprisingly) as accurate as the PES (based on CCSD(T)/cc-pVQZ(-g functions)) reported by Richter et al.[131] For trans-HONO, the NO stretch and ONO bend differ from experiment by 15 cm^{-1} which we speculate to arise from (possible) multireference character which MRCI computations can reveal. From the present work, and as shown previously[1,8] the NN-expnn method for fitting is a viable alternative to *potfit* for use in MCTDH. Additional work is underway to test its applicability towards fitting a global surface (one that contains multiple intermediates), see Chapter 5.

Chapter 5

Neural Network Exponential Fitting of a 6D Multiple-Well Potential Energy Surface: Application to HFCO

5.1 Introduction

As discussed in Chapter 3, the dynamics of HFCO and, the possible control in this small, prototype molecule, are of theoretical, and potentially, experimental interest. Therefore, in addition to the dynamics in the HFCO equilibrium and HF + CO dissociative regions, the cis-trans isomerization of HOCF could play a significant and intriguing role in the spectroscopy and controlled quantum dynamics of HFCO. While investigating intramolecular vibrational energy redistribution (IVR) of HFCO on its ground electronic (S_0) potential energy surface, Gatti and co-workers[126,128] found that exciting CH, CO or HCO vibrational modes does not facilitate the dissociation. Therefore, as speculated previously,[126] it may be possible to form trans-HOCF at the same rate as the dissociation products. The possible competition between these two processes is interesting because the barrier for HFCO to trans-HOCF conversion (~26000 cm^{-1}) is significantly higher than the activation barrier of dissociation to HF + CO (~17000 cm^{-1}). The HFCO dynamics can be compared to the analogous H_2CO molecule. H_2CO isomerizes to trans-HOCH at a faster rate than dissociation to H_2 +

CO duo to the lower activation barrier of isomerization (29938 cm^{-1}) than dissociation (30260 cm^{-1}).[282] Therefore, the unusual photochemistry of HFCO requires a detailed theoretical investigation. The lack of a global PES for HFCO limited the previous IVR studies[126–128] as the analytical PES (constructed by Yamamoto and Kato[132] and, hereafter referred to as the YK-PES) did not contain the cis- and trans-HOCF isomers. The cut-off energy for the YK[132] PES was 24000 cm^{-1} but the barrier height of HFCO to trans-HOCF conversion is 26000 cm^{-1}. To obtain new insight into the IVR dynamics and to investigate the competition between dissociation and isomerization, an accurate global PES of HFCO is desired.

In this Chapter, we develop an accurate global PES which could be used to study the wave packet dynamics in HFCO using MCTDH (or, alternative, quantum or classical dynamics approaches). Similar future directions were proposed in a series of papers on IVR dynamics of HFCO by Gatti and co-workers.[126–128] A global PES is developed using the NN-expnn method, see Sec.5.2, based on CCSD(T)-F12/cc-pVTZ-F12 ab initio data. The accuracy of the PES is tested by determining vibrational states around the 3 minimum energy structures, and comparing to available experimental measurements (only measured for the HFCO global minimum) and previous theoretical results.[202]

Besides developing a PES for examining the spectroscopy and future dynamics, we investigate the utility of the NN-expnn method for fitting a multiple-well PES. The HFCO global PES contains three minima and three transition states. If successful, the present NN-expnn fitting demonstrates its use for multiple-well PESs. Hence, a wide range of PESs involving isomerization could be developed using NN-expnn for future quantum dynamics simulations.

The work in this chapter is organized as follows. The ab initio computational methods, NN-expnn PES fitting techniques for the global surface of HFCO, and the vibrational state computations using MCTDH are discussed in Section 5.2. Section 5.3 presents the results of the optimized geometries, energies, harmonic frequencies of the intermediates, PES fitting and the MCTDH determined frequencies of cis-HOCF, trans-HOCF and equilibrium-HFCO on the S_0 global PES. The conclusions and future scope of this work are presented in Section 5.4.

5.2 Computational Methods

5.2.1 Ab initio Electronic Structure Techniques

The CCSD(T)-F12[15,16]/cc-pVTZ-F12[47–49] level of theory was used for the ab initio computations including both geometry optimizations (minima and transition states) as well as for generating the data for PES fitting. Corresponding MP2[13,14]/aug-cc-pVTZ[45] and CCSD(T)[14]/aug-cc-pVTZ computations for the stationary points have also been carried out for comparison. More importantly, anharmonic vibrational frequencies have been determined at these levels of theory using VPT2.[118–120] The CCSD(T)-F12 electronic structure computations were carried out with the Molpro package.[18,19] The MP2 and CCSD(T) computations, including for anharmonic vibrational frequencies, were carried out with CFOUR.[124]

5.2.2 PES Fitting

A body fixed polyspherical coordinate system is used to represent HFCO, see Figure 3.1. 1D cuts, 2D grids, and random data sets centred at each minimum (HFCO, trans-HOCF and cis-HOCF) and transition state geometry ($TS_{cis \leftrightarrow trans}$, $TS_{eq \leftrightarrow trans}$ and $TS_{eq \leftrightarrow diss}$) were computed with a cut-off energy, E_{cut} of 40000 cm^{-1} (relative to the equilibrium minimum). The fits of 1D cuts for cis-HOCF, trans-HOCF, HFCO and the transition states are given in Appendix D in Tables D1 and D2. The 1D and 2D cuts consist of 1500 data points at each stationary point geometry, i.e., 9000 points in all. An additional 1000 random data points at every minimum and TS were included in the training set, i.e., 6000 random data. Therefore, the entire training set is 15000 points. The test and validation sets each contain 600 random data; 100 random data centred at each stationary point and transition state. The overall 40000 cm^{-1} cut-off energy (relative to the HFCO equilibrium minimum) will include all six stationary points: cis-HOCF, trans-HOCF, $TS_{cis \leftrightarrow trans}$, HFCO (the global minimum $\equiv$ equilibrium), $TS_{eq \leftrightarrow trans}$ and $TS_{eq \leftrightarrow diss}$. The PES was fit to a sum-of-products form using NN-expnn. The details of the fitting procedure are described in Section 3.2.2.

5.2.3 MCTDH Computations

The quality of the PES was analyzed by computing vibrational energies using block improved relaxation[9] as implemented in the MCTDH software package.[3] The kinetic energy operator in body-fixed polyspherical coordinates has been described previously, see Sec.3.2.2.

5.3 Results and Discussion

5.3.1 Energies, Geometries and Fundamental Frequencies

The geometries and relative energies of the stationary points have been discussed previously in Section 3.3.1.1, see Table 3.2. To remind the reader, a schematic of the important stationary points (along with their relative energies compared to the HFCO minimum) is given in Figure 5.1. Hence, only the frequencies of the cis- and trans-HOCF isomers are discussed and compared to previous computations.[202] Currently, no experimental measurements of the fundamental frequencies of trans- or cis-HOCF are available. The fundamental harmonic frequencies of the trans- and cis-HOCF isomers as computed in the present work are given in Tables 5.1 and 5.2, respectively. While the present harmonic frequencies have been determined at a much higher level of theory than the previously reported CISD/DZ+P results,[202] the goals are to fit a global PES and determine vibrational energies beyond the fundamental frequencies.

5.3.2 The Global PES

The global PES was fit using the NN-expnn approach, see Section 3.2.2 for further details, based on the ab initio data sampled as discussed in Section 5.2.2. The RMSE of the fit utilizing different numbers of neurons is given in Table D3 in Appendix D. The best RMSE obtained is ~ 150 cm^{-1} for 100 neurons; increasing the number of neurons further does not decrease the RMSE due to the presence of the validation set. On the other hand, the RMSE is reduced to 80 cm^{-1} for an overfit PES with 80

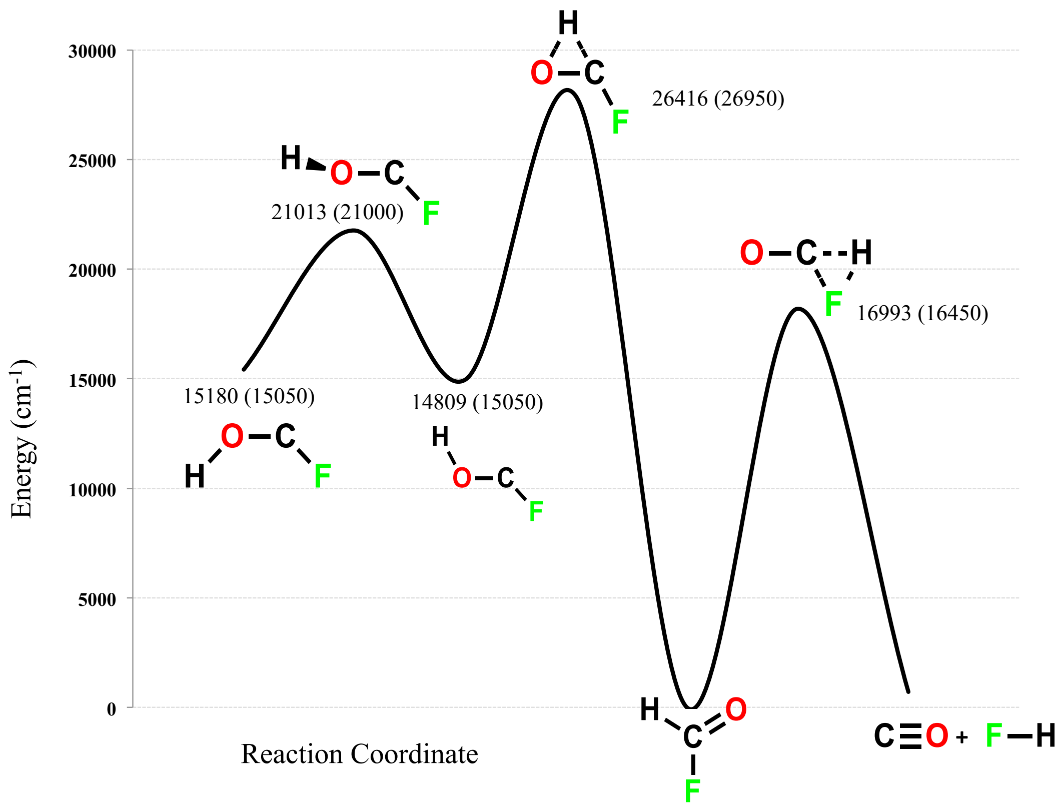

Figure 5.1: *Schematic of the stationary points on the global S_0 PES of HFCO. Energies relative to the HFCO minimum structure are provided; energies as determined at the CCSD(T)-F12/cc-pVTZ-F12 level of theory with ZPE are provided. The values in parenthesis represent the CISD/DZ+P results from Ref. 202.*

Table 5.1: *Harmonic vibrational frequencies (in cm^{-1}) of trans-HOCF compared with previous theoretical results. IR intensities (km/mol) are given in parentheses, when available.*

Mode	MP2[a]	CCSD(T)[a]	CCSD(T)-F12[b]	Ref [202][c]
ν_5 FCO bending	659.0 (3.0)	654.2 (2.8)	660.0	678
ν_6 out of plane bending	751.0 (87.1)	736.7 (87.1)	743.0	763
ν_2 CF stretching	1072.0 (273.6)	1071.2 (255.9)	1079.0	1128
ν_4 HCO bending	1284.4 (145.9)	1271.2 (159.7)	1281.0	1343
ν_3 CO stretching	1355.3 (170.1)	1360.8 (157.2)	1368.6	1441
ν_1 CH stretching	3792.9 (165.3)	3795.9 (135.2)	3811.0	3987

[a]aug-cc-pVTZ basis set; [b]cc-pVTZ-F12 basis set; [c]CISD/DZ+P

Table 5.2: *Harmonic vibrational frequencies (in cm^{-1}) of cis-HOCF compared with previous theoretical results. IR intensities (km/mol) are given in parentheses, when available.*

Mode	MP2^a	CCSD(T)^a	CCSD(T)-F12^b	Ref [202]^c
ν_5 FCO bending	643.5 (25.4)	639.0 (23.5)	644.5	665
ν_6 out of plane bending	786.5 (116.3)	769.6 (113.1)	775.8	802
ν_2 CF stretching	987.7 (123.6)	990.1 (121.4)	997.9	1056
ν_4 HCO bending	1291.1 (332.5)	1290.2 (343.9)	1297.9	1366
ν_3 CO stretching	1373.0 (41.3)	1362.9 (15.8)	1372.1	1430
ν_1 CH stretching	3587.6 (38.3)	3588.1 (26.6)	3602.4	3812

^{a}aug-cc-pVTZ basis set; ^{b}cc-pVTZ-F12 basis set; ^{c}CISD/DZ+P

neurons, where all the data is included in the training set. Without the validation set, the fitting procedure does not terminate (as happens with the validation set) to prevent overfitting. Thus, the RMSE could be reduced further to 65 cm^{-1}, if the iteration number is increased to 50000 for a single fit; however, one risks overfitting the data using this procedure and hence a validation set is always used. After NN-expnn fitting, the shape of the PES was analyzed by plotting 2D contour and 1D plots for the energy versus physical coordinates. All figures, and the subsequent MCTDH computations, are for the NN-expnn PES, determined including a validation set, with 100 neurons. These were compared to the ab initio data (see Figure 5.2). Clearly, the NN-expnn PES is accurate (as based on the RMSE) and appears smooth. Therefore, the NN-expnn fitted PES should be of suitable quality for use in quantum dynamics studies.

5.3.3 Vibrational States/Energies from MCTDH

To examine the accuracy of the global PES, the vibrational frequencies have been determined (for localized portions of the PES) at equilibrium HFCO as well as the trans- and cis- isomers, using MCTDH block-improved relaxation.[9] The numerical details regarding grid lengths, basis functions, number of primitives, number of single particle functions, and mode combinations for the MCTDH computations are provided in Appendix D, Tables D4, D5 and D6 for HFCO, cis- and trans-HOCF isomers,

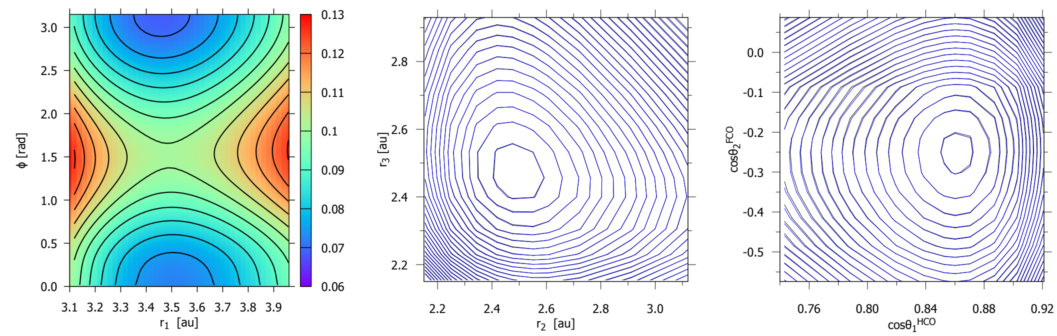

(a) **(b)** **(c)**

Figure 5.2: *Contour plots of the PES for trans-HOCF (a) ϕ vs. r_1, (b) r_3 vs. r_2, and (c) $\cos\theta_1^{HCO}$ vs. $\cos\theta_2^{FCO}$ from the NN-expnn (80 neurons) fitted surface (blue lines) and the ab initio energies (black lines, almost indistinguishable from the blue lines).*

respectively. These computations test the accuracy of the PES where comparison to experimental measurements are available. Moreover, by examing vibrational states around the minima, the presence of any "holes" in the surface should be detected. Usually if the MCTDH computation is smooth and converges to a desired state or states, the surface is then suitable for other quantum dynamics (or classical dynamics) simulations. Based on the global PES, the vibrational energies for states localized around equilibrium-HFCO were computed and compared with the previous experimental[179,196] and theoretical[196,201] results, including those from the local NN-expnn PES discussed in Chapter 3, see Table 5.3. All the fundamentals, overtones, and combination modes up to 5000 cm^{-1} were computed and assigned. The RMSE as compared to experiment is 10.2 cm^{-1} which is, not surprisingly, poorer compared to the value from the previous local PES fit only around the equilibrium HFCO geometry (RMSE of 2.5 cm^{-1}). Considering the global PES is fit to a cut-off energy of 40000 cm^{-1}, compared to 20000 cm^{-1} for the local PES, the decreased accuracy is acceptable. However, the RMSE on the present global PES is superior to computations[196] on the YK PES[132] and the WW PES.[200]

The vibrational states of both trans- and cis-HOCF isomers have also been computed. The results for the fundamental modes are given in Tables 5.4 and 5.5 for

Table 5.3: *Selected vibrational energies (in cm^{-1}) for states up to 5000 cm^{-1} for HFCO from the global PES compared with experimental measurements and previous computations, including the "local" PES discussed in Chapter 3.*

Assignment ($n_1n_2n_3n_4n_5n_6$)	This work	Expt[b]	Local	Viel-WW[196,200]	Viel-YK[132,196]	JCTC-YK[201a]
000010	663.8	662.6	664.1	626.4	659.4	658.1
000001	1005.4	1011.2	1012.8	968.8	1020.5	1019.2
010000	1075.2	1064.9	1067.8	1017.8	1051.5	1049.5
000020	1326.6	1324.1	1327.5	1255.1	1317.7	1314.8
000100	1345.9	1342.3	1338.2	1371.1	1372.2	1370.3
010010	1731.7	1719.3	1725.1	1639.5	1704.6	1699.0
001000	1841.5	1836.8	1835.6	1770.5	1827.9	1821.3
020000	2128.4	2115.6	2114.9	2029.2	2090.8	2085.3
010100	2412.7	2412.0	2399.0	2376.1	2418.3	2412.9
001010	2499.4	2494.2	2494.9	2393.4	2484.0	2474.4
001001	2840.7	2841.0	2841.0	2727.5	2843.5	2833.3
011000	2909.6	2895.0	2898.4	2787.1	2876.1	2863.9
100000	2977.2	2981.2	2976.0	2974.4	3039.2	3003.2
001020	3172.2	3150.6	3153.8	3016.2	3139.4	3126.2
002000	3665.8	3652.8	3650.9	3526.7	3648.1	3623.7
001002	3839.1	3838.1	3839.8	3686.9	3855.1	-
100020	4311.7	4302.9	4301.6	4138.3	4304.3	-
002010	4316.5	4307.5	4307.1	4335.9	4403.1	-
001200	4510.7	4493.9	4495.7	4323.5	4458.8	-
002001	4653.8	4653.1	4649.1	4474.4	4662.6	-
012000	4722.5	4705.2	4710.9	4546.4	4698.9	-
001031	4812.4	4817.6	4815.5	4649.9	4865.7	-
002020	4965.7	4955.0	4959.0	4758.0	4960.4	-
RMSE	10.0	-	2.5	92.0	28.0	12.0

[a] Vibrational assignments taken from Ref. 201
[b] Experimental values from private communication as mentioned in Ref. 196

trans- and cis-HOCF isomers, respectively. All vibrational states up to 2600 cm^{-1} (total of 30 states) above the ZPE are provided in Table D7 in Appendix D. For comparison purposes, and to provide values for the intensities which are valuable since the dipole moment cannot (readily) be determined using CCSD(T)-F12, vibrational energies (and corresponding IR intensities) for the fundamental modes as determined through VPT2 computations, see Section 5.2.1, are provided in Tables 5.4 and 5.5. In general, there is a good correspondence between the fundamental frequencies for both the cis- and trans-isomers as determined using VPT2 and the CCSD(T)/aug-cc-pVTZ level of theory and the MCTDH computations (RMSDs of 17.8 and 11.5 respectively). Interestingly and fortutously, the MCTDH computed fundamental frequencies of the MP2/aug-cc-pVTZ computed anharmonic frequencies (using VPT2 method) of trans- and cis-HOCF show better agreement than the CCSD(T)/aug-cc-pVTZ results; RMSDs were 4.4 and 10.7 cm^{-1} for cis- and trans-HOCF isomers. The present computations represent the best available vibrational energies for cis- and trans-HOCF, and, these should prove useful for future identification of these species.

The accuracy of the global PES in the local minima regions suggests that the NN-expnn method is capable of fitting a multiple well PES with the same efficiency as a single well PES. Thus the NN-expnn approach is a general, widely applicable method and the SOP form it produces will be extremely useful when using MCTDH for quantum dynamics computations.

5.4 Conclusion

In this chapter, the NN-expnn fitting procedure is shown to be capable of fitting a global 6D potential energy surface containing multiple wells for HFCO. With a sufficient number of fitting parameters (called neurons), in principle one can fit a complicated PES. The sampling of the ab initio data plays an important role in the quality of the fitting. Not surprisingly, the more complex the PES is, the more data are required; however, for the present approach, the data can be selected randomly (or, for example, by sampling with classical molecular dynamics) as data on a uniform

Table 5.4: *Fundamental vibrational frequencies (in cm^{-1}) of trans-HOCF as determined on the global PES with MCTDH compared with ab initio anharmonic vibrational frequencies. Anharmonic IR intensities (km/mol) are given in parentheses.*

Mode	MP2[a]	CCSD(T)[a]	MCTDH[b]
ν_5 FCO bending	650.7 (3.0)	645.8 (2.7)	651.4
ν_6 out of plane bending	722.8 (88.4)	707.5 (87.9)	742.9
ν_2 CF stretching	1043.3 (275.6)	1043.4 (157.6)	1043.1
ν_4 HCO bending	1243.1 (141.8)	1231.1 (153.3)	1251.5
ν_3 CO stretching	1321.0 (178.4)	1323.7 (165.2)	1321.5
ν_1 CH stretching	3610.5 (153.1)	3610.5 (120.3)	3625.0
RMSD[c]	10.7	17.8	-

[a]aug-cc-pVTZ basis set; [b]Based on the NN-expnn PES with 100 neurons fit to CCSD(T)-F12/cc-pVTZ-F12 ab initio data; [c]RMSD with respect to the CCSD(T)-F12/cc-pVTZ-F12/MCTDH computed frequencies.

Table 5.5: *Fundamental vibrational frequencies (in cm^{-1}) of cis-HOCF as determined on the global PES with MCTDH compared with ab initio anharmonic vibrational frequencies. Anharmonic IR intensities (km/mol) are given in parentheses.*

Mode	MP2[a]	CCSD(T)[a]	MCTDH[b]
ν_5 FCO bending	633.4 (24.4)	628.9 (22.3)	632.1
ν_6 out of plane bending	759.4 (113.5)	741.4 (109.7)	764.2
ν_2 CF stretching	955.6 (118.2)	959.2 (116.3)	957.0
ν_4 HCO bending	1261.8 (38.1)	1254.6 (276.4)	1265.3
ν_3 CO stretching	1336.2 (56.4)	1321.6 (24.8)	1335.6
ν_1 CH stretching	3390.2 (29.9)	3384.6 (17.9)	3381.5
RMSD[c]	4.3	11.9	-

[a]aug-cc-pVTZ basis set; [b]Based on the NN-expnn PES with 80 neurons fit to CCSD(T)-F12/cc-pVTZ-F12 ab initio data; [c]RMSD with respect to the CCSD(T)-F12/cc-pVTZ-F12/MCTDH computed frequencies.

grid is not required. Overall, the global PES developed in this work is suitable for use in further quantum, or classical, dynamics simulations, for example, the cis-trans isomerization, the equilibrium to trans-HOCF isomerization and, perhaps, unimolecular dissociation dynamics as well as the competition between them.

Chapter 6

The S_1 Excited State Potential Energy Surface of HFCO: A NN-expnn fit and vibrational energies

6.1 Introduction

HFCO is one of the series of substituted formaldehyde systems that contains the C=O chromophore. High level theoretical investigations will help to understand the excited state properties more clearly. Determining the ab initio data and then fitting a full six dimensional (6D) excited state potential energy surface is a challenging task. While there have been significant algorithmic improvements for fitting multidimensional PESs, computing the requisite numbers of ab initio data at a high enough level of theory for fitting is computationally costly. One must make a judicious choice of ab initio method; black-box single reference methods, such as EOM-CCSD or even TD-DFT, can be utilized or multireference techniques, such as CASPT2 or MRCI, can be used although then the underlying active space must be carefully considered. Whatever choice is made, there must be a compromise between accuracy and computational efficiency, especially when computing the many points required for fitting a multidimensional PES. Although the excited state potential energy surface is difficult to generate, once generated, it can be applied, when combined with a corresponding transition dipole moment surface, to simulate and interpret various spectroscopic and dynamics experiments, including absorption, photodissociation, cis-trans isomerization, intramolecular vibrational energy redistribution, and stimulated emission pumping measurements.

HFCO has very interesting photochemistry.[133,283–285] The S_1 and T_1 excited states play major roles in its photochemistry. HFCO can undergo photodissociation from excited vibrational states of the ground electronic S_0 surface,[133,183] from the first excited S_1 singlet state, it may dissociate directly or relax to highly excited vibrational states of the ground S_0 state, which then lead to the dissociated products. Alternatively, once excited, HFCO may undergo intersystem crossing from S_1 to T_1 and from T_1, it may dissociate. To-date, the experiments have focused on examining the different reaction channels. Klimek and Berry,[283] studied dissociation of HFCO after excitation at 165 nm (60606 cm^{-1}), and showed that it produces HF infrared laser emission. Although HF was the main product (≈ 7 %), fluorine atoms were also produced in the photodissociation. Moore and co-workers[133] used a range of excitation wavelengths from 193 to 248 nm (40322 cm^{-1} to 51813 cm^{-1}) to probe mode specificity in the rate HFCO unimolecular dissociation to HF + CO. Several previous investigations focused on the T_1 surface where photo excitation is initiated by S_0 to S_1 pumping followed by intersystem crossing to the T_1 surface or internal conversion back to the S_0 surface. The S_1-S_0 conical intersections[194] and S_1-T_1 crossing are particularly interesting for the photophysics of HFCO. Previous CASSCF(8,7)/cc-pVTZ computations by Wei-Hai *et al.*[194] focused on the S_1 and the T_1 surfaces. CASSCF(8,7) is a relatively modest active space compare to the full valence active space for HFCO of CASSCF(18,13). Here we investigate the choice of active space on the vertical excitation energies to S_1 and T_1, the excited state optimized geometries, and the corresponding harmonic frequencies using CASSCF, CASPT2, and MRCI computations. An EOM-CCSD investigation of the excited state structures and energies is carried out and then this methodology is utilized as a basis for PES fitting. Our goal is to compare these results with the S_1 excited state fundamental frequencies measured by Moore and co-workers.[284] They measured the fluorescence excitation spectra of jetcooled HFCO and DFCO from the S_1 electronic state for frequencies between 37500 and 40250 cm^{-1}.

Besides the spectroscopy and excited state dynamics, the geometrical structures and energetics of the HFCO excited states are also of interest. Experimental evidence shows that S_0 to S_1 or S_0 to T_1 excitation leads to an increase in C=O bond length.[286] On the S_1 and T_1 excited states, the equilibrium geometry changes from planar to pyramidal.[188] The excited S_1 and T_1 states each exhibit a double well PES with a low energy inversion barrier which leads to tunnelling splitting. The need for a S_1 PES was suggested in the work examining the control of IVR and, potentially, isomerization by Gatti and co-workers.[128] With a S_1 surface, the IVR dynamics of HFCO involving initial excitation to the S_1 surface can be investigated using MCTDH. Similarly, the control of selective HFCO to trans-HOCF or the dissociation to HF + CO can be explored.

The goal of this work is to determine the equilibrium and transition state structures and fundamental frequencies of the S_1 and T_1 electronic states. The double well depth and vertical excitation energies will be investigated and, most importantly, a 6D PES for the S_1 excited electronic state will be developed. To-date, a full PES for the excited S_1 state of the HFCO molecule has not been constructed. In terms of investigating the spectroscopy and dynamics, there is a large gap in correlating the theory with the experimental results. A S_1 PES will bridge this gap.

The scheme of this chapter is as follows: In Section 6.2.1, the ab initio computational methods used to determine the optimized structures (minima and transition state), corresponding relative energies, vertical excitation energies and harmonic frequencies are presented. In Section 6.2.2, the EOM-CCSD/aug-cc-pVTZ level of theory is selected for generating the ab initio energy data and the potential energy surface fitting of the S_1 surface using the NN-expnn technique, is discussed. In Sec.6.2.3, the MCTDH approach for determining the vibrational frequencies is presented. The results of the excited state geometry optimizations, vertical excitation energy calculations, relative energies, harmonic frequency computation, PES fitting and the MCTDH determined frequencies of the S_1 surface are analysed in Section 6.3. Finally, the conclusions of this chapter are presented in Section 6.4.

6.2 Computational Methods

6.2.1 Vertical Excitation Energy, Optimized Excited State Geometry and corresponding Harmonic Frequencies

The ground state geometry is taken to be the CCSD(T)-F12/cc-pVTZ-F12 optimized structure, see Table 3.2 and corresponding discussion in Section 3.3.1.1. The vertical excitation energies for the S_0 to S_1 and S_0 to T_1 transitions were computed with the complete active space self-consistent field (CASSCF),[23,24] complete active space second-order perturbation theory (CASPT2)[38–40] and multireference configuration interaction method (MRCI)[25–29] methods. The HFCO equilibrium geometry has C_s symmetry, but, in general, the geometries sampled on the PES do not have this symmetry; therefore, the vertical excitation energies were considered both with and without symmetry. Different active spaces were tested for the CASSCF, and subsequent CASPT2 and MRCI computations, since an accurate and efficient approach would be required for generating the ab initio points for the PES fitting. In addition to the standard CASPT2 and MRCI methods, the explicitly correlated MRCI-F12[42–44] and CASPT2-F12[41] computations were also performed. As there were some difficulties with the smoothness of the CASSCF results away from the equilibrium geometry (see discussion in Section 6.3), an equation-of-motion coupled cluster with singles and doubles (EOM-CCSD)[17] calculation of the vertical excitation energy was also performed. For all computations, the augmented correlation consistent polar triple zeta valence basis set,[45,46] aug-cc-pVTZ, was used. For the CASPT2-F12 and MRCI-F12 computations, the cc-pVTZ-F12 basis set[47] was utilized.

The optimized geometries of S_0, S_1 and T_1 surfaces were determined with the CASSCF method. In the geometry optimization, the smallest active space (8,7) (i.e., 8 electrons in 7 orbitals) to the full valence active space (18,13) (i.e., 18 electrons in 13 orbitals) was used. Including all the valence electrons in the active space is computationally costly, thus, previous CASSCF geometry optimizations for HFCO used the smaller (8,7) active space.[194] Subsequent, CASPT2 and MRCI geometry optimizations based on the different active spaces were also performed. The CASPT2 optimizations used the analytic gradients[159] while the MRCI optimizations were carried out numerically. CASPT2 and MRCI geometry optimizations were computationally too expensive to perform for the full valence active space, i.e., (18,13). Therefore, reduced active spaces, e.g., (8,7) or (12,9), were used.

On the other hand, EOM-CCSD is computationally cost effective and a more "black box" technique as compared to the multireference methods where one must worry about the choice of active space. EOM-CCSD calculations are performed for the S_1 state to compare with other methods; geometry optimizations use numerical gradients. The T_1 state was optimized using the RCCSD method.[287] For all methods, both the minimum energy structure and the inversion barrier (transition state between the symmetry equivalent minima) were determined, see discussion in Section 6.3.

The fundamental harmonic frequencies were computed after the geometry optimization to confirm the nature of the stationary points, i.e., as a minimum with no imaginary frequencies or as a transition state with a single imaginary frequency. The Molpro software package[18,19] was used to perform all the ab initio calculations. In all computations, default convergence criteria were utilized.

6.2.2 NN-expn Fitting of the PES

The neural network exponential fitting method (NN-expnn), see Section 3.2.2, was used in the PES fitting of the S_1 surface using data computed at the EOM-CCSD/aug-cc-pVTZ level of theory. The HFCO molecule was presented in a body fixed polyspherical coordinate system (Figure 3.1) where C-H, C=O and C-F bond distances were designated as R_1, R_2 and R_3, the bond angles HCO and FCO were designated as θ_1 and θ_2 and the dihedral angle between HCO and FCO was termed as ϕ. 1D, 2D, 3D and selected random energy data were computed at the EOM-CCSD/aug-cc-pVTZ level of theory for the S_1 surface. The 1D, 2D and 3D cuts were generated at the minimum and the transition state geometries. The fitting procedure is almost exactly the same as described in Chapter 3(except for the inclusion of 3D grid data in the training set in this work) .

6.2.3 Vibrational State Computations using MCTDH

Vibrational states frequencies were computed using the block improved relaxation method[9] as implemented in the MCTDH software package.[3] The fundamental mode assignment was done by using improved relaxation[7,125,265,266] with analysis of the resulting vibrational wavefunction. Since in improved relaxation, the initial overlap depends on how close the guess wavefunction is to the desired state, using a 1D cut along a physical coordinate is sometimes a poor guess for a highly coupled mode. Therefore, some specific states were difficult to converge using improved relaxation; hence, they could not be assigned by examining the final wavefunction. These states were assigned through the process of elimination, where all the other possible nearby modes were assigned and the remaining mode assigned using chemical intuition, eg, using the approximate harmonic frequency computations.

6.3 Results and Discussion

6.3.1 Vertical Excitation Energies

The S_0-S_1 and S_0-T_1 vertical excitation energies as determined using various computational methods are given in Table 6.1. It has been found that CASPT2 and CASPT2-F12 vertical excitation energies are almost 2000 cm^{-1} less than other methods. Because there is a change in the geometry following the excitation to S_1 or to T_1, the adiabatic transition energy, i.e., from the S_0 minimum to S_1 or T_1 minimum, lower than the corresponding vertical excitation energy. While the adiabatic S_0-S_1 transition energy is approximately 37000 cm^{-1}, the vertical excitation energy is around 48500 cm^{-1}. For the S_0-T_1 transition, the adiabatic transition energy is about 32000 cm^{-1} while the corresponding vertical excitation energy is $\sim$ 45000 cm^{-1}. The adiabatic S_0-S_1 transition energy computed in this work agrees well with the experimental measurement by Moore and co-workers[284] of 37500 to 40250 cm^{-1}. Most of the previous experiments investigate the role of the T_1 surface in the dissociation to

HCO + F and FCO + H, a process which requires more energy of the initial pump laser as compared to that required to access the S_1 or S_2 state.

Table 6.1: *Comparison between S_0-S_1 and S_0-T_1 vertical excitation energies (in cm^{-1}) using different electronic structure methods and the aug-cc-pVTZ basis set; cc-pVTZ-F12 basis for -F12 computations. All computations are carried out at the CCSD(T)-F12/cc-pVTZ-F12 optimized geometry, see Section 3.*

Method	S_0-S_1	S_0-T_1
EOM-CCSD	48679.5	-
CASSCF^a	48233.8	45338.7
MRCI^a	48532.7	45671.6
MRCI-F12^a	48609.1	45800.7
CASPT2^a	46502.4	43570.8
CASPT2-F12^a	46647.6	43784.6

^{a}Based on the (18,13) active space.

6.3.2 Optimized Geometries and Relative Energies

The results of geometry optimization for the excited electronic states are presented in Tables 6.2 and 6.3 for the S_1 and T_1 states, respectively. Optimized geometries of the S_0 minimum (in various excited state ab initio calculation methods) and the transition state to dissociation (HFCO to HCO+F and FCO+H on the excited S_1 and T_1 PESs) are provided in Appendix E: Table E4. The geometries of the minimum energy structures on S_1 and T_1 excited states were found to be pyramidal while the ground state (S_0) equilibrium structure is planar, see Section 3.3.1.1. Both the S_1 and T_1 states have a double well PES (shown schematically in Figure 6.1) along the out-of-plane bending mode. The EOM-CCSD/aug-cc-pVTZ geometry of the S_1 state is in very good agreement with the experimental observation.[284,288] The bond lengths are within 0.01 Å and, the bond angles agree to within 1°; however, the dihedral angle differs by 10° compared to the experimental measurement.[284] While differing from experiment, the dihedral angle of 133.4° as determined at the EOM-CCSD/aug-cc-pVTZ level of theory is in good agreement with previous computational results,[190,194] and the present high level CASPT2 and MRCI values of $\sim$ 130°. Interestingly, the

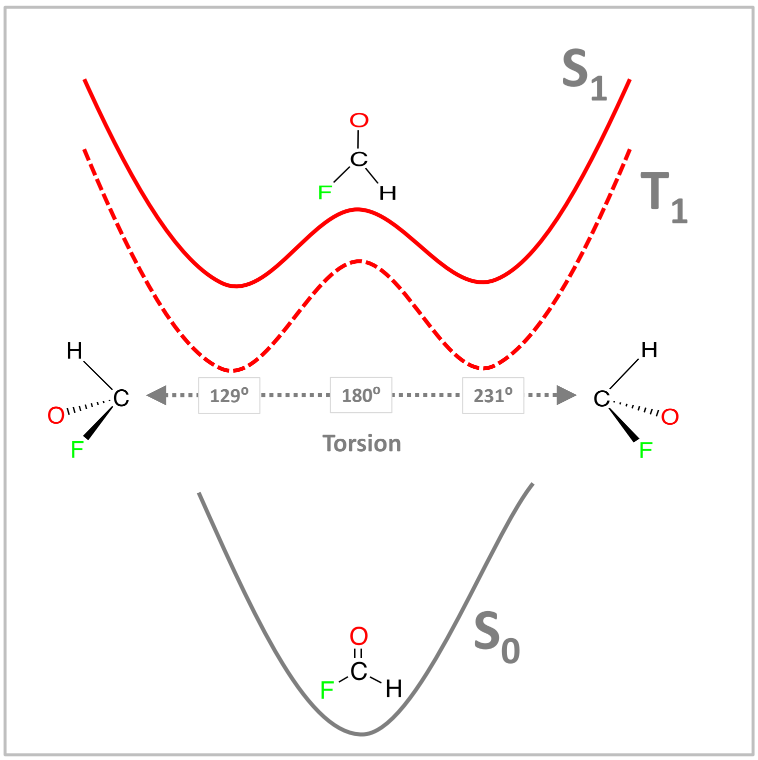

Figure 6.1: *Schematic of the S_1 double well PESs for S_1 and T_1 along the torsion mode.*

C=O bond at the S_1 equilibrium is elongated by 0.185 $\mathring{A}$ compared to its value at the S_0 minimum. Therefore, the C=O bond gains single bond character in the S_1 state. The optimized geometry on the T_1 state is similar to that of the S_1 minimum, i.e., a pyramidal geometry, a dihedral angle of approximately 128°, and an increase in the C=O bond length of 0.16 Å. A previous theoretical work[194] stated that the T_1 state originated from the n→π^* electron transition of the C=O moiety. In that work, the S_1 state was found to have mainly $^1n\pi^*$ character along with some $^1\pi\pi^*$ character mixed in. The inversion transition state between the two equivalent minima is, perhaps not surprisingly, planar on both the S_1 and T_1 PESs. The barrier height for the S_1 inversion is 1799.9 cm^{-1} at the EOM-CCSD/aug-cc-pVTZ level of theory which is in reasonable agreement with the experimental value of 2580 cm^{-1}.[284] The CASPT2(18,12) and MRCI(18,12) barrier heights of $\sim$ 2350 cm^{-1} are in excellent agreement with the experimental measurement. For the T_1 inversion, the barrier height was 2923.1 cm^{-1} at the MRCI (8,7)/aug-cc-pVTZ level of theory. No comparison is made with experiment as T_1 inversion barrier has yet to be reported.

6.3.3 Harmonic Frequency Calculation

The harmonic vibrational frequencies on the S_1 and the T_1 PESs as determined using different computational methods are given in Table 6.6. Corresponding experimental vibrational frequencies have been measured[284] for the S_1 state, see Table 6.7, to which the present theoretical results can be compared. The RMSE of the fundamental frequencies were 95.7 cm^{-1} for CASPT2(18,12)/aug-cc-pVTZ, 95.5 cm^{-1} for MRCI, and 101.4 cm^{-1} for EOM-CCSD. Previous computations examined the S_1 state using CASSCF(8,7)/cc-pVTZ, which in this work with the aug-cc-pVTZ basis, leads to an RMSE of 153.4 cm^{-1}. A full active space calculation, CASSCF(18,13), leads to a very modest improvement to 151.3 cm^{-1} RMSE.

Table 6.2: *Optimized stationary point geometries of HFCO on the S_1 surface using various computational methods and, if applicable, active spaces. Bond distances are in Å and bond angles are in degrees. All present computations use the aug-cc-pVTZ basis set. Previous experimental and theoretical results are also provided.*

Method	CH	CF	CO	HCO	FCO	ϕ
HFCO (S_1)	The first excited singlet					
CASSCF (18,13)	1.077	1.341	1.348	113.56	109.09	128.96
CASSCF (18,12)	1.075	1.342	1.388	114.08	109.04	129.34
CASSCF (12,9)	1.075	1.339	1.391	114.08	108.82	129.32
CASSCF (8,7)	1.079	1.315	1.383	113.91	109.96	129.76
CASPT2 (18,12)	1.0859	1.349	1.362	115.17	108.75	129.90
CASPT2 (12,9)	1.085	1.343	1.364	115.30	108.68	130.37
CASPT2 (8,7)	1.089	1.340	1.360	115.00	109.56	130.18
MRCI (18,12)	1.081	1.341	1.368	114.61	108.98	129.66
MRCI (12,9)	1.081	1.337	1.370	114.44	109.32	129.66
MRCI (8,7)	1.080	1.338	1.369	114.69	109.03	129.96
Ref [194][a]	1.088	1.322	1.393	113.80	109.40	130.10
Ref [194][b]	1.079	1.313	1.391	113.90	109.40	130.10
Ref [190][c]	1.098	1.346	1.346	116.10	109.82	133.70[d]
Expt.[284]	1.097	1.346	1.344	116.10	109.74	144.00[e]
Expt.[288]	1.100	1.340	1.360	129.00	110.00	145.00-150.00[f]
EOM-CCSD	1.088	1.339	1.334	116.89	109.79	133.40
HFCO (TS_{S_1})	The inversion transition state on the S_1 surface					
CASSCF (18,13)	1.060	1.335	1.390	124.30	112.93	180.00
CASSCF (18,12)	1.060	1.334	1.390	124.16	113.05	180.00
CASSCF (12,9)	1.060	1.337	1.388	124.43	113.14	180.00
CASSCF (8,7)	1.062	1.308	1.386	124.01	113.73	180.00
CASPT2 (18,12)	1.067	1.337	1.366	124.94	112.64	180.00
CASPT2 (12,9)	1.070	1.331	1.368	124.54	113.08	180.00
CASPT2 (8,7)	1.071	1.327	1.370	125.08	112.06	180.00
MRCI (18,12)	1.064	1.331	1.371	124.51	112.87	180.00
MRCI (12,9)	1.064	1.328	1.372	124.51	112.78	180.00
MRCI (8,7)	1.065	1.316	1.374	124.62	112.55	180.00
EOM-CCSD	1.073	1.330	1.339	125.01	112.91	180.00

[a] CASSCF(8,7)/cc-pVDZ from 194; [b] CASSCF(8,7)/cc-pVDZ from 194; [c] EOM-CCSD/DZP from 190; [d] Original article reports 46.3 degrees; [e] Original article reports 36.0 degrees; [f] Original article reports 30.00 to 35.00 degrees.

Table 6.3: *Optimized stationary point geometries of HFCO on the T_1 surface using various computational methods and, if applicable, active spaces. Bond distances are in Å and bond angles are in degrees. All present computations use the aug-cc-pVTZ basis set. Previous theoretical results are also provided.*

Method	CH	CF	CO	HCO	FCO	ϕ
HFCO (T_1)	First excited triplet state minimum					
CASSCF (18,13)	1.080	1.348	1.341	112.66	111.03	128.97
CASSCF (18,12)	1.078	1.344	1.365	111.97	111.41	129.03
CASSCF (12,9)	1.079	1.346	1.364	111.95	111.60	128.66
CASSCF (8,7)	1.080	1.317	1.371	111.24	111.36	129.05
CASPT2 (18,12)	1.091	1.354	1.344	110.92	111.74	127.91
CASPT2 (12,10)	1.092	1.344	1.341	111.09	111.78	128.63
CASPT2 (8,7)	1.090	1.343	1.350	111.68	111.30	128.92
MRCI (18,12)	1.085	1.346	1.349	111.47	111.54	128.51
MRCI (12,9)	1.085	1.343	1.349	111.32	111.79	128.45
MRCI (8,7)	1.086	1.331	1.353	111.23	111.57	128.86
RCCSD	1.092	1.340	1.347	111.75	111.33	128.76
Ref [194][a]	1.087	1.363	1.365	112.30	110.60	128.00
Ref [194][b]	1.078	1.349	1.364	112.60	110.70	129.00
Ref [194][c]	1.090	1.340	1.348	111.70	111.40	129.10
Ref [285][d]	1.096	1.344	1.349	111.19	111.64	128.18
HFCO (TS_{T_1})	The inversion transition state on the T_1 surface					
CASSCF (18,13)	1.062	1.336	1.367	123.39	113.66	180.00
CASSCF (18,12)	1.082	1.309	1.369	122.62	113.97	180.00
CASSCF (12,9)	1.061	1.336	1.367	123.38	114.02	180.00
CASSCF (8,7)	1.060	1.308	1.376	123.32	113.37	180.00
CASPT2 (18,12)	1.070	1.339	1.350	123.15	113.80	180.00
CASPT2 (12,10)	1.069	1.334	1.352	123.53	113.29	180.00
CASPT2 (8,7)	1.070	1.330	1.354	123.26	113.68	180.00
MRCI (8,7)	1.065	1.319	1.355	123.27	113.58	180.00
RCCSD	1.071	1.328	1.351	123.30	113.58	180.00

[a] CASSCF(8,7)/cc-pVDZ from 194; [b] CASSCF(8,7)/cc-pVTZ from 194; [c] UMP2/cc-pVTZ from 194; [d] MP4SDQ/6-311G(d,p) from 285.

Table 6.4: *Relative energy and inversion barrier height (both in cm^{-1}) of HFCO on the S_1 excited state potential energy surface as determined using different computational methods and, if applicable, active spaces. All present computations use the aug-cc-pVTZ basis set. Previous experimental and theoretical results are also provided.*

Methods	Relative energy[a]	Inversion barrier[b]
Expt.[284]	37500 - 40250	2583.0
Expt.[288]	37498.0	-
Ref [188][c]	37491.7	-
Ref [194][d]	39924.6	-
CASSCF(18,13)	36229.0	3144.0
CASSCF(18,12)	39354.6	2931.4
CASSCF(12,9)	39715.2	3140.1
CASSCF(8,7)	39209.2	3001.2
CASPT2(18,12)	36136.4	2354.3
CASPT2(12,9)	36591.4	2450.8
CASPT2(8,7)	36115.3	2386.0
MRCI(18,12)	37405.8	2633.8
MRCI(12,9)	38225.8	2577.7
MRCI(8,7)	39051.7	2766.1
EOM-CCSD	39777.8[e]	1799.9

[a] Relative energy with respect to the ground state (S_0) equilibrium structure; [b] Relative to the S_1 minimum energy; [c] EOM-CCSD/cc-pVTZ from 188; [d] CASSCF (8,7)/cc-pVTZ from 194; [e]Relative to the CCSD(T)-F12/cc-pVTZ-F12 optimized S_0 minimum structure.

Table 6.5: *Relative energy and inversion barrier height (both in cm^{-1}) of HFCO on the T_1 excited state potential energy surface. as determined using different computational methods and, if applicable, active spaces. All present computations use the aug-cc-pVTZ basis set. Previous computational results are also provided.*

Methods	Relative energy[a]	Inversion barrier[b]
Ref [188][c]	35421.0	-
Ref [194][d]	37916.5	-
Ref [285][e]	34210.0	-
CASSCF(18,13)	31596.9	4962.5
CASSCF(18,12)	35292.2	3185.3
CASSCF(12,9)	36962.7	3262.4
CASSCF(8,7)	38660.6	3560.9
CASPT2(18,13)	36120.0	-
CASPT2(18,12)	33887.9	2778.5
CASPT2(12,9)	34915.4	2760.7
CASPT2(8,7)	33397.0	3081.1
MRCI(18,12)	34782.3	
MRCI(12,9)	35633.3	
MRCI(8,7)	35841.7	2898.3
RCCSD		2842.3

[a] Relative energy with respect to the ground state (S_0) equilibrium structure; [b] Relative to the T_1 minimum energy; [c] EOM-CCSD/cc-pVTZ from 188; [d] CASSCF (8,7)/cc-pVTZ from 194; [e] MP4SDQ/6-311G(d,p) from 285.

Table 6.6: *Fundamental harmonic frequencies (in cm^{-1}) for the HFCO ground (S_0) and excited (S_1 and T_1) states minima and transition state structures using various computational methods and, if applicable, active spaces. For all computations, the aug-cc-pVTZ basis set was used.*

Method	CH str	CF str	CO str	HCO bend	FCO bend	ϕ bend
HFCO (S_1)	The first excited singlet					
CAS(18,13)	3261.7	1123.6	1165.2	1389.1	475.5	1040.0
CAS(18,12)	3297.2	1110.3	1147.8	1379.9	472.4	1044.8
CAS(12,9)	3303.4	1113.2	1162.2	1393.6	476.0	1055.9
CAS(8,7)	3220.5	1122.0	1272.5	1394.2	502.5	1049.2
CASPT2(18,12)	3160.5	1116.0	1135.2	1297.7	444.4	974.0
CASPT2(12,9)	3168.2	1129.2	1133.3	1312.1	448.5	976.2
CASPT2(8,7)	3124.1	1130.7	1143.0	1292.8	458.2	980.7
MRCI(8,7)	3225.1	1138.3	1162.5	1349.3	476.3	1017.3
EOM-CCSD	3129.5	1149.9	1215.1	1376.7	461.7	953.5
HFCO (TS_{S_1})	The inversion transition state on the S_1 surface					
CAS(18,13)	457.6	1065.5	1193.7	1380.5	3462.6	1071.9 (i)
CAS(18,12)	456.9	1066.3	1180.4	1369.5	3483.6	1044.4 (i)
CAS(12,9)	466.8	1068.3	1172.8	1377.6	3479.2	1049.3 (i)
CAS(8,7)	488.4	1066.6	1291.4	1425.5	3434.0	1070.6 (i)
CASPT2(18,12)	436.1	1087.8	1163.6	1314.2	3359.3	931.5 (i)
CASPT2(12,9)	446.9	1083.7	1171.0	1316.2	3354.2	930.8 (i)
CASPT2(8,7)	477.0	1084.0	1205.5	1333.2	3348.5	937.8 (i)
MRCI(8,7)	484.9	1099.4	1246.3	1384.4	3416.1	1005.9 (i)
EOM-CCSD	452.9	1161.1	1183.9	1396.3	3311.2	888.9 (i)
HFCO (T_1)	First excited triplet state minimum					
CAS(18,12)	3257.6	1123.4	1154.9	1382.7	464.6	1007.1
CAS(12,9)	3248.9	1120.3	1151.7	1391.2	470.4	1003.8
CAS(8,7)	3229.1	1158.5	1253.1	1421.5	487.5	1024.7
CASPT2(18,12)	3090.6	1092.5	1144.4	1310.0	424.4	921.7
CASPT2(12,9)	3067.2	1108.5	1277.9	1545.3	287.8	943.7
CASPT2(8,7)	3077.1	1114.5	1147.1	1323.9	433.2	934.1
MRCI(12,9)	3160.9	1125.2	1159.6	1348.3	455.2	960.7
MRCI(8,7)	3152.8	1145.2	1197.0	1364.5	459.1	970.4
RCCSD	3074.8	1142.8	1175.5	1352.6	457.9	978.9
HFCO (TS_{T_1})	The inversion transition state on the T_1 surface					

Continued on next page

Table 6.6 – *Continued from previous page*

Method	CH str	CF str	CO str	HCO bend	FCO bend	ϕ bend
CAS(18,12)	465.2	1106.9	1189.4	1394.2	3479.8	1096.7 (i)
CAS(12,9)	473.6	1104.5	1182.7	1402.8	3476.2	1106.2 (i)
CAS(8,7)	496.3	1122.2	1285.4	1452.5	3489.6	1206.7 (i)
CASPT2(18,12)	436.1	1087.9	1163.7	1314.2	3359.3	931.5 (i)
CASPT2(12,9)	446.9	1083.7	1171.0	1316.2	3354.2	930.8 (i)
CASPT2(8,7)	476.9	1084.0	1205.5	1333.2	3348.5	937.8 (i)
RCCSD	461.3	1125.6	1195.1	1385.0	3340.2	993.5 (i)

6.3.4 The S_1 Excited State PES

Due to difficulties with the "smoothness" of the PESs for CASSCF computations (a problem persisting for several choices of active space), the EOM-CCSD/aug-cc-pVTZ level of theory was chosen to generate the ab initio data for determining a PES for the S_1 state. The parameter ranges used to define the S_1 PES are given in Table 6.8. As discussed for the previous NN-expnn PESs, an energy cut-off (generated from analytical 1D potentials) is utilized to filter out high energy points from the PES fit. The 1D potential parameters for the analytical fits are provided in Appendix E: Tables E2 and E3 for radial and angular coordinates, respectively. A total of 180 1D, 4500 2D, 375 3D and 8000 random points were selected for the fitting. The test and the validation sets each consist of 1000 random data. The cut-off energy was selected to be 10000 cm^{-1} to cover the two torsional isomers and the transition state between them. As expected, the RMSE decreases with an increasing number of neurons (fitting parameter), see Table E1 in Appendix E. The fit with 80 neurons has a RMSE of 3.0 cm^{-1} and is selected for computing vibrational frequencies using MCTDH. Apart from the RMSE, 2D contour plots were generated to check the fitting quality with respect to the ab initio energies. From Figure 6.2, it can be seen that the shape of the fit PES shows excellent agreement with the ab initio data; as might be expected from the RMSE. A further more precise analysis of the PES quality is done in the next section by computing vibrational energies of the fundamental modes

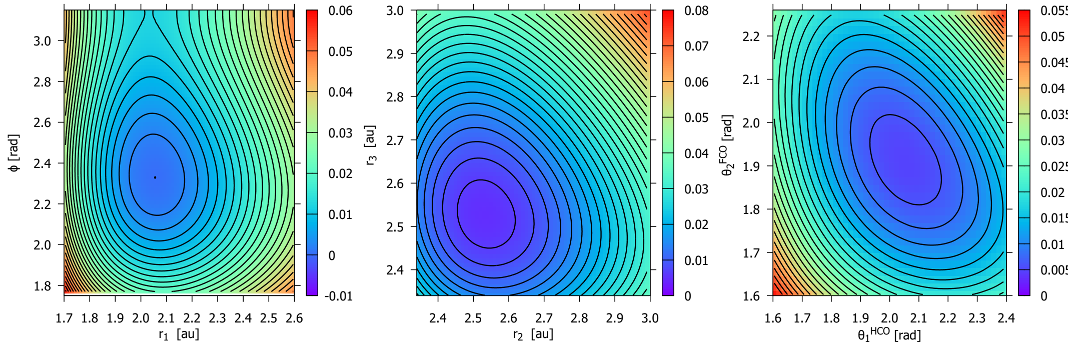

Figure 6.2: *Two dimensional (2D) contour plots of the NN-expnn fit S_1 PES of the HFCO molecule based on EOM-CCSD/aug-cc-pVTZ ab initio data; see main text for details.. (a) ϕ vs. r_1, (b) r_2 vs. r_3, and (c) θ_1^{HCO} vs. θ_2^{FCO} keeping other coordinates fixed at S_1 equilibrium values. The contour intervals are 0.002 au or 439 cm^{-1} for all the plots.*

using MCTDH.

6.3.5 Vibrational State Computations using MCTDH

6.3.5.1 EOM-CCSD S_1 surface

The vibrational energies of the fundamental modes as determined using block improved relaxation in MCTDH are given in Table 6.7 on the EOM-CCSD PES. The primitive grids, basis functions, single particle functions, and mode combinations used for the MCTDH computations are provided in Table 6.8. The RMSE of the fundamental modes is 42.6 cm^{-1} with respect to the experimental measurement.[284] The modes have been assigned based on the proximity to the harmonic frequencies. The FCO bending mode exhibits the best agreement (off by 4.5 cm^{-1}) while the HCO bending mode has the poorest (by 65.9 cm^{-1}). Additional mode combinations and overtones are also provided for the first 30 vibrational states, see Table E5 in Appendix E. Overall, the frequencies determined on the PES provide very good agreement with the experimental measurements, thus, reinforcing the overall accuracy of the surface.

Table 6.7: *MCTDH computed fundamental vibrational frequencies for the minimum energy structure on the S_1 PES fit to ab initio data at the EOM-CCSD/aug-cc-pVTZ level of theory.*

Method	CH str	CF str	CO str	HCO bend	FCO bend	ϕ bend
Expt.[284]	2935.0	1109.8	1106.0	1279.3	450.1	919.0
Expt.[288]			1112.0	1286.0	450.0	924.0
Expt.[289,290]	2935.0	(1107.0)	1111.0	(1185.0)	451.0	(570.0)
Ref [190][a]	3147.3	1149.1	1217.6	1384.7	462.3	996.5
EOM/MCTDH	2983.0	1125.7	1157.4	1345.2	454.6	876.9

[a] EOM-CCSD/DZP from 190.

Table 6.8: *Grid lengths and parameters of the primitive basis set employed for each degree of freedom. HO is the harmonic oscillator (Hermite) DVR.*

Modes	R_1	$\cos\theta_1$	R_2	$\cos\theta_2$	R_3	ϕ
Primitive basis	HO-DVR	HO-DVR	HO-DVR	HO-DVR	HO-DVR	HO-DVR
Number of basis functions	10	13	14	14	10	40
Grid length (a.u.)	[1.41,3.35]	[-0.99,0.135]	[2.06,3.62]	[-0.91,-0.055]	[1.75,2.93]	[1.48,4.82]
Mode combinations	(R_1, $\cos\theta_1$)		(R_2, $\cos\theta_2$)		(R_3,ϕ_1)	
Number of SPF	10		14		10	

6.4 Conclusion

Vertical excitation energies, optimized geometries of stationary points, and vibrational frequencies have been determined for the S_1 and the T_1 surfaces of HFCO using CASSCF, CASPT2, MRCI, and EOM-CCSD theoretical methods. The effect of the choice of active space (if applicable) on these properties was also demonstrated in this work. The capability of the NN-expnn method for fitting an excited state 6D PES is successfully demonstrated. We were able to generate the first 6D S_1 surface of HFCO based on ab initio energies at the EOM-CCSD/aug-cc-pVTZ level of theory. Further improvement in the PES quality could be accomplished using multireference MRCI or CASPT2 methods. Also, the development of a transition dipole moment surface between S_0 to S_1 would be required for future dynamics studies. Attempts are ongoing to construct MRCI and CASPT2 based 6D PESs but it is computationally costly and, hence, time consuming.

Chapter 7

Conclusions

7.1 Summary of Thesis Research

The goals of this thesis work were (i) to develop new full dimensional PESs based on high-level ab initio data, (ii) to fi the PESs to sum-of-products form using the neural network with exponential neurons technique, and (iii) to test the quality of the PESs by computing vibrational energies using methods available in MCTDH. The PESs were developed and tested for three different molecules: CS_2, HFCO, and HONO. The important conclusions from each specific study are summarized below.

In Chapter 2, new global PES and dipole moments surfaces for CS_2 based upon CASPT2/C:cc-pVTZ,S:aug-cc-pV(T+d)Z ab initio computations are reported. Using the neural network method with exponential neurons[1,2] the ab initio data is fit to sum-of-products form permitting ready use by the MCTDH software package.[3] The quality of the fits depends upon the energy cut-offs and the number of neurons, but overall excellent fits to both training (included in the fit) and test (external to the fit) data sets can be achieved with a modest number of neurons (fitting parameters). The present work in Chapter 2 represents one of the first NN fits directly to ab initio data - many NN fits are refits of analytical PESs. Importantly, the accurate global potential energy and dipole moment surfaces developed for CS_2 should permit future OCT-MCTDH studies.

In Chapter 3, a six dimensional (6D) PES was developed for HFCO based upon CCSD(T)-F12/cc-pVTZ-F12 ab initio computations. In exploring the PES, stationary points (equilibrium-HFCO, cis-HOCF, trans-HOCF, and the corresponding transition states) were determined at the same level of theory. A PES encompassing the equilibrium and transition state to dissociation (to HF + CO) was fit using the NN-expnn method. Comparatively few randomly selected points along with 1D and 2D cut points make this more efficient than *potfit*. As usual, the fitting quality depends on the number of neurons, cut-off energy and scaling of data. The new PES is far superior to the best PES previously available:[132] (i) currently based on CCSD(T)-F12/cc-pVTZ-F12 compared to MP2/cc-pVTZ (truncated) and (ii) a RMSE of only 25 cm^{-1} up to the 30000 cm^{-1} cut-off energy versus RMSE of 525 cm^{-1}. The frequencies determined for the fundamental vibrational modes on the new PES are within 2 cm^{-1} of the experimental values[181] - a factor of five improvement over those determined using the previous HFCO PES. Similarly, the vibrational state frequencies (up to 5000 cm^{-1} were much closer to the experimental measurements. A few high-energy states were provided new assignments. This PES may overcome the weaknesses of the previous PES permitting accurate calculations such as examining IVR and its control.

Following the success for HFCO presented in Chapter 3, a PES for a more complicated 6D system, HONO, was fit using the same approach and then used as a basis for computing the vibrational states (Chapter 4). In this Chapter, the capability of the NN-expnn method to fit a PES containing an asymmetric double well has been demonstrated. The CCSD(T)-F12/cc-pVTZ-F12 and CCSD(T)/CBS levels of theory have been used to generate ab initio energy data which are then used to fit two new PES. Vibrational energies for the fundamental modes have been determined to have RMSEs of 2.9 (3.9) cm^{-1} and 9.7 (7.2) cm^{-1} for the cis- and the trans-isomers. Surprisingly, the PESs do not deliver a significant accuracy as compared to the most recent CCSD(T)/cc-pVQZ (-g functions) based PES.[131] However, the CBS limit PES represent the most accurate one available for the HONO ground electronic surface in the cis-trans region.

In Chapter 5, the local HFCO PES developed in Chapter 3 is extended from just the equilibrium plus transition state to dissociation region to encompass the cis-HOCF, trans-HOCF isomers and the corresponding transition states between all minima. The PES fit demonstrates that the neural network exponential fitting procedure can be utilized for a 6D full PES containing multiple wells with proper number of fitting parameters (called neurons). The ab initio data sampling plays an important role in the quality of the fit; however, the present high quality fit (150 cm^{-1} RMSE) is to only 10000 data points. The trans-HOCF fundamental mode vibrational frequencies were computed using block improved relaxation in MCTDH. These represent the best available vibrational energies for these species and should hopefully facilitate their spectroscopic detection. The new global HFCO PES will enable the study of cis-trans isomerization , equilibrium to trans isomerization, unimolecular dissociation dynamics and the competition between these processes.

The applicability of the NN_expnn-MCTDH approach for excited state PESs has been successfully demonstrated in Chapter 6. Vertical excitation energies, optimized geometries and vibrational frequencies have been computed for the S_1 and the T_1 surfaces of the HFCO molecule using various computational approaches (CASSCF, CASPT2, MRCI and EOM-CCSD).The first 6D S_1 PES of HFCO (based on EOM-CCSD/aug-cc-pVTZ level of theory) has been generated. The fundamental frequencies as computed using block improved relaxation and the PES are improved relative to the harmonic frequencies. The excited state PES could be improved by using multireference methods like MRCI or CASPT2, but it's computationally costly and time consuming.

In brief, the main summary of achievements in this thesis are as the follows.

1. Successfully utilized sum-of-products representation of a PES using neural network fitting scheme with an exponential fitting function.

2. Interfaced the fitting method with MCTDH to generate the requisite operator files.

3. Applied the fitting method directly to newly computed high-level ab initio data (rather than refitting existing analytical PESs).

4. Successfully fit a diversity of PESs: a single well PES (Chapters 2 and 3), an asymmetric double well PES (Chapter 4), a PES containing multiple minima and the barriers between them (Chapter 5), and a symmetric double well, excited state PES (Chapter 6).

5. Used the PES to determine vibrational energies using approaches available in MCTDH.

7.2 Future Directions

There are a number of research directions that can be followed related to the specific molecules studied in this thesis as well as directions related to other molecules and/or the general PES fitting procedure.

7.2.1 Quantum Dynamics for HFCO

IVR is important because it provides all of the dynamical information about the relaxation of energy from one vibrational mode to anther or others. With the new PES, IVR without an external field can be studied for both HFCO and DFCO and compared and contrasted to previous results based upon the MP2 PES.[132] The intriguing differences observed between HFCO and DFCO can be verified. Of more interest is to examine IVR after excitation with an external laser field. After excitation, the pulse is switched off and the energy redistribution is examined as a function of time. The important step for HFCO is to investigate if control of IVR by modifying the excitation laser field is possible. This can be done by using optimal control theory.

With an excited state PES for HFCO, we can compute experimentally measured spectra, like those from Stimulated Emission pumping (SEP) experiments.[133] The use of excitation to S_1 for laser control of competition between unimolecular dissociation and cis-trans isomerization has been suggested[126,128] and the present, or new improved, excited state PES could be used for dynamics studies.

7.2.2 Studying IVR Dynamics in cis-trans HONO

With the new PES at CBS limit, IVR dynamics of HONO molecule can be studied. This includes studying the effect of IVR on cis-HONO to trans-HONO conversion. Control over cis-trans isomerization process by applying external laser pulse may also be studied.

7.2.3 PES Fitting for Higher Dimensional Systems

Before computing new ab initio data, it will be worthwhile to try the present NN-expnn approach to refit two challenging PESs: $H_3O_2^-$ and $H_5O_2^+$. There is considerable interest in fitting higher dimensional PESs, e.g., 12D, 15D, 18D . . for molecules containing 5, 6, 7 . . . atoms.

The structure of a hydroxide ion (OH^-) in water is a fundamental question in chemical physics. OH- solvation and transport share equivalent chemical and biological importance as proton solvation and transport do. Experimental[291] and theoretical[292,293] studies suggest that the most stable structure of solvated hydroxide is $H_3O_2^-$. To better interpret the experiments, a full dimensional PES was constructed and fundamental modes studied by Bowman and co-workers. This analytical PES was refitted using a newly developed Multigrid *potfit*[262,294]and quantum dynamics using MCTDH were performed. Now, with the motivation of applying the NN-expnn method for large systems, this $H_3O_2^-$ 9D analytical surface can be refit and MCTDH dynamics can be performed. This project will clearly test the advantages and disadvantages of NN-expnn in large systems. If the refitting becomes accurate enough for quantum dynamics, steps must be taken to optimize the computational effort by direct fitting of selective number of random data. If NN-expnn succeeds for this complicated, very anharmonic system, the next plan will be a 15D system and we have a classic system waiting: the protonated water dimer ($H_5O_2^+$).

The present lack of symmetry is one of the main issues for the NN-expnn approach for high dimensional potential energy surface fitting; although many intriguing problems lack symmetry. Although it is less important that we get exact permutation invariance symmetry in the types of quantum dynamics most commonly studied, there are various way one can get permutation invariance symmetry. In the future, one can include symmetry and make this approach more general applicable to other field, like classical or semiclassical molecular dynamics (MD), where exact symmetry plays crucial role in determining certain properties. The following possibilities can be pursued.

1. *Using symmetric input:* This approach was utilized in the CS_2 PES fitting (Chapter 2). Ideally, although it is not guaranteed, if the initial input layer is symmetrized, the final PES would be permutationally symmetric.

2. *Symmetric weight*: This approach is thought to gain control over the black box NN toolbox, but if possible, by initializing a symmetric weight matrix, one can achieve symmetry.

3. *Symmetric optimization*: Even if we start with symmetric input and symmetric initial weight matrix, during the optimization procedure, which is done by randomly selected step (Δx_i), the symmetry would break even by slight differences.

4. *Symmetry after fitting*: This could be done by taking the average of the difference between symmetrize points. This represents post processing procedure to the fit.

5. *PIP-NN*: The recently developed PIP-NN approach by Guo and co-workers[74–76] , can exert permutational symmetry by using permutation invariant polynomials as the fitting basis. Applied to many 6D and 9D systems but it can not be directly used in MCTDH as this is not a sum-of-products form (SOP) which is required for efficient computations in MCTDH.

6. *Product Neurons*: This is also a very recent development where a product neuron is considered (sum-of-products) instead of the natural neural network structure.[114] This method needs to be explored thoroughly. Ideally, using this

method any type of activation function, not just exponential neurons, can be utilized to obtain sum-of-products.

Appendix A

Appendix to Chapter 2

A.1 20000 cm^{-1} cut 30 NN fit PES operator file for CS_2

OP_DEFINE-SECTION
TITLE
CS2 vibrational Hamiltonian (J=0), 3 modes, valence coordinates
END-TITLE
END-OP_DEFINE-SECTION

PARAMETER-SECTION
carbon_mass = 12.0,AMU
sulphur_mass = 31.97207070,AMU #mass of S isotope 32
atomA_mass = sulphur_mass # mass of atom A in molecule A-C-B
atomB_mass = sulphur_mass # mass of atom B in molecule A-C-B
atomC_mass = carbon_mass # mass of atom C in molecule A-C-B
AC_mass = atomA_mass+atomC_mass # mass of diatom A-C
BC_mass = atomB_mass+atomC_mass # mass of diatom B-C
mass_r1 = atomA_mass*atomC_mass/AC_mass # reduced mass for mode r_1
mass_r2 = atomB_mass*atomC_mass/BC_mass # reduced mass for mode r_2
r0 = 1.29567405785
w0u0 = -0.327952912896661 , w0u1 = -0.175441733424893 , w0u2 = -0.730257421294945 , r1 = 0.0549666567879 , w1u0 = 0.304215449059582 , w1u1 = -0.872439548775528 , w1u2 = -0.119552958255330 , r2 = 0.673477940254 , w2u0 = -0.217291512437171 , w2u1 = -0.420639442155251 , w2u2 = -0.812409909595710 , r3 = 0.118682259632 , w3u0 = 0.106262384159525 , w3u1 = -0.262479393081829 , w3u2 = -0.053516186547833 , r4 = -0.548783847961 , w4u0 = -1.014535697184358 , w4u1 = -0.095112547812548 , w4u2 = -1.210651851051992 , r5 = 0.717483678682 , w5u0 = -0.105114009089433 , w5u1 = 0.008985208382246 , w5u2 = -1.029429987114359 , r6 = 25.5855779365 , w6u0 = -0.445222999271730 , w6u1 = -0.576731414555088 , w6u2 = -0.460640522111992 , r7 = 1.43336209458 , w7u0 = -0.952283525133364 , w7u1 = -0.770812382035826 , w7u2 = -0.114196579361813 , r8 = -14.86011284 , w8u0 = -0.166570817573439 , w8u1 = -0.625043950070455 , w8u2 = -0.106895306435865 , r9 = 98.82563418 , w9u0 = -2.223038559943193 , w9u1 = -0.000633559139698 , w9u2 = 0.025521912104364 , r10 = -3.51536585744 , w10u0 = -0.719302377318887 , w10u1 = -0.123190588884681 , w10u2 = 0.253549933340931 , r11 = 1.36673589343 , w11u0 = 0.235151298217273 , w11u1 = -0.205248098675018 , w11u2 = -0.233217476656203 , r12 = 97.3909184894 , w12u0 = -0.003118579239875 , w12u1 = -2.196360271285245 , w12u2 = 0.033916019893438 , r13 = -5.45284952368 , w13u0 = 0.751267028797243 , w13u1 = -0.752752411391287 , w13u2 = -2.081160311943358 , r14 = 0.882803094206 , w14u0 = 1.020309321200067 , w14u1 = -0.661256258107061 , w14u2 = -1.360757721021164 , r15 = 0.213802424947 , w15u0 = 0.037507621964053 , w15u1 = -0.998750889057260 , w15u2 = -0.404236669941202 , r16 = -0.261235348293 , w16u0 = -0.361179392439589 , w16u1 = 0.523977168477960 , w16u2 = -0.132505877927043 , r17 = -4.6282762067 , w17u0 = -0.453208942050653 , w17u1 = 0.558516249938531 , w17u2 = -2.167760944350079 , r18 = 0.312294677962 , w18u0 = -0.498849740626020 , w18u1 = -0.781952311121204 , w18u2 = -0.177180118487842 , r19 = 0.963227708137 , w19u0 = -0.452092118062645 , w19u1 = -0.528031745669198 , w19u2 = 0.653690953876505 , r20 = 0.351923103002 , w20u0

= -0.211885526880373 , w20u1 = -0.555562225984790 , w20u2 = -0.665675088460327 , r21 = 2.96746904986 , w21u0 = -0.246233992183106 , w21u1 = 0.197603854729111 , w21u2 = -0.103545628855087 , r22 = 7.4133048386 , w22u0 = -0.622739144347201 , w22u1 = -0.604210668744344 , w22u2 = -0.336806758709181 , r23 = -5.38036835509 , w23u0 = -0.405145786862715 , w23u1 = 0.118424886412600 , w23u2 = -0.320423175987198 , r24 = -0.19849288983 , w24u0 = -0.888838664449894 , w24u1 = -1.063562298440717 , w24u2 = -0.380204103114571 , r25 = -0.498759956771 , w25u0 = -0.025488617801323 , w25u1 = -1.231751972663265 , w25u2 = 0.640844936319456 , r26 = -0.602307153513 , w26u0 = 0.837344713534070 , w26u1 = -0.576477716540267 , w26u2 = -0.793949210791733 , r27 = 0.905603924045 , w27u0 = -0.288496644111838 , w27u1 = 0.648437026516376 , w27u2 = -1.342828241214197 , r28 = 165.400074001 , w28u0 = -0.337132324980444 , w28u1 = -0.411891218835125 , w28u2 = -2.535211279333682 , r29 = -0.502473529596 , w29u0 = 0.107969234506929 , w29u1 = 0.275815257854231 , w29u2 = -0.795231168133907 , c = -0.757324657839792
end-parameter-section
LABELS-SECTION
General form of the labels are given in order to save space.
qiuj = exp[wiuj, 0.0]
Where i goes from 0 to 29 and j goes from 0 to 2.
So, there will be 30x3 = 90 labels term in this operator file.
end-labels-section

HAMILTONIAN-SECTION
———————————————

modes | r1 | r2 | theta
———————————————

1.0 | 1 | KE | 1 # kinetic energy
1.0 | KE | 1 | 1
0.5/mass_r1 | 1 | q^-2 | j^2
0.5/mass_r2 | q^-2 | 1 | j^2
-1.0/atomC_mass | dq | dq | cos
1.0/atomC_mass | dq | q^-1 | dth1
1.0/atomC_mass | q^-1 | dq | dth1
-0.5/atomC_mass | q^-1 | q^-1 | cos*j^2
-0.5/atomC_mass | q^-1 | q^-1 | j^2*cos
—————————————————————

c | 1 | 1 | 1
The following lines would have the following genral form
ri | qiu0 | qiu1 | qiu2
So, total 30 lines will be there; i goes from 0 to 29
——————————————————

end-hamiltonian-section
end-operator

A.2 30000 cm^{-1} cut 30 NN fit PES operator file for CS_2

OP_DEFINE-SECTION
TITLE
CS2 vibrational Hamiltonian (J=0), 3 modes, valence coordinates
END-TITLE
END-OP_DEFINE-SECTION

PARAMETER-SECTION
carbon_mass = 12.0,AMU
sulphur_mass = 31.97207070,AMU #mass of S isotope 32
atomA_mass = sulphur_mass # mass of atom A in molecule A-C-B
atomB_mass = sulphur_mass # mass of atom B in molecule A-C-B
atomC_mass = carbon_mass # mass of atom C in molecule A-C-B
AC_mass = atomA_mass+atomC_mass # mass of diatom A-C
BC_mass = atomB_mass+atomC_mass # mass of diatom B-C
mass_r1 = atomA_mass*atomC_mass/AC_mass # reduced mass for mode r_1
mass_r2 = atomB_mass*atomC_mass/BC_mass # reduced mass for mode r_2
r0 = 16.8727225723

w0u0 = 0.263140369037430 , w0u1 = 0.599952135851169 , w0u2 = -3.945267875858313 , r1 = 2.60806149972 , w1u0 = -1.507236156822487 , w1u1 = -0.169269751497554 , w1u2 = 0.672303545495449 , r2 = -291.005926518 , w2u0 = -1.378292421059135 , w2u1 = -0.181363884492541 , w2u2 = -1.606401197908763 , r3 = -1.40060079079 , w3u0 = -0.935730150806799 , w3u1 = 0.432890827309715 , w3u2 = 0.164391443926151 , r4 = -1.48146892944 , w4u0 = 0.182567536921395 , w4u1 = -0.872004257294149 , w4u2 = 0.123707222170108 , r5 = -213.066717604 , w5u0 = -0.214242046260980 , w5u1 = -1.999972383754222 , w5u2 = -1.307333839889177 , r6 = 0.028179363993 , w6u0 = -0.602187951767044 , w6u1 = -0.584353051621127 , w6u2 = -0.449892184802155 , r7 = -1.10435549627 , w7u0 = -0.108073768270261 , w7u1 = 0.191698851035442 , w7u2 = 0.311447886221166 , r8 = -0.346750767256 , w8u0 = -0.979120507007944 , w8u1 = -0.099026607633129 , w8u2 = 1.233613172639767 , r9 = -2.88144898539 , w9u0 = 0.211164494488806 , w9u1 = 0.608158824928671 , w9u2 = -2.463361658394999 , r10 = -0.89802914654 , w10u0 = 0.138840760637955 , w10u1 = -1.075419316281596 , w10u2 = 0.125249430566725 , r11 = 0.823603900561 , w11u0 = 0.112254467591375 , w11u1 = 0.567607943439074 , w11u2 = -1.570882634854479 , r12 = 0.391655512539 , w12u0 = -1.899881611970750 , w12u1 = 1.272468738373617 , w12u2 = -1.643534080407167 , r13 = -19.8357871038 , w13u0 = -0.460389732196558 , w13u1 = -0.446528180243459 , w13u2 = 0.034547371656902 , r14 = -1.00221425597 , w14u0 = -0.323892787045409 , w14u1 = 0.130534277562755 , w14u2 = 0.760451237289668 , r15 = 1.32755490385 , w15u0 = -0.738159098771926 , w15u1 = -0.175761133518781 , w15u2 = -0.337341060699669 , r16 = 0.444714200591 , w16u0 = -1.008482447748633 , w16u1 = 0.537694216501576 , w16u2 = 0.296023464885022 , r17 = -1.5176006972 , w17u0 = -0.193481767983006 , w17u1 = 0.125050496952595 , w17u2 = -1.166282632115810 , r18 = 1.25750650261 , w18u0 = -0.601270365231147 , w18u1 = 0.049771409083551 , w18u2 = -0.319270270749412 , r19 = 448.734464614 , w19u0 = -0.867114612841849 , w19u1 = -0.522427174336340 , w19u2 = -1.629921006149796 , r20 = 1.34495349989 , w20u0 = -0.672938653078943 , w20u1 = -0.486774047661074 , w20u2 = -0.253156419768459 , r21 = 0.306783290136 , w21u0 = 0.354732612715661 , w21u1 = -1.426408560542743 , w21u2 = 0.443925378683336 , r22 = -304.451762011 , w22u0 = 0.359663841177716 , w22u1 = 0.625568902259166 , w22u2 = -6.606436410990621 , r23 = 121.764163623 , w23u0 = -2.285500853045862 , w23u1 = 0.023829938883183 , w23u2 = -0.088441956896209 , r24 = 0.162521771066 , w24u0 = -0.688226123388612 , w24u1 = -0.193951434578293 , w24u2 = -0.298662813114304 , r25 = 133.386274603 , w25u0 = 0.014085948724475 , w25u1 = -2.320888639788417 , w25u2 = -0.069083774734274 , r26 = 17.2511594055 , w26u0 = -0.431425514239506 , w26u1 = -0.799217045412624 , w26u2 = 0.090181980172482 , r27 = 1.7957466214 , w27u0 = -0.227930755587869 , w27u1 = 0.165018522130335 , w27u2 = 0.564661940876118 , r28 = 0.31215806998 , w28u0 = -0.709306541255109 , w28u1 = -0.040023174397826 , w28u2 = 1.202349535821289 , r29 = 1.65272515513 , w29u0 = -0.739787117067775 , w29u1 = -0.152901926973949 , w29u2 = -0.253868363878868 , c = 1.220684930195138
end-parameter-section

LABELS-SECTION
General form of the labels are given in order to save space.
qiuj = exp[wiuj, 0.0]
Where i goes from 0 to 29 and j goes from 0 to 2.
So, there will be 30x3 = 90 labels term in this operator file.
end-labels-section

HAMILTONIAN-SECTION

modes | r1 | r2 | theta

1.0 | 1 | KE | 1 # kinetic energy
1.0 | KE | 1 | 1
0.5/mass_r1 | 1 | q^-2 | j^2
0.5/mass_r2 | q^-2 | 1 | j^2
-1.0/atomC_mass | dq | dq | cos
1.0/atomC_mass | dq | q^-1 | dth1
1.0/atomC_mass | q^-1 | dq | dth1
-0.5/atomC_mass | q^-1 | q^-1 | cos*j^2
-0.5/atomC_mass | q^-1 | q^-1 | j^2*cos

c | 1 | 1 | 1
The following lines would have the following genral form
ri | qiu0 | qiu1 | qiu2
So, total 30 lines will be there; i goes from 0 to 29

end-hamiltonian-section
end-operator

A.3 50000 cm^{-1} cut 30 NN fit PES operator file for CS_2

OP_DEFINE-SECTION

TITLE

CS2 vibrational Hamiltonian (J=0), 3 modes, valence coordinates

END-TITLE

END-OP_DEFINE-SECTION

PARAMETER-SECTION

carbon_mass = 12.0,AMU

sulphur_mass = 31.97207070,AMU #mass of S isotope 32

atomA_mass = sulphur_mass # mass of atom A in molecule A-C-B

atomB_mass = sulphur_mass # mass of atom B in molecule A-C-B

atomC_mass = carbon_mass # mass of atom C in molecule A-C-B

AC_mass = atomA_mass+atomC_mass # mass of diatom A-C

BC_mass = atomB_mass+atomC_mass # mass of diatom B-C

mass_r1 = atomA_mass*atomC_mass/AC_mass # reduced mass for mode r_1

mass_r2 = atomB_mass*atomC_mass/BC_mass # reduced mass for mode r_2

r0 = -7.1319203778

w0u0 = -0.099809343353529 , w0u1 = -1.094154209296849 , w0u2 = -0.650828971003954 , r1 = -1.69390635501 , w1u0 = 0.324158287055998 , w1u1 = -0.733113069591260 , w1u2 = -0.622811261367949 , r2 = -0.0239336449602 , w2u0 = -0.328123810173451 , w2u1 = -0.411839647633562 , w2u2 = -0.245410838076090 , r3 = 1.47235766595 , w3u0 = 0.062616552868763 , w3u1 = -0.258099328465247 , w3u2 = 0.235048002984682 , r4 = -0.0533910208811 , w4u0 = -1.027154578475860 , w4u1 = 0.261617852984466 , w4u2 = -0.747867299992593 , r5 = 67.1748090843 , w5u0 = -2.334409898376570 , w5u1 = 0.162184751785010 , w5u2 = 0.032482951295569 , r6 = 0.871645259717 , w6u0 = -0.108682510260418 , w6u1 = 0.081242170086103 , w6u2 = -0.299859641597994 , r7 = 0.589746103021 , w7u0 = -0.839061619729243 , w7u1 = -0.740582086583470 , w7u2 = -0.639250646964926 , r8 = 0.43028242578 , w8u0 = -0.677043650714482 , w8u1 = -1.038258662654963 , w8u2 = 0.270289854591321 , r9 = -1.28368513436 , w9u0 = -2.394245305776177 , w9u1 = 0.445682003260440 , w9u2 = 0.596917223938968 , r10 = -0.343626807709 , w10u0 = -0.682062085805540 , w10u1 = 0.789878059438881 , w10u2 = -0.971144981824822 , r11 = -0.262276655431 , w11u0 = 0.139147364451021 , w11u1 = -0.034081319212657 , w11u2 = 0.115833841285072 , r12 = 0.00105795904679 , w12u0 = -0.988219689948803 , w12u1 = -0.889111453506282 , w12u2 = -0.849326196914439 , r13 = 38.1229294783 , w13u0 = -1.858216668558270 , w13u1 = -0.349330753361932 , w13u2 = 0.038142503349225 , r14 = -1.19452133252 , w14u0 = -1.100778112575936 , w14u1 = 0.145567030369686 , w14u2 = 0.438073646365512 , r15 = -120.926849215 , w15u0 = 0.489735034057426 , w15u1 = -2.002506560980035 , w15u2 = -2.422877404457820 , r16 = 1.71687502535 , w16u0 = 0.588763004709793 , w16u1 = -1.654113119458458 , w16u2 = -0.964663399685054 , r17 = 2.73520812954 , w17u0 = -0.838403751715716 , w17u1 = 0.675437957364109 , w17u2 = -1.700503072816013 , r18 = 7.68356112037 , w18u0 = 0.474057335464516 , w18u1 = -0.607461138655543 , w18u2 = -2.457723860556857 , r19 = -69.7965863517 , w19u0 = -1.923032101870550 , w19u1 = 0.450077353787281 , w19u2 = -1.845278068907596 , r20 = -16.4768350692 , w20u0 = -0.446689869973532 , w20u1 = -0.201350533176355 , w20u2 = -0.463809774230689 , r21 = 0.216429185521 , w21u0 = -0.259292870339033 , w21u1 = -1.014176882688411 , w21u2 = -0.131921602275702 , r22 = 116.897387911 , w22u0 = -0.003136718944345 , w22u1 = -2.265263434645185 , w22u2 = -0.016550216096211 , r23 = 0.0810721965561 , w23u0

= -0.627726693359049 , w23u1 = -0.479487463050294 , w23u2 = -0.125279815860544 , r24 = 121.911503659 , w24u0 = -0.581857527220109 , w24u1 = -0.493692006255399 , w24u2 = -1.215844509456250 , r25 = -2.24964023104 , w25u0 = 0.407348516112647 , w25u1 = 0.238930931522123 , w25u2 = -3.319982775925897 , r26 = -2.57815599511 , w26u0 = -0.018142218904387 , w26u1 = -0.534431165867142 , w26u2 = 0.454964862260570 , r27 = 0.631045343638 , w27u0 = -0.084988938434242 , w27u1 = -0.652415603132010 , w27u2 = 0.753368229857784 , r28 = 0.164314213612 , w28u0 = -1.622139824084987 , w28u1 = 0.266596752745178 , w28u2 = 1.010609604535488 , r29 = 0.0298603363281 , w29u0 = -0.749689190978513 , w29u1 = 0.886355982333791 , w29u2 = -0.420639340422583 , c = 0.272084269200190
end-parameter-section

LABELS-SECTION
General form of the labels are given in order to save space.
qiuj = exp[wiuj, 0.0]
Where i goes from 0 to 29 and j goes from 0 to 2.
So, there will be 30x3 = 90 labels term in this operator file.
end-labels-section

HAMILTONIAN-SECTION
——————————————
modes | r1 | r2 | theta
——————————————
1.0 | 1 | KE | 1 # kinetic energy
1.0 | KE | 1 | 1
0.5/mass_r1 | 1 | q^-2 | j^2
0.5/mass_r2 | q^-2 | 1 | j^2
-1.0/atomC_mass | dq | dq | cos
1.0/atomC_mass | dq | q^-1 | dth1
1.0/atomC_mass | q^-1 | dq | dth1
-0.5/atomC_mass | q^-1 | q^-1 | cos*j^2
-0.5/atomC_mass | q^-1 | q^-1 | j^2*cos
————————————————————-
————————————————————-
c | 1 | 1 | 1
The following lines would have the following genral form
ri | qiu0 | qiu1 | qiu2
So, total 30 lines will be there; i goes from 0 to 29
————————————————-
end-hamiltonian-section
end-operator

Appendix B

Appendix to Chapter 3

B.1 Fit to 1D Potential Energy Curves

To determine the total energy for use in the energy filter, Eq. (2) in the main text, a simple sum over 1D potential energies is computed, i.e.,

$$V^0_{total}(R_1, R_2, R_3, \theta_1, \theta_2, \phi) = \sum_{i=1}^{6} V_i^0(x_i) \tag{B.1}$$

where $V_i^0(x_i)$ is a fit to the 1D potential energy along coordinate x_i. For the distance coordinates (R_1, R_2 and R_3), the 1D potentials were fit to Morse oscillator forms. The Morse oscillator is defined in terms of the dissociation energy (a_0), predissociation factor (a_1) and equilibrium coordinate (a_2) as,

$$V_i^0(x) = a_0(1 - e^{-a_1(x-a_2)})^2. \tag{B.2}$$

The corresponding fitting parameters are defined in Table B5. For the angular coordinates ($\cos\theta_1$, $\cos\theta_2$ and ϕ), the 1D potentials were fit to n^{th} order polynomial functional forms defined as

$$V_i^0(x) = \sum_{q=0}^{n} (a_n x^n). \tag{B.3}$$

For ($\cos\theta_1$, $\cos\theta_2$), the fits were to fourth-order polynomials, while for ϕ a fifth-order polynomial was used, see Table B6 for the fitting parameters.

Table B1: *Structural Parameters (bond lengths in Å; angles in degrees) and, when available, relative energies (in cm^{-1}) of HFCO isomers at the CCSD(T)-F12/cc-pVTZ-F12 level of theory as compared to previous computational and experimental results (results provided with number of significant figures presented in the original work). Dihedral angle ϕ is 180 for equilibrium and trans-isomer and 0 for the cis-isomer.*

	R_1[a]	R_2^{CF}	R_3^{CO}	θ_1[b]	θ_2^{FCO}	Energy
Equilibrium						
This work	1.091	1.341	1.179	127.8	122.7	0
Experiment[c]	1.095±0.008	1.338±0.005	1.181±0.005	127.3±3	122.8±0.5	0
Experiment[d]	1.11±0.02	1.346±0.003	1.188±0.004	130±4	122.3±0.2	0
Experiment[e]	1.098	1.341	1.183	129	122.7	0
CCSD(T)/cc-pVQZ[f]	1.0914	1.3401	1.1800	127.7	122.8	0
CCSD(T)/cc-pVQZ(ae)[g]	1.0890	1.3368	1.1779	127.605	122.823	0
CCSD/DZ+P[h]	1.097	1.345	1.192	127.5	123.0	0
CCSD/DZP[i]	1.0947	1.3403	1.1874	127.35	123.13	0
MP2/6-31G*[j]	1.094	1.352	1.194	127.6	123.2	0
MP2/TZ2P[k]	1.087	1.350	1.183	128.0	122.9	0
MP2/6-311G**[l]	1.094	1.345	1.183	127.9	123.2	0
MP2/cc-pVTZ[m]	1.085	1.348	1.184	127.9	123.0	0
CASSCF(8,7)/cc-pVTZ[n]	1.082	1.321	1.184	127.6	122.8	0
Cis-isomer						
This work	0.976	1.341	1.295	111.2	106.8	15180
CCSD/DZ+P[h]	0.980	1.353	1.309	110.7	106.0	15000
MP2/6-31G*[j]	0.998	1.354	1.304	110.7	105.9	15700
MP2/6-311G**[l]	0.977	1.340	1.295	109.8	106.8	15900
Trans-isomer						
This work	0.964	1.317	1.308	106.1	104.5	14809
CCSD/DZ+P[h]	0.969	1.328	1.322	105.6	104.0	15000
MP2/6-31G*[j]	0.976	1.330	1.318	105.9	103.9	15500
MP2/6-311G**[l]	0.964	1.317	1.308	104.6	109.7	15200

[a] For equilibrium, $R_1 = R^{CH}$, while for cis- and trans-isomers, $R_1 = R^{OH}$; [b] For equilibrium, $\theta_1 = \theta^{HCO}$, while for cis- and trans-isomers, $\theta_1 = \theta^{HOC}$; [c] Ref. 186 ; [d] Ref. 185 ; [e] Ref. 184 ; [f] Ref. 187. Also, determined at CCSD(T)/cc-pVTZ, CCSD(T)/ANO1, and CCSD(T)/ANO2. CCSD(T)/cc-pVQZ results also available in Ref. 188 ; [g] Ref. 189. Also determined at CCSD(T)/cc-pVXZ (ae), MP2/cc-pVXZ (ae and fc), MP2/cc-pVXZ + aug(f,O) (ae and fc) (X = D, T, and Q) levels of theory; [h] Ref. 202 Relative Energy at CCSD/DZ+P with ZPE at CISD/DZ+P; [i] Ref. 190 ; [j] Ref. 191 Relative energy at MP4(SDTQ)/6-311G**//MP2/6-31G* with ZPE; [k] Ref. 192 ; [l] Ref. 193 Relative energy at MP4(SDTQ)/6-311++G**//MP2/6-311G* with ZPE.; [m] Ref. 132 *f* functions removed from F,C, and O, *d* functions from H; [n] Ref. 194 .

Table B2: *Structural Parameters (bond lengths in Å; angles in degrees) and relative energies (in cm^{-1}) of HFCO transition states at the CCSD(T)-F12/cc-pVTZ-F12 level of theory as compared to previous computational results.*

	$R_1^{OH/CH}$	R_2^{CF}	R_3^{CO}	θ_1^{HOC}	θ_2^{FCO}	ϕ	Energy
			$TS_{trans\leftrightarrow cis}$				
This work	0.964	1.320	1.332	113.4	106.5	90.3	21013
CCSD/DZ+P[a]	0.969	1.331	1.349	112.3	105.9	90.3	21000
MP2/6-31G*[b]	0.974	1.333	1.343	114.0	105.9	90.9	22300
MP2/6-311G**[c]	0.964	1.319	1.334	110.8	106.5	89.6	21900
			$TS_{eq\leftrightarrow trans}$				
This work	1.246	1.320	1.260	59.2	115.4	180	26416
CCSD/DZ+P[a]	1.235	1.330	1.269	59.7	115.6	180.0	26900
MP2/6-31G*[b]	1.260	1.336	1.279	57.6	114.3	180.0	26400
MP2/6-311G**[c]	1.240	1.325	1.269	58.0	115.1	180.0	26200
			$T_{dissociation}$				
This work	1.136	1.857	1.132	170.6	121.6	0	16993
CCSD/DZ+P[a]	1.138	1.828	1.147	171.6	122.0	0.0	16400
MP2/6-31G*[b]	1.146	1.803	1.156	170.4	121.6	0.0	16400
MP2/6-311G**[c]	1.135	1.808	1.144	188.6	122.0	0	15100
MP2/cc-pVTZ[d]	1.126	1.843	1.140	48.8	122.2	0.0	16700

[a] Ref. 202 Relative Energy at CCSD/DZ+P with ZPE at CISD/DZ+P; [b] Ref. 191 Relative energy at MP4(SDTQ)/6-311G**//MP2/6-31G* with ZPE; [c] Ref. 193 Relative energy at MP4(SDTQ)/6-311++G**//MP2/6-311G* with ZPE. [d] Ref. 132 *f* functions removed from F,C, and O, *d* functions from H;

Table B3: *Theoretical Harmonic and Experimentally Measured Fundamental Frequencies (in cm^{-1}) of DFCO.*

	Present Results				Previous Results	
Mode	MP2[a]	CCSD[a]	CCSD(T)[a]	CCSD(T)-F12[b]	CCSD(T)[c]	Expt[d]
ν_5 FCO bending	654.9	674.7	658.3	664.5	667.3	657.0
ν_6 out of plane bending	875.2	891.0	868.3	871.9	878.9	857.4
ν_2 CF stretching	1077.6	1126.1	1092.6	1099.9	1120.9	1073.2
ν_4 DCO bending	989.1	1002.5	984.0	987.2	994.7	967.9
ν_3 CO stretching	1803.8	1860.3	1814.6	1826.4	1830.7	1796.8
ν_1 CD stretching	2358.2	2355.3	2332.2	2334.1	2333.2	2261.8
RMSE	41.1	55.1	31.7	35.2	40.7	

[a]aug-cc-pVTZ basis set; [b]cc-pVTZ-F12 basis set; [c]cc-pVTZ basis set from [195]
[d] Experimental frequencies from;[182] numbers are within 0.3 cm^{-1} of measurements from [181]

Table B4: *Theoretical Anharmonic and Experimental Fundamental Frequencies (in cm^{-1}) of DFCO.*

	Present Results			Previous Results		
Mode	MP2[a]	CCSD[a]	CCSD(T)[a]	CCSD(T)[b]	Obs[c]	Intensity[d]
ν_5 FCO bending	647.3	667.9	650.9	660.2	657.0	17.3
ν_6 out of plane bending	861.8	877.7	857.7	864.9	857.4	0.4
ν_3 CF stretching	1052.3	1102.4	1068.2	1097.6	1073.2	156.4
ν_4 DCO bending	970.0	984.2	965.0	975.8	967.9	35.8
ν_3 CO stretching	1781.1	1834.4	1786.7	1795.1	1796.8	155.5
ν_1 CD stretching	2286.2	2283.4	2256.8	2258.8	2261.8	35.1
RMSE	15.3	24.3	5.7	11.1		

[a]aug-cc-pVTZ basis set; [b]cc-pVTZ basis set from.[195]
[c] Experimental frequencies from;[182] numbers are within 0.3 cm^{-1} of measurements from[181]
[d]Experimental intensities (in km/mol) from.[182]

Table B5: *One dimensional fitting parameters (in atomic units) to Morse functional form for R_1^{CH}, R_2^{CF} and R_3^{CO} physical coordinates.*

Physical Coordinates	Fitting Parameters		
	a_0	a_1	a_2
R_1^{CH}	0.177588	0.996014	2.06649
R_2^{CF}	0.161448	1.07919	2.54408
R_3^{CO}	0.335531	1.19789	2.22995

Table B6: *One dimensional fitting parameters (in atomic units) to the fourth order polynomial functional form for $\cos\theta_1^{HCO}$ and $\cos\theta_2^{FCO}$ as well as the fifth order polynomial for ϕ.*

Coordinates	Fitting Parameters					
	a_0	a_1	a_2	a_3	a_4	a_5
$\cos\theta_1^{HCO}$	0.0548669	0.139251	0.20238	0.52025	0.495075	—
$\cos\theta_2^{FCO}$	0.0974611	0.376063	0.499038	0.48174	0.399969	—
ϕ	0.814096	-0.843866	0.341579	-0.0659754	0.00524958	7.05362×10^{-8}

Table B7: *RMSE (in cm^{-1}) versus Number of Neurons (NN) for the PES with 20000 cm^{-1} and 30000 cm^{-1} cut-off Energies.*

NN	RMSE			
	30000 cm^{-1}		20000 cm^{-1}	
	train	test	train	test
25	134	132	86	80
30	80	93	67	65
35	65	82	59	53
40	58	70	48	46
45	56	64	43	39
50	53	60	28	32
55	43	56	26	29
60	39	46	24	27
65	44	50	21	25
70	33	45	22	25
75	32	40	24	25
80	31	43	21	22
85	41	45	23	25
90	33	41	24	24
95	36	42	21	23
100	35	39	20	22

Table B8: *Selected Vibrational Energies (in cm^{-1}) for States up to 5000 cm^{-1} for DFCO from the Present PES Compared with Experimental Measurements and Previous Computations.*

Assignment[b] ($\nu_1\nu_2\nu_3\nu_4\nu_5\nu_6$)	Expt[a]	This work	New Assignment ($\nu_1\nu_2\nu_3\nu_4\nu_5\nu_6$)
000010[c]	657.5	658.8	
000001[c]	857.4	859.2	
000100[c]	967.9	966.0	
010000[c]	1073.2	1074.3	
000110[c]	1624.5	1625.4	
000002[c]	1705.8	1706.8	
001000[c]	1796.8	1795.3	
010001[c]	1928.4	1928.8	000200
000200[c]	1930.6	1931.2	010001
010100[c]	2028.8	2028.8	020000
020000[c]	2137.8	2133.9	010100
100000[c]	2261.7	2258.2	
001002	3508.0	3505.8	
002000	3579.4	3576.7	
101000	4045.5	4040.1	
002010	4229.2	4227.5	
001003	4343.5	4344.3	
002001	4446.6	4446.4	
002100	4542.0	4538.7	
001031	4616.6	4622.2	
002020	4876.8	4878.6	
101001	4898.1	4894.6	
002011	5095.8	5097.0	
	RMSE	2.5	

[a] Experimental measurements and Vibrational assignments taken from[214]
[b] Vibrational states assignment from[214]
[c] Assignment and observed energies from[181]

B.2 20000 cm^{-1} cut 80 NN fit PES operator file for HFCO

OP_DEFINE-SECTION

title

HFCO in polyspherical coordinates (valence coordinates)

end-title

end-op_define-section

PARAMETER-SECTION

a11 = -0.996014

a12 = 2.06649

a21 = -1.07919

a22 = 2.54408

a31 = -1.19789

a32 = 2.22995

mh = 1.0, H-mass

mc = 12.00,AMU

mo = 15.9949146221,AMU

mf = 18.99840320,AMU

M11 = 1.0/mh+1.0/mc

M22 = 1.0/mf+1.0/mc

M33 = 1.0/mo+1.0/mc

Mu = 1.0/mc

R1eq = 2.06320d0

R2eq = 2.5340d0

R3eq = 2.228740d0

U1eq = 0.7894590d0

U2eq = 0.8414164680d0

E1eq = -0.61380310d0

E2eq = -0.54038720d0

coef1 = M11/2.0/R1eq/R1eq/U1eq/U1eq

coef2 = M33*E1eq*E1eq/2.0/R3eq/R3eq/U1eq/U1eq

coef3 = Mu*E1eq/R3eq/R1eq/U1eq/U1eq

coef4 = M22/2.0/R2eq/R2eq/U2eq/U2eq

coef5 = M33*E2eq*E2eq/2.0/R3eq/R3eq/U2eq/U2eq

coef6 = Mu*E2eq/R3eq/R2eq/U2eq/U2eq

coeff1 = coef6-coef1-coef2+coef3-coef4-coef5

coef7 = Mu*E2eq/R3eq/R1eq/U1eq/U2eq

coef8 = Mu*E1eq/R3eq/R2eq/U1eq/U2eq

coef9 = Mu/U1eq/U2eq/R1eq/R2eq

coef10 = M33*E1eq*E2eq/U1eq/U2eq/R3eq/R3eq

coeff2 = coef10+coef9-coef8-coef7

coeff3 = Mu/R3eq/R1eq

coeff4 = -1.0*Mu/R3eq/R1eq

coef11 = -1.0*M11/2.0/R1eq/R1eq

coef12 = -1.0*M33/2.0/R3eq/R3eq

coeff5 = coef11+coef12

coeff6 = Mu/R3eq/R2eq

coeff7 = -1.0*Mu/R3eq/R2eq

coef13 = -1.0*M22/2.0/R2eq/R2eq

coef14 = -1.0*M33/2.0/R3eq/R3eq

coeff8 = coef13+coef14

coef17 = -1.0*Mu*E1eq/R3eq/R1eq

coef16 = Mu*U1eq/R1eq/R2eq

coef15 = -1.0*Mu*E1eq/R1eq/R2eq

r0 = 128.124489369 , w0u0 = 0.040137487661079 , w0u1 = -2.710443139819253 , w0u2 = -0.124199393551891 , w0u3 = -0.020092703629714 , w0u4 = -0.263935236226315 , w0u5 = -0.000749269916428 , r1 = 0.0121762825833 , w1u0 = -0.036461006026643 , w1u1 = -1.141023515997769 , w1u2 = -0.334449677539109 , w1u3 = -2.227033994298276 , w1u4 = -2.058802651882234 , w1u5 = 1.086738646630416 , r2 = -0.00706861628274 , w2u0 = -0.140057097716009 , w2u1 = -0.934399651333664 , w2u2 = -0.326057709003596 , w2u3 = -8.699058955772657 , w2u4 = -1.504986635451121 , w2u5 = 0.463591994741920 , r3 = -0.166146774925 , w3u0 = 0.087879945905202 , w3u1 = -1.483220511371120 , w3u2 = -0.673177358133877 , w3u3 = -1.078538238677334 , w3u4 = -4.899817853148572 , w3u5 = -0.247092422908423 , r4 = -1.83923028522 , w4u0 = -0.159238786058514 , w4u1 = -0.896612471308449 , w4u2 = -0.441831910826347 , w4u3 = -5.244669062576353 , w4u4 = -1.834794185268330 , w4u5 = -0.579219393101293 , r5 = -0.0241405828049 , w5u0 = -0.741107400572856 , w5u1 = -0.190509952413128 , w5u2 = -0.541172076494760 , w5u3 = -1.881479155232513 , w5u4 = -4.446816665784924 , w5u5 = -0.218003741079337 , r6 = -0.000121045762459 , w6u0 = -0.171162547088383 , w6u1 = -0.917317376339388 , w6u2 = -0.304793909348580 , w6u3 = -11.824682012318728 , w6u4 = -1.675892498586720 , w6u5 = 0.162582969993692 , r7 = -0.000128369655274 , w7u0 = 0.416163100302564 , w7u1 = 0.419177728311576 , w7u2 = 1.373109953970858 , w7u3 = 0.742935216443815 , w7u4 = 0.387356785424296 , w7u5 = 0.268449817546541 , r8 = 6.21426816308 , w8u0 = -0.472020093455583 , w8u1 = -0.739533858702212 , w8u2 = -1.327328327967696 , w8u3 = -1.301418765007524 , w8u4 = -0.382319152745606 , w8u5 = 0.000579126648857 , r9 = 0.455341169598 , w9u0 = -0.167593781633230 , w9u1 = -1.068309151871655 , w9u2 = -0.487889350718625 , w9u3 = -3.349378689862172 , w9u4 = -3.003216456416223 , w9u5 = -0.322880457966888 , r10 = -0.00703043725673 , w10u0 = 0.242551413236576 , w10u1 = -0.533966908692903 , w10u2 = 0.894602043916614 , w10u3 = 0.238292759905640 , w10u4 = 0.583222250767733 , w10u5 = -0.293764447398971 , r11 = 0.00309759716838 , w11u0 = 1.006882898046506 , w11u1 = -0.278382440973430 , w11u2 = 0.586323768923906 , w11u3 = 0.203215235910327 , w11u4 = 2.264837133512882 , w11u5 = -0.479965483267225 , r12 = -0.665014409411 , w12u0 = -0.568294455330479 , w12u1 = 0.422996497113824 , w12u2 = -1.196643320868624 , w12u3 = -0.639442291754536 , w12u4 = -0.127312893508765 , w12u5 = -0.095141869112225 , r13 = -0.290884343075 , w13u0 = 0.061274991466938 , w13u1 = -0.215027949834770 , w13u2 = -0.139128151785414 , w13u3 = -0.645354793204209 , w13u4 = -1.957051786680891 , w13u5 = -1.062331822982396 , r14 = 6.06196979775d-11 , w14u0 = -0.349820362574212 , w14u1 = -1.220187849277006 , w14u2 = -0.213942002608440 , w14u3 = -24.372145402702664 , w14u4 = -1.802536957866496 , w14u5 = 0.048817607599183 , r15 = -2.43918433698 , w15u0 = -0.132515251085822 , w15u1 = -0.175382967617338 , w15u2 = -0.409489138374416 , w15u3 = -0.234092237809939 , w15u4 = -0.372054189216452 , w15u5 = 0.011177015019942 , r16 = 2.03678672153 , w16u0 = -0.239325508295263 , w16u1 = -1.333895712022472 , w16u2 = -0.295176183029563 ,

w16u3 = -2.868821616951403 , w16u4 = 1.476109672624921 , w16u5 = -0.116922835334863 , r17 = 0.133558872174 , w17u0 = -1.419620703871924 , w17u1 = 0.073980170805745 , w17u2 = 1.135394481818336 , w17u3 = 1.503555426944914 , w17u4 = 1.094321997884999 , w17u5 = -0.227655645967066 , r18 = 0.832888497006 , w18u0 = -0.413750995949658 , w18u1 = 0.921064744936459 , w18u2 = -2.479449754507122 , w18u3 = 0.101034957536337 , w18u4 = 0.975607174909722 , w18u5 = -0.064187710407504 , r19 = -0.00138226410509 , w19u0 = 0.022951747267462 , w19u1 = -0.608909827158913 , w19u2 = 0.077381774975621 , w19u3 = -0.385275996173070 , w19u4 = -2.571048312563065 , w19u5 = 1.167076039633680 , r20 = 0.162236202537 , w20u0 = 0.351569766037937 , w20u1 = -0.949042734340001 , w20u2 = 0.230540358361312 , w20u3 = 1.445478591607887 , w20u4 = -1.083383467616098 , w20u5 = -0.231136217789788 , r21 = -0.000270372496648 , w21u0 = 0.045276374742870 , w21u1 = -0.144077058248869 , w21u2 = -0.029696683501672 , w21u3 = -1.003118087326872 , w21u4 = -2.809594770329543 , w21u5 = 0.789565732410928 , r22 = -0.0153565175834 , w22u0 = 1.085706713352327 , w22u1 = -0.849445812129460 , w22u2 = -0.185122825080090 , w22u3 = -1.117618669473678 , w22u4 = -0.404643779084908 , w22u5 = -0.223196407469101 , r23 = 0.0831952014701 , w23u0 = 0.130614546488455 , w23u1 = 0.088200859437831 , w23u2 = 0.479883926629004 , w23u3 = 0.427578640287066 , w23u4 = 0.343806572140389 , w23u5 = 0.137733691501758 , r24 = -0.116671693152 , w24u0 = -0.334270377023386 , w24u1 = -0.616729669904437 , w24u2 = 0.749678069584090 , w24u3 = 0.772122579645578 , w24u4 = 0.487178585050946 , w24u5 = 0.757328001245972 , r25 = -31.8921653822 , w25u0 = -0.280336767427334 , w25u1 = -0.693884029288189 , w25u2 = 0.232194060537284 , w25u3 = 0.546033989387671 , w25u4 = 1.092290826013112 , w25u5 = -1.186501662080819 , r26 = 57.5054185738 , w26u0 = -0.064548447851620 , w26u1 = -1.060676991070500 , w26u2 = -0.486968075271273 , w26u3 = -4.308512126585911 , w26u4 = -1.848970738745815 , w26u5 = -1.209313903280875 , r27 = 0.148796960974 , w27u0 = -0.167336857520276 , w27u1 = -1.088457026950845 , w27u2 = -0.307397621308966 , w27u3 = -3.261877876216148 , w27u4 = -0.252907107188928 , w27u5 = 0.365508103275515 , r28 = -23.1353066059 , w28u0 = -0.115559632582877 , w28u1 = -0.933222295256185 , w28u2 = -0.506947699360696 , w28u3 = -5.243632621701725 , w28u4 = -1.620590420453323 , w28u5 = -1.525583574289916 , r29 = -11.3038603285 , w29u0 = -0.048683607242393 , w29u1 = -0.011458331651524 , w29u2 = -2.142147705004065 , w29u3 = -0.058270928019742 , w29u4 = 1.566534956638677 , w29u5 = -0.000569168914977 , r30 = 40.3607154387 , w30u0 = 0.085547926215999 , w30u1 = -0.574268559761161 , w30u2 = -2.397800696587281 , w30u3 = 0.787181056437170 , w30u4 = 1.004271704570243 , w30u5 = 0.022635745872854 , r31 = -0.10606449936 , w31u0 = 0.174608871588821 , w31u1 = -1.391501310314134 , w31u2 = -0.389481009177431 , w31u3 = -2.080825458073008 , w31u4 = -1.865969254256331 , w31u5 = 0.663498764642381 , r32 = 0.00588679450283 , w32u0 = -0.136859539716804 , w32u1 = -0.959208118073847 , w32u2 = -0.340782856496467 , w32u3 = -7.209010239289474 , w32u4 = -1.443806748053547 , w32u5 = 0.783441292909957 , r33 = 0.0034227725253 , w33u0 = 0.065662738510238 , w33u1 = -0.496989837299533 , w33u2 = 0.116428807746808 , w33u3 = -0.254573559976547 , w33u4 = -2.382454499584801 , w33u5 = 0.945791524094266 , r34 = -0.00306981954185 , w34u0 = -0.135474683919151 , w34u1 = -0.970956773441354 , w34u2 = -0.345387792553429 , w34u3 = -6.241157534122088 , w34u4 = -1.412809577333738 , w34u5 = 0.983456148150946 , r35 = -0.00758438070043 , w35u0 = -1.411576709037776 , w35u1 = 0.800293516086842 , w35u2 = 1.018019329249022 , w35u3 = 1.039510638104015 , w35u4 = 0.956064922001953 , w35u5 = -0.106656946358191 , r36 = -0.00702610999641 , w36u0 = 0.567705070291683 , w36u1 = -0.297276707091091 , w36u2 = 0.433970295875723 , w36u3 = 0.064202663981899 , w36u4 = 1.631866273507123 , w36u5 = -0.000492574697931 , r37 = 0.339849038205 , w37u0 = 0.610407777768204 , w37u1 = -1.472099820870112 , w37u2 = -0.482043069132616 , w37u3 = -1.260147305078096 , w37u4 = -1.221383568627253 , w37u5 = 0.173103555321636 , r38 = 12.7088266854 , w38u0 = -2.737440177062244 , w38u1 = 0.025861393665317 , w38u2 = 0.011719385200365 , w38u3 = -0.031732522880556 , w38u4 = -0.016456845018650 , w38u5 = 0.008304389416102 , r39 = -0.0183303579969 , w39u0 = 0.116393178521291 , w39u1 = -0.586650225647108 , w39u2 = 0.625668723870644 , w39u3 = 0.484638741527310 , w39u4 = -1.685443694091671 , w39u5 = 0.104332917499096 , r40 = 7.77759433329 , w40u0 = -0.142965733041113 , w40u1 = -0.880127750754475 , w40u2 = -0.542462494766485 ,

w40u3 = -6.027295673386512 , w40u4 = -1.551208043642279 , w40u5 = -1.690737807147391 , r41 = -0.00226747426829 , w41u0 = -0.083859678032972 , w41u1 = -0.043650085502563 , w41u2 = 1.126033346971153 , w41u3 = -1.181518392734956 , w41u4 = -0.279601327571284 , w41u5 = -0.114931948927245 , r42 = -30.9023338944 , w42u0 = 0.127807931965331 , w42u1 = -2.070250422380765 , w42u2 = -0.228709329613492 , w42u3 = 0.097262352748193 , w42u4 = -0.487658813801283 , w42u5 = -0.018595995921280 , r43 = 0.891007847593 , w43u0 = -0.164770896846949 , w43u1 = -1.198120353049647 , w43u2 = -0.118657945737884 , w43u3 = -1.646443646338320 , w43u4 = 2.672979934135940 , w43u5 = 0.115623469699655 , r44 = 0.0195558287965 , w44u0 = -0.646385880691343 , w44u1 = 0.315305701617019 , w44u2 = -0.647491809260882 , w44u3 = -1.861321716740193 , w44u4 = -2.619015487590776 , w44u5 = -0.122069179225815 , r45 = -0.108548531671 , w45u0 = -0.126222485566917 , w45u1 = -0.921153762624014 , w45u2 = -0.370761705855669 , w45u3 = -7.265258958225432 , w45u4 = -1.577530818980395 , w45u5 = -0.341210645185910 , r46 = -5.18167931166 , w46u0 = -0.190329797052586 , w46u1 = -1.244066704231240 , w46u2 = -0.288553234923585 , w46u3 = -2.127182742300470 , w46u4 = 1.613194296682079 , w46u5 = 0.020458649981538 , r47 = 40.2589141386 , w47u0 = -0.364310093186241 , w47u1 = -0.689195417171440 , w47u2 = 0.417802522752694 , w47u3 = 0.655338981135459 , w47u4 = 0.818987934069982 , w47u5 = -1.201779111417280 , r48 = 0.00157644621871 , w48u0 = 0.108809562276208 , w48u1 = 0.309530846700291 , w48u2 = 0.454343424517953 , w48u3 = -0.663016803412630 , w48u4 = -1.287587287538993 , w48u5 = -0.055786520740306 , r49 = -0.0746607844791 , w49u0 = -0.587716946640231 , w49u1 = -0.883548293423336 , w49u2 = -0.643331979873909 , w49u3 = -2.921870040561912 , w49u4 = -1.816406625137438 , w49u5 = 0.459537122999923 , r50 = 0.0329840165428 , w50u0 = -0.310529689421199 , w50u1 = 0.529919819441376 , w50u2 = 0.332296962128098 , w50u3 = 0.895143929786300 , w50u4 = 1.330738371098162 , w50u5 = -0.495064746567159 , r51 = 0.0780623843555 , w51u0 = -0.283034410065500 , w51u1 = -0.105591925054730 , w51u2 = 0.225365098973117 , w51u3 = -1.741562660091419 , w51u4 = 0.142899568397821 , w51u5 = -0.658811727574754 , r52 = 2.2185356864 , w52u0 = -0.359691427249907 , w52u1 = -0.221814206318625 , w52u2 = -1.095607246023340 , w52u3 = 1.170283410149247 , w52u4 = -1.155767945833338 , w52u5 = -0.064195263092470 , r53 = -5.0473713757 , w53u0 = -0.563618762326593 , w53u1 = -0.540430609983167 , w53u2 = 0.799050758528616 , w53u3 = 0.862035692328084 , w53u4 = 0.648152703410060 , w53u5 = -0.745445107284330 , r54 = 0.207559916706 , w54u0 = -0.396750410893950 , w54u1 = -0.747001565337061 , w54u2 = 0.520047785137651 , w54u3 = 0.751978021945188 , w54u4 = -0.131398403335742 , w54u5 = 0.536453848935075 , r55 = 1.30738677914 , w55u0 = -0.138001266099466 , w55u1 = -0.920412428193479 , w55u2 = -0.414287831179455 , w55u3 = -5.922573474871533 , w55u4 = -1.711368275623303 , w55u5 = -0.511952156145028 , r56 = 0.147900654962 , w56u0 = -0.225317381042958 , w56u1 = -1.011889639430318 , w56u2 = -0.352676107512078 , w56u3 = -0.892655460604594 , w56u4 = -4.247572618067967 , w56u5 = -0.109941690728107 , r57 = 0.025642201965 , w57u0 = -0.341885135992243 , w57u1 = -0.637538493684470 , w57u2 = 0.738271197610248 , w57u3 = 0.760064052564946 , w57u4 = 0.539544642131843 , w57u5 = 1.002301919871780 , r58 = -0.560452056726 , w58u0 = -0.725477787253703 , w58u1 = -0.776982637910761 , w58u2 = 0.422956766367916 , w58u3 = 0.743169041713238 , w58u4 = -0.675546980694602 , w58u5 = 0.152043706621137 , r59 = -39.3140137859 , w59u0 = -0.045176511014172 , w59u1 = -1.109589495582303 , w59u2 = -0.486428590784518 , w59u3 = -4.186595858521640 , w59u4 = -1.917848300466221 , w59u5 = -1.108610060082485 , r60 = 128.316144274 , w60u0 = -0.022370801707895 , w60u1 = 0.009355870942746 , w60u2 = -3.181407032066770 , w60u3 = -0.054030535041023 , w60u4 = 0.058845319635126 , w60u5 = -0.001864685173006 , r61 = -0.0157717438974 , w61u0 = 0.157252844828024 , w61u1 = 0.502890596700117 , w61u2 = -0.035444438155443 , w61u3 = 0.789051047017819 , w61u4 = 0.921352848473982 , w61u5 = 0.095944459206918 , r62 = 0.0219175860388 , w62u0 = 0.106145419990129 , w62u1 = 0.143128744480006 , w62u2 = 0.219737478730973 , w62u3 = -1.024403928603240 , w62u4 = -0.393595075634468 , w62u5 = -0.029306660401594 , r63 = -0.000129936047167 , w63u0 = 0.411087694424877 , w63u1 = 0.750975625859717 , w63u2 = 0.490423107112534 , w63u3 = -1.075949880626333 , w63u4 = -1.454319341412126 , w63u5 = -0.304086053797731 , r64 = 0.054055199626 , w64u0 = -0.398776241538590 , w64u1 = -0.766475447257657 , w64u2 = 1.238352531428769

, w64u3 = 0.897169371432877 , w64u4 = 0.812910445879861 , w64u5 = 0.264302617098690 , r65 = 4.37776110397d-07 , w65u0 = -0.236882708877369 , w65u1 = -0.948556551246431 , w65u2 = -0.270960362139405 , w65u3 = -1.704341779421827 , w65u4 = -14.865785742695991 , w65u5 = -0.047138689476918 , r66 = -0.229051279259 , w66u0 = 0.523855552396917 , w66u1 = 0.050983321502104 , w66u2 = -1.291952238577565 , w66u3 = 1.171929216058235 , w66u4 = -0.548845968862213 , w66u5 = -0.202806637735949 , r67 = 23.5368293675 , w67u0 = -0.028518726510973 , w67u1 = -1.065816124759037 , w67u2 = -0.927843674693096 , w67u3 = -0.363794250379981 , w67u4 = 2.667150463392842 , w67u5 = -0.033576288026181 , r68 = 0.00434652373603 , w68u0 = -0.145057036997823 , w68u1 = -0.920094275546127 , w68u2 = -0.318031312894424 , w68u3 = -9.579300240546406 , w68u4 = -1.559649253101392 , w68u5 = 0.295190319078633 , r69 = 1.19097666288 , w69u0 = -0.722956503861648 , w69u1 = -0.853986967857790 , w69u2 = 0.882040116416631 , w69u3 = 0.707690145630797 , w69u4 = -0.104312248850064 , w69u5 = -0.519757907426640 , r70 = -0.093783686581 , w70u0 = 0.496150959075417 , w70u1 = -0.574665828924528 , w70u2 = 0.709012397790081 , w70u3 = 1.122266356014727 , w70u4 = -0.045288696765434 , w70u5 = -0.784931097291497 , r71 = 0.233976888306 , w71u0 = 0.165876617215462 , w71u1 = -0.129198814914938 , w71u2 = 0.158803393360553 , w71u3 = 0.021325661380996 , w71u4 = -1.088172125699977 , w71u5 = -0.526218491213498 , r72 = -0.207733971517 , w72u0 = -0.208653494495407 , w72u1 = -0.824479416895008 , w72u2 = -0.649144816556909 , w72u3 = -7.949485349062294 , w72u4 = -1.503897098316076 , w72u5 = -2.007655018056385 , r73 = -2.33343704158d-08 , w73u0 = 0.054590900785109 , w73u1 = 0.198595428254369 , w73u2 = -0.267401286208350 , w73u3 = -10.727225727133208 , w73u4 = -3.878382223995197 , w73u5 = 0.253624478641044 , r74 = -0.00244304602301 , w74u0 = 0.806736737697331 , w74u1 = -0.454387984065477 , w74u2 = -0.362227922535493 , w74u3 = 0.462115718474676 , w74u4 = -0.171588856123621 , w74u5 = 0.674384285818280 , c = 0.01214406321949218

end-parameter-section

LABELS-SECTION

rq1 = exp1[a11,a12]

rq2 = exp1[a21,a22]

rq3 = exp1[a31,a32]

qs1 = qs[1.0]

General form of the labels are given in order to save space.

 # qiuj = exp[wiuj, 0.0]

Where i goes from 0 to 79 and j goes from 0 to 5.

So, there will be 80x6 = 480 labels term in this operator file.

end-labels-section

HAMILTONIAN-SECTION

---

modes | rch | rcf | rco | ohco | ofco | phi

-M11/2.d0 | dq^2 | 1 | 1 | 1 | 1 | 1

-M22/2.d0 | 1 | dq^2 | 1 | 1 | 1 | 1

-M33/2.d0 | 1 | 1 | dq^2 | 1 | 1 | 1

-1.0d0/mc | dq | dq | 1 | qs1 | qs1 | cos

-1.0d0/mc | dq | dq | 1 | q | q | 1

-1.0d0/mc | dq | 1 | dq | q | 1 | 1

-1.0d0/mc | 1 | dq | dq | 1 | q | 1

-1.0d0/mc | q^-1 | q^-1 | 1 | qs1 | qs1 | cos

```
-1.0d0/mc | q^1 | q^1 | 1 | q | q | 1
-1.0d0/mc | q^1 | 1 | q^1 | q | 1 | 1
-1.0d0/mc | 1 | q^1 | q^1 | 1 | q | 1
-0.5d0/mc | dq | 1 | q^1 | qs1^2*dq | 1 | 1
-0.5d0/mc | dq | 1 | q^1 | dq*qs1^2 | 1 | 1
0.5d0/mc | dq | q^1 | 1 | qs1 | qs1*q*dq | cos
0.5d0/mc | dq | q^1 | 1 | qs1 | dq*qs1*q | cos
-0.5d0/mc | dq | q^1 | 1 | q | qs1^2*dq | 1
-0.5d0/mc | dq | q^1 | 1 | q | dq*qs1^2 | 1
-0.5d0/mc | dq | 1 | q^1 | qs1 | qs1*dq | cos
-0.5d0/mc | dq | 1 | q^1 | qs1 | dq*qs1 | cos
-0.5d0/mc | 1 | dq | q^1 | 1 | qs1^2*dq | 1
-0.5d0/mc | 1 | dq | q^1 | 1 | dq*qs1^2 | 1
0.5d0/mc | q^1 | dq | 1 | qs1*q*dq | qs1 | cos
0.5d0/mc | q^1 | dq | 1 | dq*qs1*q | qs1 | cos
-0.5d0/mc | q^1 | dq | 1 | qs1^2*dq | q | 1
-0.5d0/mc | q^1 | dq | 1 | dq*qs1^2 | q | 1
-0.5d0/mc | 1 | dq | q^1 | qs1*dq | qs1 | cos
-0.5d0/mc | 1 | dq | q^1 | dq*qs1 | qs1 | cos
-0.5d0/mc | q^1 | 1 | dq | qs1^2*dq | 1 | 1
-0.5d0/mc | q^1 | 1 | dq | dq*qs1^2 | 1 | 1
-0.5d0/mc | 1 | q^1 | dq | 1 | qs1^2*dq | 1
-0.5d0/mc | 1 | q^1 | dq | 1 | dq*qs1^2 | 1
0.5d0/mc | dq | q^1 | 1 | qs1 | qs1^1 | sin*dq
0.5d0/mc | dq | q^1 | 1 | qs1 | qs1^1 | dq*sin
-0.5d0/mc | dq | 1 | q^1 | qs1 | q*qs1^1 | dq*sin
-0.5d0/mc | dq | 1 | q^1 | qs1 | q*qs1^1 | sin*dq
0.5d0/mc | q^1 | dq | 1 | qs1^1 | qs1 | sin*dq
0.5d0/mc | q^1 | dq | 1 | qs1^1 | qs1 | dq*sin
-0.5d0/mc | 1 | dq | q^1 | q*qs1^1 | qs1 | sin*dq
-0.5d0/mc | 1 | dq | q^1 | q*qs1^1 | qs1 | dq*sin
-M11/2.d0 | q^2 | 1 | 1 | dq*qs1^2*dq | 1 | 1
1.0d0/mc | q^1 | 1 | q^1 | dq*q*qs1^2*dq | 1 | 1
-M33/2.d0 | 1 | 1 | q^2 | dq*qs1^2*dq | 1 | 1
-M22/2.d0 | 1 | q^2 | 1 | 1 | dq*qs1^2*dq | 1
1.0d0/mc | 1 | q^1 | q^1 | 1 | dq*q*qs1^2*dq | 1
-M33/2.d0 | 1 | 1 | q^2 | 1 | dq*qs1^2*dq | 1
-0.5d0/mc | q^1 | q^1 | 1 | dq*qs1*q | qs1*q*dq | cos
-0.5d0/mc | q^1 | q^1 | 1 | qs1*q*dq | dq*qs1*q | cos
-0.5d0/mc | q^1 | q^1 | 1 | dq*qs1^2 | qs1^2*dq | 1
-0.5d0/mc | q^1 | q^1 | 1 | qs1^2*dq | dq*qs1^2 | 1
0.5d0/mc | q^1 | 1 | q^1 | dq*qs1*q | qs1*dq | cos
```

0.5d0/mc | q^1 | 1 | q^1 | q*qs1*dq | dq*qs1 | cos

0.5d0/mc | 1 | q^1 | q^1 | dq*qs1 | qs1*q*dq | cos

0.5d0/mc | 1 | q^1 | q^1 | qs1*dq | dq*qs1*q | cos

-M33/2.d0 | 1 | 1 | q^2 | dq*qs1 | qs1*dq | cos

-M33/2.d0 | 1 | 1 | q^2 | qs1*dq | dq*qs1 | cos

-0.5d0/mc | q^1 | q^1 | 1 | dq*qs1*q | qs1^1 | sin*dq

-0.5d0/mc | q^1 | q^1 | 1 | q*qs1*dq | qs1^1 | dq*sin

0.5d0/mc | q^1 | 1 | q^1 | dq*qs1*q | q*qs1^1 | sin*dq

0.5d0/mc | q^1 | 1 | q^1 | qs1*q*dq | q*qs1^1 | dq*sin

0.5d0/mc | 1 | q^1 | q^1 | dq*qs1 | qs1^1 | sin*dq

0.5d0/mc | 1 | q^1 | q^1 | qs1*dq | qs1^1 | dq*sin

-M33/2.d0 | 1 | 1 | q^2 | dq*qs1 | q*qs1^1 | sin*dq

-M33/2.d0 | 1 | 1 | q^2 | qs1*dq | q*qs1^1 | dq*sin

-0.5d0/mc | q^1 | q^1 | 1 | qs1^1 | dq*qs1*q | sin*dq

-0.5d0/mc | q^1 | q^1 | 1 | qs1^1 | qs1*q*dq | dq*sin

0.5d0/mc | 1 | q^1 | q^1 | q*qs1^1 | dq*qs1*q | sin*dq

0.5d0/mc | 1 | q^1 | q^1 | q*qs1^1 | qs1*q*dq | dq*sin

0.5d0/mc | q^1 | 1 | q^1 | qs1^1 | dq*qs1 | sin*dq

0.5d0/mc | q^1 | 1 | q^1 | qs1^1 | qs1*dq | dq*sin

-M33/2.d0 | 1 | 1 | q^2 | q*qs1^1 | dq*qs1 | sin*dq

-M33/2.d0 | 1 | 1 | q^2 | q*qs1^1 | qs1*dq | dq*sin

-M11/2.d0 | q^2 | 1 | 1 | qs1^2 | 1 | dq^2

1.0d0/mc | q^1 | q^1 | 1 | qs1^1 | qs1^1 | dq*cos*dq

-1.0d0/mc | q^1 | 1 | q^1 | qs1^1 | q*qs1^1 | dq*cos*dq

1.0d0/mc | q^1 | 1 | q^1 | q*qs1^2 | 1 | dq^2

-M22/2.d0 | 1 | q^2 | 1 | 1 | qs1^2 | dq^2

-1.0d0/mc | 1 | q^1 | q^1 | q*qs1^1 | qs1^1 | dq*cos*dq

1.0d0/mc | 1 | q^1 | q^1 | 1 | q*qs1^2 | dq^2

-M33/2.d0 | 1 | 1 | q^2 | q^2*qs1^2 | 1 | dq^2

-M33/2.d0 | 1 | 1 | q^2 | 1 | q^2*qs1^2 | dq^2

M33 | 1 | 1 | q^2 | q*qs1^1 | q*qs1^1 | dq*cos*dq

———————————————————-

c | 1 | 1 | 1 | 1 | 1 | 1

The following lines would have the following genral form

ri | qiu0 | qiu1 | qiu2 | qiu3 | qiu4 | qiu5

So, total 80 lines will be there; i goes from 0 to 79

———————————————————————-

end-hamiltonian-section

HAMILTONIAN-SECTION_r1i

usediag

————————————

modes | rch

-M11/2.0 | dq2̂

0.177588 | rq12̂

---

end-hamiltonian-section

HAMILTONIAN-SECTION_r2i

usediag

---

modes | rcf

-M22/2.0 | dq2̂

0.161448 | rq22̂

---

end-hamiltonian-section

HAMILTONIAN-SECTION_r3i

usediag

---

modes | rco

-M33/2.0 | dq2̂

0.335531 | rq32̂

---

end-hamiltonian-section

HAMILTONIAN-SECTION_theta1

usediag

---

modes | ohco

---

coeff3 | dq*q*qs12̂*dq

coeff4 | q

coeff5 | dq*qs12̂*dq

0.0548669 | 1

0.139251 | q

0.20238 | q2̂

0.52025 | q3̂

0.495075 | q4̂

---

end-hamiltonian-section

HAMILTONIAN-SECTION_theta2

usediag

---

modes | ofco

——————————

coef17 | 1

coef16 | qs1

coef15 | q

coeff6 | dq*q*qs1$\hat{2}$*dq

coeff7 | q

coeff8 | dq*qs1$\hat{2}$*dq

0.0974611 | 1

0.376063 | q

0.499038 | q$\hat{2}$

0.48174 | q$\hat{3}$

0.399969 | q$\hat{4}$

——————————

end-hamiltonian-section

HAMILTONIAN-SECTION_phii

usediag

——————————

modes | phi

—————————-

coeff1 | dq$\hat{2}$

coeff2 | dq*cos*dq

0.814096 | 1

-0.843866 | q

0.341579 | q$\hat{2}$

-0.0659754 | q$\hat{3}$

0.00524958 | q$\hat{4}$

7.05362d-08 | q$\hat{5}$

—————————-

end-hamiltonian-section

end-operator

Appendix C

Appendix to Chapter 4

C.1 CCSD(T)-F12/VTZ-F12 along Normal Mode results

CCSD(T)-F12/VTZ-F12 results along normal mode are performed to check if normal mode cuts (1D and 2D) gives any new results. So, we choose normal mode eigen vector from the ab initio frequency calculation output and take 1D and 2D cuts by propagating the eigen vector along each normal mode. The random data sets were the same. The results will be presented in a separate table along with physical coordinate, potfit-MCTDH and experiments for cis and trans HONO.

C.2 CBS extrapolation

In this work, the equilibrium geometry for the CBS calculation was taken to be the CCSD(T)-F12/cc-pVTZ-F12 computed equilibrium geometry. 1D and 2D cuts of the CCSD(T)-F12 equilibrium geometry and the random data set were also same for all of them. Three different combinations for the 2 points extrapolation (34, 35 and 45, results in Table C13 and C14) were computed. The 3 points extrapolation results are presented in the main chapter (see Chapter 4).

Table C1: *CCSD(T)-F12/cc-pVTZ-F12 (F12) optimized geometries including bond distances (Å) and angles (degrees), of H-NO_2, $TS^{\#}_{trans \leftrightarrow H-NO_2}$ and $TS^{\#}_{HONO \leftrightarrow 1,3HONO}$. Also provided are experimental and previous theoretical results.*

Methods	$R_1{}^{N=O}$	$R_2{}^{O-N}$	$R_3{}^{O-H}$	$\theta_1{}^{O-N-O}$	$\theta_2{}^{H-O-N}$	ϕ
			H-NO_2			
Ref [240][a]	1.225	1.225	1.917	128.20	28.97	180.00
Ref [272][b]	1.231	1.231	1.936	128.70	29.29	180.00
F12[c]	1.217	1.217	1.911	128.00	29.09	180.00
			$TS^{\#}_{trans \leftrightarrow H-NO_2}$			
CCSD(T)[d]	1.194	1.325	1.304	53.32	123.34	180.00
Ref [272][b]	1.188	1.317	1.300	53.80	123.50	180.00
F12[c]	1.189	1.319	1.301	53.57	123.23	180.00
			$TS^{\#}_{HONO \leftrightarrow 1,3HONO}$			
CCSD(T)[d]	1.268	1.268	1.298	104.86	76.84	0.00
Ref [272][b]	1.260	1.260	1.304	105.30	77.40	0.00
Ref [131][e]	1.265	1.265	1.298	105.10	76.90	0.00
F12[c]	1.262	1.262	1.299	105.06	76.99	0.00

[a] CCSD(T)/TZ2P; [b] B3LYP/6-311G(3df,3pd); [c] CCSD(T)-F12/cc-pVTZ-F12 in this work; [d] CCSD(T)/aug-cc-pVTZ in this work; [e] CCSD(T)/aug-cc-pVQZ(-g functions).

Table C2: *Anharmonic vibrational frequencies, zero point energies (ZPE) (both in cm^{-1}), relative energies (in cm^{-1}) without (ΔE) and with (ΔE_{ZPE}) zero-point energy corrections for the trans-HONO and cis-HONO as determined at the CCSD(T)/aug-cc-pVTZ level of theory. Energies reported relative to the lowest energy trans-HONO isomer.*

Mode	trans-HONO	cis-HONO
OH	3576.0	3421.4
N=O	1690.0	1629.2
HON	1259.0	1288.7
O-N	785.8	844.5
ONO	596.0	604.8
Torsion	534.0	628.2
ZPE	4220.4	4208.4
ΔE	0.0	124.0
Δ_{ZPE}	0.0	-12.0
ΔE_{ZPE}	0.0	112.0

Table C3: *Grid lengths used for the Physical Coordinates for the HONO PES. Also provided are the type and number of primitive basis functions and single particle functions (SPFs) used in the MCTDH computations.*

Coordinates	$R_1^{N=O}$	$\cos\theta_2^{HON}$	$\cos\theta_1^{ONO}$	R_2^{ON}	R_3^{OH}	ϕ
Grid Length [min , max]	[1.9,2.6]	[-0.65,0.25]	[-0.65,-0.1]	[2.1,3.25]	1,3,2.45]	[0,3.14]
Primitive Basis	13	18	16	16	18	32
Basis Function Types	HO	HO	HO	HO	HO	sin/cos[a]
SPF	16		16		5	11

[a] sin DVR for A' and cos DVR for A'' state computations.

Table C4: *Fitting Parametersof bond lengths (in au) for trans-HONO*

Fitting Parameter	A_0	A_1	A_2
	trans-HONO		
N=O	0.234724	1.3613	2.2109
ON	0.071236	1.21988	2.68149
OH	0.1772	1.2145	1.8254
	cis-HONO		
N=O	0.22438	1.3443	2.2355
ON	0.07585	1.27968	2.6172
OH	0.156615	1.24114	1.84378

Table C5: *Fitting parameters for bond angles and dihedral angle of cis- and trans-HONO isomers.*

Fitting Parameter	A_0	A_1	A_2	A_3	A_4
			trans-HONO		
$\cos\theta_1^{ONO}$	0.0454297	0.289274	0.57919	0.445615	0.265011
$\cos\theta_2^{HON}$	0.00483919	0.0470909	0.123341	0.0478834	0.0299907
ϕ	0.0103183	0.00118698	-0.0096204	-0.000340861	-0.000142621
			cis-HONO		
$\cos\theta_1^{ONO}$	0.0675922	0.398938	0.786201	0.662467	0.357884
$\cos\theta_2^{HON}$	0.0081536	0.062814	0.145385	0.0737161	0.045309
ϕ	0.0111641	-0.000004713	-0.0104423	-0.00032032	0.000195262

Table C6: *trans-HONO 2D grid. Bond lengths are in a.u. and bond angles are in degrees.*

Coordinates	Grid points
$R_1^{N=O}$	[1.99,2.05,2.1,2.15,2.21,2.246,2.28,2.32,2.4,2.5]
R_2^{O-N}	[2.33,2.45,2.53,2.61,2.681,2.765,2.845,2.96,3.14,3.32]
R_3^{O-H}	[1.56,1.67,1.72,1.77,1.825,1.874,1.91,1.99,2.09,2.24]
Θ_1^{ONO}	[98,101,104,107,109,110.69,112.5,114.8,119,123,130]
Θ_2^{HON}	[80,89,94,97,100,102.26,104.5,108,112,117,125]
Torsion (Φ)	[90,120,140,155,165,170,174,177,179,180]

Table C7: *cis-HONO 2D grid. Bond lengths are in a.u. and bond angles are in degrees.*

Coordinates	Grid points
$R_1^{N=O}$	[1.99,2.05,2.1,2.15,2.2515,2.246,2.28,2.32,2.4,2.5]
R_2^{O-N}	[2.33,2.45,2.53,2.61,2.62194,2.765,2.845,2.96,3.14,3.32]
R_3^{O-H}	[1.56,1.67,1.72,1.77,1.85268,1.874,1.91,1.99,2.09,2.24]
Θ_1^{ONO}	[98,101,104,107,109,113.3026,112.5,114.8,119,123,130]
Θ_2^{HON}	[80,89,94,98,101,104.6118,106,108,112,117,125]
Torsion (ϕ)	[70,60,45,35,25,15,9,6,3,0]

Table C8: *TS_ct-HONO 2D grid. Bond lengths are in a.u. and bond angles are in degrees.*

Coordinates	Grid points
$R_1^{N=O}$	[1.99,2.06,2.12,2.16,2.194,2.23,2.29,2.34,2.45,2.57]
R_2^{O-N}	[2.35,2.5,2.6,2.71,2.819,2.93,3.06,3.19,3.47,3.9]
R_3^{O-H}	[1.57,1.65,1.73,1.76,1.827,1.875,1.94,2.0,2.13,2.3]
Θ_1^{ONO}	[99,102,105,107.5,109.5,111.19,113,115,119,122,125]
Θ_2^{HON}	[81,88,93,97.5,101,103.439,106,109,112.5,119,127]
Torsion (ϕ)	[37,54,65,74,82,86.91,90.5,97,106,117,137]

Table C9: *RMSE vs NN of HONO*

Number of	RMSE (in cm^{-1})		
Neurons (NN)	Testset	Trainset	Validation set
20	115.0	118.0	129.0
30	66.0	59.6	64.9
40	41.3	36.5	42.0
50	29.3	24.8	29.9
60	24.8	21.7	25.9
70	19.3	16.3	21.6
80	14.4	11.0	16.3
90	13.3	10.4	15.0
100	15.0	12.0	16.9

Table C10: *RMSE in different energy range of a PES. This is a testset data analyzed below 10000 cm^{-1} and 80N fit.*

Energy Range	RMSE (cm^{-1})	Number of Points
0.0 - 3000.0	4.6	59
3000.0 - 6000.0	6.3	340
6000.0 - 10000.0	12.4	978
0.0 - 10000.0	10.6	1377

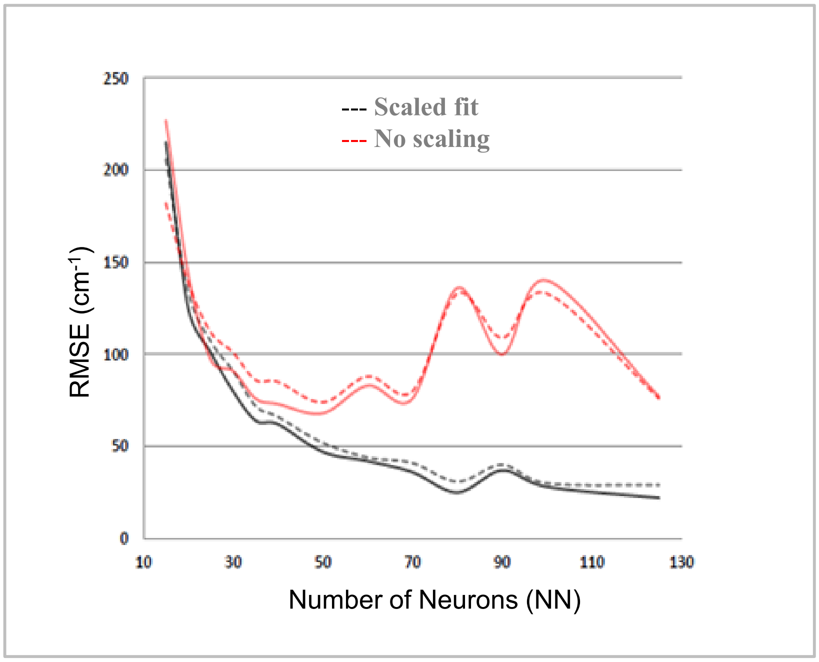

Figure C1: *Effect of Scaling data sets on the fitting quality*

Table C11: *Refitting previous PES[131] with NN-expnn; MCTDH vibrational states of trans-HONO, compared with PES generated from normal mode 1D, 2D and random energy data. Number of neurons is 80 here. 5k, 7k, 8k, 9k, and 10k represent 5000, 700, 8000, 9000, and 10000 cm^{-1} cut-off energy PES, respectively.*

	Torsion	ONO bend	ON str	HON bend	N=O str	OH str	ZPE
Expt.[a]	543.8	595.6	790.1	1263.1	1699.8	3590.7	
Ref [131][b]	538.0	601.0	796.0	1267.0	1698.0	3590.0	4367.6
Normal mode[c]	541.5	612.4	803.7	1270.4	1705.5	3590.9	4369.2
5k	538.4	601.1	796.1	1267.5	1690.0	3587.0	4364.2
7k	538.0	601.0	795.0	1268.0	1690.0	3589.0	4365.4
8k	539.2	600.7	795.6	1268.2	1689.4	3586.0	4364.6
9k	537.5	600.5	794.4	1267.5	1689.0	3586.7	4366.8
10K	534.5	601.0	796.0	1268.6	1685.0	3587.5	4371.6

[a](Torsion, ONO bend) from,[275](ON streching, HON bend) from,[276] N=O stretching from[237] and OH stretching from.;[277] [b] Previous MCTDH work by Gatti and co-workers.; [c] Normal mode cuts data upto 10000 cm^{-1} cut-off energy included in the PES.

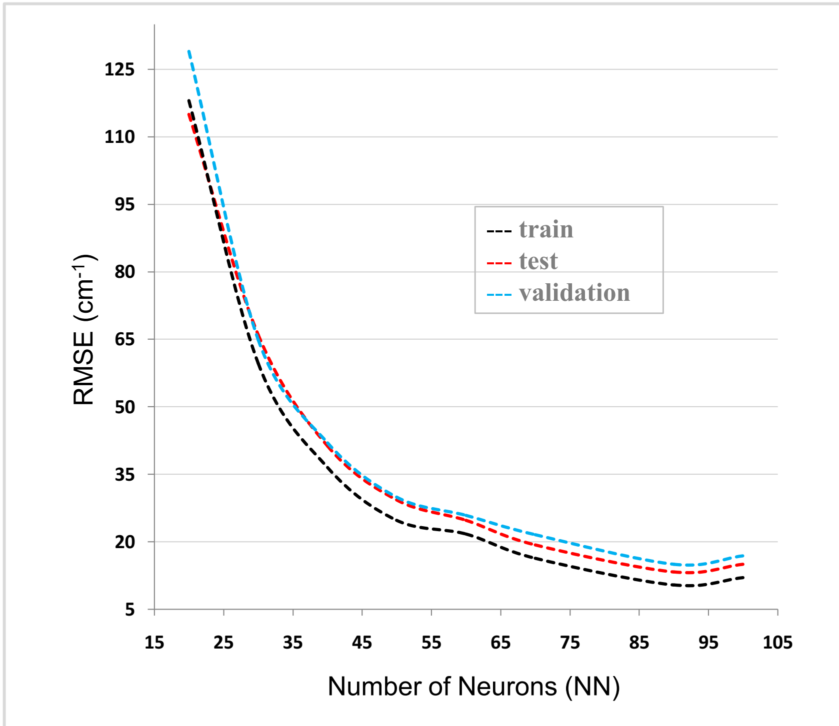

Figure C2: *RMSE vs NN*

Table C12: *Refitting Gatti PES with NN-expnn; MCTDH vibrational states of cis-HONO, compared with PES generated from normal mode 1D, 2D and random energy data. 5k, 7k, 8k, 9k, and 10k represent 5000, 700, 8000, 9000, and 10000 cm^{-1} cut-off energy PES, respectively.*

	Torsion	ONO bend	ON str	HON bend	N=O str	OH str	ZPE
Expt.[a]	638.5	609.0	851.0	1315.2	1640.5	3426.2	
Ref [131][b]	632.0	617.0	850.0	1312.0	1637.0	3436.0	4461.5
Normal mode[c]	639.1	621.2	866.4	1322.5	1646.4	3427.5	4491.7
5k	632.2	617.2	850.1	1311.4	1632.8	3432.5	4457.7
7k	631.3	617.0	850.5	1311.0	1632.4	3436.0	4457.1
8k	629.2	616.3	850.3	1310.0	1634.0	3432.0	4458.5
9k	629.1	616.0	850.0	1310.0	1631.6	3434.3	4458.3
10k	632.0	616.0	848.5	1307.6	1633.6	3437.4	4458.7

[a](Torsion, ONO bend) from,[275] (OH stretching, N=O stretching) from,[238] HON bending in a Kr matrix from[254] and ON stretching from;[276] [b] Previous MCTDH work by Gatti and co-workers; [c] Normal mode cuts data upto 10000 cm^{-1} cut-off energy included in the PES.

Table C13: *CBS limit of HONO PES from CCSD(T)/AVTZ,AVQZ and AV5Z compared with Gatti PES and the experiment: trans-HONO results*

	Torsion	ONO bend	ON str	HON bend	N=O str	OH str	ZPE
Expt.[a]	543.8	595.6	790.1	1263.1	1699.8	3590.7	
Ref [131][b]	538.0	601.0	796.0	1267.0	1698.0	3590.0	4367.6
CCSD(T)/AVTZ	530.7	596.8	788.3	1258.7	1688.0	3577.4	4328.7
CCSD(T)/AVQZ	539.4	608.6	799.8	1267.4	1701.6	3593.0	4364.4
CCSD(T)/AV5Z	543.9	612.3	802.8	1268.8	1705.0	3595.0	4370.3
CBS_TQ	542.9	609.9	802.5	1266.1	1703.8	3593.6	4362.7
CBS_Q5	534.6	610.0	801.4	1265.6	1702.3	3589.2	4360.3
CBS_TQ5	542.7	608.5	800.1	1266.6	1700.1	3586.4	4350.5

[a](Torsion, ONO bend) from,[275](ON streching, HON bend) from,[276] N=O stretching from[237] and OH stretching from;[277] [b] Previous MCTDH work by Gatti and co-workers.

Table C14: *CBS limit of HONO PES from CCSD(T)/AVTZ,AVQZ and AV5Z compared with Gatti PES and the experiment: cis-HONO results*

	Torsion	ONO bend	ON str	HON bend	N=O str	OH str	ZPE
Expt.[a]	638.5	609.0	851.0	1315.2	1640.5	3426.2	
Ref [131][b]	632.0	617.0	850.0	1312.0	1637.0	3436.0	4461.5
CCSD(T)/AVTZ	627.4	605.2	847.6	1306.6	1628.9	3418.0	4491.5
CCSD(T)/AVQZ	634.0	616.9	865.0	1322.0	1643.0	3429.0	4499.0
CCSD(T)/AV5Z	637.5	620.0	865.6	1321.8	1645.8	3431.0	4495.3
CBS_TQ	635.6	618.2	865.7	1321.3	1644.5	3432.0	4487.8
CBS_Q5	631.6	618.5	864.5	1320.3	1642.8	3425.0	4476.4
CBS_TQ5	636.4	617.6	861.2	1318.4	1640.7	3426.0	4469.8

[a](Torsion, ONO bend) from,[275] (OH stretching, N=O stretching) from,[238] HON bending in a Kr matrix from[254] and ON stretching from;[276] [b] Previous MCTDH work by Gatti and co-workers.

Table C15: *Vibrational frequencies of selected overtones and combination modes (in cm^{-1}) of trans-HONO for the CBS_345 80 NN fit PES.*

$(\nu_1\ \nu_2\ \nu_3\ \nu_4\ \nu_5\ \nu_6)^a$	This work	Previous Expt.	Guilmot *et al.*[237]	Richter *et al.*[131]
020000	3374.5	3372.1[b]	3372.1	3367.4
101000	4384.2	4379.0[c]	4378.3	
100100	4830.1	4829.0[c]	4829.6	
100200	6052.4		6045.8	
200000	7012.1	7017.0[c]	7016.8	
300000	10297.0	10279.0[c]	10280.5	
400000	13507.0	13385.0[c]		

[a] ν_1: CH stretch. (A'), ν_2: N=O stretch. (A'), ν_3: ON stretch. (A'), ν_4: HON bend. (A'), ν_5:ONO bend. (A') and ν_6: out-of-plane bend. (A''); [b] From Ref. 279; [c] From Ref. 280

Table C16: *Vibrational frequencies of selected overtones and combination modes (in cm^{-1}) of cis-HONO for the CBS_345 80 NN fit PES.*

$(\nu_1\ \nu_2\ \nu_3\ \nu_4\ \nu_5\ \nu_6)^a$	This work	Previous Expt.	Guilmot *et al.*[238]	Richter *et al.*[131]
011000	2515.9	2493.0[b]	2492.9	2476.7
020000	3264.7	3257.9[c]	3257.9	3253.6
101000	4297.8	4281.0[d]	4281.0	
200000	6676.7	6665.0[d]	6664.4	

[a] ν_1: CH stretch. (A'), ν_2: N=O stretch. (A'), ν_3: ON stretch. (A'), ν_4: HON bend. (A'), ν_5:ONO bend. (A') and ν_6: out-of-plane bend. (A''); [b] From Ref. 281; [c] From Ref. 275; [d] From Ref. 280

C.3 CBS_345 Extrapolated PES of HONO using 80 NN: Operator file

OP_DEFINE-SECTION

title

HONO r1 = OH, r2 = N=O, r3 = ON, th1 = HON, th2 = ONO, p1 = torsion

This operator file is for cos-DVR for p_1 defined on [0,pi].

end-title

end-op_define-section

PARAMETER-SECTION

q20 = 2.696732586 , q30 = 1.822912197 , q10 = 2.21332641 , q11 = 1.8653 , th20 = 1.777642018 , th10 = 1.9315017 , mh = 1.0, H-mass , mc = 12.0,AMU , mo = 15.9949,AMU , mn = 13.9939,AMU , M11 = 1.0/mo+1.0/mh , M22 = 1.0/mo+1.0/mn , M33 = M22 , M13 = 1.0/mo , M23 = -1.0/mn , p1 = PI/2.0 , p2 = 3.0*PI/2.0

, r0 = 215.033298376 , w0u0 = 0.125823534531891 , w0u1 = -1.806035654434605 , w0u2 = -0.136998979298039 , w0u3 = 0.338250129812485 , w0u4 = -0.361491345675920 , w0u5 = 0.095141353516250 , r1 = -0.708473537487 , w1u0 = -0.210381681518466 , w1u1 = -0.447015055533330 , w1u2 = -0.038602335795481 , w1u3 = -1.959115130022963 , w1u4 = -1.018487355760621 , w1u5 = -0.277829182688022 , r2 = 83.9689779887 , w2u0 = -0.771685038364569 , w2u1 = -1.260299658252386 , w2u2 = 0.487090587125463 , w2u3 = 2.622113502878132 , w2u4 = 1.734331845853653 , w2u5 = -0.178116680144332 , r3 = -2.23874546314 , w3u0 = 0.235335596499319 , w3u1 = -1.311359141632936 , w3u2 = 0.054695242716243 , w3u3 = -1.784466867582287 , w3u4 = 0.440080169072798 , w3u5 = 0.166020227963305 , r4 = 0.000102243324097 , w4u0 = 0.058266485690154 , w4u1 = 1.365158385417139 , w4u2 = 0.211264413395750 , w4u3 = 0.577910496455408 , w4u4 = -0.205169940469451 , w4u5 = 0.287098008216782 , r5 = -635.314882534 , w5u0 = 0.103364007738257 , w5u1 = -1.576766228592027 , w5u2 = -0.099218493004741 , w5u3 = 0.212006630085992 , w5u4 = -0.481785373545057 , w5u5 = 0.088661350753319 , r6 = 0.0234213127706 , w6u0 = -2.082550943640675 , w6u1 = 1.176586426580983 , w6u2 = 0.402671476454461 , w6u3 = 1.367468909657925 , w6u4 = -0.714440236204393 , w6u5 = 0.047012220632286 , r7 = 0.206464429698 , w7u0 = -0.379420359845496 , w7u1 = -0.311133141916230 , w7u2 = -0.018890450307341 , w7u3 = -2.071792886395266 , w7u4 = -1.076104856733825 , w7u5 = -0.591349020627664 , r8 = -1.79339528347 , w8u0 = 0.307272070048732 , w8u1 = -1.265611185448160 , w8u2 = 0.019999792672684 , w8u3 = -2.004830275188881 , w8u4 = 0.552983691951995 , w8u5 = -0.809710372839196 , r9 = 0.159973819578 , w9u0 = 0.255908865067018 , w9u1 = -0.151370137417048 , w9u2 = -0.930178870819283 , w9u3 = -0.113111112497356 , w9u4 = 0.112641921420822 , w9u5 = -0.946037923928646 , r10 = 0.3367210372 , w10u0 = -0.538804280776509 , w10u1 = -0.717183574945979 , w10u2 = -0.398953826388468 , w10u3 = 1.691463032037448 , w10u4 = -2.935766121160888 , w10u5 = 0.177123547045084 , r11 = 382.930491391 , w11u0 = -0.864581908148141 , w11u1 = -2.861822574339154 , w11u2 = 0.158267925646723 , w11u3 = -1.869927286775813 , w11u4 = 0.030130646797633 , w11u5 = -0.029466799709394 , r12 = -4.99303304942e-08 , w12u0 = 1.243935963393556 , w12u1 = 0.098045838957343 , w12u2 = 3.089091390362069 , w12u3 = 0.680225432885033 , w12u4 = -1.539241705181553 , w12u5 = 0.160953697119371 , r13 = 23.7591918778 , w13u0 = -1.425350635293963 , w13u1 = -0.385338624445347 , w13u2 = -1.224791768253172 , w13u3 = 0.169886446398477 , w13u4 = 0.322504267513744 , w13u5 = -0.128901143540096 , r14 = -0.0871982129012 , w14u0 = 0.098005176576224 , w14u1 = 0.124102922754623 , w14u2 = -1.580897776883444 , w14u3 = -0.726095336765562 , w14u4 = -0.002073543593550 , w14u5 = 0.441546026621100 , r15 = 115.3480285 , w15u0 = 0.060639080019321 , w15u1 = -1.536262327770898 , w15u2 = -0.106976756491459 , w15u3 = 0.456052777546998 , w15u4 = -0.525328643863887 , w15u5 = 0.444163906462205 , r16 = 23.6350250287 , w16u0 = -0.211883845421597 , w16u1 = -0.967194232561933 , w16u2 = -0.224056968426485 , w16u3 = 0.928050648041108 , w16u4 = -1.410364914927638 , w16u5 = -1.610387048364686 , r17 = -1237.96922576 , w17u0 = 0.160503257852956 , w17u1 = -1.494570083280115 , w17u2 = -0.103853200619006 , w17u3 = -0.222896763508138 , w17u4 = -0.655234312104624 , w17u5 = -0.714563190714063 , r18 = 38.1670430153 , w18u0 = 0.286156508346835 , w18u1 = -1.508125244636193 , w18u2 = -0.248448310561833 , w18u3 = -0.815118479703325 , w18u4 = -1.204116460890554 , w18u5 = -2.107457921622166 , r19 = 22.5516846217 , w19u0 = -0.483970110922961 , w19u1 = -1.128462930367552 , w19u2 = -0.179632869376950 , w19u3 = 3.130610900806947 , w19u4 = -0.103261851573917 , w19u5 = 0.109607730501244 , r20 = 0.830288709995 , w20u0 = 0.787558999336503 , w20u1 = -2.031293984137298 , w20u2 = 0.102639312526616 , w20u3 = -2.355258927500568 , w20u4 = 1.890281289683642 , w20u5 = -0.059070088510453 , r21 = 0.918334874384 , w21u0 = -2.646368651671837 , w21u1 = 0.452974952194262 , w21u2 = 0.107400849566796 , w21u3 = -1.938416736949235 , w21u4 = -0.041402694944184 , w21u5 = -0.026312386418054 , r22 = -321.969395459 , w22u0 = 0.226185718475238 , w22u1 = -1.481014211025087 , w22u2 = -0.180363344718838 , w22u3 = -0.542047682033697 , w22u4 = -0.982811116232047 , w22u5 = -1.553831626888309 , r23 = -3.98494199893 , w23u0 = -0.367100500645524 , w23u1 = -1.408642314411877 , w23u2 = 0.435437966924311 , w23u3 = 3.424047955307278 , w23u4 = 0.807171158792301 , w23u5 = 0.227731668938768 , r24 = -22.791224454 , w24u0 = -0.166042119995561 , w24u1 = -1.183473502484889 , w24u2 = -0.254267673204818 , w24u3 = 2.042991894109432 , w24u4 = -0.514564307476311 , w24u5 = -0.136140506624085 , r25 = -0.0134173644718 , w25u0 = 1.038369760154856 , w25u1 = -0.290263433006996 , w25u2 = -1.123941134480203 , w25u3 = -2.100084780723947 , w25u4 = -0.853930572845061 , w25u5 = -0.335551957025956 , r26 = 8.55436345147 , w26u0 = 0.206757386989288 , w26u1 = -1.429827359179757 , w26u2 = 0.105320840637524 , w26u3 = -1.596391393355998 , w26u4 = 0.487445191393735 , w26u5 = -0.448411020098712 , r27 = 41.5238151983 , w27u0 = -0.824214653524812 , w27u1 = -0.857389373382693 , w27u2 = -0.243953674329364 , w27u3 = 1.365125429252300 , w27u4 = 2.540847922960905 , w27u5 = -0.148226223559230 , r28 = 0.843867858846 , w28u0 = -0.063531958793103 , w28u1 = -0.583829077214041 , w28u2 = -0.097794871176437 , w28u3 = -1.898849996913780 , w28u4 = -0.575446111842980 , w28u5 = 0.011735225813560 , r29 = -22.8343173701 , w29u0 = -0.877276555793962 , w29u1 = -0.655234492586132 , w29u2 = -0.598449785886289 , w29u3 = 1.270183070726200 , w29u4 = 2.753317702506051 , w29u5 = -0.210528489922387 , r30 = 38.860410417 , w30u0 = -1.374254458427669 , w30u1 = -1.242429565665795 , w30u2 = 0.146362209782475 , w30u3 = -2.281578500953064 , w30u4 = 0.076975574052538 , w30u5 = -0.022579104403494 , r31 = -217.028708752 , w31u0 = -0.785106775143492 , w31u1 = -1.421326261434761 , w31u2 = 0.728257719542637 , w31u3 = 2.757656011707904 , w31u4 = 2.353281853955700 , w31u5 = -0.571311107203414 , r32 = -7.77193688281 , w32u0 = -0.847959247269636 , w32u1 = -0.222804407658939 , w32u2 = -0.251473843505371 , w32u3 = -0.132407796413705 , w32u4 = -0.032303669523464 , w32u5 = 0.057115709304850 , r33 = -0.838521027988 , w33u0 = -0.706731846243094 , w33u1 = -0.080266093459614 , w33u2 = -0.264545873458030 , w33u3 = 2.109671263231354 , w33u4 = -1.280354945522662 , w33u5 = -0.055731334393189 , r34 = 190.455191043 , w34u0 = -0.837965600803032 , w34u1 = -1.655391872381884 , w34u2 = 1.157180514787483 , w34u3 = 3.131983580236994 , w34u4 = 2.834310557245700 , w34u5 = -1.019679841186801 , r35 = -8.17656146002e-05 , w35u0 = -0.254814355947369 , w35u1 = 1.741252817765529 , w35u2 = 0.290070980730520 , w35u3 = 0.318314065914855 , w35u4 = -0.340559673947432 , w35u5 = 0.154156182965224 , r36 = -2.26851606494 , w36u0 = -0.052411078604690 , w36u1 = -0.196490144464146 , w36u2 = -1.061265269264264 , w36u3 = 1.241302539855455 , w36u4 = 0.558202639349858 , w36u5 = -0.262926764023980 , r37 = 0.00904528386081 , w37u0 = -0.550042415864926 , w37u1 = 0.436154131149496 , w37u2 = -0.126808067524024 , w37u3 = -0.075011926917543 , w37u4 = -2.399571902912988 , w37u5 = 0.031068927795595 , r38 = -1.39176742612 , w38u0 = 0.717035549136906 , w38u1 = -1.999122402350024 , w38u2 = 0.179260968725505 , w38u3 = -1.914022048834026 , w38u4 = 1.810483394123775 , w38u5 = 0.056134570830038 , r39 = -4.30610890888 , w39u0 = -0.112283033331136 , w39u1 = -1.252950958745576 , w39u2 = -0.295102937619947 , w39u3 = 0.219852987502287 , w39u4 = -2.026266663199123 , w39u5 = -0.100838204865778 , r40 = 0.681425148941 , w40u0 = -0.265051927260367 , w40u1 = -0.892044252972442 , w40u2 = -0.259998360323446

, w40u3 = -0.787611449614359 , w40u4 = -2.459497607683900 , w40u5 = -0.315898028685410 , r41 = 0.271046615988 , w41u0 = -0.749065822385963 , w41u1 = 0.613799722370821 , w41u2 = -1.258128385410575 , w41u3 = 2.151844305187226 , w41u4 = 1.105096771046574 , w41u5 = -0.391199709045411 , r42 = 1.17635621753 , w42u0 = 0.377967478598610 , w42u1 = -1.695171134161845 , w42u2 = 0.205494910261157 , w42u3 = -1.508720434375944 , w42u4 = 1.043393114409791 , w42u5 = 0.638083665855028 , r43 = -34.1288492855 , w43u0 = -0.919383651615041 , w43u1 = -0.962946362205706 , w43u2 = -0.049448502709749 , w43u3 = 1.635704267316419 , w43u4 = 1.556078410083341 , w43u5 = 0.165829720282759 , r44 = 30.4589623727 , w44u0 = -0.482600312487793 , w44u1 = -0.753918894339439 , w44u2 = -0.143471536464763 , w44u3 = 1.420016423669167 , w44u4 = -1.255728427348348 , w44u5 = -0.790966117387628 , r45 = 50.3885510604 , w45u0 = -0.771117881473166 , w45u1 = -1.136670350231372 , w45u2 = -0.313192983843149 , w45u3 = 1.478167109274165 , w45u4 = 0.481917480894273 , w45u5 = 0.354430541949418 , r46 = 968.908407916 , w46u0 = 0.130576845419502 , w46u1 = -1.513465473590139 , w46u2 = -0.091342719233646 , w46u3 = -0.029368857801711 , w46u4 = -0.561190632534115 , w46u5 = -0.303127856911043 , r47 = 70.8946842702 , w47u0 = -0.733063179278421 , w47u1 = -1.629622268758132 , w47u2 = 0.789288490550507 , w47u3 = 3.119801098928447 , w47u4 = 2.833654296722980 , w47u5 = -0.963018041078552 , r48 = -0.192642883066 , w48u0 = 0.359753464519960 , w48u1 = -1.783499081094813 , w48u2 = 0.269243759223069 , w48u3 = -1.447535437057270 , w48u4 = 1.213211437552736 , w48u5 = 1.011257311999415 , r49 = 0.011869646682 , w49u0 = -0.143991820237945 , w49u1 = 0.200844814797353 , w49u2 = -1.180018573305406 , w49u3 = -1.095635231927168 , w49u4 = -0.350765412341257 , w49u5 = 0.775973256634383 , r50 = -9.39586901388 , w50u0 = -2.004309249331419 , w50u1 = -0.348256403951743 , w50u2 = 0.144238997687260 , w50u3 = -2.098013287385470 , w50u4 = 0.135390114574372 , w50u5 = -0.036724431677873 , r51 = 906.419898421 , w51u0 = 0.189854169070978 , w51u1 = -1.481879417275660 , w51u2 = -0.134510143992100 , w51u3 = -0.374948885582379 , w51u4 = -0.801011921988930 , w51u5 = -1.117580506591630 , r52 = -16.5334309005 , w52u0 = -0.426400232194459 , w52u1 = -1.423232829076349 , w52u2 = -0.244414910595229 , w52u3 = 1.791512601764764 , w52u4 = 0.085854872270283 , w52u5 = 0.665073600460340 , r53 = 1.43810060947 , w53u0 = -0.669062418107514 , w53u1 = -1.366090909969609 , w53u2 = 0.305453426383842 , w53u3 = -3.406465584755819 , w53u4 = 0.790076269496740 , w53u5 = -0.285603889194554 , r54 = 147.478476375 , w54u0 = -3.018202027177908 , w54u1 = -0.132093357359990 , w54u2 = 0.047434140523326 , w54u3 = -0.117839746945070 , w54u4 = 0.051998282988900 , w54u5 = -0.002837615036507 , r55 = -6.92467973017 , w55u0 = 0.011488582748737 , w55u1 = -1.568871508251123 , w55u2 = -0.134962055690593 , w55u3 = 0.994255295760675 , w55u4 = -0.558971505282510 , w55u5 = 1.021569390272837 , r56 = -2.8416146856e-07 , w56u0 = 1.357756237248721 , w56u1 = 1.784003603369558 , w56u2 = 0.218199177303585 , w56u3 = 1.813149410401791 , w56u4 = 1.802099182282840 , w56u5 = -0.252698519050476 , r57 = 21.6055106955 , w57u0 = 0.020012126388130 , w57u1 = -0.018321059320640 , w57u2 = -3.196031325819046 , w57u3 = 0.009350138300733 , w57u4 = 0.021145863768890 , w57u5 = 0.002856387050370 , r58 = 2.9259381122 , w58u0 = -0.255661616517409 , w58u1 = -0.421969079850881 , w58u2 = -0.599367040714134 , w58u3 = 2.151826593418869 , w58u4 = -0.627492778644224 , w58u5 = -0.388097130059263 , r59 = -209.785154924 , w59u0 = -1.172419618035117 , w59u1 = -1.291375794533033 , w59u2 = 0.064627662413098 , w59u3 = 2.974821834874014 , w59u4 = 1.551932038871447 , w59u5 = -1.678507872993984 , r60 = 0.0136798542056 , w60u0 = 0.094386687568331 , w60u1 = 0.209609217477351 , w60u2 = -1.557337854229193 , w60u3 = -1.932519291250121 , w60u4 = -0.374202173603191 , w60u5 = -0.115627571695610 , r61 = -0.00932807811812 , w61u0 = -0.252074212151064 , w61u1 = -0.134991482653103 , w61u2 = -0.266888403868647 , w61u3 = -1.331512410318276 , w61u4 = -1.232011543256694 , w61u5 = 0.688811809987881 , r62 = -0.643838644364 , w62u0 = -0.520697944359742 , w62u1 = 0.201035790325336 , w62u2 = -0.906898264410254 , w62u3 = 0.091010738975916 , w62u4 = 0.024420165039072 , w62u5 = -0.399686201820311 , r63 = 0.00219545075621 , w63u0 = 1.008239811634577 , w63u1 = -0.336070310343361 , w63u2 = -0.515744153110423 , w63u3 = -3.226657712453456 , w63u4 = -1.035846871554554 , w63u5 = -0.717393631207543 , r64 = -189.338621623 , w64u0 = -0.824691611377172 , w64u1 = -1.898474435953118 , w64u2 = 1.447451751619065

, w64u3 = 3.484504759277509 , w64u4 = 3.206227354234469 , w64u5 = -1.557545504958584 , r65 = -12.3358784709 , w65u0 = -0.576295269930288 , w65u1 = -1.836166011584152 , w65u2 = 0.378995406829392 , w65u3 = -2.637604522206471 , w65u4 = 0.632565347484929 , w65u5 = -0.246706657591886 , r66 = 0.000766953486858 , w66u0 = 2.074636612590538 , w66u1 = -1.844010684390077 , w66u2 = 1.250713716020937 , w66u3 = 2.883255359685029 , w66u4 = 0.605356782536396 , w66u5 = -0.115865077198536 , r67 = -75.9225630503 , w67u0 = -0.702818638851484 , w67u1 = -1.482794343603591 , w67u2 = -1.017936814079278 , w67u3 = 0.990517438361159 , w67u4 = 0.072153241787141 , w67u5 = 0.007356552198966 , r68 = 0.193896558034 , w68u0 = 0.343368723057545 , w68u1 = -0.387305905759735 , w68u2 = -0.460052438480687 , w68u3 = 0.232330238926853 , w68u4 = 1.391149769715387 , w68u5 = -0.125365834831055 , r69 = 28.8888781331 , w69u0 = -1.649239150151173 , w69u1 = -0.988113699673671 , w69u2 = -0.441781225893546 , w69u3 = 0.532298327444435 , w69u4 = -1.465506511665277 , w69u5 = -0.010855597674084 , r70 = 75.1831647295 , w70u0 = -0.832228790818582 , w70u1 = -2.045506455909168 , w70u2 = 1.631883447581282 , w70u3 = 3.683620571834991 , w70u4 = 3.379681735585193 , w70u5 = -2.009808496825519 , r71 = 0.00387317118305 , w71u0 = -0.581294984580651 , w71u1 = -0.868811687075429 , w71u2 = -0.036430139136950 , w71u3 = -1.057795650817691 , w71u4 = 1.660469379409591 , w71u5 = 1.389556592961171 , r72 = 0.0759996165006 , w72u0 = -0.035182558644811 , w72u1 = 0.288218611363679 , w72u2 = 0.298576455500861 , w72u3 = 0.085805434564398 , w72u4 = -0.077207653848329 , w72u5 = -0.010765516171013 , r73 = -0.734951132865 , w73u0 = -1.319427009409104 , w73u1 = 0.230525317724424 , w73u2 = 0.416757268484731 , w73u3 = 0.482362403342543 , w73u4 = -0.144213079439785 , w73u5 = -0.042561940888112 , r74 = -49.9940952069 , w74u0 = -0.329964175182422 , w74u1 = -0.868847751777221 , w74u2 = -0.186776117921342 , w74u3 = 1.177320195724601 , w74u4 = -1.307902219159446 , w74u5 = -1.221807095074365 , r75 = -1.16392292794 , w75u0 = -1.296798053895331 , w75u1 = -0.268706575054995 , w75u2 = -0.240623346263197 , w75u3 = 0.608796940960312 , w75u4 = -2.555126580224502 , w75u5 = -0.165413990829340 , r76 = 242.912093143 , w76u0 = -1.094886387046626 , w76u1 = -1.241993682396458 , w76u2 = 0.012077152754223 , w76u3 = 2.874193202426282 , w76u4 = 1.333880639289986 , w76u5 = -1.345831920493652 , r77 = -48.3138284073 , w77u0 = -1.267062327346737 , w77u1 = -0.839344564402828 , w77u2 = -0.236605744128114 , w77u3 = 3.248150385632202 , w77u4 = 0.503356528245979 , w77u5 = -0.338486279189680 , r78 = 0.978964667455 , w78u0 = -0.076477277381700 , w78u1 = -1.581762041423235 , w78u2 = -0.145453889657714 , w78u3 = 1.607094109233751 , w78u4 = -0.434806942211019 , w78u5 = 1.370789113319065 , r79 = -277.010485191 , w79u0 = -1.207736452990555 , w79u1 = -2.272118210510676 , w79u2 = 0.107259914309597 , w79u3 = -2.097955708597492 , w79u4 = -0.038908519827878 , w79u5 = 0.001497224334231

c = 0.017982894

end-parameter-section

LABELS-SECTION

q1 = exp1[-0.70,q10]

q2 = exp1[-0.70,q20]

q3 = exp1[-0.70,q30]

t1 = acos[1.0 0.0 th20]

t2 = acos[1.0 0.0 th10]

qs1 = qs[1.0]

g1 = gauss[1.0,q10]

g2 = gauss[1.0/9.0,q20]

g3 = gauss[0.25,q30]

g4 = tgauss[0.25,th10]

g5 = tgauss[0.25,th20]

c1 = gauss[-4.0,q10]

c2 = gauss[-1.0,q20]

c3 = gauss[-4.0,q30]

c4 = tgauss[-4.0,th10]

c5 = tgauss[-4.0,th20]

g0pi = gauss[2.0,0.0]

g1pi = gauss[2.0,PI]

g2pi = gauss[2.0,2.0*PI]

cos2 = cos[2.0]

cos3 = cos[3.0]

cos4 = cos[4.0]

st1 = step[p1]

st2 = rstep[p2]

#Labels are adapted in a general form to save space end-labels-section

HAMILTONIAN-SECTION

---

modes | r_2 | r_3 | r_1 | t_2 | t_1 | p_1

-M11/2.0 | 1 | 1 | dq^2 | 1 | 1 | 1

-M22/2.0 | dq^2 | 1 | 1 | 1 | 1 | 1

-M33/2.0 | 1 | dq^2 | 1 | 1 | 1 | 1

-M13 | 1 | dq | dq | 1 | q | 1

M23 | dq | dq | 1 | q | 1 | 1

-M13 | 1 | q^-1 | q^-1 | 1 | q | 1

M23 | q^-1 | q^-1 | 1 | q | 1 | 1

-M13 | 1 | q^-1 | dq | 1 | udq2 | 1

M13 | 1 | q^-1 | dq | udq | qs1 | cos

-M23 | dq | q^-1 | 1 | qs1 | udq | cos

M23 | dq | q^-1 | 1 | udq2 | 1 | 1

-M13 | 1 | dq | q^-1 | 1 | udq2 | 1

M23 | q^-1 | dq | 1 | udq2 | 1 | 1

M13 | 1 | q^-1 | dq | q*qs1^-1 | qs1 | sdq

-M23 | dq | q^-1 | 1 | qs1 | q*qs1^-1 | sdq

-M11/2.0 | 1 | 1 | q^-2 | 1 | dq*qs1^2*dq | 1

-M33/2.0 | 1 | q^-2 | 1 | 1 | dq*qs1^2*dq | 1

M13 | 1 | q^-1 | q^-1 | 1 | dq*qs1^2*q*dq | 1

-M22/2.0 | q^-2 | 1 | 1 | dq*qs1^2*dq | 1 | 1

-M33/2.0 | 1 | q^-2 | 1 | dq*qs1^2*dq | 1 | 1

-M23 | q^-1 | q^-1 | 1 | dq*qs1^2*q*dq | 1 | 1

-M13/2.0 | 1 | q^-1 | q^-1 | qs1*dq | dq*q*qs1 | cos

-M13/2.0 | 1 | q^-1 | q^-1 | dq*qs1 | q*qs1*dq | cos

M23/2.0 | q^-1 | q^-1 | 1 | q*qs1*dq | dq*qs1 | cos

M23/2.0 | q^-1 | q^-1 | 1 | dq*q*qs1 | qs1*dq | cos

M33/2.0 | 1 | q^2 | 1 | qs1*dq | dq*qs1 | cos

M33/2.0 | 1 | q^2 | 1 | dq*qs1 | qs1*dq | cos

-M13/2.0 | 1 | q^1 | q^1 | q*qs1^1 | dq*q*qs1 | sdq

-M13/2.0 | 1 | q^1 | q^1 | q*qs1^1 | q*qs1*dq | sdq

-M13/4.0 | 1 | q^1 | q^1 | q*qs1^1 | q^2*qs1^1 | cos

M13/4.0 | 1 | q^1 | q^1 | q*qs1^1 | qs1 | cos

M23 | q^1 | q^1 | 1 | qs1^1 | udq | sdq

-0.25*M23 | q^1 | q^1 | 1 | qs1^1 | q*qs1^1 | cos

M33 | 1 | q^2 | 1 | q*qs1^1 | udq | sdq

M23/2.0 | q^1 | q^1 | 1 | dq*q*qs1 | q*qs1^1 | sdq

M23/2.0 | q^1 | q^1 | 1 | q*qs1*dq | q*qs1^1 | sdq

M23/4.0 | q^1 | q^1 | 1 | q^2*qs1^1 | q*qs1^1 | cos

-M23/4.0 | q^1 | q^1 | 1 | qs1 | q*qs1^1 | cos

-M13 | 1 | q^1 | q^1 | udq | qs1^1 | sdq

-M13/4.0 | 1 | q^1 | q^1 | q*qs1^1 | qs1^1 | cos

M33 | 1 | q^2 | 1 | udq | q*qs1^1 | sdq

-M11/2.0 | 1 | 1 | q^2 | 1 | qs1^2 | dq^2

M13/2.0 | 1 | q^1 | q^1 | q*qs1^1 | qs1^1 | cos*dq^2

M13/2.0 | 1 | q^1 | q^1 | q*qs1^1 | qs1^1 | dq^2*cos

M13/2.0 | 1 | q^1 | q^1 | q*qs1^1 | qs1^1 | cos

M13 | 1 | q^1 | q^1 | 1 | q*qs1^2 | dq^2

-M22/2.0 | q^2 | 1 | 1 | qs1^2 | 1 | dq^2

-M23/2.0 | q^1 | q^1 | 1 | qs1^1 | q*qs1^1 | dq^2*cos

-M23/2.0 | q^1 | q^1 | 1 | qs1^1 | q*qs1^1 | cos*dq^2

-M23 | q^1 | q^1 | 1 | q*qs1^2 | 1 | dq^2

-M33/2.0 | 1 | q^2 | 1 | 1 | q^2*qs1^2 | dq^2

-M33/2.0 | 1 | q^2 | 1 | q^2*qs1^2 | 1 | dq^2

-M33/2.0 | 1 | q^2 | 1 | q*qs1^1 | q*qs1^1 | dq^2*cos

-M33/2.0 | 1 | q^2 | 1 | q*qs1^1 | q*qs1^1 | cos*dq^2

---

c | 1 | 1 | 1 | 1 | 1 | 1

The following lines would have the following genral form

ri | qiu0 | qiu1 | qiu2 | qiu3 | qiu4 | qiu5

So, total 80 lines will be there; i goes from 0 to 79

---

end-hamiltonian-section

HAMILTONIAN-SECTION_cis

usediag

---

modes | r_2 | r_3 | r_1 | t_2 | t_1 | p_1

5.862318d-6 | q^1 | 1 | 1 | 1 | 1 | 1

-3.674923d-5 | dq2̂ | 1 | 1 | 1 | 1 | 1

0.199815 | q10̂ | 1 | 1 | 1 | 1 | 1

-0.1995720744 | g1 | 1 | 1 | 1 | 1 | 1

-0.02919914 | g1*q1 | 1 | 1 | 1 | 1 | 1

0.4880250 | g1*q12̂ | 1 | 1 | 1 | 1 | 1

-1.303379 | g1*q13̂ | 1 | 1 | 1 | 1 | 1

0.9694112 | g1*q14̂ | 1 | 1 | 1 | 1 | 1

———————————————————— 1.152891d-5 | 1 | qˆ1 | 1 | 1 | 1 | 1 -3.6749237d-5 | 1 | dq2̂ | 1 | 1 | 1 | 1 0.199815 | 1 | q20̂ | 1 | 1 | 1 | 1 -0.19939010 | 1 | g2 | 1 | 1 | 1 | 1 0.017770776 | 1 | g2*q2 | 1 | 1 | 1 | 1 0.1326029 | 1 | g2*q22̂ | 1 | 1 | 1 | 1 -0.19864533 | 1 | g2*q23̂ | 1 | 1 | 1 | 1 0.0963012354 | 1 | g2*q24̂ | 1 | 1 | 1 | 1 ———————————————————— 3.243973d-6 | 1 | 1 | qˆ1 | 1 | 1 | 1 -2.893093d-4 | 1 | 1 | dq2̂ | 1 | 1 | 1 0.199815 | 1 | 1 | q30̂ | 1 | 1 | 1 -0.1997286 | 1 | 1 | g3 | 1 | 1 | 1 -0.01330962 | 1 | 1 | g3*q31̂ | 1 | 1 | 1 0.41641177 | 1 | 1 | g3*q32̂ | 1 | 1 | 1 -0.50147370 | 1 | 1 | g3*q33̂ | 1 | 1 | 1 0.23521044 | 1 | 1 | g3*q34̂ | 1 | 1 | 1 -0.4574862 | 1 | 1 | g3*q35̂ | 1 | 1 | 1 0.8193689 | 1 | 1 | g3*q36̂ | 1 | 1 | 1 ———————————————————— -6.65897d-6 | 1 | 1 | 1 | q | 1 | 1 -1.26493d-5 | 1 | 1 | 1 | dq*qs12̂*dq | 1 | 1 6.65897d-6 | 1 | 1 | 1 | dq*q*qs12̂*dq | 1 | 1 0.199815 | 1 | 1 | 1 | t20̂ | 1 | 1 -0.1992434 | 1 | 1 | 1 | g4 | 1 | 1 -0.026653980 | 1 | 1 | 1 | g4*t2 | 1 | 1 0.27134390 | 1 | 1 | 1 | g4*t22̂ | 1 | 1 -0.26446122 | 1 | 1 | 1 | g4*t23̂ | 1 | 1 0.23762334 | 1 | 1 | 1 | g4*t24̂ | 1 | 1 ———————————————————— -7.07777d-6 | 1 | 1 | 1 | 1 | q | 1 -9.06079d-5 | 1 | 1 | 1 | 1 | dq*qs12̂*dq | 1 7.07777d-6 | 1 | 1 | 1 | 1 | dq*q*qs12̂*dq | 1 0.199815 | 1 | 1 | 1 | 1 | t10̂ | 1 -0.1996101 | 1 | 1 | 1 | 1 | g5 | 1 -0.00931089145 | 1 | 1 | 1 | 1 | g5*t1 | 1 0.058163918856 | 1 | 1 | 1 | 1 | g5*t12̂ | 1 -0.05969423564 | 1 | 1 | 1 | 1 | g5*t13̂ | 1 0.02626388225 | 1 | 1 | 1 | 1 | g5*t14̂ | 1 ————————————————————- -1.14605d-4 | 1 | 1 | 1 | 1 | 1 | dq2̂ -3.07824d-6 | 1 | 1 | 1 | 1 | 1 | dq2̂*cos -3.07824d-6 | 1 | 1 | 1 | 1 | 1 | cos*dq2̂ -7.172084d-5 | 1 | 1 | 1 | 1 | 1 | cos -0.0104828 | 1 | 1 | 1 | 1 | 1 | cos2 -0.000334943 | 1 | 1 | 1 | 1 | 1 | cos3 0.000171863 | 1 | 1 | 1 | 1 | 1 | cos4 0.006 | 1 | 1 | 1 | 1 | 1 | g1pi ————————————————————- end-hamiltonian-section

HAMILTONIAN-SECTION_trans

usediag

————————————————————

modes | r_2 | r_3 | r_1 | t_2 | t_1 | p_1

————————————————————

5.130465d-6 | qˆ1 | 1 | 1 | 1 | 1 | 1 -3.674923d-5 | dq2̂ | 1 | 1 | 1 | 1 | 1 0.200239252946 | q10̂ | 1 | 1 | 1 | 1 | 1 -0.200239252946 | g1 | 1 | 1 | 1 | 1 | 1 0.47224 | g1*q12̂ | 1 | 1 | 1 | 1 | 1 -1.28108 | g1*q13̂ | 1 | 1 | 1 | 1 | 1 1.01278 | g1*q14̂ | 1 | 1 | 1 | 1 | 1 ———————————————————— 1.0114998d-5 | 1 | qˆ1 | 1 | 1 | 1 | 1 -3.6749237d-5 | 1 | dq2̂ | 1 | 1 | 1 | 1 0.200239252946 | 1 | q20̂ | 1 | 1 | 1 | 1 -0.200239252946 | 1 | g2 | 1 | 1 | 1 | 1 0.148565 | 1 | g2*q22̂ | 1 | 1 | 1 | 1 -0.20644 | 1 | g2*q23̂ | 1 | 1 | 1 | 1 0.1018 | 1 | g2*q24̂ | 1 | 1 | 1 | 1 ———————————————————— 2.611952d-6 | 1 | 1 | qˆ1 | 1 | 1 | 1 -2.893093d-4 | 1 | 1 | dq2̂ | 1 | 1 | 1 0.2002393 | 1 | 1 | q30̂ | 1 | 1 | 1 -0.2002393 | 1 | 1 | g3 | 1 | 1 | 1 0.42615 | 1 | 1 | g3*q32̂ | 1 | 1 | 1 -0.49848 | 1 | 1 | g3*q33̂ | 1 | 1 | 1 0.29256 | 1 | 1 | g3*q34̂ | 1 | 1 | 1 -0.36536 | 1 | 1 | g3*q35̂ | 1 | 1 | 1 0.54825 | 1 | 1 | g3*q36̂ | 1 | 1 | 1 ———————————————————— -6.56776d-6 | 1 | 1 | 1 | q | 1 | 1 -1.25549d-5 | 1 | 1 | 1 | dq*qs12̂*dq | 1 | 1 6.56776d-6 | 1 | 1 | 1 | dq*q*qs12̂*dq | 1 | 1 0.200239252946 | 1 | 1 | 1 | t20̂ | 1 | 1 -0.200239252946 | 1 | 1 | 1 | g4 | 1 | 1 0.28985 | 1 | 1 | 1 | g4*t22̂ | 1 | 1 -0.173188 | 1 | 1 | 1 | g4*t23̂ | 1 | 1 0.16913 | 1 | 1 | 1 | g4*t24̂ | 1 | 1 ———————————————————— -6.97676d-6 | 1 | 1 | 1 | 1 | q | 1 -9.21157d-5 | 1 | 1 | 1 | 1 | dq*qs12̂*dq | 1 6.97676d-6 | 1 | 1 | 1 | 1 | dq*q*qs12̂*dq | 1 0.200239252946 | 1 | 1 | 1 | 1 |

t1$\hat{0}$ | 1 -0.200239252946 | 1 | 1 | 1 | 1 | g5 | 1 0.0471315 | 1 | 1 | 1 | 1 | g5*t1$\hat{2}$ | 1 -0.0446942 | 1 | 1 | 1 | 1 | g5*t1$\hat{3}$ | 1 0.0120094 | 1 | 1 | 1 | 1 | g5*t1$\hat{4}$ | 1 ——————————————————————— -1.131196d-4 | 1 | 1 | 1 | 1 | 1 | dq$\hat{2}$ -2.481013d-6 | 1 | 1 | 1 | 1 | 1 | dq$\hat{2}$*cos -2.481013d-6 | 1 | 1 | 1 | 1 | 1 | cos*dq$\hat{2}$ 0.001091769 | 1 | 1 | 1 | 1 | 1 | cos -0.00967354 | 1 | 1 | 1 | 1 | 1 | cos2 -0.358768d-3 | 1 | 1 | 1 | 1 | 1 | cos3 0.122464d-3 | 1 | 1 | 1 | 1 | 1 | cos4 0.005 | 1 | 1 | 1 | 1 | 1 | g0pi 0.005 | 1 | 1 | 1 | 1 | 1 | g2pi ———————————————————————

end-hamiltonian-section

end-operator

Appendix D

Appendix to Chapter 5

Table D1: *Fitting Parameters of bond lengths (in Å) for HFCO global PES*

Fitting Parameter	A_0	A_1	A_2
	HFCO		
CH	0.170523	1.91503	1.09197
CF	0.140033	2.19966	1.34058
CO	0.323817	2.31931	1.17885
	trans-HOCF		
CH	0.40318	1.15625	1.8253
CF	0.161191	2.1032	1.32096
CO	0.180574	2.25003	1.3078
	cis-HOCF		
CH	0.27858	1.3776	1.88176
CF	0.126212	2.202258	1.34323
CO	0.207766	2.16394	1.29538
	$TS^{\#}_{cis\leftrightarrow trans}$		
CH	0.384223	1.23925	1.93094
CF	0.125528	2.24039	1.32174
CO	0.188859	2.10828	1.33224
	$TS^{\#}_{trans\leftrightarrow eq.}$		
CH	0.19022	1.37438	1.24565
CF	0.138298	2.18594	1.32527
CO	0.251685	2.15293	1.26038
	$TS^{\#}_{eq.\leftrightarrow diss.}$		
CH	0.122952	1.86676	1.13992
CF	0.207685	0.965338	1.85693
CO	0.37914	2.38939	1.13183

Table D2: *Fitting Parameters for bond angles and dihedral angle of HFCO global PES*

Fitting Parameter	A_0	A_1	A_2	A_3	A_4
			HFCO		
$\cos\theta_1^{HCO}$	-0.00941689	0.655782	-0.712589	0.246601	-0.0260739
$\cos\theta_2^{FCO}$	4.12442	-6.47744	3.91998	-1.1034	0.123926
ϕ	0.148051	0.184528	0.0410732	0.00456629	-0.0000426235
			trans-HOCF		
$\cos\theta_1^{HCO}$	1.16407	-5.92812	10.5444	-7.68789	2.01949
$\cos\theta_2^{FCO}$	3.16337	-5.32248	3.32299	-0.929076	0.101849
ϕ	0.0169521	0.00183211	-0.0155756	0.0000674612	0.000531103
			cis-HOCF		
$\cos\theta_1^{HCO}$	0.845562	-4.62362	8.89735	-7.10876	2.08893
$\cos\theta_2^{FCO}$	6.0662	-10.8735	7.29698	-2.18907	0.250653
ϕ	0.0145962	-0.00004804	-0.0151842	0.000175393	0.000485224
			$TS^{\#}_{cis\leftrightarrow trans}$		
$\cos\theta_1^{HCO}$	0.766402	-4.42355	8.9767	-7.56858	2.36852
$\cos\theta_2^{FCO}$	4.142	-7.22621	4.73598	-1.40105	0.161227
ϕ	-0.014438	0.000262282	-0.0139564	0.000145259	0.000469644
			$TS^{\#}_{trans\leftrightarrow eq.}$		
$\cos\theta_1^{HCO}$	1.42998	-5.50878	7.73936	-4.68779	1.02693
$\cos\theta_2^{FCO}$	3.04765	-4.78936	2.81346	-0.743932	0.0767932
ϕ	0.0351776	0.03771	0.00122596	-0.00200	-0.000713794
			$TS^{\#}_{eq.\leftrightarrow diss.}$		
$\cos\theta_1^{HCO}$	33.663	-45.4056	22.8712	-5.09897	0.424502
$\cos\theta_2^{FCO}$	1.50609	-2.41497	1.43761	-0.376511	0.0366299
ϕ	0.514862	-0.835363	0.435901	-0.133681	0.0182813

Table D3: *RMSE vs NN for HFCO global PES*

Number of	RMSE (in cm^{-1})	
Neurons (NN)	Testset	Trainset
10	2238.6	2348.4
20	1229.0	1295.0
40	307.3	263.4
60	205.7	164.5
80	140.5	112.9
100	133.6	90.8
120	131.6	92.4
140	138.4	95.7

Table D4: *Grid lengths and parameters of the primitive basis set employed for each degree of freedom of HFCO. HO is the harmonic oscillator (Hermite) DVR.*

Modes	R_1 $\cos\theta_1$	R_2 $\cos\theta_2$	R_3 ϕ
Primitive basis	HO-DVR HO-DVR	HO-DVR HO-DVR	HO-DVR HO-DVR
Number of basis functions	16 18	16 18	25 25
Grid length (a.u.)	[1.30,3.39] [-0.98,0.12]	[1.98,3.85] [-0.90,-0.06]	[1.83,2.94] [1.4586,4.8245]
Mode combinations	(R_1, $\cos\theta_1$)	(R_2, $\cos\theta_2$)	(R_3,ϕ_1)
Number of SPF	25	30	25

Table D5: *Grid lengths and parameters of the primitive basis set employed for each degree of freedom of trans-HOCF. HO is the harmonic oscillator (Hermite) DVR.*

Modes	R_1 $\cos\theta_1$	R_2 $\cos\theta_2$	R_3 ϕ
Primitive basis	HO-DVR HO-DVR	HO-DVR HO-DVR	HO-DVR HO-DVR
Number of basis functions	16 18	16 18	25 25
Grid length (a.u.)	[3.0,4.5] [0.74,0.97]	[2.10,3.28] [-0.707,0.129]	[2.15,3.01] [1.5714,4.8246]
Mode combinations	(R_1, $\cos\theta_1$)	(R_2, $\cos\theta_2$)	(R_3,ϕ_1)
Number of SPF	25	30	25

Table D6: *Grid lengths and parameters of the primitive basis set employed for each degree of freedom of cis-HOCF. HO is the harmonic oscillator (Hermite) DVR.*

Modes	R_1 $\cos\theta_1$	R_2 $\cos\theta_2$	R_3 ϕ
Primitive basis	HO-DVR HO-DVR	HO-DVR HO-DVR	HO-DVR HO-DVR
Number of basis functions	16 18	16 18	25 25
Grid length (a.u.)	[3.0,4.5] [0.74,0.97]	[2.10,3.28] [-0.707,0.129]	[2.15,3.01] [-1.5714,1.57142]
Mode combinations	(R_1, $\cos\theta_1$)	(R_2, $\cos\theta_2$)	(R_3,ϕ_1)
Number of SPF	25	30	25

Table D7: *Selected vibrational energies (in cm^{-1}) for states up to 2600 cm^{-1} for cis- and trans-HOCF from the global PES compared with CCSD(T)/aug-cc-pVTZ anharmonic frequencies (using VPT2 method). Vibrational states assignment is based upon comparing with corresponding VPT2 assignment.*

cis-HOCF			trans-HOCF		
Assignment ($\nu_1\nu_2\nu_3\nu_4\nu_5\nu_6$)	CCSD(T)[a]	MCTDH[b]	Assignment ($\nu_1\nu_2\nu_3\nu_4\nu_5\nu_6$)	CCSD(T)	MCTDH[b]
0 0 0 0 1 0	628.9	632.0	0 0 0 0 1 0	645.8	651.4
0 0 0 0 0 1	741.4	764.2	0 0 0 0 0 1	707.5	742.9
0 1 0 0 0 0	959.2	957.0	0 1 0 0 0 0	1043.3	1043.1
0 0 0 1 0 0	1254.6	1240.2	0 0 0 1 0 0	1231.1	1251.5
0 0 0 0 2 0	1254.7	1265.3	0 0 0 0 2 0	1291.3	1302.9
0 0 1 0 0 0	1321.6	1335.6	0 0 1 0 0 0	1323.7	1321.5
0 0 0 0 1 1	1370.3	1397.2	0 0 0 0 1 1	1354.2	1394.9
0 0 0 0 0 2	1468.8	1512.9	0 0 0 0 0 2	1398.9	1457.5
0 1 0 0 1 0	1580.6	1582.6	0 1 0 0 1 0	1683.7	1688.7
0 1 0 0 0 1	1701.2	1719.2	0 1 0 0 0 1	1751.7	1789.1
0 0 0 0 3 0	1877.3	1860.6	0 0 0 1 1 0	1870.1	1898.8
0 0 0 1 1 0	1883.3	1897.8	0 0 0 1 0 1	1928.1	1954.2
0 2 0 0 0 0	1898.5	1898.6	0 0 0 0 3 0	1936.6	1970.4
0 0 1 0 1 0	1946.8	1962.5	0 0 1 0 1 0	1966.6	1986.8
0 0 0 1 0 1	1988.4	1996.5	0 0 0 0 2 1	2000.6	2047.1
0 0 0 0 1 2	1996.2	2030.4	0 0 1 0 0 1	2026.7	2067.2
0 0 1 0 0 1	2046.6	2075.0	0 0 0 0 1 2	2046.6	2074.9
0 0 0 0 2 1	2097.9	2145.2	0 2 0 0 0 0	2073.0	2109.8
0 0 0 0 0 3	2182.4	2187.1	0 0 0 0 0 3	2074.5	2145.5
0 1 0 0 2 1	2198.9	2209.9	0 1 0 1 0 0	2272.9	2301.5
0 1 0 1 0 0	2206.9	2249.3	0 1 0 0 2 0	2323.8	2334.8
0 1 1 0 0 0	2277.2	2290.8	0 1 1 0 0 0	2352.7	2355.2
0 1 0 0 1 1	2322.7	2346.4	0 1 0 0 1 1	2390.3	2435.4
0 1 0 0 0 2	2429.3	2449.5	0 0 0 2 0 0	2441.5	2495.2
0 0 0 2 0 0	2489.6	2466.7	0 1 0 0 0 2	2444.1	2506.4
0 0 0 1 2 0	2508.9	2483.5	0 0 0 1 2 0	2508.8	2545.9
0 2 0 0 1 0	2512.4	2517.0	0 0 1 1 0 0	2542.1	2575.1
0 1 1 0 0 0	2555.8	2531.2	0 0 0 1 1 1	2568.0	2695.1
0 0 1 0 2 0	2568.9	2552.4	0 0 0 1 0 2	2609.2	2619.9
0 0 0 1 1 1	2617.2	2590.5	0 0 1 0 2 0	2609.3	2630.7

[a] Using aug-cc-pVTZ basis set and VPT2 method in CFOUR.[124]
[b]Based on CCSD(T)-F12/cc-pVTZ-F12 computed 100 NN fit PES.

D.1 40000 cm^{-1} cut 100 NN fit PES operator file for HFCO

The operator file is exactly the same structure as the Appendix D. Only the fitting parameters are provided here.

PARAMETER-SECTION

a11 = -0.996014, a12 = 2.06649, a21 = -1.07919, a22 = 2.54408, a31 = -1.19789, a32 = 2.22995, mh = 1.0, H-mass, mc = 12.00,AMU, mo = 15.9949146221,AMU, mf = 18.99840320,AMU, M11 = 1.0/mh+1.0/mc, M22 = 1.0/mf+1.0/mc, M33 = 1.0/mo+1.0/mc Mu = 1.0/mc # Mu = Mij; i neq j, R1eq = 2.06320d0, R2eq = 2.5340d0, R3eq = 2.228740d0, U1eq = 0.789459, U2eq = 0.8414164680d0, E1eq = -0.61380310d0, E2eq = -0.54038720d0

, r0 = -4.16991810462d-05 , w0u0 = 0.577739296615502 , w0u1 = 0.364802012405860 , w0u2 = 1.318909354162213 , w0u3 = 0.530745606677309 , w0u4 = 1.177607033196864 , w0u5 = 0.279174788467111 , r1 = 3.64022403025 , w1u0 = -0.839578266364988 , w1u1 = -0.378396502067425 , w1u2 = 0.741431950733731 , w1u3 = 3.420498531258265 , w1u4 = -0.029708769550532 , w1u5 = -0.006113340164022 , r2 = 3.71295435763 , w2u0 = 0.287063556606475 , w2u1 = -1.170412715728625 , w2u2 = -0.459604502987128 , w2u3 = 1.118723673469369 , w2u4 = -0.712149197836188 , w2u5 = -0.281633732843197 , r3 = -7.31328671614 , w3u0 = 0.121474155060917 , w3u1 = -0.525901917292006 , w3u2 = -0.478778964855351 , w3u3 = 0.291914605518526 , w3u4 = -0.141371698899919 , w3u5 = -0.929991950773385 , r4 = 207.404100493 , w4u0 = -0.017559838694596 , w4u1 = -0.050448373149514 , w4u2 = -3.381897564963545 , w4u3 = 0.071857169973141 , w4u4 = -0.139735254297427 , w4u5 = -0.016408565919342 , r5 = -5.9321139127 , w5u0 = 0.061221955872117 , w5u1 = -1.158090327090918 , w5u2 = -0.143579510332362 , w5u3 = -3.171292275778967 , w5u4 = -2.078722271047108 , w5u5 = -0.209967147073400 , r6 = -5.19943885979 , w6u0 = 0.284872559605997 , w6u1 = -1.021450857962388 , w6u2 = -0.492366950862660 , w6u3 = -1.095118394447858 , w6u4 = -1.566440854272596 , w6u5 = 0.191517393180694 , r7 = -57.1319109211 , w7u0 = -0.526353686978408 , w7u1 = -1.167036170493288 , w7u2 = -0.187032676966528 , w7u3 = 0.935337817766746 , w7u4 = -1.123466878119092 , w7u5 = -0.433972084392229 , r8 = -8.59531994183 , w8u0 = 0.543725766548193 , w8u1 = -1.089351285318377 , w8u2 = -0.725904622166933 , w8u3 = -0.658271720208572 , w8u4 = -1.484857932547301 , w8u5 = -0.281063176364276 , r9 = 0.463823077686 , w9u0 = 0.008058500708986 , w9u1 = -1.069193528178423 , w9u2 = -0.030649557355871 , w9u3 = -8.449486616517992 , w9u4 = -1.700457212974302 , w9u5 = -0.516729247260890 , r10 = -0.00229962451386 , w10u0 = 0.468576521992768 , w10u1 = 0.862258373414940 , w10u2 = -0.654193728290914 , w10u3 = -2.729228779726665 , w10u4 = -2.806676450408779 , w10u5 = -0.506996125056840 , r11 = 31.8160542028 , w11u0 = 0.161721884546187 , w11u1 = -0.406057209459314 , w11u2 = -0.646494684947232 , w11u3 = 1.438734883123415 , w11u4 = 0.138540759909740 , w11u5 = 0.313015572510880 , r12 = 0.0122833724562 , w12u0 = 0.600215817411941 , w12u1 = 0.665383992089364 , w12u2 = -0.634162704977210 , w12u3 = -2.345399291678224 , w12u4 = -2.908815513711600 , w12u5 = -0.456669662038281 , r13 = -0.00424282679862 , w13u0 = -0.398210209755173 , w13u1 = -0.488281120111609 , w13u2 = 2.191476288558438 , w13u3 = 2.126589113185838 , w13u4 = 0.966685063567495 , w13u5 = 0.043684264364885 , r14 = 4.31190827317 , w14u0 = -0.030690714208931 , w14u1 = -0.406735929759648 , w14u2 = -0.230485544824226 , w14u3 = 1.097362496582178 , w14u4 = -0.066300472127542 , w14u5 = -0.554489261660661 , r15 = -11.5084713591 , w15u0 = 0.353367121732586 , w15u1 = -0.254275628481591 , w15u2 = -0.762259629407990 , w15u3 = 3.097338664752718 , w15u4 = 0.028979790764896 , w15u5 = -0.752782414614103 , r16 = -7.59924122327 , w16u0 = 0.433749217345842 , w16u1 = -0.684673999221812 , w16u2 = -0.685845525531516 , w16u3 = 1.090024897772241 , w16u4 = 0.021219446085162 , w16u5 = 0.021636346022023 , r17 = -0.00461754764621 , w17u0 = -0.665735504566998 , w17u1 = 0.905682778554172 , w17u2 = 0.633994984711044 , w17u3 = 0.551742068621788 , w17u4 = 1.519454264999029 , w17u5 = -0.156274770594540 , r18 = 0.00795747492259 , w18u0 = -0.038796112314585

, w18u1 = 1.076216717337046 , w18u2 = -0.825691015735533 , w18u3 = -0.809142346036502 , w18u4 = -0.975799759546187 , w18u5 = -0.473339310092979 , r19 = 88.6201185897 , w19u0 = 0.446381139638723 , w19u1 = -0.296811866573782 , w19u2 = -0.803629662916175 , w19u3 = 3.413657552720172 , w19u4 = 0.054631178201507 , w19u5 = -1.138080370340223 , r20 = -5.99219063657 , w20u0 = -0.696467072657822 , w20u1 = -0.586241508333827 , w20u2 = 0.559043490016027 , w20u3 = 1.537837246094041 , w20u4 = -0.145506329632145 , w20u5 = -0.139355290118540 , r21 = -0.417067601991 , w21u0 = 0.455887639880311 , w21u1 = -0.526833845620239 , w21u2 = -0.488632254894506 , w21u3 = -1.376522177412964 , w21u4 = 0.465017387670366 , w21u5 = 0.220403918699748 , r22 = 5.23006770681 , w22u0 = 0.779564757949549 , w22u1 = -1.087499078151688 , w22u2 = -0.931199238724953 , w22u3 = -0.374625829636220 , w22u4 = -0.020807492023271 , w22u5 = -0.096992615633671 , r23 = 6.83318000677 , w23u0 = 0.251414719873395 , w23u1 = -1.168767717600650 , w23u2 = -0.540194717548044 , w23u3 = -0.609562104659726 , w23u4 = -2.182528126897380 , w23u5 = -0.341970748588511 , r24 = -0.0222699872628 , w24u0 = -0.002702641852643 , w24u1 = -0.728027483966623 , w24u2 = -0.257008088894586 , w24u3 = 0.002357876281161 , w24u4 = -0.871443585070177 , w24u5 = -0.088749972825090 , r25 = 17.455356004 , w25u0 = 0.225543020785034 , w25u1 = -0.442633655955038 , w25u2 = -0.734109220396171 , w25u3 = 0.853574588991114 , w25u4 = 0.154909409446326 , w25u5 = -0.568907415605138 , r26 = 0.747104265829 , w26u0 = -0.326598594039228 , w26u1 = -0.190904919851986 , w26u2 = -0.162837517462372 , w26u3 = 8.094063279767193 , w26u4 = 0.250955763396014 , w26u5 = 0.111973151392174 , r27 = -11.5865857737 , w27u0 = 0.492936827694900 , w27u1 = -0.301249415648155 , w27u2 = -0.817341666836425 , w27u3 = 3.614809149630531 , w27u4 = 0.029366374465673 , w27u5 = -1.327906843676313 , r28 = -3161.44268893 , w28u0 = 0.254770521195832 , w28u1 = -0.283474441373207 , w28u2 = -0.731789550400320 , w28u3 = 2.750510545800161 , w28u4 = 0.157462010940399 , w28u5 = -0.143600184859073 , r29 = -0.0309177874382 , w29u0 = 0.675558883788327 , w29u1 = 0.500783708233544 , w29u2 = -0.633120221935511 , w29u3 = -1.745730773334296 , w29u4 = -2.906907255262786 , w29u5 = -0.377391706809615 , r30 = -525.775979337 , w30u0 = 0.387071561152176 , w30u1 = -0.291650217321996 , w30u2 = -0.784950046540488 , w30u3 = 3.164862798929071 , w30u4 = 0.087408418339530 , w30u5 = -0.878334977277496 , r31 = 10.1289395675 , w31u0 = -2.627102240724649 , w31u1 = 0.078770051718374 , w31u2 = -0.006306013396358 , w31u3 = -0.024189819387966 , w31u4 = 0.031475151712836 , w31u5 = 0.065666403280857 , r32 = -0.689241721099 , w32u0 = -0.344317068088799 , w32u1 = -0.190039624930709 , w32u2 = -0.142855504479063 , w32u3 = 8.196776944827237 , w32u4 = 0.249715920562343 , w32u5 = 0.109882786183660 , r33 = -0.437349492037 , w33u0 = -1.170476209199126 , w33u1 = -0.170712382672496 , w33u2 = 1.038788269435308 , w33u3 = 10.585954547350145 , w33u4 = 0.207264895125130 , w33u5 = 0.064793501596819 , r34 = 0.015683806253 , w34u0 = 0.656889774485164 , w34u1 = 1.009702242396779 , w34u2 = -1.503593816064203 , w34u3 = -0.230835832296360 , w34u4 = 1.059802232929915 , w34u5 = 0.047838356600411 , r35 = -22.5157972808 , w35u0 = 0.174575467751591 , w35u1 = -0.356968836276332 , w35u2 = -0.672194326109733 , w35u3 = 1.825404294725173 , w35u4 = 0.136064169023028 , w35u5 = 0.399663690073619 , r36 = 0.0392931532675 , w36u0 = 0.135090857616445 , w36u1 = 0.654364264853994 , w36u2 = -0.930140526904383 , w36u3 = 1.808186883597199 , w36u4 = -0.131400675231109 , w36u5 = -0.274250965339362 , r37 = 15.2929285496 , w37u0 = 0.066509998641655 , w37u1 = -1.113180635628618 , w37u2 = -0.124744205730496 , w37u3 = -4.129204997447228 , w37u4 = -2.245509055280770 , w37u5 = -0.537035439917634 , r38 = 489.193857491 , w38u0 = 0.052000941607351 , w38u1 = -4.187793668976839 , w38u2 = -0.093954971314386 , w38u3 = -0.040098708254868 , w38u4 = 0.060200568780177 , w38u5 = 0.049184817855449 , r39 = 0.00612313164389 , w39u0 = -0.384758597990867 , w39u1 = 0.240151316396118 , w39u2 = 0.259574894304137 , w39u3 = 0.052345668481917 , w39u4 = 0.021756067600526 , w39u5 = 0.036494002634463 , r40 = -1.9031624045 , w40u0 = -0.949604348790300 , w40u1 = -0.294642675953554 , w40u2 = 0.933143824804099 , w40u3 = 4.846531048792728 , w40u4 = 0.031779958757153 , w40u5 = 0.044085152962012 , r41 = -15.5851404636 , w41u0 = -0.513512141622168 , w41u1 = -0.663322315510871 , w41u2 = -0.345684141464899 , w41u3 = -0.544752964283277 , w41u4 = -0.199348654023021 , w41u5 = -0.069343947840589 , r42 = 0.00539419312219 , w42u0 = -0.147715877658163

, w42u1 = -0.137847056586809 , w42u2 = 0.519002201686035 , w42u3 = -0.818930998249140 , w42u4 = 0.814517216354192 , w42u5 = -0.381079203962102 , r43 = 0.0802132573347 , w43u0 = -0.352497111997417 , w43u1 = 0.211410840637369 , w43u2 = 0.224016073307244 , w43u3 = 1.007219249052409 , w43u4 = 0.046646846172278 , w43u5 = -0.130883773049865 , r44 = -0.0743591852798 , w44u0 = -0.285678973528675 , w44u1 = 0.352536050132551 , w44u2 = -0.287013019371255 , w44u3 = -0.247100748184672 , w44u4 = 0.527142213642225 , w44u5 = 0.437949863206590 , r45 = 0.0129882902067 , w45u0 = -0.480586972159899 , w45u1 = 0.302821864413237 , w45u2 = 0.488977601531796 , w45u3 = 0.367944819227344 , w45u4 = -1.885838597623759 , w45u5 = -0.289228918131450 , r46 = 7.31205881331 , w46u0 = 0.040883012167856 , w46u1 = -1.211212216290000 , w46u2 = -0.198441408518460 , w46u3 = -2.173309025249773 , w46u4 = -2.251650205986686 , w46u5 = -0.062020702177717 , r47 = -0.0566793098901 , w47u0 = -0.047878064578809 , w47u1 = 0.332623830404475 , w47u2 = -0.462833106160332 , w47u3 = -1.186886226328104 , w47u4 = -1.553680328466275 , w47u5 = -0.218222514833004 , r48 = 0.0901676771813 , w48u0 = -0.031450559380997 , w48u1 = 0.838964347021116 , w48u2 = -1.429430504618531 , w48u3 = 0.462860965910763 , w48u4 = 0.425938848123677 , w48u5 = 0.263676275007881 , r49 = 1.22727013778 , w49u0 = 0.151270444434554 , w49u1 = -0.886340828938803 , w49u2 = -0.337156862492473 , w49u3 = -2.292712310183083 , w49u4 = -0.856436484110062 , w49u5 = 0.134749575265030 , r50 = 5.33766124186 , w50u0 = 0.061963737521786 , w50u1 = -0.786071539838896 , w50u2 = -0.760391047485215 , w50u3 = 0.114386885942747 , w50u4 = 3.247341852731722 , w50u5 = -0.119944773648415 , r51 = -1.76460495656 , w51u0 = -0.219915469625617 , w51u1 = -0.624647032196350 , w51u2 = -0.276261756865753 , w51u3 = 0.348769778157179 , w51u4 = 0.239111342976674 , w51u5 = 0.678633907381688 , r52 = -0.000539915387304 , w52u0 = 1.357816398981088 , w52u1 = 0.639815270541873 , w52u2 = -1.189131780446365 , w52u3 = -2.014177051533041 , w52u4 = 0.060482603638121 , w52u5 = -0.245693085367951 , r53 = 0.220878597777 , w53u0 = -0.249074007644993 , w53u1 = -0.836504150274033 , w53u2 = 0.984100764147841 , w53u3 = 0.991768129459050 , w53u4 = -0.292679270071117 , w53u5 = -0.304139504325273 , r54 = 1.70798124224 , w54u0 = 0.174368017520032 , w54u1 = -1.056514601489333 , w54u2 = -0.201191074288665 , w54u3 = -3.010796602910186 , w54u4 = -2.728783891196509 , w54u5 = -0.877357379185521 , r55 = 5.28169675655d-05 , w55u0 = -1.400863608004426 , w55u1 = -0.151264448841782 , w55u2 = 1.294861026017208 , w55u3 = 14.774353999911385 , w55u4 = 0.371387153177501 , w55u5 = 0.046510954044298 , r56 = 0.100029860699 , w56u0 = -0.004943870963242 , w56u1 = 0.293637008736924 , w56u2 = 0.158032146937629 , w56u3 = 0.196928360943084 , w56u4 = 0.389259524298499 , w56u5 = 0.132918671044628 , r57 = 0.0147242216392 , w57u0 = -0.716662004535817 , w57u1 = -0.421103960582040 , w57u2 = 1.969127244627034 , w57u3 = 3.230171524953269 , w57u4 = 0.683905257473096 , w57u5 = 0.040155869081459 , r58 = 2211.17542976 , w58u0 = 0.337373828585744 , w58u1 = -0.287720683642584 , w58u2 = -0.767081908814244 , w58u3 = 2.971082998176700 , w58u4 = 0.112902046862304 , w58u5 = -0.640081226522553 , r59 = -0.553838329765 , w59u0 = -1.075867303103811 , w59u1 = -0.196124907178188 , w59u2 = 0.960695162870240 , w59u3 = 8.134297888880029 , w59u4 = 0.097876548467491 , w59u5 = 0.072185388848856 , r60 = 37.8017892618 , w60u0 = -0.756868501845973 , w60u1 = -1.033122580370870 , w60u2 = -1.205489675411792 , w60u3 = -0.341287091376902 , w60u4 = 1.367282355418201 , w60u5 = 0.192354697887263 , r61 = 1.03776631908 , w61u0 = -1.041472147460211 , w61u1 = -0.220462600174668 , w61u2 = 0.958703540367636 , w61u3 = 6.915054344152382 , w61u4 = 0.059052873345051 , w61u5 = 0.069984958703455 , r62 = 0.0124733625296 , w62u0 = 0.142300973682369 , w62u1 = -0.493715418857844 , w62u2 = 0.792312244464035 , w62u3 = 0.437526867769169 , w62u4 = 0.389884177464348 , w62u5 = 0.151824380011441 , r63 = 0.0223874433445 , w63u0 = 0.381749206400599 , w63u1 = -0.145609261982420 , w63u2 = -0.465266250771509 , w63u3 = -0.701631321868313 , w63u4 = 1.660869357962825 , w63u5 = 0.658509180332857 , r64 = 0.00400815968505 , w64u0 = -0.371134527241616 , w64u1 = 0.518384250132498 , w64u2 = 0.410003161586691 , w64u3 = -0.724630298030106 , w64u4 = 1.258538662245388 , w64u5 = -0.143371703680463 , r65 = 96.6011345954 , w65u0 = -0.590904599571934 , w65u1 = -1.123538832347626 , w65u2 = -0.128364236888470 , w65u3 = 0.456025071807558 , w65u4 = -0.971074279346625 , w65u5 = -0.445189234440927 , r66 = 1.55922768359d-05 , w66u0 = 0.838102824707261

, w66u1 = -0.160433198746739 , w66u2 = 1.993550985526628 , w66u3 = 0.219351996026708 , w66u4 = 1.805489873861869 , w66u5 = 0.170737027441086 , r67 = -0.0873969495752 , w67u0 = -0.212437270876071 , w67u1 = 0.499826983220182 , w67u2 = -0.356931235130331 , w67u3 = 0.646014646150175 , w67u4 = -1.493271324517211 , w67u5 = -0.052609507095137 , r68 = 0.519112511853 , w68u0 = -1.164040150752691 , w68u1 = -0.171487049137076 , w68u2 = 1.031117672798583 , w68u3 = 10.468526485530296 , w68u4 = 0.201670376172516 , w68u5 = 0.065309578998843 , r69 = -0.0025029582161 , w69u0 = 0.640343024505876 , w69u1 = 0.749485470323417 , w69u2 = -0.398000012456532 , w69u3 = -0.197315357142888 , w69u4 = -1.185673505124250 , w69u5 = -0.036547764498961 , r70 = 3.6948100147 , w70u0 = 0.455290628949746 , w70u1 = -0.996682206487039 , w70u2 = -0.640272560957080 , w70u3 = -0.820666673017353 , w70u4 = -1.502177631261605 , w70u5 = 0.152114542066331 , r71 = -1.54249916742 , w71u0 = 0.022046457278402 , w71u1 = -1.062116553734765 , w71u2 = -0.044310401563896 , w71u3 = -7.923116834322894 , w71u4 = -1.763576647757806 , w71u5 = -0.545931576546123 , r72 = 5.05503437942 , w72u0 = 0.052204315763714 , w72u1 = -1.055490500404144 , w72u2 = -0.075253961762354 , w72u3 = -6.666234978735950 , w72u4 = -1.931030914640736 , w72u5 = -0.597707606092860 , r73 = -0.0557984859314 , w73u0 = 0.027546661097965 , w73u1 = -0.997307556701072 , w73u2 = 0.931228728627617 , w73u3 = 0.824985346906503 , w73u4 = -0.798798642102170 , w73u5 = -0.522818522762574 , r74 = 0.000647421620573 , w74u0 = 0.716104402668682 , w74u1 = 0.415582350679438 , w74u2 = 0.207756138919516 , w74u3 = -1.069469432346300 , w74u4 = -0.236805526981045 , w74u5 = 0.096413948561824 , r75 = -0.000768015124329 , w75u0 = 0.185650008183667 , w75u1 = -0.039973343512557 , w75u2 = 0.508006514420574 , w75u3 = -0.255846298774271 , w75u4 = 0.241109580643783 , w75u5 = -0.019039345115434 , r76 = -11.5298741098 , w76u0 = 0.071562745716792 , w76u1 = -1.067427059424005 , w76u2 = -0.102522368981235 , w76u3 = -5.443562639495840 , w76u4 = -2.103536322301759 , w76u5 = -0.613535322627714 , r77 = 0.0215638964981 , w77u0 = 0.970396625459726 , w77u1 = 0.189829125882600 , w77u2 = -0.793217081592396 , w77u3 = -1.377360248200592 , w77u4 = -2.228507489036832 , w77u5 = -0.226238259974719 , r78 = 0.156566652271 , w78u0 = -0.232141783339805 , w78u1 = -0.549967839714569 , w78u2 = -0.321509806474215 , w78u3 = 0.268553749698811 , w78u4 = 0.082323161115334 , w78u5 = 1.059247326790769 , r79 = -14.4600403732 , w79u0 = 0.205112096912156 , w79u1 = -0.270839623753977 , w79u2 = -0.700266006098565 , w79u3 = 3.071219903530748 , w79u4 = 0.196680886011015 , w79u5 = 0.338366664893728 , r80 = 0.0220640145375 , w80u0 = 0.444369314211184 , w80u1 = 0.539477869617900 , w80u2 = -0.593082847280868 , w80u3 = -0.890061558142355 , w80u4 = -2.797671414383015 , w80u5 = -0.216338218351844 , r81 = -1.21007262626 , w81u0 = -1.276351400735217 , w81u1 = -0.094207824444882 , w81u2 = -0.325499817922146 , w81u3 = 3.457571482497354 , w81u4 = -0.165817408172000 , w81u5 = 0.144676343767072 , r82 = 0.303208575475 , w82u0 = 0.037668022172578 , w82u1 = 0.050396277192387 , w82u2 = -0.858377947229910 , w82u3 = 1.078709828738378 , w82u4 = -1.179001044612128 , w82u5 = 0.214990758595530 , r83 = 2.3700103426 , w83u0 = 0.189551796365068 , w83u1 = -0.292661516550572 , w83u2 = -0.685303358570454 , w83u3 = 2.829312119879968 , w83u4 = 0.186135028050196 , w83u5 = 0.557621799193029 , r84 = 0.65772948445 , w84u0 = 0.307426918706072 , w84u1 = -0.242648479011099 , w84u2 = -0.536500675212424 , w84u3 = 1.103664828006365 , w84u4 = -0.580487936952305 , w84u5 = -0.518200620828503 , r85 = -0.356919755492 , w85u0 = 0.495415218257807 , w85u1 = -0.315793158948306 , w85u2 = -0.560231822228178 , w85u3 = 0.471150075185933 , w85u4 = 0.823335744455845 , w85u5 = 0.243157937244943 , r86 = 810.413455758 , w86u0 = 0.238441014164608 , w86u1 = -0.282153990449833 , w86u2 = -0.723290358957124 , w86u3 = 2.750037336462124 , w86u4 = 0.167072085120639 , w86u5 = -0.003100071801093 , r87 = -0.0298368390829 , w87u0 = -0.515786133815231 , w87u1 = 0.176188810579050 , w87u2 = 0.259524928506412 , w87u3 = 0.945676241219544 , w87u4 = 0.896456836874206 , w87u5 = 0.117326720065308 , r88 = -0.646688594738 , w88u0 = -0.087316525132470 , w88u1 = -0.291831486471338 , w88u2 = -0.092947174909537 , w88u3 = 2.723847604076803 , w88u4 = -0.077778787070632 , w88u5 = -0.287502791746024 , r89 = 2.04964528234 , w89u0 = -0.735005492268909 , w89u1 = -0.059945125918544 , w89u2 = -0.568941585783969 , w89u3 = 2.849402078332382 , w89u4 = 0.273625829602798 , w89u5 = 0.138693215291586 , r90 = -4824.75364157 , w90u0 = 0.302727623569067 , w90u1 = -0.286136547191467 , w90u2 = -0.753338483712698 , w90u3 = 2.851968612682050 , w90u4 = 0.131519852933756 , w90u5 = -0.454767746422297 , r91 = -32.0687616821 , w91u0 = 0.108053139259059 , w91u1 = -0.353981644783447 , w91u2 = -0.626370978281938 , w91u3 = 1.408920670114594 , w91u4 = 0.143009908711770 , w91u5 = -0.109037622390768 , r92 = -12.8688517017 , w92u0 = 0.006003232157463 , w92u1 = -1.232602916817761 , w92u2 = -0.163345698581569 , w92u3 = -2.321775355793676 , w92u4 = -2.544712145650465 , w92u5 = -0.413095022944811 , r93 = 5448.94682317 , w93u0 = 0.276282241962728 , w93u1 = -0.284881224735465 , w93u2 = -0.741848750841652 , w93u3 = 2.782198674140654 , w93u4 = 0.145590155023437 , w93u5 = -0.295291952664330 , r94 = -0.153315917674 , w94u0 = 0.822488803360089 , w94u1 = 0.005498433202169 , w94u2 = -1.564099744499153 , w94u3 = -0.189520421939817 , w94u4 = -1.466409595622114 , w94u5 = 0.112462085754964 , r95 = 0.00870603655818 , w95u0 = 0.463918922665083 , w95u1 = -0.008071656975637 , w95u2 = -0.495743554993691 , w95u3 = -0.845850818890365 , w95u4 = -0.653379728711700 , w95u5 = -0.087495123702144 , r96 = -0.263859337385 , w96u0 = 0.137626496474963 , w96u1 = 0.767375382029750 , w96u2 = -1.207663355724944 , w96u3 = 0.231624854880772 , w96u4 = 0.708869825270077 , w96u5 = -0.071150495884325 , r97 = -0.00658084310416 , w97u0 = -0.106661228405277 , w97u1 = 1.046665870947527 , w97u2 = -1.362077966456989 , w97u3 = 0.625872478671948 , w97u4 = 0.107836783646556 , w97u5 = 0.577304279533526 , r98 = 0.213420915519 , w98u0 = -0.991744128003810 , w98u1 = -0.540167162227647 , w98u2 = 0.443804527270521 , w98u3 = -0.114870690389039 , w98u4 = 1.660173308524129 , w98u5 = 0.061951503772172 , r99 = 4.18108546396 , w99u0 = -0.344027446888542 , w99u1 = -0.972300537838800 , w99u2 = -0.039931175625579 , w99u3 = 0.166929688667627 , w99u4 = 0.168199598407611 , w99u5 = 0.311138200462158

c = 0.219898906

end-parameter-section

Appendix E

Appendix to Chapter 6

Table E1: *RMSE vs NN for HFCO on the S_1 PES*

Number of Neurons (NN)	RMSE (in cm^{-1})	
	Testset	Trainset
10	157.5	137.9
20	38.3	33.0
40	8.6	6.7
60	5.2	3.9
80	3.1	2.1
100	1.4	0.9

The Morse oscillator is defined in terms of the dissociation energy (a_0), predissociation factor (a_1) and equilibrium coordinate (a_2) as,

$$V(x) = a_0(1 - e^{-a_1(x-a_2)})^2 \tag{E.1}$$

Table E2: *One dimensional fitting parameters to Morse functional form for ${R_1}^{CH}$, ${R_2}^{CF}$ and ${R_3}^{CO}$ physical coordinates*

Physical Coordinates	Fitting Parameters		
	a_0	a_1	a_2
${R_1}^{CH}$	0.164216	1.02917	2.05681
${R_2}^{CF}$	0.157972	1.15394	2.52932
${R_3}^{CO}$	0.204523	1.04952	2.5215

Table E3: *One dimensional fitting parameters to the fourth order Polynomial functional form for ${\theta_1}^{HCO}$, ${\theta_2}^{FCO}$ and fifth order for ϕ physical coordinates*

Physical Coordinates	Fitting Parameters				
	a_0	a_1	a_2	a_3	a_4
${\theta_1}^{HCO}$	0.0261503	0.123836	0.192181	0.160517	0.129113
${\theta_2}^{FCO}$	0.0211551	0.140332	0.29972	0.273869	0.202697
ϕ	0.608371	-0.601016	0.15261	0.00866992	-0.0049585

n^{th} order polynomial functional form of coordinate x is defined as,

$$V(x_n) = \sum_{q=0}^{n} (a_n x^n) \tag{E.2}$$

Table E4: *Optimized geometries of HFCO ground and excited states minimum and intermediates conformers at various methods and active space. Bond distances are in Å and bond angles are in degrees. All present computations use the aug-cc-pVTZ basis set. Previous computational results are also provided.*

Method	CH	CF	CO	HCO	FCO	ϕ
HFCO (S_0)	The minimum at the singlet ground state					
CASSCF(18,13)	1.078	1.347	1.187	127.40	122.26	180.00
mrci (18,12)	1.075	1.373	1.190	127.68	122.48	180.00
mrci (12,9)	1.086	1.354	1.183	128.13	122.72	180.00
mrci (8,7)	1.088	1.348	1.184	128.03	122.76	180.00
Ref:[194]/A	1.091	1.330	1.187	128.00	122.80	180.00
Expt.[185,186,213]	1.09	1.34	1.18	127.3	122.8	180.00
HFCO ($TSD1_{T_1}$)	HCO + F dissociation transiton state on T_1 surface					
CASSCF(8,7)[a]	1.096	1.739	1.230	122.60	95.10	109.20
CASSCF(8,7)[b]	1.087	1.749	1.220	123.00	95.10	108.40
UMP2[b]	1.103	1.764	1.200	125.40	86.40	100.80
CASSCF(18,12)	1.083	1.772	1.239	121.82	96.80	108.19
CASSCF(8,7)	1.085	1.837	1.210	123.55	94.11	106.47
CASSCF(12,9)	1.083	1.764	1.240	121.71	96.50	108.51
HFCO ($TSD2_{T_1}$)	FCO + H dissociation transition state on T_1 surface					
CASSCF(8,7)[a]	1.542	1.312	1.239	97.30	122.40	110.90
CASSCF(8,7)[b]	1.531	1.302	1.235	97.00	122.90	111.00
UMP2[b]	1.452	1.339	1.202	89.40	128.20	102.30
CASSCF(18,12)	1.531	1.302	1.234	97.03	122.86	110.99
CASSCF(12,9)	1.531	1.303	1.234	97.13	122.89	110.84
CASSCF(8,7)	1.528	1.301	1.235	96.88	123.19	111.03
HFCO ($TSD1_{S_1}$)	HCO + F dissociation transition state on S_1 surface					
CASSCF(8,7)[a]	1.089	1.732	1.238	125.90	97.00	103.20
CASSCF(8,7)[b]	1.087	1.743	1.229	126.40	96.60	102.00
CASSCF(18,12)	1.076	1.786	1.248	125.95	96.28	99.43
CASSCF(12,9)	1.076	1.784	1.249	125.32	96.87	100.46
CASSCF(8,7)	1.077	1.874	1.216	126.63	94.37	95.34

[a] CASSCF (8,7)/cc-pVDZ results from 194; [b] CASSCF (8,7)/cc-pVTZ results from 194.

Table E5: *Selected vibrational energies (in cm^{-1}) of first 30 states for S_1 excited state 80 NN fit NN-expnn PES of HFCO. See Section 6.3.5 for details of assignment procedure.*

Assignment ($\nu_1\nu_2\nu_3\nu_4\nu_5\nu_6$)	EOM-CCSD-MCTDH	Assignment ($\nu_1\nu_2\nu_3\nu_4\nu_5\nu_6$)	EOM-CCSD-MCTDH
0 0 0 0 1 0	454.6	0 0 0 0 1 2	2022.3
0 0 0 0 0 1	876.9	0 0 0 0 3 1	2060.6
0 0 0 0 2 0	916.1	0 2 0 0 0 0	2091.8
0 1 0 0 0 0	1125.7	0 0 0 0 5 0	2118.3
0 0 1 0 0 0	1187.4	0 0 2 0 0 0	2222.2
0 0 0 0 1 1	1331.2	0 1 0 0 1 1	2225.6
0 0 0 1 0 0	1345.2	0 1 0 0 3 0	2231.3
0 0 0 0 3 0	1411.0	0 0 1 0 1 1	2244.8
0 1 0 0 1 0	1592.8	0 0 1 0 3 0	2282.9
0 0 1 0 1 0	1637.8	0 0 0 0 0 3	2304.9
0 0 0 0 0 2	1664.5	0 0 0 0 2 2	2367.7
0 0 0 0 2 1	1777.9	0 0 0 2 0 0	2446.9
0 0 0 0 4 0	1793.1	0 0 0 0 4 1	2456.5
0 1 0 0 2 0	1822.9	0 2 0 0 1 0	2461.8
0 0 1 0 2 0	2000.4	0 0 2 0 1 0	2474.8

E.1 10000 cm^{-1} cut 80 NN fit PES operator file for the S_1 state of HFCO

The operator file structure is exactly same as the Appendix B. Only the fitting parameters are given here.

PARAMETER-SECTION

, a11 = -1.02917 , a12 = 2.05681 , a21 = -1.15394 , a22 = 2.52932 , a31 = -1.04952 , a32 = 2.5215 , mh = 1.0, H-mass , mc = 12.00,AMU , mo = 15.9949146221,AMU , mf = 18.99840320,AMU , M11 = 1.0/mh+1.0/mc , M22 = 1.0/mf+1.0/mc , M33 = 1.0/mo+1.0/mc , Mu = 1.0/mc # Mu = Mij; i neq j , R1eq = 2.0570d0 , R2eq = 2.53050d0 , R3eq = 2.52140d0 , U1eq = 0.89187640d0 , U2eq = 0.94093980d0 , E1eq = -0.4522790d0 , E2eq = -0.33857370d0 , r0 = 3.55420057021d-07 , w0u0 = 1.171156666982833 , w0u1 = -1.099094250794489 , w0u2 = -0.299296758083863 , w0u3 = 1.629189842813214 , w0u4 = 1.700425983652629 , w0u5 = 5.192321482065484 , r1 = 0.000268488901303 , w1u0 = -0.026238641062026 , w1u1 = 0.653819993913979 , w1u2 = 0.265365515066824 , w1u3 = 0.068210259361839 , w1u4 = 0.669286173611580 , w1u5 = 1.710309813270403 , r2 = 0.000145995289083 , w2u0 = 2.413443774422379 , w2u1 = -2.070855939004337 , w2u2 = -1.822597474374239 , w2u3 = -1.087531212488764 , w2u4 = 1.216221746221809 , w2u5 = 3.373787800041887 , r3 = -16.2685106239 , w3u0 = -1.249943974805711 , w3u1 = 0.273739418113034 , w3u2 = -1.735327823669221 , w3u3 = -0.242269254407064 , w3u4 = 1.962769801495739 , w3u5 = -0.655605049991432 , r4 = -102.285026975 , w4u0 = 0.143101737332200 , w4u1 = -1.274327872276258 , w4u2 = 0.043276733161153 , w4u3 = -1.003571441183166 , w4u4 = -0.796218921195865 , w4u5 = -2.042976521318406 , r5 = 0.0345692079037 , w5u0 = -3.528401290726351 , w5u1 = 1.425130181267610 , w5u2 = 0.741448966316332 , w5u3 = 1.347547151510961 , w5u4 = -0.525524859200215 , w5u5 = 0.054424004259404 , r6 = -0.0141887552846 , w6u0 = 0.213339113636840 , w6u1 = 0.213923348181382 , w6u2 = -0.255452637186345 , w6u3 = -2.500317919760658 , w6u4 = 0.725264452325959 , w6u5 = 0.260228772860919 , r7 = -2.89686352613 , w7u0 = -0.027905438513155 , w7u1 = -0.136875667592787 , w7u2 = -0.283463862423174 , w7u3 = -0.037427199345287 , w7u4 = 0.108497129508539 , w7u5 = 0.075183505365319 , r8 = 0.045837723141 , w8u0 = 0.175820726916132 , w8u1 = 0.082648398691942 , w8u2 = -0.258244315902518 , w8u3 = -2.381964287474481 , w8u4 = 0.485966088949358 , w8u5 = 0.074653398725381 , r9 = -0.00925306725576 , w9u0 = -0.159732671288696 , w9u1 = 0.993982046526610 , w9u2 = -0.176355751591068 , w9u3 = -1.429543646510991 , w9u4 = -0.017887323697675 , w9u5 = -0.494462347857475 , r10 = 0.774947089855 , w10u0 = -0.023855080928849 , w10u1 = -0.077807923040876 , w10u2 = -0.768597251248800 , w10u3 = 2.432008739884567 , w10u4 = 0.013038295087428 , w10u5 = 0.428783012781158 , r11 = -0.395147511801 , w11u0 = 1.617349238871167 , w11u1 = -0.264929576787361 , w11u2 = -1.062895656924539 , w11u3 = 2.251160100438413 , w11u4 = 3.139614568876533 , w11u5 = 1.784041290255702 , r12 = -4.20365148106 , w12u0 = 1.681580561792374 , w12u1 = 0.020408668035945 , w12u2 = -1.406332347060500 , w12u3 = 2.833938830950114 , w12u4 = 3.825017232128297 , w12u5 = 0.256473806379301 , r13 = -0.00817625729811 , w13u0 = 0.791113827579508 , w13u1 = 0.150435378578124 , w13u2 = -0.038453743320958 , w13u3 = -0.570645227900161 , w13u4 = 0.229807798606093 , w13u5 = 0.046748805008813 , r14 = -2.20851724781d-05 , w14u0 = 2.516023767312669 , w14u1 = -0.216220407944076 , w14u2 = -0.121687069365532 , w14u3 = 3.069022289431679 , w14u4 = 3.666764374368822 , w14u5 = 0.815019701368257 , r15 = 859.355241707 , w15u0 = 0.194070056821249 , w15u1 = 0.259807081011087 , w15u2 = -3.384074761380140 , w15u3 = 0.705014445365372 , w15u4 = -3.822884538368623 , w15u5 = -1.322325271069581 , r16 = 0.464978244643 , w16u0 = -0.360155154849525 , w16u1 = -1.399554337677334 , w16u2 = 0.364179834864968 , w16u3 = -5.089749932794002 , w16u4 = -2.923864676882602 , w16u5 = -1.378785370918360 , r17 = -18.1018316403 , w17u0 = 0.445378696638515 , w17u1 = -1.789423961540532 , w17u2 = -0.646658326228650 , w17u3 = 1.284822464845653 , w17u4 = 2.960322724483682 , w17u5 = -0.218096176505548 , r18 = -1.26415578474d-06 , w18u0 = 0.189844551417092

, w18u1 = -0.138020724126611 , w18u2 = -0.344663490520063 , w18u3 = -1.323001913758728 , w18u4 = 0.318791173009525 , w18u5 = 3.794002374620306 , r19 = -20.0008817846 , w19u0 = -0.008666612383633 , w19u1 = -0.638730910367066 , w19u2 = -0.450492840832808 , w19u3 = 1.332043381176530 , w19u4 = 1.713996742658584 , w19u5 = -0.373264985937916 , r20 = -1.69789482032 , w20u0 = 0.383133871392605 , w20u1 = 0.015347897087061 , w20u2 = -2.302005222378397 , w20u3 = 2.258847893360300 , w20u4 = -0.204158996903534 , w20u5 = 0.835244067404298 , r21 = 0.384017093505 , w21u0 = 0.171086130970682 , w21u1 = 0.117975254904918 , w21u2 = 0.012538692313811 , w21u3 = -0.098574342062176 , w21u4 = 0.047873685274962 , w21u5 = 0.020125416600241 , r22 = 0.0787880520089 , w22u0 = 1.550880961081798 , w22u1 = -0.375530640951121 , w22u2 = -0.927842099064458 , w22u3 = 2.008520340008002 , w22u4 = 2.865152210025270 , w22u5 = 2.420266739322893 , r23 = 88.4077303872 , w23u0 = 0.043164876043188 , w23u1 = -2.812997139678137 , w23u2 = 0.000899626043813 , w23u3 = 0.261917102523249 , w23u4 = 0.063491705421291 , w23u5 = 0.033646632621666 , r24 = 83.0840659929 , w24u0 = -0.095902121388073 , w24u1 = 0.021647048291347 , w24u2 = -2.759567053856676 , w24u3 = -0.111774438918134 , w24u4 = -0.125934278184276 , w24u5 = -0.025410207737020 , r25 = 0.0978453575197 , w25u0 = 0.227131481116360 , w25u1 = -0.188938661636874 , w25u2 = -0.583989672828324 , w25u3 = 0.307803787568596 , w25u4 = 0.486433315321691 , w25u5 = 1.109821017846900 , r26 = -1.74305265946d-05 , w26u0 = 1.282823401435111 , w26u1 = -0.865609011098150 , w26u2 = -0.455951192551653 , w26u3 = 1.545205174831154 , w26u4 = 2.022700924773130 , w26u5 = 4.471709053136204 , r27 = -2.6421398437d-05 , w27u0 = 0.017407487169398 , w27u1 = 0.317476283497371 , w27u2 = 0.305268552305961 , w27u3 = 0.095006445966786 , w27u4 = 0.523027595566540 , w27u5 = 2.616423901372888 , r28 = -210.971260264 , w28u0 = -0.165263198261548 , w28u1 = -1.146401256502281 , w28u2 = 0.070882129322945 , w28u3 = -1.228952275688558 , w28u4 = -1.039116651352781 , w28u5 = -2.398502996627870 , r29 = -0.0255407682085 , w29u0 = -1.160045828985586 , w29u1 = -0.659401130410642 , w29u2 = -0.523603803711810 , w29u3 = -2.661474216225630 , w29u4 = -9.886691750140885 , w29u5 = -2.971153112533248 , r30 = -0.0168125160283 , w30u0 = -1.246485138475861 , w30u1 = 1.017831868166547 , w30u2 = -3.086972470344355 , w30u3 = -3.349372171643084 , w30u4 = -4.227043136038438 , w30u5 = 0.394889104578549 , r31 = 2.63749341372 , w31u0 = -1.508726798661946 , w31u1 = -0.320041654918139 , w31u2 = 0.139307877166800 , w31u3 = -0.532148534749809 , w31u4 = 0.620808028577890 , w31u5 = -0.530400990769081 , r32 = 62.5162615994 , w32u0 = 0.328359883553525 , w32u1 = -0.128228997528182 , w32u2 = -3.133806345277390 , w32u3 = 0.927098864772183 , w32u4 = 0.919598565019283 , w32u5 = -0.504669666075170 , r33 = -0.0719322621191 , w33u0 = 0.274809816131287 , w33u1 = -0.512128060357561 , w33u2 = -1.104723805124439 , w33u3 = 1.494170069693616 , w33u4 = 0.410324821805319 , w33u5 = 1.392674787384642 , r34 = -0.00942804949407 , w34u0 = 1.474103316838892 , w34u1 = -0.495948312237105 , w34u2 = -0.789158585933010 , w34u3 = 1.792539091490017 , w34u4 = 2.602997318279916 , w34u5 = 3.047005339073372 , r35 = -1.87408969352d-06 , w35u0 = 0.716522201031320 , w35u1 = -0.698296528003879 , w35u2 = -0.411543420915645 , w35u3 = -1.031047960123738 , w35u4 = 0.856960908280349 , w35u5 = 3.737185019577849 , r36 = 1.73770321135 , w36u0 = 0.421285282611504 , w36u1 = -0.031089974053124 , w36u2 = -2.466191601532332 , w36u3 = 2.156647504505738 , w36u4 = 0.085301891112349 , w36u5 = 0.945154335369147 , r37 = 9.42376598363d-07 , w37u0 = 0.036020032487762 , w37u1 = 0.128741171491332 , w37u2 = 0.343974361128390 , w37u3 = -0.051870278955370 , w37u4 = 0.189035099123102 , w37u5 = 3.352607936513188 , r38 = -0.202329388784 , w38u0 = -0.175131616252240 , w38u1 = -0.067661788615826 , w38u2 = -0.658089028073966 , w38u3 = 3.229904048316191 , w38u4 = -0.068604713259307 , w38u5 = 0.444271565074747 , r39 = -27.2262624039 , w39u0 = 1.290539453381701 , w39u1 = 0.417622481103595 , w39u2 = -1.853729362389350 , w39u3 = 3.142287141819980 , w39u4 = 4.247125342121761 , w39u5 = -1.338122338383461 , r40 = 6.06565889874d-05 , w40u0 = -0.356739851924167 , w40u1 = -0.718895846391489 , w40u2 = 0.011436032503426 , w40u3 = -1.296836126060803 , w40u4 = -8.705209970969264 , w40u5 = 0.011661557249701 , r41 = -1.88605543016 , w41u0 = -0.737235745529193 , w41u1 = -0.632319241554324 , w41u2 = 0.350859159765471 , w41u3 = -0.533028599702045 , w41u4 = 0.275308841028644 , w41u5 = -0.626898283414772 , r42 = 0.0032801511183 , w42u0 = -0.153896127469758 , w42u1 = 0.085758726422497 , w42u2 = -1.075955498540534 , w42u3 = 1.387548173902996 , w42u4 = -2.726076766481954 , w42u5 = 1.535934711709153 , r43 = -52.2829924163 , w43u0 = 0.278424270104819 , w43u1 = 0.069746992880547 , w43u2 = -2.063440458468953 , w43u3 = 0.829186148005168 , w43u4 = 5.489996132621749 , w43u5 = -0.696086406491536 , r44 = 1.35158007085 , w44u0 = 1.670005163365882 , w44u1 = -0.144265365169987 , w44u2 = -1.210793619252976 , w44u3 = 2.524941188071885 , w44u4 = 3.450433384216361 , w44u5 = 1.090077825917100 , r45 = 29.3718699407 , w45u0 = 0.124029093305129 , w45u1 = -1.443237770331561 , w45u2 = 0.000142660829358 , w45u3 = 0.860051663031763 , w45u4 = 0.516370524882737 , w45u5 = -0.594233485218134 , r46 = -0.158846632236 , w46u0 = 0.036259021528496 , w46u1 = -1.022049295401776 , w46u2 = -0.304790535175516 , w46u3 = -1.940500786749442 , w46u4 = -2.522539000148388 , w46u5 = -0.137425458272470 , r47 = -0.000151392397125 , w47u0 = 2.469178265674428 , w47u1 = -2.098194001157384 , w47u2 = -1.863692926987774 , w47u3 = -1.069154722064659 , w47u4 = 1.203094874721098 , w47u5 = 3.349836830452504 , r48 = 0.000585572631915 , w48u0 = 1.385324023324369 , w48u1 = -0.649684413771371 , w48u2 = -0.633107569958711 , w48u3 = 1.617236766169625 , w48u4 = 2.329139568682493 , w48u5 = 3.716316428590288 , r49 = 12.7686345859 , w49u0 = 0.258051196166153 , w49u1 = -0.568313683238482 , w49u2 = -1.590247034042726 , w49u3 = 0.359021653383828 , w49u4 = 5.269992469834441 , w49u5 = -0.203559666537561 , r50 = -0.00120439526935 , w50u0 = 0.184632923468849 , w50u1 = -0.170168583064895 , w50u2 = -0.480434396416797 , w50u3 = -0.656241740312302 , w50u4 = 0.542502376969987 , w50u5 = 2.270702731215742 , r51 = 0.0158692264252 , w51u0 = -0.191173769357014 , w51u1 = -0.988146477963124 , w51u2 = -0.269748430142647 , w51u3 = -2.605323181965038 , w51u4 = -2.683599695188490 , w51u5 = 0.442675074826798 , r52 = 486.775797863 , w52u0 = -0.049011466705645 , w52u1 = -1.193369083165663 , w52u2 = 0.071926610412018 , w52u3 = -0.927130200993672 , w52u4 = -1.108675270090148 , w52u5 = -2.216980796525117 , r53 = 2.25750378047d-06 , w53u0 = -0.039811148297532 , w53u1 = -1.047139970812603 , w53u2 = 0.029824632534913 , w53u3 = -11.179585764301164 , w53u4 = -1.470158012106983 , w53u5 = 0.225359265647942 , r54 = -0.000458291361587 , w54u0 = -0.010430799768616 , w54u1 = 1.027072165347232 , w54u2 = 0.213807628598379 , w54u3 = -0.557899336476453 , w54u4 = 0.752969647295462 , w54u5 = 0.961552008451534 , r55 = 0.443039464606 , w55u0 = 1.036822182268231 , w55u1 = -0.933627749142066 , w55u2 = -0.449056185454432 , w55u3 = -0.115111528763321 , w55u4 = -0.368083928045229 , w55u5 = -1.023338546002750 , r56 = -24.4097346861 , w56u0 = 0.483611416467720 , w56u1 = -0.668030613292850 , w56u2 = -0.921591644726321 , w56u3 = 1.565109452422065 , w56u4 = 1.728041607852819 , w56u5 = -0.295424399695306 , r57 = 0.000969764772141 , w57u0 = -0.158609506942595 , w57u1 = 1.262768871053726 , w57u2 = -0.005300647727663 , w57u3 = -1.203899020384625 , w57u4 = 0.598616691513922 , w57u5 = 0.261437430166769 , r58 = 40.2907155695 , w58u0 = -0.138503656993572 , w58u1 = -2.259254550555071 , w58u2 = -0.277723433059147 , w58u3 = -0.519871128458581 , w58u4 = 0.151208826140915 , w58u5 = -0.282172640744977 , r59 = -885.888577215 , w59u0 = 0.195977016598176 , w59u1 = 0.249061374131947 , w59u2 = -3.366034837158871 , w59u3 = 0.683127693267584 , w59u4 = -3.795421666172456 , w59u5 = -1.329207804034171 , r60 = 12.4848776895 , w60u0 = -2.900917698831391 , w60u1 = 0.084521348214542 , w60u2 = 0.021967315137997 , w60u3 = 0.077063117514900 , w60u4 = -0.004360094467221 , w60u5 = 0.042951582135449 , r61 = -0.0806723574819 , w61u0 = -3.395982656507708 , w61u1 = 1.238820782035821 , w61u2 = 0.614144621369395 , w61u3 = 1.153647907607316 , w61u4 = -0.360232884491086 , w61u5 = 0.110569620791515 , r62 = -7.59254214055d-05 , w62u0 = 0.358380155310094 , w62u1 = -0.364877398419629 , w62u2 = 2.012202343401440 , w62u3 = 0.408653341254073 , w62u4 = -0.016511016616444 , w62u5 = 0.162256516895884 , r63 = -0.398206375634 , w63u0 = -0.363884460552878 , w63u1 = -1.412345992782474 , w63u2 = 0.383988440878303 , w63u3 = -5.314807024829985 , w63u4 = -2.947262708894936 , w63u5 = -1.460740181772298 , r64 = 1.42663263585 , w64u0 = 0.350611805932449 , w64u1 = -0.855141918286774 , w64u2 = -0.844618832442666 , w64u3 = -0.809908676803381 , w64u4 = -3.382813629833590 , w64u5 = -0.254881598044187 , r65 = 80.6381176153 , w65u0 = 0.215129790234729 , w65u1 = 0.241114612092929 , w65u2 = -2.356025781938511 , w65u3 = 0.973149813181353 , w65u4 = 5.963303334126470 , w65u5 = -0.979981315952972 , r66 = 0.000137235310169 ,

w66u0 = 0.429093897140132 , w66u1 = -0.514965299137968 , w66u2 = 1.717870518004942 , w66u3 = 0.744833828623217 , w66u4 = 0.174739202906955 , w66u5 = 0.442559196567081 , r67 = -0.249827081841 , w67u0 = 0.139538355117664 , w67u1 = 1.422024855707526 , w67u2 = -2.827792395992360 , w67u3 = -0.466334043267081 , w67u4 = 0.303737324487712 , w67u5 = -0.245859191910363 , r68 = -169.993011768 , w68u0 = -0.028367417364525 , w68u1 = -1.208327031749608 , w68u2 = 0.085601541995079 , w68u3 = -0.622991872123809 , w68u4 = -1.422664834955042 , w68u5 = -2.197961136038069 , r69 = 58.8792500161 , w69u0 = 0.277854417060480 , w69u1 = -1.136487866719021 , w69u2 = -0.601521759157689 , w69u3 = 1.217306859225153 , w69u4 = 1.527257696966378 , w69u5 = -0.174488167334597 , r70 = -2.86191326596d-07 , w70u0 = 1.121418571091532 , w70u1 = -1.601810793265924 , w70u2 = 0.009830214692608 , w70u3 = -7.606406214300840 , w70u4 = -2.244711517747978 , w70u5 = 1.127421920293229 , r71 = -1.1392881138 , w71u0 = 0.439013165929856 , w71u1 = -0.876793314583145 , w71u2 = -0.978300712417195 , w71u3 = -0.814034289083154 , w71u4 = -3.561495319708979 , w71u5 = -0.237618096675690 , r72 = 13.7267389737 , w72u0 = 1.573525065909979 , w72u1 = 0.230839683737639 , w72u2 = -1.646815261663597 , w72u3 = 3.080335068960788 , w72u4 = 4.162950985780570 , w72u5 = -0.641133634531616 , r73 = 4.87913642217d-05 , w73u0 = 0.225382142475718 , w73u1 = -0.207849358865932 , w73u2 = -0.385308248740076 , w73u3 = -1.092578037680616 , w73u4 = 0.512592053309786 , w73u5 = 3.152384750458141 , r74 = -51.395369559 , w74u0 = 0.162936178873633 , w74u1 = -1.640149559405016 , w74u2 = -0.099784991996545 , w74u3 = 0.748756369626001 , w74u4 = 0.539915352725742 , w74u5 = -0.241971410269628 , r75 = 26.2553824806 , w75u0 = 0.280998863144045 , w75u1 = -0.162294790644787 , w75u2 = -1.079605181464803 , w75u3 = 1.925790930303141 , w75u4 = 2.294567729044204 , w75u5 = -0.821800825219680 , r76 = -0.00848668195271 , w76u0 = 0.166327175489812 , w76u1 = 0.369107740371492 , w76u2 = -0.300661930558245 , w76u3 = 1.084015521399461 , w76u4 = 0.310937532127148 , w76u5 = 0.926421390002950 , r77 = -0.00574769018717 , w77u0 = -0.159614552910174 , w77u1 = -0.030439634025100 , w77u2 = -0.931496340603121 , w77u3 = 1.290869091944860 , w77u4 = -2.757881922574533 , w77u5 = 1.348223031286090 , r78 = 5.73933095597d-05 , w78u0 = 0.605613429872508 , w78u1 = 0.810359167475118 , w78u2 = -0.022376208106600 , w78u3 = -1.460670759454577 , w78u4 = 1.202595730149319 , w78u5 = 0.958758827609009 , r79 = 3.54701191404 , w79u0 = -0.090406804443713 , w79u1 = -0.485789812050632 , w79u2 = -0.291023169422437 , w79u3 = 0.650332579265194 , w79u4 = 1.613378317275738 , w79u5 = -0.196801249137671 , c = 0.005883354

end-parameter-section

Label section is exactly same as Appendix B

HAMILTONIAN-SECTION is also same as Appendix B

HAMILTONIAN-SECTION_r1i usediag ———————— modes | rch ———————— -M11/2.0 | dq2̂ 0.164216 | rq12̂ ———————— end-hamiltonian-section HAMILTONIAN-SECTION_r2i usediag ———————— modes | rcf ———————— -M22/2.0 | dq2̂ 0.157972 | rq22̂ ———————— end-hamiltonian-section HAMILTONIAN-SECTION_r3i usediag ———————— modes | rco ———————— -M33/2.0 | dq2̂ 0.204523 | rq32̂ ———————— end-hamiltonian-section HAMILTONIAN-SECTION_theta1 usediag ———————— modes | ohco ———————— coeff3 | dq*q*qs12̂*dq coeff4 | q coeff5 | dq*qs12̂*dq 0.0261503 | 1 0.123836 | q 0.192181 | q2̂ 0.160517 | q3̂ 0.129113 | q4̂ ———————— end-hamiltonian-section HAMILTONIAN-SECTION_theta2 usediag ———————— modes | ofco ———————— coef17 | 1 coef16 | qs1 coef15 | q coeff6 | dq*q*qs12̂*dq coeff7 | q coeff8 | dq*qs12̂*dq 0.0211551 | 1 0.140332 | q 0.29972 | q2̂ 0.273869 | q3̂ 0.202697 | q4̂ ———————— end-hamiltonian-section HAMILTONIAN-SECTION_phii usediag ———————— modes | phi ————————- coeff1 | dq2̂ coeff2 | dq*cos*dq 0.608371 | 1 -0.601016 | q 0.15261 | q2̂ 0.00866992 | q3̂ -0.0049585 | q4̂ ————————- end-hamiltonian-section end-operator

Bibliography

[1] Manzhos, S.; Carrington, T. *J. Chem. Phys.* **2006**, *125*, 194105.

[2] Manzhos, S.; Carrington, T. *J. Chem. Phys.* **2008**, *129*, 224104.

[3] Worth, G. A.; Beck, M. H.; Jäckle, A.; Meyer, H. D. The Heidelberg MCTDH Software package, Version 8.3.17 and 8.4.6. 2010; see http://mctdh.uni-hd.de.

[4] Beck, M. H.; Jäckle, A.; Worth, G. A.; Meyer, H. D. *Phys. Rep.* **2000**, *324*, 1–105.

[5] Meyer, H. D.; Manthe, U.; Cederbaum, L. S. *Chem. Phys. Lett.* **1990**, *165*, 73–78.

[6] Manthe, U.; Meyer, H. D.; Cederbaum, L. S. *J. Chem. Phys.* **1992**, *97*, 3199–3213.

[7] Meyer, H. D.; Worth, G. A. *Theor. Chem. Acc.* **2003**, *109*, 251–267.

[8] Pradhan, E.; Carren-Macedo, J. L.; Cuervo, J. E.; Schröder, M.; Brown, A. *J. Phys. Chem. A* **2013**, *117*, 6925–6931.

[9] Bowman, J. M.; Carrington, T.; Meyer, H. D. *Mol. Phys.* **2008**, *106*, 2145–2182.

[10] Hartree, D. R. *Proc. Cambridge Phil. Soc.* **1928**, *24*, 89–110.

[11] Fock, V. *Z. Angew. Phys.* **1930**, *61*, 126–148.

[12] Møller, C.; Plesset, M. S. *Phys. Rev.* **1934**, *46*, 618–622.

[13] Hampel, C.; Peterson, K. A.; Werner, H. J. *Chem. Phys. Lett.* **1992**, *190*, 1 – 12.

[14] Deegan, M. J.; Knowles, P. J. *Chem. Phys. Lett.* **1994**, *227*, 321 – 326.

[15] Adler, T. B.; Knizia, G.; Werner, H. J. *J. Chem. Phys.* **2007**, *127*, 221106.

[16] Werner, H. J.; Knizia, G.; Manby, F. R. *Mol. Phys.* **2011**, *109*, 407–417.

[17] Korona, T.; Werner, H. J. *J. Chem. Phys.* **2003**, *118*, 3006–3019.

[18] Werner, H. J. et al. MOLPRO, version 2008.1, a package of ab initio programs. 2008; see http://www.molpro.net.

[19] Werner, H. J.; Knowles, P. J.; Knizia, G.; Manby, F. R.; Schtz, M. *WIREs Comput. Mol. Sci.* **2012**, *2*, 242–253.

[20] Roos, B. O.; Taylor, P. R.; Siegbahn, P. E. *Chem. Phys.* **1980**, *48*, 157 – 173.

[21] Siegbahn, P. E. M.; Almlöf, J.; Heiberg, A.; Roos, B. O. *J. Chem. Phys.* **1981**, *74*, 2384–2396.

[22] Siegbahn, P.; Heiberg, A.; Roos, B.; Levy, B. *Phys. Scr.* **1980**, *21*, 323–327.

[23] Werner, H. J.; Knowles, P. J. *J. Chem. Phys.* **1985**, *82*, 5053–5063.

[24] Knowles, P. J.; Werner, H. J. *Chem. Phys. Lett.* **1985**, *115*, 259–267.

[25] Werner, H. J.; Knowles, P. J. *J. Chem. Phys.* **1988**, *89*, 5803–5814.

[26] Knowles, P. J.; Werner, H. J. *Chem. Phys. Lett.* **1988**, *145*, 514–522.

[27] Shamasundar, K. R.; Knizia, G.; Werner, H. J. *J. Chem. Phys.* **2011**, *135*, 054101.

[28] Werner, H. J.; Reinsch, E. A. *J. Chem. Phys.* **1982**, *76*, 3144–3156.

[29] Knowles, P.; Werner, H. J. *Theor. Chim. Acta* **1992**, *84*, 95–103.

[30] Paldus, J. *J. Chem. Phys.* **1974**, *61*, 5321–5330.

[31] Shavitt, I. *Chem. Phys. Lett.* **1979**, *63*, 421 – 427.

[32] Brooks, B. R.; Schaefer, H. F. *J. Chem. Phys.* **1979**, *70*, 5092–5106.

[33] Tavan, P.; Schulten, K. *J. Chem. Phys.* **1980**, *72*, 3547–3576.

[34] Liu, B.; Yoshimine, M. *J. Chem. Phys.* **1981**, *74*, 612–616.

[35] Taylor, P. R. *J. Chem. Phys.* **1981**, *74*, 1256–1270.

[36] Malmqvist, P.; Rendell, A.; Roos, B. O. *J. Phys. Chem.* **1990**, *94*, 5477–5482.

[37] Andersson, K.; Malmqvist, P. A.; Roos, B. O. *J. Chem. Phys.* **1992**, *96*, 1218–1226.

[38] Werner, H. J. *Mol. Phys.* **1996**, *89*, 645–661.

[39] Celani, P.; Werner, H. J. *J. Chem. Phys.* **2000**, *112*, 5546–5557.

[40] Shiozaki, T.; Gyrffy, W.; Celani, P.; Werner, H. J. *J. Chem. Phys.* **2011**, *135*, 081106.

[41] Shiozaki, T.; Werner, H. J. *J. Chem. Phys.* **2010**, *133*, 141103.

[42] Shiozaki, T.; Knizia, G.; Werner, H. J. *J. Chem. Phys.* **2011**, *134*, 034113.

[43] Shiozaki, T.; Werner, H. J. *J. Chem. Phys.* **2011**, *134*, 184104.

[44] Shiozaki, T.; Werner, H. J. *Mol. Phys.* **2013**, *111*, 607–630.

[45] Dunning Jr., T. H. *J. Chem. Phys.* **1990**, *90*, 1007–1023.

[46] Kendall, R. A.; Dunning Jr., T. H.; Harrison, R. J. *J. Chem. Phys.* **1992**, *96*, 6796–6806.

[47] Peterson, K. A.; Adler, T. B.; Werner, H. J. *J. Chem. Phys.* **2008**, *128*, 084102.

[48] Hill, J. G.; Peterson, K. A. *Phys. Chem. Chem. Phys.* **2010**, *12*, 10460–10468.

[49] Hill, J. G.; Peterson, K. A. *J. Chem. Phys.* **2014**, *141*, 094106.

[50] Feller, D. *J. Chem. Phys.* **1992**, *96*, 6104–6114.

[51] Peterson, K. A.; Dunning, T. H. *J. Phys. Chem.* **1995**, *99*, 3898–3901.

[52] Peterson, K. A.; Kendall, R. A.; Dunning, T. H. *J. Chem. Phys.* **1993**, *99*, 9790–9805.

[53] Morse, P. M. *Phys. Rev.* **1929**, *34*, 57–64.

[54] Manzhos, S.; Carrington, T. *Can. J. Chem.* **2009**, *87*, 864–871.

[55] Kauppi, E. *J. Chem. Phys.* **1996**, *105*, 7986–7994.

[56] Car, R.; Parrinello, M. *Phys. Rev. Lett.* **1985**, *55*, 2471–2474.

[57] Truhlar, D. G.; Steckler, R.; Gordon, M. S. *Chem. Rev.* **1987**, *87*, 217–236.

[58] Schatz, G. C. *Rev. Mod. Phys.* **1989**, *61*, 669–688.

[59] Kuhn, B.; Rizzo, T. R.; Luckhaus, D.; Quack, M.; Suhm, M. A. *J. Chem. Phys.* **1999**, *111*, 2565–2587.

[60] Marquardt, R.; Sagui, K.; Zheng, J.; Thiel, W.; Luckhaus, D.; Yurchenko, S.; Mariotti, F.; Quack, M. *J. Phys. Chem. A* **2013**, *117*, 7502–7522.

[61] Press, W. H.; Teukolsky, S. A.; Vetterling, W. T.; Flannery, B. P. *Numerical Recipes - The art of Scientific Computing*; Cambridge University Press, Cambridge, 2007.

[62] de Boor, C. *A Practical Guide to Splines*; Springer, Berlin, 2001.

[63] Maisuradze, G. G.; Thompson, D. L.; Wagner, A. F.; Minkoff, M. *J. Chem. Phys.* **2003**, *119*, 10002–10014.

[64] Dawes, R.; Thompson, D. L.; Guo, Y.; Wagner, A. F.; Minkoff, M. *J. Chem. Phys.* **2007**, *126*, 184108.

[65] Ischtwan, J.; Collins, M. A. *J. Chem. Phys.* **1994**, *100*, 8080–8088.

[66] Jordan, M. J. T.; Thompson, K. C.; Collins, M. A. *J. Chem. Phys.* **1995**, *102*, 5647–5657.

[67] Makarov, D. E.; Metiu, H. *J. Chem. Phys.* **1998**, *108*, 590–598.

[68] Bartok, A. P.; Payne, M. C.; Kondor, R.; Csanyi, G. *Phys. Rev. Lett.* **2010**, *104*, 136403.

[69] Czako, G.; Shepler, B. C.; Braams, B. J.; Bowman, J. M. *J. Chem. Phys.* **2009**, *130*, 084301.

[70] Brown, A.; Braams, B. J.; Christoffel, K.; Jin, Z.; Bowman, J. M. *J. Chem. Phys.* **2003**, *119*, 8790–8793.

[71] Park, S. C.; Braams, B. J.; Bowman, J. M. *J. Theor. Comput. Chem.* **2005**, *4*, 163–173.

[72] Huang, X. C.; Braams, B. J.; Bowman, J. M. *J. Chem. Phys.* **2005**, *122*, 044308.

[73] Braams, B. J.; Bowman, J. M. *Int. Rev. Phys. Chem.* **2009**, *28*, 577–606.

[74] Jiang, B.; Guo, H. *J. Chem. Phys.* **2014**, *141*, 034109.

[75] Li, J.; Jiang, B.; Guo, H. *J. Chem. Phys.* **2013**, *139*, 204103.

[76] Jiang, B.; Guo, H. *J. Chem. Phys.* **2013**, *139*, 054112.

[77] Manzhos, S.; Wang, X.; Dawes, R.; Carrington, T. *J. Phys. Chem. A* **2006**, *110*, 5295–304.

[78] Manzhos, S.; Carrington, T. *J. Chem. Phys.* **2006**, *125*, 084109.

[79] Manzhos, S.; Carrington, T. *J. Chem. Phys.* **2007**, *127*, 014103.

[80] Malshe, M.; Raff, L. M.; Rockley, M. G.; Hagan, M.; Agrawal, P. M.; Komanduri, R. *J. Chem. Phys.* **2007**, *127*, 134105.

[81] Manzhos, S.; Yamashita, K.; Carrington Jr., T. *Comp. Phys. Comm.* **2009**, *180*, 2002–2012.

[82] Manzhos, S.; Yamashita, K. *Surf. Sci.* **2010**, *604*, 555–561.

[83] Handley, C. M.; Popelier, P. L. A. *J. Phys. Chem. A* **2010**, *114*, 3371–3383.

[84] Behler, J. *Phys. Chem. Chem. Phys.* **2011**, *13*, 17930–17955.

[85] Halverson, T.; Poirier, B. *J. Chem. Phys.* **2012**, *137*, 224101.

[86] Leclerc, A.; Carrington, T. *J. Chem. Phys.* **2014**, *140*, 174111.

[87] Jäckle, A.; Meyer, H. D. *J. Chem. Phys.* **1996**, *104*, 7974–7984.

[88] Jäckle, A.; Meyer, H. D. *J. Chem. Phys.* **1998**, *109*, 3772–3779.

[89] Kohonen, T. *Neural Networks* **1988**, *1*, 3–16.

[90] Sumpter, B. G.; Getino, C.; Noid, D. W. *Ann. Rev. Phys. Chem.* **1994**, *45*, 439–481.

[91] Zupan, J.; Gasteiger, J. *Anal. Chim. Acta* **1991**, *248*, 1–30.

[92] Spining, M. T.; Darsey, J. A.; Sumpter, B. G.; Noid, D. W. *J. Chem. Educ.* **1994**, *71*, 406–411.

[93] Thomsen, J. U.; Meyer, B. *J. Magn. Reson.* **1989**, *84*, 212–217.

[94] Curry, B.; Rumelhart, D. E. *Tetrahedron Comput. Methodol.* **1990**, *3*, 213 – 237.

[95] Holley, L. H.; Karplus, M. *Proc. Natl. Acad. Sci. U. S. A.* **1989**, *86*, 152–156.

[96] Rabow, A. A.; Scheraga, H. A. *J. Mol. Biol.* **1993**, *232*, 1157–1168.

[97] So, S. S.; Karplus, M. *J. Med. Chem.* **1996**, *39*, 1521–1530.

[98] Agrafiotis, D. K.; Cedeno, W.; Lobanov, V. S. *J. Chem. Inf. Comput. Sci.* **2002**, *42*, 903–911.

[99] Gasteiger, J.; Teckentrup, A.; Terfloth, L.; Spycher, S. *J. Phys. Org. Chem.* **2003**, *16*, 232–245.

[100] Reibnegger, G.; Weiss, G.; Wernerfelmayer, G.; Judmaier, G.; Wachter, H. *Proc. Natl. Acad. Sci. U. S. A.* **1991**, *88*, 11426–11430.

[101] Curteanu, S.; Petrila, C. *Int. J. Quantum Chem.* **2006**, *106*, 1445–1456.

[102] Gernoth, K. A.; Clark, J. W.; Prater, J. S.; Bohr, H. *Phys. Lett. B* **1993**, *300*, 1–7.

[103] Peterson, K. L. *Phys. Rev. A* **1990**, *41*, 2457–2461.

[104] Peterson, K. L. *Phys. Rev. a* **1991**, *44*, 126–138.

[105] Brunak, S.; Engelbrecht, J.; Knudsen, S. *Nature* **1990**, *343*, 123–123.

[106] Sugawara, M. *Comput. Phys. Commun.* **2001**, *140*, 366–380.

[107] Lagaris, I. E.; Likas, A.; Fotiadis, D. I. *Comput. Phys. Commun.* **1997**, *104*, 1–14.

[108] Darsey, J. A.; Noid, D. W.; Upadhyaya, B. R. *Chem. Phys. Lett.* **1991**, *177*, 189–194.

[109] Manzhos, S.; Yamashita, K.; Jr., T. C. *Chem. Phys. Lett.* **2009**, *474*, 217–221.

[110] Braunheim, B. B.; Bagdassarian, C. K.; Schramm, V. L.; Schwartz, S. D. *Int. J. Quantum Chem.* **2000**, *78*, 195–204.

[111] Silva, G. M. E.; Acioli, P. H.; Pedroza, A. C. *J. Comput. Chem.* **1997**, *18*, 1407–1414.

[112] Balabin, R. M.; Lomakina, E. I. *J. Chem. Phys.* **2009**, *131*, 074104.

[113] Munoz-Caro, C.; Nino, A. *Comput. Chem.* **1998**, *22*, 355–361.

[114] Koch, W.; Zhang, D. H. *J. Chem. Phys.* **2014**, *141*, 021101.

[115] Kalman, R. E. *J. Basis Eng.* **1960**, *82*, 35–45.

[116] Levenberg, K. *Q. Appl. Math.* **1944**, *2*, 164–168.

[117] Marquardt, D. W. *J. Soc. Ind. Appl. Math.* **1963**, *11*, 431 – 441.

[118] Schneider, W.; Thiel, W. *Chem. Phys. Lett.* **1989**, *157*, 367 – 373.

[119] Stanton, J. F.; Lopreore, C. L.; Gauss, J. *J. Chem. Phys.* **1998**, *108*, 7190–7196.

[120] Stanton, J. F.; Gauss, J. *Int. Rev. Phys. Chem.* **2000**, *19*, 61–95.

[121] Frisch, M. J. et al. Gaussian 09 Revision B.1. Gaussian Inc. Wallingford CT 2009.

[122] Schmidt, M. W.; Baldridge, K. K.; Boatz, J. A.; Elbert, S. T.; Gordon, M. S.; Jensen, J. H.; Koseki, S.; Matsunaga, N.; Nguyen, K. A.; Su, S.; Windus, T. L.; Dupuis, M.; Montgomery, J. A. *J. Comput. Chem.* **1993**, *14*, 1347–1363.

[123] Gordon, M. S.; Schmidt, M. W. In *Theory and Applications of Computational Chemistry: the first forty years*; Dykstra, C. E., Frenking, G., Kim, K. S., Scuseria, G. E., Eds.; Elsevier: Amsterdam, 2005; 1167–1189.

[124] Stanton, J. F.; Gauss, J.; Harding, M. E.; Szalay, P. G. CFOUR, Coupled-Cluster techniques for Computational Chemistry, a quantum-chemical program package. 2010; For the current version, see http://www.cfour.de.

[125] Meyer, H. D.; Qur, F. L.; Lonard, C.; Gatti, F. *Chem. Phys.* **2006**, *329*, 179 – 192.

[126] Pasin, G.; Gatti, F.; Iung, C.; Meyer, H. D. *J. Chem. Phys.* **2006**, *124*, 194304.

[127] Pasin, G.; Iung, C.; Gatti, F.; Meyer, H. D. *J. Chem. Phys.* **2007**, *126*, 024302.

[128] Pasin, G.; Iung, C.; Gatti, F.; Richter, F.; Léonard, C.; Meyer, H. D. *J. Chem. Phys.* **2008**, *129*, 144304.

[129] Richter, F.; Rosmus, P.; Gatti, F.; Meyer, H. D. *J. Chem. Phys.* **2004**, *120*, 6072–6084.

[130] Richter, F.; Gatti, F.; Lonard, C.; Le Qur, F.; Meyer, H. D. *J. Chem. Phys.* **2007**, *127*, 164315.

[131] Richter, F.; Hochlaf, M.; Rosmus, P.; Gatti, F.; Meyer, H. D. *J. Chem. Phys.* **2004**, *120*, 1306–1317.

[132] Yamamoto, T.; Kato, S. *J. Chem. Phys.* **1997**, *107*, 6114–6122.

[133] Choi, Y. S.; Moore, C. B. *J. Chem. Phys.* **1992**, *97*, 1010–1021.

[134] Scaria, A.; Konradi, J.; Namboodiri, V.; Materny, A. *J. Raman Spectrosc.* **2008**, *39*, 739–746.

[135] Schröeder, M.; Carreón-Macedo, J. L.; Brown, A. *Phys. Chem. Chem. Phys.* **2008**, *10*, 850–856.

[136] Schröeder, M.; Brown, A. *J. Chem. Phys.* **2009**, *131*, 034101.

[137] Kummli, D. S.; Frey, H. M.; Leutwyler, S. *J. Chem. Phys.* **2006**, *124*, 144307.

[138] Kolbuszewski, M.; Bunker, P. R.; Jensen, P. *J. Mol. Spectrosc.* **1994**, *170*, 158–165.

[139] Smith Jr., D. F.; Overend, J. *J. Chem. Phys.* **1971**, *54*, 3632–3639.

[140] Maki, A. G. *J. Mol. Spectrosc.* **1973**, *47*, 217–225.

[141] Blanquet, G.; Baeten, E.; Cauuet, I.; Walrand, J.; Courtoy, C. *J. Mol. Spectrosc.* **1985**, *112*, 55–70.

[142] Desiderio, R. A.; Gerrity, D. P.; Hudson, B. S. *Chem. Phys. Lett.* **1985**, *115*, 29–33.

[143] Suzuki, I. *Bull. Chem. Soc. Jpn.* **1975**, *48*, 1685–1690.

[144] Lindenmayer, J.; Jones, H. *J. Mol. Spectrosc.* **1985**, *110*, 65–73.

[145] Walrand, J.; Humblet, V.; Blanquet, G. *J. Mol. Spectrosc.* **1988**, *127*, 304–323.

[146] Zhou, C.; Xie, D.; Chen, R.; Yan, G.; Guo, H.; Tyng, V.; Kellman, M. E. *Spectrochim. Acta A: Mol. Biomol. Spectrosc.* **2002**, *58*, 727–746.

[147] Zúñiga, J.; Bastida, A.; Requena, A.; Sibert, E. L. *J. Chem Phys.* **2002**, *116*, 7495–7508.

[148] Zúñiga, J.; Bastida, A.; Alacid, M.; Requena, A. *Chem Phys. Lett.* **1999**, *313*, 670–678.

[149] Murrell, J. N.; Guo, H. *J. Chem. Soc., Faraday Trans. 2* **1987**, *83*, 683–692.

[150] Coriani, S.; Marchesan, D.; Gauss, J.; Hättig, C.; Helgaker, T.; Jørgensen, P. *J. Chem. Phys.* **2004**, *123*, 184107.

[151] Bahou, M.; Lee, Y. C.; Lee, Y. P. *J. Am. Chem. Soc.* **2000**, *122*, 661–667.

[152] Wiberg, K. B.; Wang, Y. G.; de Oliveira, A. E.; Perera, S. A.; Vaccaro, P. H. *J. Phys. Chem. A* **2005**, *109*, 466–477.

[153] Tseng, D. C.; Poshusta, R. D. *J. Chem. Phys.* **1994**, *100*, 7481–7486.

[154] Zhang, Q.; Vaccaro, P. H. *J. Phys. Chem.* **1995**, *99*, 1799–1813.

[155] Latino, D. A. R. S.; Fartaria, R. P. S.; Freitas, F. F. M.; Aires-De-Sousa, J.; Silva Fernandes, F. M. S. *Int. J. Quant. Chem.* **2010**, *110*, 432–445.

[156] NIST Computational Chemistry Comparison and Benchmark Database, NIST Standard Reference Database Number 101, Release 15b, August 2011, Editor: Russell D. Johnson III, http://ccdb.nist.gov. 2011.

[157] Brasen, G.; Demtröder, W. *J. Chem. Phys.* **1999**, *110*, 11841–11849.

[158] Dunning, T. H.; Peterson, K. A.; Wilson, A. K. *J. Chem. Phys.* **2001**, *114*, 9244–9253.

[159] Celani, P.; Werner, H. J. *J. Chem. Phys.* **2003**, *119*, 5044–5057.

[160] Lo, W. J.; Lee, Y. P. *Chem. Phys. Lett.* **2001**, *336*, 71–75.

[161] Cao, Z.; Bu, Y.; Han, K. *Chin. J. Chem. Phys.* **2004**, *17*, 415–420.

[162] Carter, S.; Handy, N. C. *Mol. Phys.* **1986**, *57*, 175–185.

[163] Lanczos, C. *J. Res. Natl. Bur. Stand.* **1950**, *45*, 255–282.

[164] Parlett, B. N. *The Symmetric Eigenvalue Problem*; Prentice-Hall: Englewood Cliffs, NJ, 1980.

[165] Cullum, J. K.; Willoughby, R. A. *Lanczos algorithms for large symmetric eigenvalue computations*; Birkhäuser: Boston, 1985; Vol. 1.

[166] Beck, M. H.; Meyer, H. D. *J. Chem. Phys.* **2001**, *114*, 2036–2046.

[167] Rabitz, H.; de Vivie-Riedle, R.; Motzkus, M.; Kompa, K. *Science* **2000**, *288*, 824–828.

[168] Shapiro, M.; Brumer, P. *Quantum Control of Molecular Processes, 2nd Rev Enl edition*; Wiley, 2012.

[169] Rice, S.; Zhao, M. *Optical Control of Molecular Dynamics*; John Wiley & Sons: New York, 2000.

[170] Balint-Kurti, G. G.; Zou, S.; Brown, A. *Adv. Chem. Phys.* **2008**, *138*, 43–56.

[171] Gordon, R. J.; Rice, S. A. *Annu. Rev. Phys. Chem.* **1997**, *48*, 601–641.

[172] Zhu, L.; Kleimann, V. D.; Li, X.; Lu, S. P.; Trentleman, K.; Gordon, R. J. *Science* **1995**, *270*, 77.

[173] Prokhorenko, V. I.; Nagy, A. M.; Waschuk, S. A.; Brown, L. S.; Birge, R. R.; Miller, R. J. D. *Science* **2006**, *313*, 1257–1261.

[174] Arango, C.; Brumer, P. *J. Chem. Phys.* **2013**, *138*, 071104.

[175] Bardeen, C. J.; Yakovlev, V. V.; Squier, J. A.; Wilson, K. R. *J. Am. Chem. Soc.* **1998**, *120*, 13023–13027.

[176] Saab, M.; Doriol, L. J.; Lasorne, B.; Gurin, S.; Gatti, F. *Chem. Phys.* **2014**, *442*, 93 – 102.

[177] Sala, M.; Gatti, F.; Lauvergnat, D.; Meyer, H. D. *Phys. Chem. Chem. Phys.* **2012**, *14*, 3791–3801.

[178] Choi, Y. S.; Bradley Moore, C. *J. Chem. Phys.* **1989**, *90*, 3875–3876.

[179] Choi, Y. S.; Moore, C. B. *J. Chem. Phys.* **1991**, *94*, 5414–5425.

[180] Choi, Y. S.; Moore, C. B. *J. Chem. Phys.* **1995**, *103*, 9981–9988.

[181] Stratton, R. F.; Nielsen, A. H. *J. Mol. Spectrosc.* **1960**, *4*, 373 – 387.

[182] Martins, H.; Haiduke, R.; Bruns, R. *Spectrochimica Acta Part A: Molecular and Biomolecular Spectroscopy* **2004**, *60*, 2947 – 2952.

[183] Saito, K.; Kuroda, H.; Kakumoto, T.; Munechika, H.; Murakami, I. *Chem. Phys. Lett.* **1985**, *113*, 399 – 402.

[184] Le Blanc, A. H.; Laurie, V. H.; Gwinn, W. D. *J. Chem. Phys.* **1960**, *33*, 598–600.

[185] Huisman, P.; Klebe, K.; Mijlhoff, F.; Renes, G. *J. Mol. Struct.* **1979**, *57*, 71 – 82.

[186] Miller, R. F.; Curl, R. F. *J. Chem. Phys.* **1961**, *34*, 1847–1848.

[187] Vazquez, J.; Stanton, J. F. *Mol. Phys.* **2006**, *104*, 377–388.

[188] Bokarev, S.; Dolgov, E. K.; Bataev, V. A.; Godunov, I. A. *Int. J. Quant. Chem.* **2009**, *109*, 569–585.

[189] Margulès, L.; Demaison, J.; Boggs, J. E. *J. Phys. Chem. A* **1999**, *103*, 7632–7638.

[190] Stanton, J. F.; Gauss, J. *Theor. Chim. Acta* **1995**, *91*, 267–289.

[191] Kamiya, K.; Morokuma, K. *J. Chem. Phys.* **1991**, *94*, 7287–7298.

[192] Green, W. H.; Jayatilaka, D.; Willetts, A.; Amos, R. D.; Handy, N. C. *J. Chem. Phys.* **1990**, *93*, 4965–4981.

[193] Francisco, J. S.; Zhao, Y. *J. Chem. Phys.* **1992**, *96*, 7587–7596.

[194] Fang, W. H.; Liu, R. Z. *J. Chem. Phys.* **2001**, *115*, 5411–5417.

[195] Davisson, J. L.; Brinkmann, N. R.; Polik, W. F. *Mol. Phys.* **2012**, *110*, 2587–2598.

[196] Viel, A.; Leforestier, C. *J. Chem. Phys.* **2000**, *112*, 1212–1220.

[197] Yamamoto, T.; Kato, S. *J. Chem. Phys.* **1998**, *109*, 9783–9794.

[198] Yamamoto, T.; Kato, S. *J. Chem. Phys.* **2000**, *112*, 8006–8016.

[199] Iung, C.; Ribeiro, F.; III, E. L. S. *J. Phys. Chem. A* **2006**, *110*, 5420–5429.

[200] Wei, T. G.; Wyatt, R. E. *J. Phys. Chem.* **1993**, *97*, 13580–13585.

[201] Vazquez, J.; Harding, M. E.; Stanton, J. F.; Gauss, J. *J. Chem. Theory Comput.* **2011**, *7*, 1428–1442.

[202] Goddard, J. D.; III, H. F. S. *J. Chem. Phys.* **1990**, *93*, 4907–4915.

[203] Iung, C.; Pasin, G. *J. Phys. Chem. A* **2007**, *111*, 10426–10433.

[204] Pasin, G.; Iung, C.; Gatti, F.; Meyer, H. D. *J. Chem. Phys.* **2007**, *126*, 024302.

[205] Otto, F. *J. Chem. Phys.* **2014**, *140*, 014106.

[206] Knizia, G.; Adler, T. B.; Werner, H. J. *J. Chem. Phys.* **2009**, *130*, 054104.

[207] Bartlett, R.; Silver, D. *Phys. Rev. A* **1974**, *10*, 1927–1931.

[208] Bartlett, R. J.; Silver, D. M. *J. Chem. Phys.* **1975**, *62*, 3258–3268.

[209] Pople, J. A.; Binkley, J. S.; Seeger, R. *Int. J. Quantum Chem.* **1976**, *10*, 1–19.

[210] Raghavachari, K.; Trucks, G. W.; Pople, J. A.; Head-Gordon, M. *Chem. Phys. Lett.* **1989**, *157*, 479–483.

[211] Bartlett, R. J.; Watts, J. D.; Kucharski, S. A.; Noga, J. *Chem. Phys. Lett.* **1990**, *165*, 513–522.

[212] Stanton, J. F. *Chem. Phys. Lett.* **1997**, *281*, 130–134.

[213] Herzberg, G. *Van Nostrand Reinhold, New York,* **1966**, 616.

[214] Crane, J. C.; Kawai, A.; Nam, H.; Clauberg, H.; Beal, H. P.; Guinn, P.; Moore, C. *J. Mol. Spectrosc.* **1997**, *183*, 273 – 284.

[215] Zhou, X.; Zhang, N.; TerAvest, M.; Tang, D.; Hou, J.; Bertman, S.; Alaghmand, M.; Shepson, P. B.; Carroll, M. A.; Griffith, S.; Dusanter, S.; Stevens, P. S. *Nat. Geosci.* **2011**, *4*, 440–443.

[216] Wong, K. W.; Tsai, C.; Lefer, B.; Haman, C.; Grossberg, N.; Brune, W. H.; Ren, X.; Luke, W.; Stutz, J. *Atoms. Chem. Phys.* **2012**, *12*, 635–652.

[217] Platt, U.; Perner, D.; Harris, G. W.; Winer, A. M.; Pitts, J. N. *Nature* **1980**, *285*, 312–314.

[218] Li, S.; Matthews, J.; Sinha, A. *Science* **2008**, *319*, 1657–1660.

[219] Hofzumahaus, A.; Rohrer, F.; Lu, K.; Bohn, B.; Brauers, T.; Chang, C.-C.; Fuchs, H.; Holland, F.; Kita, K.; Kondo, Y.; Li, X.; Lou, S.; Shao, M.; Zeng, L.; Wahner, A.; Zhang, Y *Science* **2009**, *324*, 1702–1704.

[220] Bejan, I.; Abd El Aal, Y.; Barnes, I.; Benter, T.; Bohn, B.; Wiesen, P.; Kleffmann, J. *Phys. Chem. Chem. Phys.* **2006**, *8*, 2028–2035.

[221] Ammann, M.; Kalberer, M.; Jost, D. T.; Tobler, L.; Rossler, E.; Piguet, D.; Gaggeler, H. W.; Baltensperger, U. *Nature* **1998**, *395*, 157–160.

[222] Acker, K.; Moller, D.; Wieprecht, W.; Meixner, F. X.; Bohn, B.; Gilge, S.; Plass-Dulmer, C.; Berresheim, H. *Geophys. Res. Lett.* **2006**, *33*, L02809.

[223] Edwards, P. M.; Brown, S. S.; Roberts, J. M.; Ahmadov, R.; Banta, R. M.; deGouw, J. A.; Dube, W. P.; Field, R. A.; Flynn, J. H.; Gilman, J. B.; Graus, M.; Helmig, D.; Koss, A.; Langford, A. O.; Lefer, B. L.; Lerner, B. M.; Li, R.; Li, S.-M.; McKeen, S. A.; Murphy, S. M.; Parrish, D. D.; Senff, C. J.; Soltis, J.; Stutz, J.; Sweeney, C.; Thompson, C. R.; Trainer, M. K.; Tsai, C.; Veres, P. R.; Washenfelder, R. A.; Warneke, C.; Wild, R. J.; Young, C. J.; Yuan, B.; Zamora, R. *Nature* **2014**, *514*, 351–354.

[224] VandenBoer, T. C.; Young, C. J.; Talukdar, R. K.; Markovic, M. Z.; Brown, S. S.; Roberts, J. M.; Murphy, J. G. *Nat. Geosci.* **2015**, *8*, 55–60.

[225] Li, X.; Rohrer, F.; Hofzumahaus, A.; Brauers, T.; Haeseler, R.; Bohn, B.; Broch, S.; Fuchs, H.; Gomm, S.; Holland, F.; Jaeger, J.; Kaiser, J.; Keutsch, F. N.; Lohse, I.; Lu, K.; Tillmann, R.; Wegener, R.; Wolfe, G. M.; Mentel, T. F.; Kiendler-Scharr, A.; Wahner, A. *Science* **2014**, *344*, 292–296.

[226] Novicki, S.; Vasudev, R. *Chem. Phys. Lett.* **1991**, *176*, 118 – 122.

[227] Pagsberg, P.; Bjergbakke, E.; Ratajczak, E.; Sillesen, A. *Chem. Phys. Lett.* **1997**, *272*, 383 – 390.

[228] Dixon, R. N.; Rieley, H. *Chem. Phys.* **1989**, *137*, 307 – 321.

[229] Brust, A.; Becker, K.; Kleffmann, J.; Wiesen, P. *Atmospheric Environment* **2000**, *34*, 13 – 19.

[230] Stockwell, W. R.; Calvert, J. G. *Journal of Photochemistry* **1978**, *8*, 193 – 203.

[231] Yu, S. Y.; Zhang, C. G.; Huang, M. B. *Chem. Phys. Lett.* **2007**, *440*, 187 – 193.

[232] Dixon, R. N.; Rieley, H. *J. Chem. Phys.* **1989**, *91*, 2308–2320.

[233] Vasudev, R.; Zare, R. N.; Dixon, R. N. *J. Chem. Phys.* **1984**, *80*, 4863–4878.

[234] Hennig, S.; Untch, A.; Schinke, R.; Nonella, M.; Huber, J. *Chem. Phys.* **1989**, *129*, 93 – 107.

[235] Suter, H.; Huber, J. *Chem. Phys. Lett.* **1989**, *155*, 203 – 209.

[236] Deeley, C. M.; Mills, I. M.; Halonen, L. O.; Kauppinen, J. *Can. J. Phys.* **1985**, *63*, 962–965.

[237] Guilmot, J.; Godefroid, M.; Herman, M. *J. Mol. Spectrosc.* **1993**, *160*, 387 – 400.

[238] Guilmot, J. M.; Melen, F.; Herman, M. *J. Mol. Spectrosc.* **1993**, *160*, 401–410.

[239] McGraw, G. E.; Bernitt, D. L.; Hisatsune, I. C. *J. Chem. Phys.* **1966**, *45*, 1392–1399.

[240] Lee, T. J. *Chem. Phys. Lett.* **1993**, *216*, 194 – 199.

[241] Deeley, C. M.; Mills, I. M. *Mol. Phys.* **1985**, *54*, 23–32.

[242] Varma, R.; Curl, R. F. *J. Phys. Chem.* **1976**, *80*, 402–409.

[243] Hall, R. T.; Pimentel, G. C. *J. Chem. Phys.* **1963**, *38*, 1889–1897.

[244] Mielke, Z.; Latajka, Z.; Kolodziej, J.; Tokhadze, K. G. *J. Phys. Chem.* **1996**, *100*, 11610–11615.

[245] Baldeschwieler, J. D.; Pimentel, G. C. *J. Chem. Phys.* **1960**, *33*, 1008–1015.

[246] Guillory, W. A.; Hunter, C. E. *J. Chem. Phys.* **1971**, *54*, 598–603.

[247] Crowley, J. N.; Sodeau, J. R. *J. Phys. Chem.* **1989**, *93*, 4785–4790.

[248] Mielke, Z.; Tokhadze, K. G.; Latajka, Z.; Ratajczak, E. *J. Phys. Chem.* **1996**, *100*, 539–545.

[249] Wierzejewska, M.; Mielke, Z.; Wieczorek, R.; Latajka, Z. *Chem. Phys.* **1998**, *228*, 17 – 29.

[250] Krajewska, M.; Mielke, Z.; Tokhadze, K. G. *J. Mol. Struct.* **1997**, *404*, 47–53.

[251] Mielke, Z.; Wierzejewska, M.; Olbert, A.; Krajewska, M.; Tokhadze, K. G. *J. Mol. Struct.* **1997**, *436437*, 339 – 347.

[252] Mcdonald, P. A.; Shirk, J. S. *J. Chem. Phys.* **1982**, *77*, 2355–2364.

[253] Shirk, A. E.; Shirk, J. S. *Chem. Phys. Lett.* **1983**, *97*, 549–552.

[254] Khriachtchev, L.; Lundell, J.; Isoniemi, E.; Rasanen, M. *J. Chem. Phys.* **2000**, *113*, 4265–4273.

[255] Koch, T. G.; Sodeau, J. R. *J. Phys. Chem.* **1995**, *99*, 10824–10829.

[256] Luckhaus, D. *J. Chem. Phys.* **2003**, *118*, 8797–8806.

[257] Pham, P.; Guo, Y. *J. Chem. Phys.* **2013**, *138*, 144304.

[258] Bulychev, V. P.; Buturlimova, M. V.; Tokhadze, K. G. *J. Phys. Chem. A* **2015**, *119*, 9910–9916.

[259] Madsen, C. B.; Madsen, L. B.; Viftrup, S. S.; Johansson, M. P.; Poulsen, T. B.; Holmegaard, L.; Kumarappan, V.; Jrgensen, K. A.; Stapelfeldt, H. *J. Chem. Phys.* **2009**, *130*, 234310.

[260] Madsen, C. B.; Madsen, L. B.; Viftrup, S. S.; Johansson, M. P.; Poulsen, T. B.; Holmegaard, L.; Kumarappan, V.; Jørgensen, K. A.; Stapelfeldt, H. *Phys. Rev. Lett.* **2009**, *102*, 73007–73010.

[261] Hansen, J. L.; Stapelfeldt, H.; Dimitrovski, D.; Abu-samha, M.; Martiny, C. P. J.; Madsen, L. B. *Phys. Rev. Lett.* **2011**, *106*, 073001.

[262] Pelez, D.; Meyer, H. D. *J. Chem. Phys.* **2013**, *138*, 014108.

[263] Manzhos, S.; Dawes, R.; Carrington, T. *Int. J. Quantum Chem.* **2015**, *115*, 1012–1020.

[264] Worth, G. A.; Beck, M. H.; Jäckle, A.; Meyer, H. D. The MCTDH Package, Version 8.2, (2000). H. D. Meyer, Version 8.3 (2002). See http://www.pci.uni-heidelberg.de/tc/usr/mctdh/.

[265] Doriol, L. J.; Gatti, F.; Iung, C.; Meyer, H. D. *J. Chem. Phys.* **2008**, *129*, 224109.

[266] Meyer, H. D. *WIREs Comput. Mol. Sci.* **2012**, *2*, 351–374.

[267] Cox, A. P.; Brittain, A. H.; Finnigan, D. J. *Trans. Faraday Soc.* **1971**, *67*, 2179–2194.

[268] Lee, T. J.; Rendell, A. P. *J. Chem. Phys.* **1991**, *94*, 6229–6236.

[269] Skaarup, S.; Boggs, J. E. *J. Mol. Struct.* **1976**, *30*, 389 – 398.

[270] Benioff, P.; Das, G.; Wahl, A. C. *J. Chem. Phys.* **1976**, *64*, 710–717.

[271] Coffin, J. M.; Pulay, P. *J. Phys. Chem.* **1991**, *95*, 118–122.

[272] Jursic, B. S. *Chem. Phys. Lett.* **1999**, *299*, 334–344.

[273] Agrawal, P. M.; Thompson, D. L.; Raff, L. M. *J. Chem. Phys.* **1994**, *101*, 9937–9945.

[274] Reiche, F.; Abel, B.; Beck, R. D.; Rizzo, T. R. *J. Chem. Phys.* **2000**, *112*, 8885–8898.

[275] Deeley, C.; Mills, I. *J. Mol. Struct.* **1983**, *100*, 199 – 213.

[276] Barney, W. S.; Wingen, L. M.; Lakin, M. J.; Brauers, T.; Stutz, J.; Finlayson-Pitts, B. J. *J. Phys. Chem. A* **2000**, *104*, 1692–1699.

[277] Guilmot, J.; Carleer, M.; Godefroid, M.; Herman, M. *J. Mol. Spectrosc.* **1990**, *143*, 81 – 90.

[278] Murto, J.; Rsnen, M.; Aspiala, A.; Lotta, T. *J. Mol. Struct. THEOCHEM* **1985**, *122*, 213 – 224.

[279] Maki, A. G. *J. Mol. Spectrosc.* **1988**, *127*, 104–111.

[280] Holland, S. M.; Stickland, R. J.; Ashfold, M. N. R.; Newnham, D. A.; Mills, I. M. *J. Chem. Soc., Faraday Trans.* **1991**, *87*, 3461–3471.

[281] Allegrini, M.; Johns, J. W. C.; Mckellar, A. R. W.; Pinson, P. *J. Mol. Spectrosc.* **1980**, *79*, 446–454.

[282] Zhang, X.; Zou, S.; Harding, L. B.; Bowman, J. M. *J. Phys. Chem. A* **2004**, *108*, 8980–8986.

[283] Klimek, D. E.; Berry, M. J. *Chem. Phys. Lett.* **1973**, *20*, 141 – 145.

[284] Crane, J. C.; Nam, H.; Beal, H. P.; Clauberg, H.; Choi, Y. S.; Moore, C.; Stanton, J. F. *J. Mol. Spectrosc.* **1997**, *181*, 56 – 66.

[285] Maul, C.; Dietrich, C.; Haas, T.; Gericke, K.-H.; Tachikawa, H.; R. Langford, S.; Kono, M.; L. Reed, C.; N. Dixon, R.; N. R. Ashfold, M. *Phys. Chem. Chem. Phys.* **1999**, *1*, 767–772.

[286] Godunov, I.; Yakovlev, N. *J. Struct. Chem.* **1995**, *36*, 238–253.

[287] Knowles, P. J.; Hampel, C.; Werner, H. J. *J. Chem. Phys.* **2000**, *112*, 3106–3107.

[288] Fischer, G. *J. Mol. Spectrosc.* **1969**, *29*, 37 – 53.

[289] Giddings, L.; Innes, K. *J. Mol. Spectrosc.* **1961**, *6*, 528 – 549.

[290] Giddings, L.; Innes, K. *J. Mol. Spectrosc.* **1962**, *8*, 328 – 337.

[291] Diken, E. G.; Headrick, J. M.; Roscioli, J. R.; Bopp, J. C.; Johnson, M. A.; McCoy, A. B. *J. Phys. Chem. A* **2005**, *109*, 1487–1490.

[292] Huang, X.; Braams, B. J.; Carter, S.; Bowman, J. M. *J. Am. Chem. Soc.* **2004**, *126*, 5042–5043.

[293] McCoy, A. B.; Huang, X.; Carter, S.; Bowman, J. M. *J. Chem. Phys.* **2005**, *123*, 064317.

[294] Pelez, D.; Sadri, K.; Meyer, H. D. *Spectrochim. Acta, Part A* **2014**, *119*, 42 – 51.